Daniel Waltner

Semiclassical Approach to Mesoscopic Systems

Classical Trajectory Correlations and Wave Interference



Springer Tracts in Modern Physics

Volume 245

Managing Editor

G. Höhler, Karlsruhe, Germany

Series Editors

A. Fujimori, Tokyo, Japan J. Kühn, Karlsruhe, Germany Th. Müller, Karlsruhe, Germany F. Steiner, Ulm, Germany W. C. Stwalley, Storrs, CT, USA J. E. Trümper, Garching, Germany P. Wölfle, Karlsruhe, Germany

For further volumes: http://www.springer.com/series/426

Springer Tracts in Modern Physics

Springer Tracts in Modern Physics provides comprehensive and critical reviews of topics of current interest in physics. The following fields are emphasized: elementary particle physics, solid-state physics, complex systems, and fundamental astrophysics.

Suitable reviews of other fields can also be accepted. The editors encourage prospective authors to correspond with them in advance of submitting an article. For reviews of topics belonging to the above mentioned fields, they should address the responsible editor, otherwise the managing editor.

See also springer.com

Managing Editor

Gerhard Höhler

Institut für Theoretische Teilchenphysik Karlsruhe Institut für Technologie KIT Postfach 69 80

76128 Karlsruhe, Germany Phone: +49 (7 21) 6 08 33 75 Fax: +49 (7 21) 37 07 26 Email: gerhard.hoehler@KIT.edu www-ttp.physik.uni-karlsruhe.de/

Elementary Particle Physics, Editors

Johann H. Kühn

Institut für Theoretische Teilchenphysik Karlsruhe Institut für Technologie KIT Postfach 69 80

76049 Karlsruhe, Germany Phone: +49 (7 21) 6 08 33 72 Fax: +49 (7 21) 37 07 26 Email: johann.kuehn@KIT.edu www-ttp.physik.uni-karlsruhe.de/~ik

Thomas Müller

Institut für Experimentelle Kernphysik Karlsruhe Institut für Technologie KIT Postfach 69 80

76049 Karlsruhe, Germany Phone: +49 (7 21) 6 08 35 24 Fax: +49 (7 21) 6 07 26 21 Email: thomas.muller@KIT.edu www-ekp.physik.uni-karlsruhe.de

Fundamental Astrophysics, Editor

Joachim Trümper

Max-Planck-Institut für Extraterrestrische Physik

Postfach 13 12 85741 Garching, Germany

Phone: +49 (89) 30 00 35 59 Fax: +49 (89) 30 00 33 15 Email: jtrumper@mpe.mpg.de www.mpe-garching.mpg.de/index.html

Solid-State Physics, Editors

Atsushi Fujimori

Editor for The Pacific Rim

Department of Physics University of Tokyo 7-3-1 Hongo, Bunkyo-ku Tokyo 113-0033, Japan

Email: fujimori@phys.s.u-tokyo.ac.jp http://wyvern.phys.s.u-tokyo.ac.jp/

welcome_en.html

Peter Wölfle

Institut für Theorie der Kondensierten Materie Karlsruhe Institut für Technologie KIT

Postfach 69 80

76049 Karlsruhe, Germany Phone: +49 (7 21) 6 08 35 90 Fax: +49 (7 21) 6 08 77 79 Email: peter.woelfle@KIT.edu www-tkm.physik.uni-karlsruhe.de

Complex Systems, Editor

Frank Steiner

Institut für Theoretische Physik Universität Ulm Albert-Einstein-Allee 11 89069 Ulm, Germany

Phone: +49 (7 31) 5 02 29 10 Fax: +49 (7 31) 5 02 29 24 Email: frank.steiner@uni-ulm.de

www.physik.uni-ulm.de/theo/qc/group.html

Atomic, Molecular and Optical Physics

William C. Stwalley

University of Connecticut Department of Physics 2152 Hillside Road, U-3046 Storrs, CT 06269-3046, USA Phone: +1 (860) 486 4924

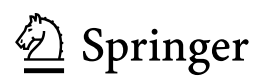
Phone: +1 (860) 486 4924 Fax: +1 (860) 486 3346 Email: w.stwalley@uconn.edu

www-phys.uconn.edu/faculty/stwalley.html

Daniel Waltner

Semiclassical Approach to Mesoscopic Systems

Classical Trajectory Correlations and Wave Interference



Dr. Daniel Waltner Institut für Theoretische Physik Universität Regensburg Regensburg Germany

ISSN 0081-3869 ISBN 978-3-642-24527-5 DOI 10.1007/978-3-642-24528-2 Springer Heidelberg Dordrecht London New York e-ISSN 1615-0430 e-ISBN 978-3-642-24528-2

Library of Congress Control Number: 2011941856

© Springer-Verlag Berlin Heidelberg 2012

This work is subject to copyright. All rights are reserved, whether the whole or part of the material is concerned, specifically the rights of translation, reprinting, reuse of illustrations, recitation, broadcasting, reproduction on microfilm or in any other way, and storage in data banks. Duplication of this publication or parts thereof is permitted only under the provisions of the German Copyright Law of September 9, 1965, in its current version, and permission for use must always be obtained from Springer. Violations are liable to prosecution under the German Copyright Law.

The use of general descriptive names, registered names, trademarks, etc. in this publication does not imply, even in the absence of a specific statement, that such names are exempt from the relevant protective laws and regulations and therefore free for general use.

Printed on acid-free paper

Springer is part of Springer Science+Business Media (www.springer.com)

Preface

This book explains how to describe quantum effects in mesoscopic systems by semiclassical methods. These methods combine on the one hand concepts of classical mechanics as classical trajectories and on the other hand of quantum mechanics as interference effects. By this they are especially suited to describe the transition region between the macroscopic and the microscopic world, i.e. the mesoscopic regime. Within the semiclassical framework *classical* orbits alone can lead to a basic understanding of quantum effects, e.g. of quantum spectra. However for a full understanding *quantum* interference between different paths need to be taken into account. These attracted huge interest during the last years. We thus want to review here the most important developments and present recent advances.

The content of this book originates from my Ph.D. thesis *Semiclassical Approach to Mesoscopic Systems: Classical Trajectory Correlations and Wave Interference* at the Institute for Theoretical Physics at the University of Regensburg in 2011. This work was supervised by Prof. Klaus Richter. Him I would like to thank for his guidance and encouragement during the last years.

I am grateful to some colleagues in Regensburg with whom I had the pleasure of discussing several topics of semiclassics: İnanc Adagideli, Marcus Bonanca, Tobias Dollinger, Christopher Eltschka, Arseni Goussev, Martha Gutiérrez, Tobias Kramer, Jack Kuipers, Cyril Petitjean, Peter Schlagheck, Gregor Tanner and Juan-Diego Urbina. Furthermore I enjoyed the fruitful discussions with other members of the quantum chaos community during their visits in Regensburg or at workshops and conferences especially with Jens Bolte, Piet Brouwer, Stefan Heusler, Philippe Jacquod, Sebastian Müller, Dima Savin, Martin Sieber and Robert Whitney to mention just a few.

I want to thank Jack Kuipers for proof reading this book and commenting on it and Tobias Dollinger, Christopher Eltschka and Juan-Diego Urbina for critically reading different parts of it.

Furthermore I am grateful to Prof. Frank Steiner for recommending the publication of this book and his suggestions to improve the presentation and Ute Heuser and Jacqueline Lenz from the Springer Verlag for the editorial guidance.

vi Preface

The results presented in this book were obtained at the Institute for Theoretical Physics of the University of Regensburg. In this context I acknowledge financial support by the DFG-Graduiertenkolleg "Nonlinearity and Nonequilibrium in Condensed Matter".

Finally I thank my family and especially my parents for their generous support and encouragement.

Regensburg, August 2011

Daniel Waltner

Contents

1	Intr	oductio	n	1		
	1.1	Consid	dered Systems and Methods of Description	1		
		1.1.1	Mesoscopic Systems: Methods of Description	1		
		1.1.2	Quantum Chaos: Considered Systems	3		
		1.1.3	Quantum Chaos and Semiclassical Methods	5		
	1.2	Outlin	e of the Book	8		
	Refe	rences		10		
2	Semiclassical Techniques					
	2.1		Features of Classical and Quantum Systems	13		
	2.2	Introd	uction into Semiclassical Techniques	16		
	2.3	Quant	um Corrections to the Transmission	21		
		2.3.1	Diagonal Contribution	22		
		2.3.2	First Quantum Correction: Configuration-Space			
			Approach	23		
		2.3.3	Quantum Transmission: Phase-Space Approach	29		
	2.4	Spectral Statistics				
	Refe	References				
3	Sur	vival Pr	robability and Fidelity Decay	41		
	3.1					
			Approximation			
		3.1.1	Survival Probability	41		
		3.1.2	Fidelity Amplitude and Fidelity	44		
	3.2	Unitar	ity in Semiclassics	48		
	3.3	Higher-Order Contributions and the Effect of Spin-Orbit				
		Interaction				
		3.3.1	Higher-Order Contributions	52 52		
		3.3.2	Unitary Case	58		

viii Contents

		3.3.3	Orthogonal Case	59		
		3.3.4	Spin-Orbit Interaction and the Symplectic Case	61		
	3.4	Contir	nuity Equation	62		
		3.4.1	Higher-Order Contributions to the Integrated			
			Current Density	66		
		3.4.2	Fourier Transforms	66		
		3.4.3	Recursion Relations	68		
		3.4.4	Implications for Transport	72		
		3.4.5	Application of Recursion Relations			
			to the Fidelity Amplitude	75		
	3.5		s not Accessed by RMT	81		
		3.5.1	Lyapunov Decay of the Fidelity	81		
		3.5.2	Effect of a Time-Dependent Perturbation	83		
	Refe	erences		86		
4	Fhr	anfact_7	Fime Effects in Mesoscopic Systems	89		
7	4.1	L eadir	ng-Order Quantum Correction to the Conductance	90		
	4.2		ero Ehrenfest-Time for Time-Dependent Processes	90		
	4.3		nce of the Conductance	97		
	4.4		to-Leading Order Quantum Corrections	102		
		4.4.1	Transmission and Reflection for dc Transport	103		
		4.4.2	Frequency Dependence of Transmission	100		
		2	and Reflection	112		
		4.4.3	Spectral Form Factor	116		
	4.5		lation Function of an Arbitrary Number of Pairs	110		
			attering Matrices	121		
		4.5.1	Influence of the Ehrenfest-Time on Orbits			
			with Encounters	123		
		4.5.2	Trajectories Always Correlated	137		
		4.5.3	Mixed Terms	137		
	4.6	The D	Density of States of Chaotic Andreev Billiards	139		
		4.6.1	Scattering Approach for the Andreev Billiard			
			and the RMT Density of States	140		
		4.6.2	Density of States for Non-vanishing Ehrenfest-Time	143		
	Refe	erences		146		
_	C	! -1 ·	al Al 4. Et al Element d'al 17004.	149		
5	Sem 5.1					
	3.1		ral Form Factor for $\tau > 1$ and Unitarity in Semiclassics Semiclassical Approximations for the Spectral	149		
		5.1.1	11	149		
		512	Determinant	149		
	5.0	5.1.2	Spectral Form Factor for $\tau > 1$	152		
	5.2		ture and Multiple Traversals of Periodic Orbits	157		
		J.4.1	Dennerassical Calculation	130		

Contents ix

	5.2.2	Field-Theoretical Calculation: The Curvature						
		Contribution	160					
	5.2.3	Semiclassical Interpretation of Curvature Effects	162					
	5.2.4	Consistency with Former Results	164					
	References		166					
6		s and Outlook	167 171					
Appendix A: Recursion Relations for Transport								
Appendix B: Encounter Integrals for Non-zero Ehrenfest-Time								
Αı	Appendix C: Conductance Variance with Tunnel Barriers							

Chapter 1 Introduction

1.1 Considered Systems and Methods of Description

Improved experimental and numerical techniques generated an increasing interest in theoretical methods to describe mesoscopic systems. Such systems with the size of a few micrometers are situated with respect to their dimensions between the microscopic and the macroscopic world. The motion of microscopic particles is described by quantum mechanics, i.e. the Schrödinger equation, whereas the dynamics of macroscopic bodies is described by classical mechanics, i.e. Newton's equation of motion. If the number of conserved quantities in a classical system is less than the number of degrees of freedom, the dynamics is no longer regular but becomes mixed or even chaotic. The last case is characterised by the fact that most of the neighboring trajectories approach or deviate from each other exponentially and almost all long trajectories cover the accessible space uniformly.

1.1.1 Mesoscopic Systems: Methods of Description

Due to phase-coherent motion through the underlying system, an exact description of mesoscopic systems is only possible by means of quantum mechanics, i.e. of the Schrödinger equation. As, however, the systems are already relatively large compared to microscopic systems, using an exact quantum mechanical description quite often reaches the computational limits. Three alternative theoretical approaches are used here: numerical methods, Random Matrix Theory (RMT) and semiclassical methods.

Due to the large size of the considered systems compared to microscopic ones, numerical investigations based on quantum calculations already need a lot of computer power. Additionally in most cases they do not lead to an intuitive explanation of the observed phenomena. However they can be used to confirm and to correct results obtained by the other approximate methods. For this purpose this method will be applied in this book.

1

2 1 Introduction

The second method, RMT¹ [1], was originally invented to study the correlations in the rather complex spectra of nuclei. The basic idea of this method is that matrices appearing in the corresponding quantum mechanical description of the system, e.g. the Hamiltonian, are replaced by random matrices, i.e. averages over all possible matrix entries. The only constraint comes from the symmetries of the underlying system leading to several ensembles of matrices used for the calculation. For Hermitian matrices to be analysed in the case of no time-reversal symmetry the Gaussian unitary ensemble (GUE), in the case of time-reversal symmetry and no spin-orbit interaction the Gaussian orthogonal ensemble (GOE) and in the case of time-reversal symmetry and spin-orbit interaction the Gaussian symplectic ensemble (GSE) is used. When unitary instead of Hermitian matrices are considered, e.g. scattering matrices, the corresponding circular instead of Gaussian ensembles have to be studied. For more details see [1]. A newer related method, supersymmetry [2], performs the ensemble averages not directly but at cost of introducing further integrals over commuting and anticommuting variables. Furthermore for disordered systems there is the perturbative diagrammatic technique that is known to be equivalent to the supersymmetric method for these systems. For an overview over disordered systems and the diagrammatic technique see for example [3]. The connection between RMT and the study of classically chaotic mesoscopic systems was made in the so-called Bohigas, Giannoni, Schmit (BGS) conjecture [4]. It states, based on numerical results that the statistics of energy levels of individual classically chaotic systems is well described by RMT. Although RMT is quite often the only feasible way of describing analytically systems with complex dynamics, this approach has disadvantages: A dynamical interpretation is not available and additionally its applicability to quantum systems with classically chaotic counterpart relies on the BGS conjecture.

In this work we will mainly present results obtained by using semiclassical methods. This method contains on the one hand elements of classical mechanics like classical orbits and on the other hand also elements of quantum mechanics like interference effects. In this approach exact quantum mechanical expressions are replaced by approximations that are asymptotically valid in the semiclassical limit. This limit usually means that the Fermi wavelength λ_F of the considered particles is much smaller than the typical system size \mathcal{L} , but not fully negligible, which is fulfilled in the considered mesoscopic systems. Here we will mostly take the semiclassical limit by considering $\hbar \to 0$ and mean by this that \hbar is much smaller than all relevant classical actions like the classical actions of the considered orbits.

Despite semiclassical expressions as introduced below are quite complicated to analyse, this method has several advantages compared to the ones mentioned before: It is applicable to regular and chaotic mesoscopic systems; not only to chaotic systems like RMT. Second it makes it possible to develop a dynamical understanding of phenomena obtained by RMT calculations or by numerical simulations based on the elements of a semiclassical theory, i.e. in terms of properties of classical trajectories and interference effects. Third it is even possible to identify corrections to the RMT

We will sometimes use RMT synonymous with supersymmetry and refer to these theories as field-theoretical methods.

results for example due to the Ehrenfest-time, the time up to that spatially localised initial wave packets follow the classical dynamics, or due to non universal effects, which we will come back to soon. Semiclassics is thus a very useful tool to examine and understand mesoscopic systems.

1.1.2 Quantum Chaos: Considered Systems

The interest in mesoscopic systems often comes together with interest in the research field of quantum chaos [5]. The central question in this field is the following: Consider two classical systems, one of them with chaotic and one with regular dynamics, how are the quantum properties of the systems that get important when we shrink them down, influenced by the underlying classical dynamics?

As the semiclassical expressions given below are quite complicated to analyse already for relatively simple physical systems, one often considers in quantum chaos simple low-dimensional model systems such as two-dimensional billiards. The dynamics in these systems is ballistic, i.e. free motion inside and specular reflection at the boundary. The boundary in this context determines if the system possesses chaotic or regular motion. For example the circular and rectangular billiard possess regular dynamics. In the rectangular billiard the magnitudes of the momenta along the rectangle's axes are conserved and in the circular billiard apart from the energy also the angular momentum is conserved. The number of conserved quantities is thus equal to the number of degrees of freedom. The stadium billiard obtained by attaching two half circles to two opposite sides of a rectangle, the Sinai billiard, a quadratic or rectangular billiard with a circular hole in the centre and the desymmetrised diamond (DD) billiard, see Fig. 1.1 are examples of billiards with chaotic dynamics. Billiards are studied analytically, numerically and also experimentally. Experimentally they are realised for example as quantum dots—the electrons are confined to interfaces in semiconductor heterostructures, see Fig. 1.2—, quantum wells and quantum corrals probing the dynamics of electrons, for an overview see for example [5]. However due to the structural similarity of the stationary Schrödinger equation and the electromagnetic wave equation also two-dimensional microwave billiards confining microwaves to metallic or superconducting cavities are studied. Also cold atoms confined by laser beams are realised experimentally [6].

Also, periodic arrays as the antidot superlattice, obtained by etching a regular lattice of circular nanometer sized holes into the interface region of a semiconductor heterostructure containing a two-dimensional electron gas are considered. In the case of a steep potential at the holes in the antidot this represents another example of a chaotic system, the Lorentz gas.

Apart from these Euclidean billiards in quantum chaos, mainly in theoretical studies, also systems endowed with a non-Euclidean metric like surfaces of constant negative curvature [7] can be considered. Although they are hard to study experimentally, in analytical calculations they lead, compared to Euclidean billiards, to simplifications. For example the semiclassical approximation for the density of

4 1 Introduction

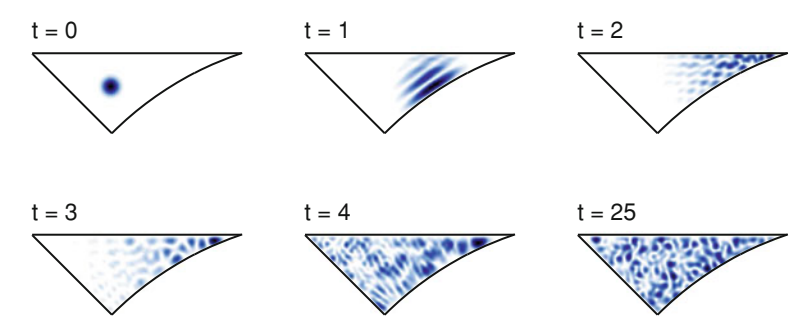


Fig. 1.1 Quantum mechanical wave packet launched into a mesoscopic cavity with the geometry of a desymmetrised diamond billiard. The wave packet evolution is monitored at times t = 1, 2, 3, 4, and 25, in units of the average time between collisions with the walls of a corresponding classical particle. (Courtesy of A. Goussey)

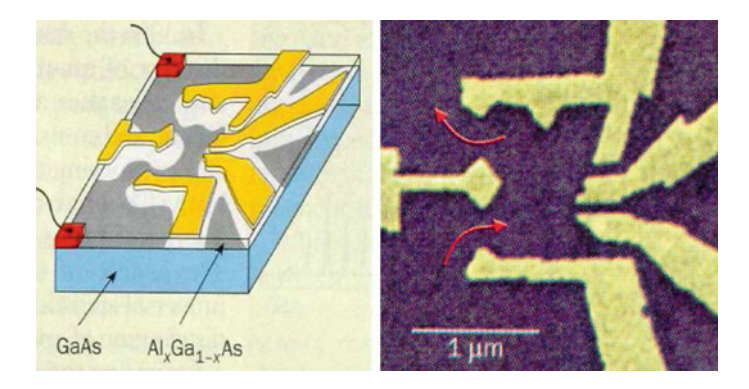


Fig. 1.2 A mesoscopic quantum dot obtained by confining electrons at a two-dimensional interface between GaAs and AlGaAs [taken from [8]]. The motion of the electrons is further confined by negatively charged surface gates to the dot, this allows the electrons to enter and leave only through the two openings indicated in the right figure

states is sometimes exact. Another example of a model system are quantum graphs [9, 10]. Here one considers a set of vertices connected by a set of edges. The propagation of an initial state ψ_0 on a graph is normally determined by the following rule: On the edges the state is propagated according to the one-dimensional free Schrödinger equation and at the vertices the state is scattered into one of the edges reaching this vertex. The scattering is determined by scattering matrices at each vertex. Also for these systems the semiclassical expression for the density of states is exact. Compared to surfaces of constant negative curvature these systems possess the advantage that they are often studied numerically and realized experimentally as microwave networks, see for example [11]. Another example for model systems often studied numerically are maps, i.e. discrete mappings of position and momentum. One example is the kicked rotator; i.e. a pendulum that is driven by instantaneous kicks resulting from a gravitational potential. It shows, depending on the kicking parameter

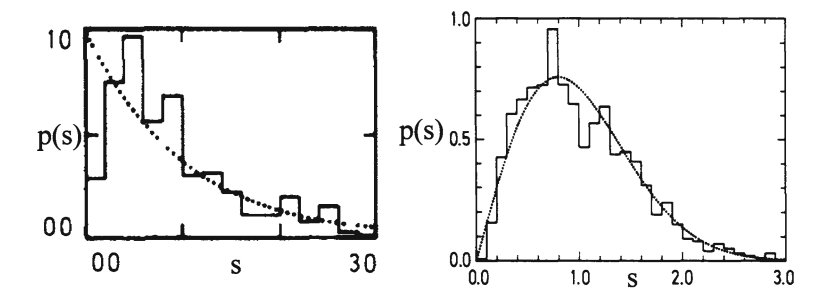


Fig. 1.3 Experimentally measured histogram for distances *s* between successive eigenenergies shown for a regular system on the left and for a chaotic system on the right hand side probing a microwave billiard [taken from [12]]. The dotted curves indicate a Wigner distribution in the chaotic and a Poisson distribution in the regular case. The decrease of the first data point in the left histogram is due to imperfections of the resonator

K, a transition from almost regular dynamics via a mixed phase space to complete chaos.

1.1.3 Quantum Chaos and Semiclassical Methods

In applying semiclassical methods, quantum chaotic questions are of course of interest. We first show here, considering different examples, how the quantum properties are influenced by the kind of the underlying classical dynamics. A first example is the nearest neighbour distribution of the eigenenergies of a system. One finds a Wigner distribution with a characteristic suppression of small level distances, referred to as level repulsion, for classically chaotic systems [4] (see the right diagram in Fig. 1.3). For classically regular systems like the rectangular billiard, however, one expects a Poisson distribution as shown semiclassically in Ref. [13], see the left panel in Fig. 1.3, as all the energies can be assumed in this case to be distributed in an uncorrelated manner. In the latter figure the experimental results studying the difference between the spectral properties of chaotic and regular systems obtained from a microwave billiard are shown. In this case the number of eigenenergies p(s)in the interval of successive eigenenergies between s and $s + \Delta s$ is plotted for a regular system, a rectangular billiard, on the left and for a chaotic system, a Sinai billiard of the same size, on the right. The decrease in the regular case for small s is due to imperfections of the resonator. To describe the functional form of p(s) for mixed dynamics several approaches were developed, for example the Berry Robnik distribution [14] was obtained by assuming that the subspectra of the chaotic and the regular part of the phase space can be superimposed uncorrelatedly. The function p(s) determined within this approach is however larger for $s \to 0$ than the one found numerically. This region is better explained by the purely phenomenological Brody distribution [15]. Recently it was shown that by additionally taking into account 6 1 Introduction

dynamical tunnelling between the chaotic and the regular parts of the phase space the Berry Robnik distribution also yields the correct behaviour for $s \to 0$ [16].

A further example is the dependence of the transmission through a quantum dot on the applied magnetic field. Here one observes weak localisation, i.e. a decrease of the conductance with decreasing magnetic field. Probing an ensemble of circular cavities one here finds for the dependence of the conductance on the magnetic field a triangular curve; this curve is in general system dependent, whereas for chaotic cavities, here stadium shaped billiards, one finds an universal Lorentzian [5], predicted also by RMT and by semiclassics, see Fig. 1.4.

A third example to which we will return in Chap. 4 is the density of states of Andreev billiards, i.e. normal conducting billiards with a superconductor attached. Whereas, as just mentioned, in normal conducting billiards correlations between energy levels are considered in order to find traces of the underlying classical dynamics, these traces can be found in Andreev billiards directly in the density of states. In the chaotic case, i.e. a superconductor attached to a chaotic billiard one finds a gap in the density of states for small energies above the Fermi energy E=0 in accordance with RMT [17] and semiclassics (as shown in this book). In the regular case the density of states is in general system dependent, for a circular cavity it increases linearly with increasing energy (exact quantum calculations are shown in the left panel in Fig. 1.5). For the corresponding result for chaotic systems—here a Sinai billiard—see the right diagram in Fig. 1.5.

Besides the comparison of quantum features of systems with different underlying classical dynamics, semiclassical methods have several other applications. First they can be used to explain quantum spectra by relating certain peaks in the quantum spectrum to contributions of certain classical trajectories. Also the semiclassical calculation of spectra is an important field of interest. In this case one faces however the problem that the spectral density expressed as a sum over periodic-orbit contributions (see below) yields a divergent result when evaluated for real energies E. Only grouping the trajectory contributions together in a sophisticated way, as it is done within the cycle expansion method [20], that makes the cancellation of a huge part of the contributions obvious, leads to convergent results. Another interesting research topic starts from the similarity of the semiclassical expression for the density of states in terms of classical orbits and the formula determining the density of the nontrivial zeros of the Riemann zeta function in terms of a summation over prime numbers, for an introduction see for example [21]. Apart from similarities between the latter formulas, there are further parallels between these two branches. For example there is strong evidence that the distribution of zeros is given by the GUE, i.e. here it shows the same behaviour as a chaotic system without time-reversal symmetry. However there are also differences between the two research directions: The action of the trajectories depends linearly on the length of the trajectory, the corresponding quantities for the primes logarithmically on the prime number. Furthermore primes are not randomly distributed, i.e. the probability to find a prime in the neighbourhood of another one is *not* independent of the difference between the two. This is stated by the Hardy-Littlewood conjecture. A corresponding correlation for orbits is not known. The ultimate goal of this research is to find a self-adjoint operator that

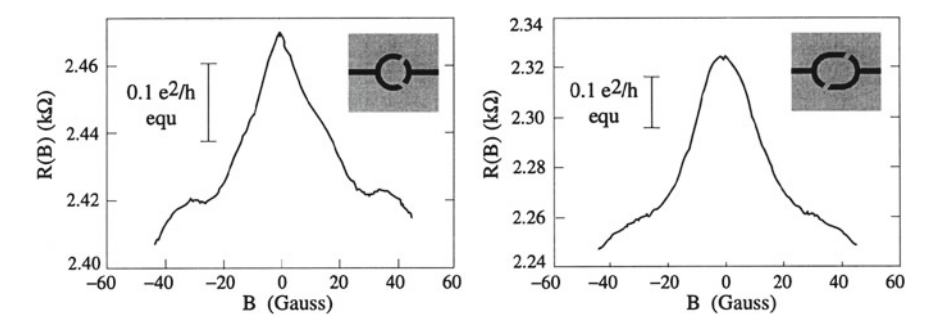


Fig. 1.4 Measured resistance as a function of the applied magnetic field for an ensemble of circular—i.e. regular—billiards on the left and an ensembles of stadium—i.e. chaotic—billiard on the right [adapted from [18]]. For regular dynamics here a triangular curve and for chaotic systems a Lorentzian lineshape is observed

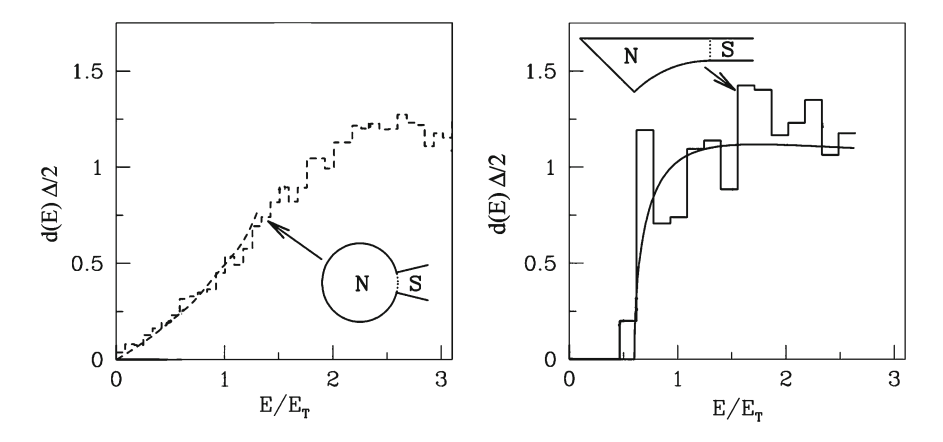


Fig. 1.5 Numerically calculated average density of states d(E) multiplied by one half of the mean level spacing Δ of the normal conducting billiard, i.e. the inverse of twice the mean spectral density, as a function of the energy divided by the Thouless energy E_T defined in Chap. 4, for a regular billiard in the left diagram and a chaotic Andreev billiard in the right one [taken from [19]]. Whereas in the chaotic case a pronounced gap is observed for small energies, the density of states increases here linearly for small energies in the regular case. The continuous curve on the right is the RMT prediction, the one on the left is obtained from a semiclassical calculation

possesses the eigenvalues y, where z = 1/2 + iy are the zeros of the Riemann zeta function. This would prove that y always has to be real and thus prove the Riemann hypothesis. Although a possible Hamiltonian was conjectured about ten years ago, this connection is still not understood and an subject of ongoing research, see for example [22, 23].

8 1 Introduction

1.2 Outline of the Book

In this book we study classically chaotic mesoscopic systems by means of semiclassical techniques. On the one hand we confirm and explain in terms of correlations between classical trajectories results obtained before by RMT. On the other hand we also study effects beyond RMT, mostly the effects of a non-zero Ehrenfest-time, and check in this case some of our predictions by comparison with numerics.

First we explain the main assumptions made in our calculations and the corresponding requirements that need to be fulfilled by potential systems: We use semiclassical techniques. In order to make them applicable the Fermi wavelength λ_F should be the shortest length scale in the system. In order to obtain all considered interference effects between different paths, phase-coherent motion is assumed. When probing electron transport thus low temperatures are required to suppress electron-phonon scattering. To obtain ballistic and not diffusive dynamics impurity scattering should be strongly suppressed. Finally we neglect all kinds of interaction effects, e.g. electron-electron interaction, for a justification of this approximation and its limits see for example [24].

Now we summarise the contents of the chapters: In Chap. 2 we introduce, after reviewing basic features of classical and quantum systems, semiclassical expressions for the time evolution operator, the Green function, the density of states and the conductance. Afterwards we explain the two known methods to calculate semiclassically contributions to the conductance and the Fourier transform of the two-point autocorrelation function of spectral densities, the so-called spectral form factor, in agreement with RMT.

In Chap. 3 we study time-dependent processes. More precisely we consider on the one hand decay of open chaotic systems and calculate the quantum survival probability as a function of the time for that systems, for a possible initial situation see the left panel in Fig. 1.6. On the other hand we study the effect of perturbations on closed chaotic systems and treat the spatially integrated overlap of the wavefunctions characterising the perturbed and the unperturbed systems. A possible situation is illustrated in the right part of Fig. 1.6. We there evolve a wave packet up to time t in the unperturbed system, then we perform a perturbation—here a deformation of the boundary—and then evolve the state for the time t backwards in time keeping the perturbation. Finally we consider the overlap between the initial and final wavefunctions, i.e. the ones obtained for the two billiards on the left. We first show in this chapter how to obtain in a way consistent with RMT the leading-order quantum corrections in \hbar to the classical contributions. We check that our semiclassical and the RMT results coincide order by order in \hbar for the GUE, GOE and GSE. Furthermore we confirm that exact relations as for example the continuity equation are also fulfilled within our semiclassical approach. We show a relation between the spectral form factor and the spatially integrated overlap of perturbed and unperturbed wavefunction obtained previously using RMT within our approach. Finally we treat effects not accessed by RMT. We there extend our studies on the effect of a perturba1.2 Outline of the Book 9

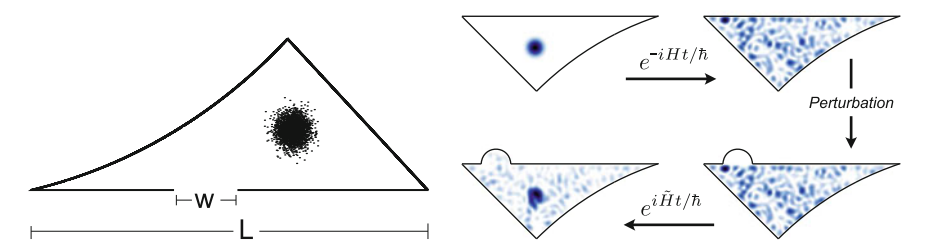
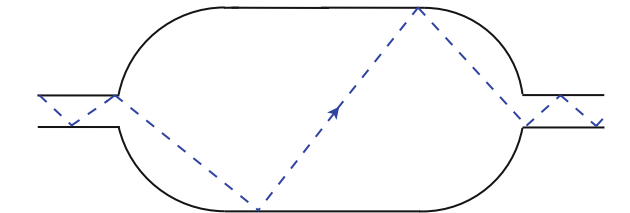


Fig. 1.6 *Left*: Possible initial state for the calculation of the survival probability, a localised wave packet inside the DD billiard, *Right*: Situation studied when analysing the effect of a perturbation [taken from [25, 26]]

Fig. 1.7 An example of a possible system for studying transport, a stadium billiard with two leads attached. The *dashed* line indicates a possible classical trajectory traversing the system



tion on additional contributions occurring in the regime of strong perturbations and on time-dependent perturbations.

Chaper 4 is devoted to the probably most prominent effects apart from the ones obtained by RMT, the effects of a non-zero Ehrenfest-time. We first consider a chaotic system containing two semi-infinite straight leads, see Fig. 1.7. We review the calculation of [27] determining semiclassically the Ehrenfest-time dependence of the transmission up to the first subleading order in the number of open channels in the leads. We then consider the effect of a non-vanishing Ehrenfest-time when studying a perturbation and the decay as in Chap. 3. Our results for the latter quantity are additionally checked by numerical simulations. For the next application we include tunnel barriers in the leads. We study in this case the Ehrenfest-time dependence of the variance of the conductance to leading order in the number of open channels in dependence of the tunnelling rate, these results are confirmed by numerical simulations. We then return to the transmission and the reflection of the chaotic system with perfectly coupled leads and calculate the next-order quantum correction in the number of open channels for non-zero Ehrenfest-time.

Next we study the spectral form factor and confirm previous field-theoretical results predicting the Ehrenfest-time dependence that are in contrast to previous semiclassical findings. We furthermore study the leading-order contribution in the number of open channels in the leads to the correlation function of n pairs ($n \in \mathbb{N}$) of scattering matrices for non-zero Ehrenfest-time, that can be used for calculating the Ehrenfest-time dependence of the density of states of a chaotic Andreev billiard that we determine afterwards.

10 1 Introduction

The following chapter is devoted to a semiclassical interpretation of RMT effects. We first show the connection between the unitarity of the semiclassical time evolution and the form of the two-point autocorrelation function of spectral densities predicted by RMT. Afterwards we give an interpretation of the integration over a curved manifold in field theory in terms of multiply surrounded periodic orbits in semiclassics for the two-point correlation function of spectral determinants.

Most of the results presented in this work have been published in Refs. [25, 28–37], and the presentation follows these articles to a large extent.

References

- 1. Mehta, M.L.: Random matrices. Elsevier, Amsterdam (2004)
- 2. Efetov, K.B.: Adv. Phys. 32, 53 (1983)
- 3. Kramer, B., MacKinnon, A.: Rep. Prog Phys. 56, 1469 (1993)
- 4. Bohigas, O., Giannoni, M.J., Schmit, C.: Phys. Rev. Lett. **52**, 1 (1984)
- Stöckmann, H.-J.: Quantum chaos-an introduction. Cambridge University Press, Cambridge (1999)
- 6. Milner, V., Hanssen, J.L., Campbell, W.C., Raizen, M.G.: Phys. Rev. Lett. 86, 1514 (2001)
- 7. Balazs, N.L., Voros, A.: Phys. Rep. 143, 109 (1986)
- 8. Kouwenhoven, L., Marcus, C.: Physics World 11, 35 (1998)
- 9. Kottos, T., Smilansky, U.: Phys. Rev. Lett. 79, 4794 (1997)
- 10. Kottos, T., Smilansky, U.: Ann. Phys 274, 76 (1999)
- 11. Hul, O., Tymoshchuk, O., Bauch, S., Koch, P.M., Sirko, L.: J. Phys. A 138, 10489 (2005)
- 12. Stöckmann, H.-J., Stein, J.: Phys. Rev. Lett. 64, 2215 (1990)
- 13. Berry, M.V., Tabor, M.: Proc. R. Soc. Lond. A 356, 375 (1977)
- 14. Berry, M.V., Robnik, M.: J. Phys. A 17, 2413 (1984)
- 15. Brody, T.A.: Lett. Nuo. Cim. 7, 482 (1973)
- 16. Bäcker, A., Ketzmerick, R., Löck, S., Mertig, N.: Phys. Rev. Lett. 106, 024101 (2011)
- 17. Melsen, J.A., Brouwer, P.W., Frahm, K.M., Beenakker, C.W.J.: Europhys. Lett. 35, 7 (1996)
- 18. Chang, A.M., Baranger, H.U., Pfeiffer, L.N., West, K.W.: Phys. Rev. Lett. 73, 2111 (1994)
- Melsen, J.A., Brouwer, P.W., Frahm, K.M., Beenakker, C.W.J.: Physica Scripta T 69, 223 (1997)
- 20. Artuso, R., Aurell, E., Cvitanović, P.: Nonlinearity 3, 325 (1990)
- 21. Berry, M.V., Keating, J.P.: SIAM Rev. 41, 236 (1999)
- 22. Endres, S., Steiner, F.: J. Phys. A 43, 095204 (2010)
- 23. Sierra, G., Townsend, P.K.: Phys. Rev. Lett. 101, 110201 (2008)
- Richter, K.: Semiclassical Theory of Mesoscopic Quantum Systems, Springer Tracts in Modern Physics, Vol. 161. Berlin, Heidelberg (2000)
- 25. Waltner, D., Gutiérrez, M., Goussev, A., Richter, K.: Phys. Rev. Lett. 101, 174101 (2008)
- 26. Goussev, A., Richter, K.: Phys. Rev. E 75, 015201(R) (2007)
- 27. Adagideli, İ. Phys. Rev. B 68, 233308 (2003)
- Waltner, D., Richter, K.: Classical correlations and quantum interference in ballistic conductors. In: Radons, G., Schuster, H.G., Rumpf, B. (eds.) Nonlinear Dynamics of Nanosystems. Wiley-VCH, Berlin (2010)
- 29. Gutiérrez, M., Waltner, D., Kuipers, J., Richter, K.: Phys. Rev. E 79, 046212 (2009)
- 30. Kuipers, J., Waltner, D., Gutiérrez, M., Richter, K.: Nonlinearity 22, 1945 (2009)
- 31. Gutkin, B., Waltner, D., Gutiérrez, M., Kuipers, J., Richter, K.: Phys. Rev. E 81, 036222 (2010)
- Kuipers, J., Waltner, D., Petitjean, C., Berkolaiko, G., Richter, K.: Phys. Rev. Lett. 104, 027001 (2011)

References 11

- 33. Waltner, D., Kuipers, J.: Phys. Rev. E 82, 066205 (2010)
- 34. Waltner, D., Kuipers, J., Richter, K.: Phys. Rev. B 83, 195315 (2011)
- 35. Waltner, D., Heusler, S., Urbina, J.-D., Richter, K.: J. Phys. A 42, 292001(F) (2009)
- 36. Petitjean, C., Waltner, D., Kuipers, J., Adagideli, İ., Richter, K.: Phys. Rev. B 80, 115310 (2009)
- Kuipers, J., Engl, T., Berkolaiko, G., Petitjean, C., Waltner, D., Richter, K.: Phys. Rev. B 83, 195316 (2011)

Chapter 2 Semiclassical Techniques

We start this chapter with describing the main features of classical and quantum systems. We focus in contrast to the previous chapter here on expressing them in terms of formulas. Afterwards we introduce basic semiclassical techniques yielding approximations for the time evolution operator, the Green function, the density of states and the conductance. In the next two sections we explain how to calculate semiclassically the contributions from correlated orbit pairs using the configuration-[1, 2] and the phase-space approach [3–6] in the case of the conductance and the spectral form factor.

2.1 Basic Features of Classical and Quantum Systems

Classical mechanics completely describes the state of a particle at time t by its position and its momentum. These are solutions of Newton's equations of motion at time t for given initial conditions. The motion of a particle in classical mechanics is thus deterministic. This however does not imply that the motion of a particle is easy to predict, for example in the case of a strong dependence of the motion on the initial conditions. This strong dependence is one main characteristic of classically chaotic systems. In order to quantify this dependence one studies how the motion changes under the influence of a perturbation of the initial conditions. We therefore consider one orbit in a system with initial conditions (\mathbf{r} , \mathbf{p}) with position \mathbf{r} and with momentum \mathbf{p} and one with slightly perturbed initial conditions ($\mathbf{r} + \epsilon \delta \mathbf{r}$, $\mathbf{p} + \epsilon \delta \mathbf{p}$) with $\epsilon \ll 1$. We calculate now the difference between the two phase-space coordinates at time t and expand it in a Taylor series in ϵ

$$(\mathbf{r} + \epsilon \delta \mathbf{r}, \mathbf{p} + \epsilon \delta \mathbf{p})(t) - (\mathbf{r}, \mathbf{p})(t) = \epsilon D \phi^{t}(\mathbf{r}, \mathbf{p})(\delta \mathbf{r}, \delta \mathbf{p}) + \mathcal{O}(\epsilon^{2})$$
(2.1)

In this work we only consider Hamiltonian systems, that are not explicitly time dependent. In particular this excludes dissipation.

with the differential of the Hamiltonian flow $D\phi^t(\mathbf{r}, \mathbf{p})$ defined as

$$D\phi^{t}(\mathbf{r}, \mathbf{p}) = \begin{pmatrix} \frac{\partial \mathbf{r}(t)}{\partial \mathbf{r}} & \frac{\partial \mathbf{r}(t)}{\partial \mathbf{p}} \\ \frac{\partial \mathbf{p}(t)}{\partial \mathbf{r}} & \frac{\partial \mathbf{p}(t)}{\partial \mathbf{p}} \end{pmatrix}$$
(2.2)

with $(\mathbf{r}, \mathbf{p})(t) \equiv (\mathbf{r}(t), \mathbf{p}(t))$ and $(\mathbf{r} + \epsilon \delta \mathbf{r}, \mathbf{p} + \epsilon \delta \mathbf{p})(t)$ defined analogously. The differential in Eq. (2.2) containing the derivatives of the momenta and positions at time t with respect to the initial momenta and positions thus determines the stability of an orbit. Of special interest in chaotic systems are orbits deviating from each other or approaching each other exponentially with t. In order to quantify this exponential separation one usually considers the 2d positive eigenvalues of the symmetric matrix $D\phi^t(\mathbf{r}, \mathbf{p})^T D\phi^t(\mathbf{r}, \mathbf{p})$ denoted by $\mu_i^2(\mathbf{r}, \mathbf{p}, t)$ in a d-dimensional system. The exponent T denotes here the transposed of a matrix. A measure for the exponential separation is then obtained by defining the Lyapunov exponent

$$\lambda_i(\mathbf{r}, \mathbf{p}) \equiv \lim_{t \to \infty} \left(\frac{1}{t} \ln \mu_i(\mathbf{r}, \mathbf{p}, t) \right).$$
 (2.3)

The above quantity has the following properties: If $\lambda_i > 0$, the initial perturbation $(\delta \mathbf{r}, \delta \mathbf{p})$ increases exponentially like $e^{\lambda_i t}$, for $\lambda_i < 0$ it decreases exponentially and for $\lambda_i = 0$ there is a non-exponential change of the perturbation with time. The Lyapunov exponents always come in pairs. For each $\lambda_i > 0$ there exists an exponent $-\lambda_i < 0$. Two exponents vanish in every system, the one in the direction of the flow and the one perpendicular to the surface of constant energy. Definition (2.3) leads us to a first property of chaotic systems: Hyperbolicity, meaning that (2d-2) Lyapunov exponents λ_i (\mathbf{r} , \mathbf{p}) are different from zero for almost all (\mathbf{r} , \mathbf{p}).

We define here the monodromy matrix \mathbb{M} that will appear later in this work: It is a $(2d-2)\times(2d-2)$ -matrix in the case of a d-dimensional system and is obtained from the differential of the flow $D\phi^t(\mathbf{r},\mathbf{p})$ by restricting it to the directions where the Lyapunov exponents do not vanish thus reducing the dimension by two.

A further property of chaotic system is ergodicity: This means that almost all orbits with duration $t \to \infty$ are equidistributed in the part of the energy surface at energy E filled by the system. This implies for almost all initial conditions in closed systems, that time averages are equal to phase-space averages, in terms of formulas,

$$\lim_{t \to \infty} \frac{1}{t} \int_{0}^{t} dt' f\left(\mathbf{r}(t'), \mathbf{p}(t')\right) = \frac{\int d\mathbf{r} \int d\mathbf{p} f\left(\mathbf{r}, \mathbf{p}\right) \delta\left(E - H\left(\mathbf{r}, \mathbf{p}\right)\right)}{\Omega(E)}$$
(2.4)

for a smooth function $f(\mathbf{r}, \mathbf{p})$ of position and momentum and the Hamilton function $H(\mathbf{r}, \mathbf{p})$ of the considered system. The phase-space integrals here are performed with respect to the phase-space parts filled by the system. We defined in this context the volume of the energy shell of the system

$$\Omega(E) \equiv \int d\mathbf{r} \int d\mathbf{p} \, \delta \left(E - H(\mathbf{r}, \mathbf{p}) \right). \tag{2.5}$$

These two conditions are the main characteristics of chaotic systems that we will use in this book. There are however also stronger conditions as mixing, that implies ergodicity: This means that correlations between the starting point of a trajectory and the phase-space point one obtains for the trajectory at time t can be neglected for $t \to \infty$ implying in terms of formulas

$$\lim_{t \to \infty} \frac{1}{\Omega(E)} \int d\mathbf{r} \int d\mathbf{p} h (\mathbf{r}(t), \mathbf{p}(t)) f (\mathbf{r}, \mathbf{p}) \delta (E - H (\mathbf{r}, \mathbf{p}))$$

$$= \frac{1}{\Omega(E)^{2}} \int d\mathbf{r} \int d\mathbf{p} h (\mathbf{r}, \mathbf{p}) \delta (E - H (\mathbf{r}, \mathbf{p}))$$

$$\times \int d\mathbf{r}' \int d\mathbf{p}' f (\mathbf{r}', \mathbf{p}') \delta (E - H (\mathbf{r}', \mathbf{p}')) \qquad (2.6)$$

with another smooth function $h(\mathbf{r}, \mathbf{p})$ of position and momentum.

Up to now we only considered one class of classical systems, chaotic ones. The counterpart, integrable systems, possess in d-dimensions apart from the Hamilton function d-1 conserved quantities F_i (\mathbf{r} , \mathbf{p}). This means that all F_i , F_j (i, $j \in \{1, \ldots, d\}$) are in involution, i.e. that their Poisson brackets

$$\left\{F_{i}, F_{j}\right\}(\mathbf{r}, \mathbf{p}) \equiv \frac{\partial F_{i}(\mathbf{r}, \mathbf{p})}{\partial \mathbf{r}} \frac{\partial F_{j}(\mathbf{r}, \mathbf{p})}{\partial \mathbf{p}} - \frac{\partial F_{i}(\mathbf{r}, \mathbf{p})}{\partial \mathbf{p}} \frac{\partial F_{j}(\mathbf{r}, \mathbf{p})}{\partial \mathbf{r}}$$
(2.7)

vanish. In this context we defined $F_d(\mathbf{r},\mathbf{p}) \equiv H(\mathbf{r},\mathbf{p})$. These systems show linear stability, i.e. neighbouring trajectories deviate from each other linearly with time. An ergodicity relation as in (2.4) can be also obtained for these systems, however the integration range is no longer given by the energy shell but further restricted by additional conserved quantities. The motion in phase space can be shown by studying the dynamics in terms of action-angle variables to take place on tori.

In the intermediate case of mixed dynamics the two kinds of phase-space dynamics coexist in a single system: The phase space contains regions of chaotic, i.e. ergodic, motion and regular motion, i.e. motion on tori.

In contrast to macroscopic systems, the theory to describe the dynamics of microscopic systems is quantum mechanics. In this case the state of the system at time t is described by a wavefunction obtained as solution of the Schrödinger equation for a certain initial state at time zero. The state of the underlying system cannot, in contrast to classical mechanics, be described by a point in phase space due to the Heisenberg uncertainty principle. It is not even possible to derive joint probability distributions for position and momentum, only functions that are similar to these distributions, for example Wigner or Husimi functions. Another difference between classical and quantum mechanics is that the Schrödinger equation is, in contrast to the Newton equation, always a linear differential equation leading only to a linear dependence of the state at time t on a perturbation of the initial state.

2.2 Introduction into Semiclassical Techniques

After having introduced the methods to describe classical and quantum systems we now want to explain in more detail the method used in this book for describing mesoscopic systems, that contains features of both theories: semiclassics. How does this method really work? We explain the procedure in detail for the quantum propagator. The propagator $K(\mathbf{r}, \mathbf{r}', t)$ evolves the initial quantum state $\psi_0(\mathbf{r}')$ describing a system at time t=0 into the state at time t, $\psi(\mathbf{r}, t)$, i.e.

$$\psi\left(\mathbf{r},t\right) = \int d\mathbf{r}' K\left(\mathbf{r},\mathbf{r}',t\right) \psi_{0}\left(\mathbf{r}'\right),\tag{2.8}$$

with the integration over the configuration space of the considered system. In order to find a semiclassical approximation for $K(\mathbf{r}, \mathbf{r}', t)$ we start by making a WKB-ansatz

$$K\left(\mathbf{r},\mathbf{r}',t\right) = \left(\frac{1}{2\pi\hbar}\right)^{d} \int_{\mathbb{R}^{d}} d\mathbf{p}' \sum_{\nu \in \mathbb{N}_{0}} \hbar^{\nu} a_{\nu}\left(\mathbf{r},\mathbf{p}',t\right) \exp\left[\left(i/\hbar\right)\left(R\left(\mathbf{r},\mathbf{p}',t\right) - \mathbf{r}'\mathbf{p}'\right)\right],$$
(2.9)

with the (for the moment) arbitrary scalar functions $R\left(\mathbf{r},\mathbf{p}',t\right)$ and $a_{\nu}\left(\mathbf{r},\mathbf{p}',t\right)$. The initial condition $K\left(\mathbf{r},\mathbf{r}',0\right)=\delta^{(d)}\left(\mathbf{r}-\mathbf{r}'\right)$ that guarantees that Eq. (2.8) is fulfilled for t=0 leads to $R\left(\mathbf{r},\mathbf{p}',0\right)=\mathbf{r}\mathbf{p}',\ a_{0}\left(\mathbf{r},\mathbf{p}',0\right)=1$ and $a_{\nu}\left(\mathbf{r},\mathbf{p}',0\right)=0$ for $\nu>0$. The ansatz (2.9) is then inserted into the Schrödinger equation for the propagator with the Hamilton operator \hat{H} governing the dynamics of the quantum system

$$\left(\hat{H} - i\hbar \frac{\partial}{\partial t}\right) K\left(\mathbf{r}, \mathbf{r}', t\right) = 0$$
(2.10)

with \hat{H} acting on the **r**-coordinate. In the next step the result is sorted by powers of \hbar . This yields that $R(\mathbf{r}, \mathbf{p}', t)$ solves to leading order in \hbar the classical Hamilton-Jacobi equation [7]

$$H\left(\mathbf{r}, \frac{\partial R}{\partial \mathbf{r}}\right) + \frac{\partial R}{\partial t} = 0 \tag{2.11}$$

with the classical Hamilton function $H(\mathbf{r}, \partial R/\partial \mathbf{r})$ corresponding to the Hamilton-operator \hat{H} , that is obtained by replacing the position operator $\hat{\mathbf{r}}$ by the position coordinate \mathbf{r} and the momentum operator $\hat{\mathbf{p}}$ by the momentum $\partial R/\partial \mathbf{r}$. Following Hamilton-Jacobi theory there exists a classical trajectory of duration t connecting $(\partial R/\partial \mathbf{p}', \mathbf{p}')$ and $(\mathbf{r}, \partial R/\partial \mathbf{r})$. Furthermore this implies that the Legendre transform of $R(\mathbf{r}, \mathbf{p}', t)$ from \mathbf{p}' to \mathbf{r} given by

$$S(\mathbf{r}, \mathbf{r}', t) = R(\mathbf{r}, \mathbf{p}', t) - \mathbf{r}'\mathbf{p}'$$
(2.12)

is Hamilton's principal function [8]

$$S\left(\mathbf{r}, \mathbf{r}', t\right) = \int_0^t dt' L\left(\mathbf{r}(t'), \dot{\mathbf{r}}(t'), t'\right)$$
(2.13)

with the Lagrange function $L\left(\mathbf{r}(t'), \dot{\mathbf{r}}(t'), t'\right)$ and the velocity $\dot{\mathbf{r}}(t')$ of the particle at time t'.

By considering now the equation next-to-leading order in \hbar the prefactor $a_0(\mathbf{r}, \mathbf{p}', t)$ can be determined to be given by [7]

$$a_0\left(\mathbf{r}, \mathbf{p}', t\right) = \sqrt{\det\left(\frac{\partial R\left(\mathbf{r}, \mathbf{p}', t\right)}{\partial \mathbf{r} \partial \mathbf{p}'}\right)}$$
(2.14)

with $R(\mathbf{r}, \mathbf{p}', t)$ again the solution of the Hamilton Jacobi equation (2.11).

From now on we will neglect the higher-order terms $a_{\nu}(\mathbf{r}, \mathbf{p}', t)$ with $\nu > 0$ and insert the expressions for $a_0(\mathbf{r}, \mathbf{p}', t)$ and $R(\mathbf{r}, \mathbf{p}', t)$ into the ansatz (2.9).

Next we perform the \mathbf{p}' -integral. Therefore we use the method of stationary phase that extracts from integrals containing rapidly oscillating phases the leading contributions in \hbar yielding [9]

$$\int_{\mathbb{R}^{d}} d\mathbf{r} \, a\left(\mathbf{r}, \mathbf{r}'\right) e^{(i/\hbar)\phi(\mathbf{r}, \mathbf{r}')} = (2\pi\hbar)^{d/2} \sum_{j} a\left(\mathbf{r}_{0,j}, \mathbf{r}'\right) e^{(i/\hbar)\phi(\mathbf{r}_{0,j}, \mathbf{r}')} \\
\times \frac{\exp\left(i\frac{\pi}{4}\operatorname{sign}\left(\frac{\partial^{2}\phi}{\partial r_{k}\partial r_{l}}\left(\mathbf{r}_{0,j}, \mathbf{r}'\right)\right)\right)}{\left|\det\frac{\partial^{2}\phi}{\partial r_{k}\partial r_{l}}\left(\mathbf{r}_{0,j}, \mathbf{r}'\right)\right|} + \mathcal{O}\left(\hbar^{d/2+1}\right) \tag{2.15}$$

with the scalar functions $a(\mathbf{r}, \mathbf{r}')$ and $\phi(\mathbf{r}, \mathbf{r}')$. The sum on the right hand side of the last equation runs over all stationary points $\mathbf{r}_{0,j}$ of the integral on the left hand side defined as $\partial \phi(\mathbf{r}, \mathbf{r}')/\partial \mathbf{r} = 0$. Here $\mathrm{sign}(A)$ denotes the difference of the number of positive and negative eigenvalues of the matrix A. The intuitive interpretation of this method is: For $\hbar \to 0$ the integrand on the left hand side of Eq. (2.15) is rapidly oscillating in dependence of \mathbf{r} everywhere except for regions close to points where $\partial \phi(\mathbf{r}, \mathbf{r}')/\partial \mathbf{r} = 0$. Thus only those points contribute in leading order in \hbar . To apply relation (2.15) these points need to be isolated and the determinant of second derivatives needs to be non-zero at the stationary points

$$\det \frac{\partial^2 \phi}{\partial r_k \partial r_l} \left(\mathbf{r}_{0,j}, \mathbf{r}' \right) \neq 0. \tag{2.16}$$

For a more detailed description of the assumptions, see for example [8, 9].

Using now the method of stationary phase we find the semiclassical expression for the quantum propagator, the so-called van Vleck-Gutzwiller propagator [10, 11]

$$K_{\rm sc}\left(\mathbf{r},\mathbf{r}',t\right) = \left(\frac{1}{\sqrt{2\pi i\hbar}}\right)^{d} \sum_{\gamma(\mathbf{r}'\to\mathbf{r},t)} A_{\gamma} e^{(i/\hbar)S_{\gamma}\left(\mathbf{r},\mathbf{r}',t\right) - i(\pi/2)\mu_{\gamma}}, \qquad (2.17)$$

given by a sum over classical orbits from \mathbf{r}' to \mathbf{r} of duration t. Each summand contains the prefactor $A_{\gamma} = \sqrt{\left|\det\left(-\frac{\partial^2 S_{\gamma}(\mathbf{r},\mathbf{r}',t)}{\partial \mathbf{r}\partial \mathbf{r}'}\right)\right|} = \sqrt{\left|\det\left(\frac{\partial \mathbf{p}_0^{\gamma}}{\partial \mathbf{r}}\right)\right|}$ obtained first by Morette and van Hove [12] with the initial momentum \mathbf{p}_0^{γ} and a phase with the aforementioned principal function. The phase factor $e^{-i\pi\mu_{\gamma}/2}$ results from the \hbar -independent phase in Eq. (2.15) and the sign of $a_0\left(\mathbf{r},\mathbf{p}',t\right)$ in Eq. (2.14). This so-called Maslov phase can be expressed by the number of conjugated points along the orbit, so-called caustics, i.e. by the number of times the prefactor A_{γ} gets singular along the orbit plus twice the number of hard wall boundary reflections [11]. The number of vanishing eigenvalues of the inverse matrix $\frac{\partial \mathbf{r}}{\partial \mathbf{p}_0^{\gamma}}$ determines the order of a caustic. If the number is equal to the dimension of configuration space, we have a focal point: Changing \mathbf{p}_0^{γ} leaves all components of \mathbf{r} unchanged.

The expression (2.17) contains as classical element the sum over classical orbits and as quantum mechanical one phases with the principal functions of the underlying trajectories in the exponentials, that can cause interference effects.

Starting from the semiclassical formula for the propagator, semiclassical expressions can be also obtained for other quantities that we will need here like Green functions, or the density of states of a system. In that cases, relation (2.17) is again the building block: One uses in the derivation of semiclassical expressions for these quantities the exact relation between the propagator and the Green function (a Fourier transformation) and the exact relation between the Green function and the density of states (a trace integral) plus the semiclassical form of the propagator to obtain an approximate formula for these quantities. This yields for the (retarded) Green function $G(\mathbf{r}, \mathbf{r}', E)$ at energy E given in terms of the propagator by

$$G\left(\mathbf{r},\mathbf{r}',E\right) = \frac{1}{i\hbar} \lim_{\epsilon \to 0} \int_{0}^{\infty} dt K\left(\mathbf{r},\mathbf{r}',t\right) e^{(i/\hbar)(E+i\epsilon)t}$$
(2.18)

the semiclassical expression [11] by performing the t-integral by stationary phase

$$G_{\rm sc}\left(\mathbf{r},\mathbf{r}',E\right) = \frac{1}{i\hbar} \left(\frac{1}{\sqrt{2\pi i\hbar}}\right)^{d-1} \sum_{\gamma(\mathbf{r}'\to\mathbf{r},E)} B_{\gamma} e^{(i/\hbar)S_{\gamma}\left(\mathbf{r},\mathbf{r}',E\right) - i(\pi/2)\nu_{\gamma}}$$
(2.19)

with the orbits γ connecting \mathbf{r}' and \mathbf{r} at energy E, the prefactors B_{γ} calculated in [11] are given by $B_{\gamma} = \left(1/\left(|\dot{\mathbf{r}}'|\,|\dot{\mathbf{r}}'|\right)\,|\det\left(\partial^2S_{\gamma}/\partial\mathbf{r}_{\perp}\partial\mathbf{r}'_{\perp}\right)|\right)^{1/2}$ and the classical actions of γ , $S_{\gamma}\left(\mathbf{r},\mathbf{r}',E\right) = \int_{\mathbf{r}'}^{\mathbf{r}}d\mathbf{y}\,\mathbf{p}\left(\mathbf{y},E\right)$, in the exponentials. Here $\dot{\mathbf{r}}$ and $\dot{\mathbf{r}}'$ are the final and initial velocities and \mathbf{r}_{\perp} and \mathbf{r}'_{\perp} denote the (d-1) final and initial spatial coordinates perpendicular to the trajectory, respectively. The Maslov phases ν_{γ} are determined by the ones of the propagator and the phases resulting from performing the t-integral in (2.18) within stationary phase [8].

The spectral density is defined in terms of the spectrum $\{E_n\}$ as

$$d(E) = \sum_{n=1}^{\infty} \delta(E - E_n).$$
 (2.20)

It is proportional to the imaginary part of trace of $G(\mathbf{r}, \mathbf{r}', E)$

$$d(E) = -\frac{1}{\pi} \Im \operatorname{Tr} [G(E)] = -\frac{1}{\pi} \Im \int d\mathbf{r} G(\mathbf{r}, \mathbf{r}, E)$$
 (2.21)

with \Im denoting the imaginary part, the real part will be denoted by \Re . The famous Gutzwiller trace formula [11] for chaotic systems is obtained by performing the **r**-integral within stationary phase yielding

$$\Im \operatorname{Tr} G_{\operatorname{sc}}(E) = -\frac{\pi \Omega(E)}{(2\pi \hbar)^d} + \Im \underbrace{\frac{-i}{\hbar} \sum_{\gamma} T_{\gamma}^{\operatorname{prim}} C_{\gamma} e^{(i/\hbar) S_{\gamma}(E) - i(\pi/2) \tau_{\gamma}}}_{\operatorname{Tr} G_{\operatorname{sc}}^{+\operatorname{osc}}(E)}$$
(2.22)

with the oscillatory part of the trace of the Green function $\text{Tr}G_{\text{sc}}^{+\text{osc}}(E)$ defined for later reference. The spectral density can thus be expressed semiclassically as

$$d_{\rm sc}(E) = \frac{\Omega(E)}{(2\pi\hbar)^d} + \frac{1}{\pi\hbar} \Re \sum_{\gamma} T_{\gamma}^{\rm prim} C_{\gamma} e^{(i/\hbar)S_{\gamma}(E) - i(\pi/2)\tau_{\gamma}}. \tag{2.23}$$

The first summand, the so-called Weyl term, follows after performing the **r**-integral by stationary phase from very short trajectories contained in (2.19). It can be interpreted as the number of Planck cells of the volume $(2\pi\hbar)^d$ in d dimensions fitting into the volume of the energy shell $\Omega(E)$. The second summand is rapidly oscillating as function of the energy and characterises the oscillations of the density of states around the mean part. It contains a sum over periodic orbits γ of primitive duration T_γ^{prim} with the prefactor $C_\gamma = 1/\left|\det\left(\mathbb{M}_\gamma - \mathbb{1}_{2d-2}\right)\right|^{1/2}$ containing the monodromy matrix \mathbb{M}_γ defined before Eq. (2.4) and the actions $S_\gamma(E) = \oint d\mathbf{y} \, \mathbf{p}(\mathbf{y}, E)$. The Maslov phases τ_γ contain the phases μ_γ from the Green function and the additional phases from the additional stationary phase.

Note that the stationary phase approximation in Eq. (2.22) can only be performed for isolated stationary points, i.e. isolated orbits. For integrable systems they form families covering the tori, here a different formula developed by Berry, Tabor and Balian, Bloch applies, see [13–17].

Whereas the semiclassical expression for the spectral density is of interest itself, the semiclassical Green function will be mainly used here to derive a semiclassical form of the transmission coefficients; i.e. the elements of the scattering matrix S(E) at energy E. Considering a two lead geometry this matrix contains the reflection and transmission subblocks r(E), t(E) for the incoming wave in the lead 1 and r'(E), t'(E) for the incoming wave in the lead 2, respectively

$$S(E) = \begin{pmatrix} r(E) \ t'(E) \\ t(E) \ r'(E) \end{pmatrix}. \tag{2.24}$$

The dimension of the matrices is determined by the condition that the longitudinal wavefunction possesses positive energy, i.e. by the largest number N_i fulfilling

 $E - \hbar^2/(2m)(N_i\pi/W_i)^2 > 0$ with the total energy E and the energy of the transverse wavefunction $\hbar^2/(2m)(N_i\pi/W_i)^2$ containing the width of the ith lead, W_i . The dimension of S(E) is then given by $N \equiv N_1 + N_2$. Using the Landauer-Büttiker formalism [18–20] an expression for the conductance G can be obtained in terms of the subblock t

$$G = 2\frac{e^2}{h} \text{Tr} \left(t t^{\dagger} \right) \tag{2.25}$$

with the factor 2 accounting for spin degeneracy in the absence of spin-orbit interaction. These scattering-matrix elements $t_{\alpha,\beta}(E)$, that we will in the following consider as a function of the absolute value of the wave vector $k = \sqrt{2mE}/\hbar$ with the particle mass m, are related to the Green function by the Fisher Lee relations [21]

$$t_{\alpha,\beta}(k) = -i\hbar\sqrt{v_{\alpha}v_{\beta}} \int_{0}^{W_{1}} dy \int_{0}^{W_{2}} dy' \Phi_{\alpha}^{*}(y) G(y, y', E) \Phi_{\beta}(y'), \qquad (2.26)$$

i.e. the scattering-matrix elements are given by the projections of the Green function onto the transverse eigenfunctions in the leads of width W_1 and W_2 . The star denotes here complex conjugation. These eigenfunctions are, for hard wall boundary conditions, given by $\Phi_{\alpha}(y) = \sqrt{2/W_1} \sin{(\alpha \pi y/W_1)}$ and $\Phi_{\beta}(y') = \sqrt{2/W_2} \sin{(\beta \pi y'/W_2)}$. The longitudinal velocities in the left and right lead are denoted v_{β} and v_{α} , respectively. For the matrix elements of the reflection subblock a relation similar to Eq. (2.26) can be obtained [21]

$$r_{\alpha,\beta}(k) = \delta_{\alpha,\beta} - i\hbar\sqrt{v_{\alpha}v_{\beta}} \int_{0}^{W_{1}} dy \int_{0}^{W_{1}} dy' \Phi_{\alpha}^{*}(y) G(y, y', E) \Phi_{\beta}(y') \quad (2.27)$$

with y, y' now both lying in the same lead.

To obtain a semiclassical form of Eq. (2.26) [22, 23], the semiclassical expression of the Green function (2.19) is used and the integrals with respect to y and y' are performed within stationary phase yielding the condition

$$\frac{\partial S_{\gamma}}{\partial y'} = -p_{y'} = -\frac{\overline{\beta}\pi\hbar}{W_2} \tag{2.28}$$

with $\overline{\beta} \equiv \pm \beta$. An analogous condition is obtained for the momenta p_y . Thus only those paths which enter into the cavity at (x', y') with a fixed angle $\sin \theta' = \pm \beta \pi / (kW_2)$ and exit the cavity at (x, y) with angle $\sin \theta = \pm \alpha \pi / (kW_1)$ contribute to $t_{\alpha,\beta}(k)$. There is an intuitive explanation for this condition: The trajectories are those whose transverse wave vectors on entrance and exit match the wave vectors of the modes in the leads. One then obtains for the semiclassical expression for the transmission amplitudes $t_{\alpha,\beta}(k)$

$$t_{\alpha,\beta}^{\rm sc}(k) = -\frac{\sqrt{\pi i \hbar}}{\sqrt{2W_1 W_2}} \sum_{\gamma(\overline{\alpha},\overline{\beta})} \operatorname{sign}(\overline{\alpha}) \operatorname{sign}(\overline{\beta}) D_{\gamma} \exp\left(\frac{i}{\hbar} \widetilde{S}_{\gamma} \left(\overline{\alpha},\overline{\beta},E\right) - i \frac{\pi}{2} \eta_{\gamma}\right)$$
(2.29)

with the reduced actions

$$\widetilde{S}_{\gamma}\left(\overline{\alpha}, \overline{\beta}, E\right) \equiv S_{\gamma}(\mathbf{r}, \mathbf{r}', E) + \hbar k y' \sin \theta' - \hbar k y \sin \theta. \tag{2.30}$$

Furthermore one obtains $D_{\gamma} = \sqrt{|(\partial y/\partial \theta')|/(\hbar k |\cos \theta'|)}$; the index η_{γ} contains the Maslov index appearing in the Green function and additional phases due to the two stationary phase integrals. For the reflection (2.27) an analogous expression in terms of trajectories returning to the same lead holds. The $\delta_{\alpha,\beta}$ in Eq. (2.27) is cancelled by direct trajectories not entering the cavity.

The three Eqs. (2.17, 2.23, 2.29) are the basic semiclassical formulas we will use in this book.

In the next two sections we want to present the main advances in showing how the RMT results can be derived with semiclassical methods: First we analyse the transmission through a chaotic system based on the Landauer-Büttiker formalism and afterwards we consider the spectral form factor.

2.3 Quantum Corrections to the Transmission

In this section we want to study the expression obtained by inserting the semiclassical approximation (2.29) into the Landauer-Büttiker formula (2.25). Here we obtain with $G \equiv 2\frac{e^2}{h}T$

$$T^{\text{sc}} = \sum_{\alpha=1}^{N_1} \sum_{\beta=1}^{N_2} \left| t_{\alpha,\beta}^{\text{sc}}(k) \right|^2 = \frac{\pi \hbar}{2W_1 W_2} \sum_{\alpha=1}^{N_1} \sum_{\beta=1}^{N_2} \sum_{\gamma,\gamma'} F_{\alpha,\beta}^{\gamma,\gamma'}$$
(2.31)

with

$$F_{\alpha,\beta}^{\gamma,\gamma'} \equiv D_{\gamma} D_{\gamma'} \exp\left[\frac{i}{\hbar} \left(S_{\gamma} - S_{\gamma'} - i\frac{\pi}{2}\mu_{\gamma,\gamma'}\right)\right]$$
 (2.32)

with $\mu_{\gamma,\gamma'}$ containing the indices η_{γ} and $\eta_{\gamma'}$, the sign-factors in Eq. (2.29) and the phases due to the two last summands in Eq. (2.30). For $\hbar \to 0$ the function in (2.32) is rapidly oscillating in dependence of the energy due to the factor $\mathrm{e}^{(i/\hbar)\left(S_{\gamma}-S_{\gamma'}\right)}$. In the following we wish to identify those contributions to Eq. (2.31) which survive an average over a classically small but quantum mechanically large k-window Δk . Important contributions to (2.31) will result from very similar trajectories γ and γ' . Afterwards we wish to evaluate their contributions to $\left|t_{\alpha,\beta}(k)\right|^2$ using basic principles of chaotic dynamics: For our calculation we will need hyperbolicity and ergodicity.

This section is divided into three subsections: After showing how to obtain the diagonal contribution in the first subsection we describe the calculation of the simplest non-diagonal contribution in the second part and study its behaviour as a function of a magnetic field. In the third subsection we introduce an approach to calculate further quantum corrections.

2.3.1 Diagonal Contribution

The simplest approximation is $\gamma = \gamma'$, the so-called diagonal approximation, yielding

$$\left|t_{\alpha,\beta}(k)\right|_{\text{diag}}^{2} = \frac{\pi\hbar}{2W_{1}W_{2}} \sum_{\gamma} \left|D_{\gamma}\right|^{2}.$$
 (2.33)

The remaining sum over classical trajectories in Eq. (2.33) can be calculated using a classical sum rule [24] that can be derived using in the ergodicity relation (2.4) a proper function $f(\mathbf{r}, \mathbf{p})$, see for a derivation of a similar rule [25] and for a detailed derivation of this sum rule [26]. It yields

$$\sum_{\gamma} |D_{\gamma}|^2 \approx \frac{4W_1 W_2}{\Omega(E)} \int_0^{\infty} dT \rho(T), \qquad (2.34)$$

where $\Omega(E)$ again denotes the phase-space volume of the system at energy E, and $\rho(T)$ is the classical probability to find a particle still inside an open system after a time T if it was inside at T=0. For long times this function decays exponentially $\rho(T)\sim e^{-T/\tau_D}$ for $T\to\infty$ for a chaotic system, with the dwell time $\tau_D=\frac{\Omega(E)}{2\pi\hbar(N_1+N_2)}$. This exponential decay can be easily understood based on the equidistribution of trajectories: The number ΔN of particles leaving the system during ΔT is given by the overall number of particles N times the ratio of the phase-space volume from which the particles leave during ΔT and the whole phase-space volume of the system. The differential equation for N, obtained in the case of infinitesimal ΔT , has obviously an exponential solution.

By inserting Eq. (2.34) into Eq. (2.33), we obtain

$$\left| t_{\alpha,\beta}(k) \right|_{\text{diag}}^2 = \frac{1}{N_1 + N_2}.$$
 (2.35)

Its derivation required ergodicity valid only for long trajectories. We will assume that the classical dwell time is large enough, i.e. the opening is small enough, in order to have a statistically relevant number of long trajectories left after time T. The result in Eq. (2.35) allows for a very simple interpretation: It is just the probability of reaching one of the $N_1 + N_2$ channels if each of the channels can be reached equally likely.

Next we want to evaluate off-diagonal (interference) contributions to the quantum transmission. We will present here two approaches: The first one, the configuration-space approach, that was also chronologically the first one to calculate off-diagonal contributions is very illustrative as it measures the difference between the orbit and its partner in terms of the crossing angle of the crossing orbit and not in terms of the phase-space difference as the second one, the phase-space approach [3–6]. The latter one is however more general as the configuration-space approach relies on assumptions valid only for two-dimensional systems. Originally developed for surfaces of constant negative curvature [1, 2], it could later be generalised to general hyperbolic chaotic systems with two degrees of freedom [27].

2.3.2 First Quantum Correction: Configuration-Space Approach

In the following we will describe the calculation of the contributions from pairs of different trajectories, however with similar actions.

We want to remark that this calculation was motivated by the existence of RMT results for $|t_{\alpha,\beta}(k)|^2$ [28]

$$\left| t_{\alpha,\beta}(k) \right|_{\text{RMT}}^2 = \frac{1}{N_1 + N_2}$$
 (2.36)

for the circular unitary ensemble, i.e. for systems without time-reversal symmetry, and

$$|t_{\alpha,\beta}(k)|_{\text{RMT}}^2 = \frac{1}{N_1 + N_2 + 1} = \frac{1}{N_1 + N_2} \sum_{k=0}^{\infty} \left(\frac{-1}{N_1 + N_2}\right)^k$$
 (2.37)

for the circular orthogonal ensemble, i.e. for systems with time-reversal symmetry. The result (2.36) shows that in the absence of time-reversal symmetry semiclassically there are no additional contributions expected when semiclassical and RMT results coincide apart from the one obtained in diagonal approximation above. In the presence of time-reversal symmetry there exist apart from the diagonal contribution—the k=0-term in (2.37)—further contributions that need to be explained semiclassically, if semiclassics reproduces RMT results.

For a long time it was not clear how orbits could look like that are on the one hand correlated but on the other hand different. There are many orbit pairs in a chaotic system having accidentally nearly equal actions. Their number is usually exponentially increasing as a function of their duration T_{ν} , as can be seen by applying the sum rule (2.34) directly in Eq. (2.29) and taking into account that usually $D_{\nu} \propto$ $e^{-\lambda T_{\gamma}/2}$ for large T_{γ} . These contributions are however assumed to appear randomly and to be cancelled by the energy average. In order to describe universal features of a chaotic system after energy averaging, one has to find orbits that are correlated in a systematic way. These orbits were first identified and analysed in 2000 in the context of spectral statistics [1]. There, *periodic* orbits were studied to compute correlations between energy eigenvalues of quantum systems with classically chaotic counterpart, we will come to this point in the next section. Based on open, lead-connecting trajectories, in Ref. [24] this approach was generalised to the conductance we study here. Still, the underlying mechanism to form pairs of classically correlated orbits is the same in the two cases. In Fig. 2.1 we show a representative example of such a correlated (periodic) orbit pair in the chaotic hyperbola billiard. The two partner orbits are topologically the same up to the region marked by the circle where one orbit exhibits a self-crossing (left panel) while the partner orbit an "avoided crossing" (right panel). Usually, such trajectory pairs are drawn schematically as shown in Fig. 2.2.

We here consider very long orbits with self-crossings characterised by crossing angles $\epsilon \ll \pi$. In Refs. [1, 2] it was shown that there exists for each orbit a partner orbit starting and ending (exponentially) close to the first one. It follows the first

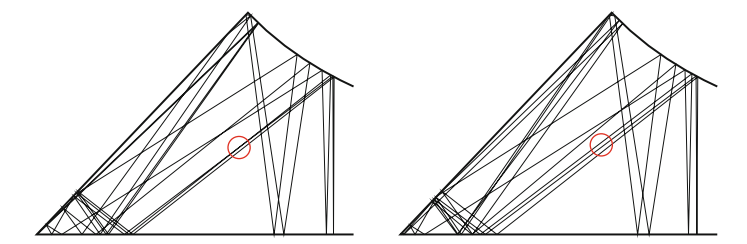
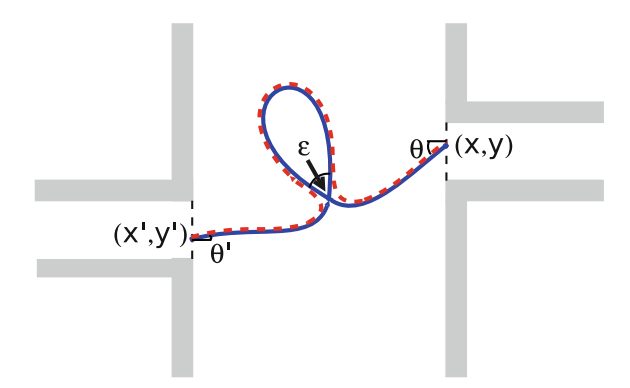


Fig. 2.1 Pair of two periodic orbits in the hyperbola billiard differing from each other essentially in the region marked by the *circle*, where the *left* orbit exhibits a self-crossing while the *right* partner orbit shows an "avoided crossing" (taken from [29])

Fig. 2.2 Schematic drawing of a pair of orbits yielding the first non-diagonal contribution to the transmission considered in Ref. [24]. One of the orbits crosses itself under an angle ϵ , the other one possesses an "avoided crossing". Except for the crossing region both orbits are almost identical



orbit until the crossing, avoids this, however, traverses the loop in reversed direction and avoids the crossing again.

In order to quantify the contribution of these trajectory pairs to Eq. (2.31) we need two inputs: an expression for the action difference and for the density quantifying how often an orbit of time T exhibits a self-intersection, both quantities expressed as a function of the parameter ϵ . The formula for the action difference ΔS can be derived by linearising the dynamics of the orbit without crossing around the reference orbit with crossing giving, in the limit $\epsilon \ll \pi$, [1, 2]

$$\Delta S \approx \frac{p^2 \epsilon^2}{2m\lambda} \tag{2.38}$$

with p the absolute value of the momentum. At this point we can justify our assumption of small crossing angles ϵ : In the limit $\hbar \to 0$, we expect important contributions to Eq. (2.31) only from orbit pairs with small action differences, larger action differences will yield rapidly oscillating contributions as a function of the energy. This implies that the crossing angles have to be small, as we see from Eq. (2.38).

Before deriving the number of self-crossings, $P(\epsilon, T) d\epsilon$, in the range between ϵ and $\epsilon + d\epsilon$ for an orbit of time T, we give rough arguments how this expression depends on ϵ and T for trajectories in billiards. There, each orbit is composed of a chain of N chords connecting the reflection points. Following an orbit, the first two

chords cannot intersect, the third chord can cross with up to one, the fourth chord with up to two segments, and so on. Hence, the overall number of self-crossings will be proportional to $\sum_{n=3}^{N} (n-2) \propto N^2$, to leading order in N, i.e. proportional to T^2 .

The crossing-angle dependence of $P(\epsilon, T)$ can be estimated for small ϵ as follows: Given a trajectory chord of length L, a second chord, tilted by an angle ϵ with respect to the first one, will cross it inside the billiard (with area of order L^2) only if the distance between the reflection points of the two chords at the boundary is smaller than $L \sin \epsilon$. The triangle formed in the latter case includes a fraction $\sin \epsilon$ of the entire billiard size. From this rough estimation we expect $P(\epsilon, T) \propto T^2 \sin \epsilon$.

More rigorously, the quantity $P(\epsilon, T) d\epsilon$, can be expressed for an arbitrary orbit γ as [1, 2]

$$P(\epsilon, T) d\epsilon = \left\langle \int_{T_{\min}(\epsilon)}^{T - T_{\min}(\epsilon)} dt_l \int_{T_{\min}(\epsilon)/2}^{T - t_l - T_{\min}(\epsilon)/2} dt_s |J| \delta\left(\mathbf{r}\left(t_s\right) - \mathbf{r}\left(t_s + t_l\right)\right) \right\rangle$$

$$\times \delta\left(\epsilon - \alpha\left(t_s, t_s + t_l\right)\right) d\epsilon$$
(2.39)

with the average $\langle ... \rangle$ taken over different initial conditions $(\mathbf{x}_0, \mathbf{p}_0)$. The time of the closed loop of the trajectory is denoted by t_l and the time before the loop by t_s . $\alpha(t_s, t_s + t_l)$ denotes the absolute value of the angle between the velocities $\mathbf{v}(t_s)$ and $\mathbf{v}(t_s + t_l)$. |J| is the Jacobian for the transformation from the argument of the first delta function to t_l and t_s ensuring that $P(\epsilon, T) d\epsilon$ yields a 1 for each crossing of γ . With the absolute value of the velocity, v, it can be expressed as

$$|J| = |\mathbf{v}(t_s) \times \mathbf{v}(t_s + t_l)| = v^2 \sin \alpha (t_s, t_s + t_l). \tag{2.40}$$

As the derivation [1] of the formula for $P(\epsilon, T)$ for a chaotic system, starting from the formal expression (2.39), is instructive to see how information can be extracted from the basic principles of chaotic dynamics beyond the diagonal approximation, we will present it here in detail. Hyperbolicity will yield a justification for the minimal time $T_{\min}(\epsilon)$ already introduced in Eq. (2.39); we will come back to that point later and first study the effect of ergodicity. To proceed we interchange the phase-space integral of the average with the time integrals, substitute $(\mathbf{r}(t_s), \mathbf{p}(t_s)) \longmapsto (\mathbf{r}_0, \mathbf{p}_0)$ in Eq. (2.39) and obtain

$$P(\epsilon, T) = 2m \int_{T_{\min}(\epsilon)}^{T - T_{\min}(\epsilon)} dt_l v^2 \sin \epsilon p_E(\epsilon, t_l) (T - t_l - T_{\min}(\epsilon)), \qquad (2.41)$$

with the averaged classical return probability density

$$p_{E}(\epsilon, t_{l}) = \frac{1}{2m} \langle \delta(\mathbf{r}_{0} - \mathbf{r}(t_{l})) \delta(\epsilon - | \measuredangle(\mathbf{v}_{0}, \mathbf{v}(t_{l})) |) \rangle.$$
 (2.42)

This yields the probability density that a particle possessing the energy E returns after the time t_l to its starting point with the angle $|\angle (\mathbf{v}_0, \mathbf{v}(t_l))| = \epsilon$. For long times this can be replaced by $1/\Omega(E)$, assuming ergodicity. Then we obtain

$$P(\epsilon, T) \approx 2m \int_{T_{\min}(\epsilon)}^{T - T_{\min}(\epsilon)} dt_l v^2 \sin \epsilon \frac{1}{\Omega(E)} (T - t_l - T_{\min}(\epsilon))$$

$$= \frac{mv^2}{\Omega(E)} \sin \epsilon (T - 2T_{\min}(\epsilon))^2. \tag{2.43}$$

Now we return to our assumption of hyperbolicity and explain the cutoff time $T_{\min}(\epsilon)$, introduced in the equations above. To this end, we consider two classical paths leaving their crossing with a small angle ϵ . The initial deviation of their velocities is $\delta v_i \approx \epsilon v$. In order to form a closed loop, the deviation of the velocities δv_f , when both paths have traversed half of the closed loop, has to be given by $\delta v_f = cv$ with c of the order unity. Then we get for the minimal time $T_{\min}(\epsilon)$ to form a closed loop, due to the maximally exponential divergence of neighboring orbits for $T_{\min}(\epsilon) \to \infty$,

$$c \sim \epsilon e^{(\lambda T_{\min}(\epsilon))/2},$$
 (2.44)

implying

$$T_{\min}(\epsilon) \sim \frac{2}{\lambda} \ln\left(\frac{c}{\epsilon}\right).$$
 (2.45)

An argument similar to the one used here for the closed loop can also be applied to the other two parts of the trajectory leaving the crossing with an angle ϵ towards the opening of the conductor. Suppose t_s in Eq. (2.39) has a length between 0 and $T_{\min}(\epsilon)/2$, then both parts have to be so close together that they must leave both through the same lead. As we are interested in the transmission, we also have to exclude in that case a length of t_s between 0 and $T_{\min}(\epsilon)/2$. A similar argument holds for the case where the last part of the orbit has a length between 0 and $T_{\min}(\epsilon)/2$, in this case the orbit has to come very close to the opening already before the crossing and leave before it could have crossed. Accounting for all these restrictions, gives the integration limits in Eq. (2.39).

We want to remark here that the restrictions of the time integrals given above only hold for the transmission T. If we would calculate the reflection $R \equiv \sum_{\alpha,\beta=1}^{N_1} |r_{\alpha,\beta}(k)|^2$ with the reflection elements of the scattering matrix $r_{\alpha,\beta}(k)$, the effect of short legs—to the corresponding contribution is referred as coherent backscattering—has to be taken into account, see for example [23, 30]. This contribution was actually the first off-diagonal contribution that could be calculated semiclassically and that is changed by a magnetic field as the orbit and its partner enclose non-zero flux, because both traverse the loop in different directions. In the articles [23, 30] this contribution was then used to explain the Lorentzian lineshap of the reflection in dependence of the magnetic field for weak magnetic fields that do

not change the shape of the trajectories significantly. Via the current conservation relation

$$T + R = N, (2.46)$$

that follows from the unitarity of the scattering matrix—for a proof of the latter relation see for example [26, 31]—the lineshape of the transmission T was then predicted semiclassically.

Now we are prepared to calculate the contribution of the considered trajectory pairs to the transmission. Therefore we keep in Eq. (2.31) one sum over trajectories that we will perform using the same classical sum rule as in diagonal approximation, the other we can replace by a sum over all the partner trajectories of one trajectory, which can be calculated using $P(\epsilon,T)$. There is, however, one subtlety concerning the survival probability $\rho(T)$ in the sum rule: We argued already, that if the crossing happens near the opening, both parts of the orbit act in a correlated way; $\rho(T)$ is changed in the case of the trajectory pairs considered here for a similar reason: Because we know that the two parts of the orbit leaving the crossing on each side are very close to each other, the orbit can either leave the cavity during the first stretch, i.e. during the first time it traverses the crossing region, or cannot leave at all. This implies that we have to change 2 the survival probability from $\rho(T)$ to $\rho(T-T_{\min}(\epsilon))$. Then we arrive at the loop (L) contribution

$$\begin{aligned} \left| t_{\alpha,\beta}(k) \right|_{L}^{2} &= \frac{\pi \hbar}{2W_{1}W_{2}} \sum_{\gamma} \sum_{P} \left| D_{\gamma} \right|^{2} 2\Re \exp \left(i \frac{p^{2} \epsilon_{P}^{2}}{2m \lambda \hbar} \right) \\ &= \frac{4\pi \hbar}{\Omega(E)} \int_{0}^{\pi} d\epsilon \int_{2T_{\min}(\epsilon)}^{\infty} dT e^{-(T - T_{\min}(\epsilon))/\tau_{D}} P(\epsilon, T) \cos \left(\frac{p^{2} \epsilon^{2}}{2m \lambda \hbar} \right) \\ &= \frac{8\pi \hbar m v^{2} \tau_{D}^{3}}{\Omega(E)^{2}} \int_{0}^{\pi} d\epsilon e^{-T_{\min}(\epsilon)/\tau_{D}} \sin \epsilon \cos \left(\frac{p^{2} \epsilon^{2}}{2m \lambda \hbar} \right) \end{aligned} \tag{2.47}$$

with the sum over the partner trajectories P in the first line. As the important contributions require very small action differences, i.e. very similar trajectories, and as the prefactor D_{γ} is not as sensitive as the actions to small changes of the trajectories, we can neglect differences between γ and γ' in the prefactor. In the second line we

² This effect together with the requirement of a finite length of the orbit parts leaving towards the opening was originally not taken into account in Ref. [24]. In that calculation, the contributions from these two effects cancel each other, they will be only important when considering more complicated diagrams as in the next subsection.

³ We assumed here that the two trajectories possess the same Maslov index: Although this was not yet shown for pairs of open orbits considered here there are several reasons why the Maslov indices can be assumed not to influence properties of chaotic systems showing behaviour predicted by RMT: For special chaotic systems like surfaces of constant negative curvature the Maslov indices do not depend on the specific orbit and thus drop out in Eq. (2.47). Furthermore the following interpretation is helpful: The Maslov index is given by the number of times the stable and unstable manifolds rotate by half a turn plus twice the number of reflections on walls with Dirichlet boundary

applied the classical sum rule with the modification explained before Eq. (2.47) and used $P(\epsilon, T)$ to evaluate the sum over P. After performing the simple time integral in the third line, we can do the ϵ -integration as for example in Ref. [34] by taking into account that the important contributions come from very small ϵ , yielding

$$\begin{aligned} \left| t_{\alpha,\beta}(k) \right|_{L}^{2} &= \frac{8\pi\hbar m v^{2} \tau_{D}^{3}}{\Omega(E)^{2}} \int_{0}^{\pi} d\epsilon (\epsilon/c)^{\frac{2}{\lambda \tau_{D}}} \sin \epsilon \cos \left(\frac{p^{2} \epsilon^{2}}{2m\lambda \hbar} \right) \\ &= \frac{8\pi\hbar m v^{2} \tau_{D}^{3}}{\Omega(E)^{2}} \int_{0}^{\infty} dz \frac{m\lambda \hbar}{p^{2}} \left(\frac{1}{c} \right)^{\left(\frac{2}{\lambda \tau_{D}} \right)} \left(\frac{2m\lambda \hbar z}{p^{2}} \right)^{\frac{1}{\lambda \tau_{D}}} \cos z \\ &= -\frac{8\pi\hbar m v^{2} \tau_{D}^{2}}{\Omega(E)^{2}} \int_{0}^{\infty} dz \frac{m\hbar}{p^{2}} \left(\frac{1}{c} \right)^{\left(\frac{2}{\lambda \tau_{D}} \right)} \left(\frac{2m\lambda \hbar z}{p^{2}} \right)^{\frac{1}{\lambda \tau_{D}}} \frac{\sin z}{z}. \end{aligned} (2.48)$$

In the first line we already rewrote $e^{-T_{\min}(\epsilon)/\tau_D}$ as $(\epsilon/c)^{\frac{2}{\lambda\tau_D}}$, and in the second line we approximated $\sin\epsilon \approx \epsilon$ and substituted $z=p^2\epsilon^2/\left(2m\lambda\hbar\right)$. Then we perform a partial integration with respect to z neglecting rapidly oscillating terms that are cancelled by the k-average, introduced after Eq. (2.32). Eventually, we perform the z-integral by pushing the upper limit to infinity, i.e. $\hbar \to 0$ and taking into account our assumption of large dwell times, i.e. $\lambda\tau_D \to \infty$. Additionally we assume $\left(2m\lambda\hbar/p^2\right)^{\frac{1}{\lambda\tau_D}} \approx 1$; we will return to the last point in Chap. 4

Finally, we arrive at the leading non-diagonal contribution to the quantum transmission [24],

$$|t_{\alpha,\beta}(k)|_{\mathcal{L}}^2 = -\frac{1}{(N_1 + N_2)^2},$$
 (2.49)

that agrees with the k = 1-term in the RMT expression given in (2.37).

2.3.2.1 Magnetic Field Dependence of the Non-diagonal Contribution

Up to now we assumed time-reversal symmetry. If this symmetry is destroyed, for example by applying a strong magnetic field, the latter contribution will vanish, because the closed loop has to be traversed in different directions by the trajectory and its partner. Here we study the transition region between zero and weak magnetic field. In particular, we consider a homogeneous magnetic field B_z perpendicular to the sample that is assumed weak enough not to change the classical trajectories, but

Footnote 3 (continued)

conditions [32]. This yields for periodic orbits that the Maslov indices of the orbit and its partner are equal: First both are classically very similar and second the manifolds have to return to their original positions for the orbits to become periodic. These facts exclude that stable and unstable manifolds of orbit and partner differ by at least half a turn. For open orbits similar arguments were applied in [33]. In the following we will thus always assume that there are no additional contributions due to Maslov phases.

only the actions in the exponents. Since the closed loop is traversed in different directions by the two trajectories, we obtain an additional phase difference $(4\pi AB_z/\phi_0)$ between the two trajectories with the enclosed area A of the loop and the flux quantum $\phi_0 = (hc/e)$. We further need the distribution of enclosed areas for a trajectory with a closed loop of time T in chaotic systems, given by

$$P(A,T) = \frac{1}{\sqrt{2\pi T\beta'}} \exp\left(-\frac{A^2}{2T\beta'}\right)$$
 (2.50)

with a system specific parameter β' . A derivation of this formula can be found for example in Ref. [35]. Equation (2.50) can be interpreted in the following way [36]: Long orbits accumulate their enclosed areas in a random way leading due to the central limit theorem to a Gaussian area distribution. Including the phase difference due to the magnetic field and the area distribution in a modified $P(\epsilon, T)$ yields

$$P_{B}(\epsilon, T) \approx \frac{2mv^{2}}{\Omega(E)} \sin \epsilon \int_{T_{\min}(\epsilon)}^{T - T_{\min}(\epsilon)} dt_{l} (T - t_{l} - T_{\min}(\epsilon))$$

$$\times \int_{-\infty}^{\infty} dA P (A, t_{l} - T_{\min}(\epsilon)) \cos \frac{4\pi A B_{z}}{\phi_{0}}$$

$$= \frac{2mv^{2}}{\Omega(E)} \sin \epsilon \int_{T_{\min}(\epsilon)}^{T - T_{\min}(\epsilon)} dt_{l} (T - t_{l} - T_{\min}(\epsilon)) e^{-(t_{l} - T_{\min}(\epsilon))/t_{B}}$$
(2.51)

with $t_B = \frac{\phi_0^2}{8\pi^2\beta'B_z^2}$. In the first step we used that paths leaving the crossing to form a closed loop, enclose a negligible flux, as long as they are correlated; for a more detailed analysis see Appendix D of Ref. [37]. Performing the T- and ϵ -integrals similar to the case without magnetic field, yields [24]

$$|t_{\alpha,\beta}(k,B_z)|_{L}^2 = -\frac{1}{(N_1 + N_2)^2} \frac{1}{1 + \tau_D/t_B}.$$
 (2.52)

We obtain in dependence of B_z an inverted Lorentzian with minimum at zero magnetic field, implying that the transmission through our sample increases with increasing magnetic field. This weak-localisation phenomenon is visible as the reduction of the average quantum transmission in Fig. 2.3.

After this introduction into the semiclassical methods for the evaluation of non-diagonal contributions in configuration space, we will now turn to the generalisation to phase space which also allows for an elegant way to compute higher-order corrections in 1/N than the leading weak-localisation contribution presented above.

2.3.3 Quantum Transmission: Phase-Space Approach

The above configuration-space treatment, based on self-crossings, is restriced to systems with two degrees of freedom. For higher-dimensional, dynamical chaotic systems one cannot assume to find a one-to-one correspondence between partner

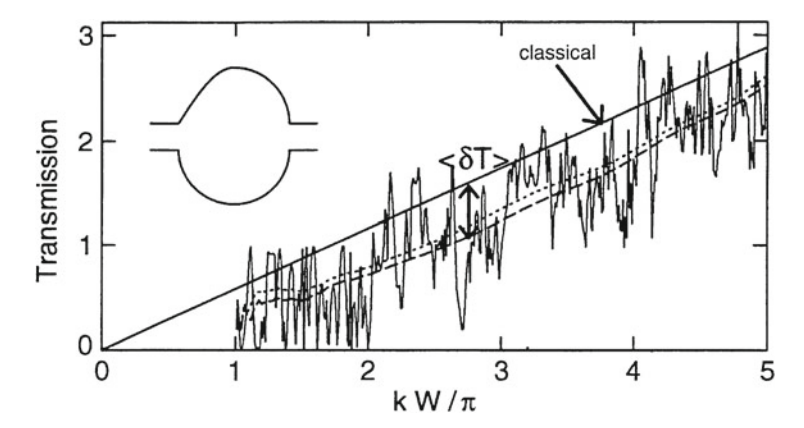


Fig. 2.3 Transmission of the depicted geometry as a function of kW/π for $W_1 = W_2 \equiv W$. The *straight full line* is the resulting transmission in diagonal approximation, the *fluctuating full line* the numerically determined quantum transmission. The *dashed* and the *dotted curve* are smoothed curves for the quantum transmission without and with a weak magnetic field, respectively (taken from [23]). Note the large fluctuations around these curves. They are universal in chaotic systems and referred to as universal conductance fluctuations. We will come back to their semiclassical description in Chap. 4

orbits and crossings of an orbit [3, 4]. In order to overcome these difficulties, a phase-space approach was developed for calculating the spectral form factor in spectral statistics in [3–5] involving periodic orbits. The next challenge was the generalisation of this theory to trajectory pairs differing from each other at several places, solved again first for the spectral form factor [6] and generalised to the transport situation considered here in Ref. [38] which serves as the basis of the following discussion.

We now first explain the phase-space approach and use it afterwards in the way developed in Refs. [6, 38] for the calculation of the quantum transmission involving also higher-order semiclassical diagrams.⁴

2.3.3.1 Phase-Space Approach

Compared to the last subsection, we first switch the role of the reference orbit. Whereas we used there the crossing orbit as reference and calculated then the action difference and the crossing-angle distribution in terms of the crossing angle ϵ , we will consider here the orbit without the crossing that is close to itself in the encounter region, where the partner orbit crossed in configuration space itself in the last subsection. To the region, where the orbit is close to itself, we will refer as encounter region and to the parts of the orbit inside as encounter stretches. These are connected by so-called links. Imagining this encounter in phase space, we place

⁴ We restrict for simplicity of presentation to two-dimensional systems with one constant Lyapunov exponent, generalisations can be found for example in [39, 40].

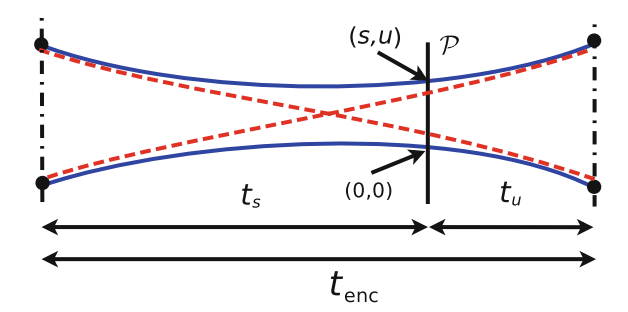


Fig. 2.4 An encounter with the ingredients considered in the phase-space approach: The duration of the encounter is given by $t_{\rm enc}$, the sum of the times t_s and t_u traversed on the *left* and on the *right* of a Poincaré surface of section \mathcal{P} , respectively. The piercing points of the trajectory indicated by the fat (*blue*) line are given by (0,0) and (s,u). The partner trajectory is indicated by the *dashed* (*red*) line

a Poincaré surface of section \mathcal{P} with its origin at $\tilde{x} = (\mathbf{r}, \mathbf{p})$ inside this region. The section consists of all points $\tilde{x} + \delta \tilde{x} = (\mathbf{r} + \delta \mathbf{r}, \mathbf{p} + \delta \mathbf{p})$ in the same energy shell as the reference point with the $\delta \mathbf{r}$ perpendicular to the momentum \mathbf{p} of the trajectory. For the two-dimensional systems mostly considered here \mathcal{P} is a two-dimensional surface, where every vector $\delta \tilde{x}$ can be expressed in terms of the stable direction $e_s(\tilde{x})$ and the unstable one $e_u(\tilde{x})$ [41]

$$\delta \tilde{x} = se_s(\tilde{x}) + ue_u(\tilde{x}). \tag{2.53}$$

The expressions stable and unstable refer to the following: Consider two orbits, one starting at \tilde{x} and the other one at $\tilde{x} + \delta \tilde{x}_0$, then the difference between the stable coordinates will decrease exponentially for positive times and increase for negative time exponentially in the limit of long time T, unstable coordinates behave just the other way round. The functional form of the exponentials can be written as $e^{\lambda T}$ and $e^{-\lambda T}$. Now we can come back to the trajectory with the encounter region, where we have put the Poincaré surface of section. The reference trajectory considered here, the fat (blue) line in Fig. 2.4, will pierce the Poincaré section twice: One of these points we will consider as the origin of the section the other piercing will take place at the distance (s,u), see Fig. 2.4. The coordinates of the piercing points of the partner trajectory, the dashed (red) one in Fig. 2.4 are determined in the following way: The unstable coordinate of the partner trajectory has to be the same as the one of that part of the first trajectory that the partner will follow for positive times. The stable coordinate is determined by the same requirement for negative times.

After this introduction into the determination of the (s, u)-coordinates, we are now ready to treat trajectory pairs that differ in encounters of arbitrary complexity. Following Refs. [6, 39, 40] and using the notation introduced there we will allow here that the two trajectories differ in arbitrarily many encounters involving an arbitrary number of stretches. In order to organise this encounter structure we introduce a vector $\mathbf{v} = (v_2, v_3, \ldots)$ with the component v_l determining the number of encounters

with l stretches involved. The overall number of encounters during an orbit will be denoted by $V = \sum_{l=2}^{\infty} v_l$, the overall number of encounter stretches by $L = \sum_{l=2}^{\infty} l v_l$. In an encounter of l stretches, we will get l-1 (s,u)-coordinates.

Now we can proceed by replacing the former expressions for the minimal loop time, the action difference and the crossing-angle distribution depending on the former small parameter ϵ , by the corresponding expressions depending on the new small parameters (s, u).

We start with the minimal loop time, to that one also refers as the duration of the encounter as the two parts of the trajectory are close, i.e. linearisable, to each other during that time, as we saw in the last subsection. Shifting the Poincaré surface of section through the encounter, the stable components will asymptotically decrease, the unstable ones will increase for increasing time. We then claim that both components have to be smaller than a classical constant c, giving the upper bound for the two trajectories to be linearisable. Its exact value will again, as in the last subsection, be unimportant for our final results. We then obtain the encounter duration $t_{\rm enc}$ as the sum of the times t_u , that the trajectory needs from $\mathcal P$ till the point where the first unstable component reaches c, and the time t_s , that the trajectory needs from $\mathcal P$ till the point where the last stable component falls below c, for an illustration see Fig. 2.4. Thus we get for $t_{\rm enc} \to \infty$

$$t_{\text{enc}} = t_s + t_u \sim \frac{1}{\lambda} \ln \frac{c^2}{\max_i \{|s_i|\} \max_j \{|u_j|\}}.$$
 (2.54)

Now we treat the action difference between the two trajectories. Expressing the actions of the paired trajectories as the line integral of the momentum along the trajectory as defined after Eq. (2.19), we can expand [3, 4] one action around the other by linearising the motion on the two trajectories around each other and express the result in terms of the (s, u)-coordinates. This yields for an l-encounter⁵

$$\Delta S \approx \sum_{j=1}^{l-1} u_j s_j. \tag{2.55}$$

The action difference of a trajectory pair is then obtained by adding the differences resulting from all encounters.

Finally we come to the crossing-angle distribution that will be replaced here by a weight function for the stable and unstable coordinates for a trajectory of time T. We first notice that the uniformity of the trajectory distribution implies in terms of our coordinates in \mathcal{P} that a trajectory pierces through the section with the coordinates (u, u + du) and (s, s + ds) within the time interval (t, t + dt) with the probability $dsdudt/\Omega(E)$. In general, we obtain for an l-encounter $ds^{l-1}du^{l-1}dt^{l-1}\left(1/\Omega(E)\right)^{l-1}$. Integrating the product of the latter quantities for

⁵ Strictly speaking [6] the (s, u)-coordinates used here and in the following calculation are for encounters involving more than two stretches *not* the same as the ones described before, but related to them via a linear and volume preserving transformation.

all encounters over all possible durations of the L-V intra-encounter links, in a way that their durations are positive yields our weight function for a fixed position of \mathcal{P} . To take into account all possible positions of \mathcal{P} , we also integrate over all possible positions where it can be placed, and divide by $t_{\rm enc}$ to avoid overcounting of equivalent positions. Taking all link times positive, we obtain for the weight function⁶

$$w(\boldsymbol{u}, \boldsymbol{s}, T) \approx \frac{1}{\Omega^{L-V} \prod_{\alpha=1}^{V} t_{\text{enc}}^{\alpha}} \int_{0}^{\infty} dt_{1} \dots dt_{L} \Theta \left(T - \sum_{\alpha=1}^{V} l_{\alpha} t_{\text{enc}}^{\alpha} - \sum_{\alpha=1}^{L} t_{\alpha} \right)$$

$$= \frac{\left(T - \sum_{\alpha=1}^{V} l_{\alpha} t_{\text{enc}}^{\alpha} \right)^{L}}{L! \Omega^{L-V} \prod_{\alpha=1}^{V} t_{\text{enc}}^{\alpha}}.$$
(2.56)

with the Heaviside theta function $\Theta(x)$.

One additional problem arises, when treating trajectory pairs differing not only in one 2-encounter like in the last subsection: One can construct for one \mathbf{v} different trajectory pairs, varying for example in the relative orientation or order in which the encounter stretches are traversed. We will count this number by a function $N(\mathbf{v})$ and describe briefly later in this section how it can be calculated.

2.3.3.2 Calculation of the Full Transmission

After the introduction into the phase-space approach we are now ready to calculate the contributions of orbit pairs differing in an arbitrary number of encounters of arbitrary size to the transmission. Taking the weight function, the action difference and the number of structures, we can transform the off-diagonal part of the summands in Eq. (2.31) into

$$\left| t_{\alpha,\beta}(k) \right|_{\text{off}}^{2} = \frac{\pi \hbar}{2W_{1}W_{2}} \sum_{\gamma} \sum_{\mathbf{v}} \left| D_{\gamma} \right|^{2} N(\mathbf{v})$$

$$\times \left\langle \int_{-c}^{c} ds d\mathbf{u} \exp\left(\frac{i}{\hbar} \Delta S\right) w(\mathbf{u}, \mathbf{s}, T) \right\rangle_{\Delta k}$$
(2.57)

with the average over a small k-window denoted by $\langle \ldots \rangle_{\Delta k}$. Inserting the formulas for the action difference (2.55), the weight function (2.56) and using the classical sum rule with the modification of the survival probability due to encounters, discussed in the last subsection, we can transform [38] the integral with respect to the length of the trajectory into one over the last link and obtain

⁶ A derivation of this expression starting from a formula analogous to (2.39) and using the mixing property can be found in Appendix B of [39].

$$\begin{aligned} \left| t_{\alpha\beta}(k) \right|_{\text{off}}^{2} &= \frac{2\pi\hbar}{\Omega} \sum_{\mathbf{v}} N\left(\mathbf{v}\right) \left(\prod_{i=1}^{L+1} \int_{0}^{\infty} dt_{i} \exp\left(-\frac{t_{i}}{\tau_{D}}\right) \right) \\ &\times \left\langle \int_{-c}^{c} \frac{ds d\mathbf{u}}{\Omega^{L-V}} \prod_{\alpha=1}^{V} \frac{\exp\left(-\frac{t_{\text{enc}}^{\alpha}}{\tau_{D}} + \frac{i}{\hbar} \sum_{j=1}^{l_{\alpha}-1} u_{\alpha j} s_{\alpha j}\right)}{t_{\text{enc}}^{\alpha}} \right\rangle_{\Delta k} \\ &= \frac{1}{N_{1} + N_{2}} \sum_{n=1}^{\infty} \left(\frac{1}{N_{1} + N_{2}} \right)^{n} \sum_{\mathbf{v}}^{L-V=n} (-1)^{V} N\left(\mathbf{v}\right) \end{aligned} \tag{2.58}$$

with the L+1 link times t_i . The (s,u)-integrals are calculated using the rule [6], that after expanding the exponential $e^{t_{\rm enc}/\tau_D}$ into a Taylor series, only the $t_{\rm enc}$ -independent term contributes and yields for $\hbar \to 0$

$$\left\langle \frac{1}{\Omega} \int_{-c}^{c} ds du \exp\left(\frac{ius}{\hbar}\right) \right\rangle_{\Delta k} \sim \frac{1}{T_H}$$
 (2.59)

with the Heisenberg time $T_H = \Omega/(2\pi\hbar) = 2\pi\hbar\bar{d}(E)$. Due to the last relation T_H can be, following the Heisenberg uncertainty principle, regarded as the time needed to resolve energy levels separated by distances of the order of the mean level spacing $\Delta(E) = 1/\bar{d}(E)$.

For the sum with respect to \mathbf{v} , one can derive recursion relations, yielding [6, 38]

$$\sum_{\mathbf{v}}^{L-V=n} (-1)^{V} N(\mathbf{v}) = \left(1 - \frac{2}{\beta}\right)^{n}$$
 (2.60)

with $\beta=1$ and $\beta=2$ for the case with and without time-reversal symmetry, respectively. Relations of this kind are derived from recursion relations obtained by expressing the connections inside and between encounters by permutations and considering the effect of shrinking one link in an arbitrarily complicated structure to zero.

We then obtain for T(k) in the case with time-reversal symmetry [38]

$$T(k)^{\beta=1} \approx \frac{N_1 N_2}{N_1 + N_2} + \frac{N_1 N_2}{N_1 + N_2} \sum_{n=1}^{\infty} \left(\frac{-1}{N_1 + N_2}\right)^n = \frac{N_1 N_2}{N_1 + N_2 + 1}$$
 (2.61)

and in the case without time-reversal symmetry

$$T(k)^{\beta=2} \approx \frac{N_1 N_2}{N_1 + N_2},$$
 (2.62)

which agrees with the diagonal contribution, already obtained in the first subsection of this section. Both results are in agreement with RMT predictions [28] given in (2.36) and (2.37).

(2.66)

2.4 Spectral Statistics

After this introduction to transport through open systems we now want to analyse the spectral properties of chaotic systems. We first introduce the quantities usually studied in this context and afterwards show how the spectral form factor, for its definition see below, is calculated semiclassically within the phase-space approach.

In the context of spectral statistics often the autocorrelator of two spectral densities d(E) (we will come to another quantity characterising the spectral properties of a chaotic system in Chap. 5) is considered, defined as

$$C(\epsilon) = \frac{1}{\bar{d}^2} \left\langle d\left(E + \frac{\epsilon}{2\pi \bar{d}}\right) d\left(E - \frac{\epsilon}{2\pi \bar{d}}\right) \right\rangle_{Ak} - 1. \tag{2.63}$$

The (-1) subtracts the contributions due to the mean spectral densities \overline{d} contained in the first term. The function $C(\epsilon)$ can be expressed semiclassically using (2.23) and linearising the actions around the mean energy E, $S_{\gamma}\left(E+\epsilon/(2\pi\bar{d})\right)\approx S_{\gamma}(E)+\epsilon\hbar T_{\gamma}/T_{H}$, as

$$C_{\text{sc}}(\epsilon) = \Re \frac{2}{T_H^2} \left\langle \sum_{\gamma,\gamma'} T_{\gamma}^{\text{prim}} T_{\gamma'}^{\text{prim}} C_{\gamma} C_{\gamma'} e^{(i/\hbar) \left(S_{\gamma} - S_{\gamma'} \right) + (i\epsilon/T_H) \left(T_{\gamma} + T_{\gamma'} \right) - i(\pi/2) \left(\tau_{\gamma} - \tau_{\gamma'} \right)} \right\rangle_{\Delta k}.$$
(2.64)

We also define

$$R(\epsilon) = \frac{1}{4\pi^2 \bar{d}^2} \left\langle \text{Tr} G^{+\text{osc}} \left(E + \frac{\epsilon}{2\pi \bar{d}} \right) \text{Tr} G^{-\text{osc}} \left(E - \frac{\epsilon}{2\pi \bar{d}} \right) \right\rangle_{\Delta k}, \quad (2.65)$$

expressed by using $TrG^-(E) = [TrG^+(E)]^*$ and Eq. (2.22) semiclassically as

$$R_{\rm sc}(\epsilon) = \frac{1}{T_H^2} \left\langle \sum_{\gamma,\gamma'} T_{\gamma}^{\rm prim} T_{\gamma'}^{\rm prim} C_{\gamma} C_{\gamma'} e^{(i/\hbar) \left(S_{\gamma} - S_{\gamma'} \right) + (i\epsilon/T_H) \left(T_{\gamma} + T_{\gamma'} \right) - i(\pi/2) \left(\tau_{\gamma} - \tau_{\gamma'} \right)} \right\rangle_{\Delta k}.$$

Often also the corresponding Fourier transform, the spectral form factor is considered

$$K(\tau) = \frac{1}{\pi} \left\langle \int_{-\infty}^{\infty} d\epsilon e^{-2i\epsilon\tau} R(\epsilon) \right\rangle_{\Delta k, \Delta \tau}, \tag{2.67}$$

that we want to study here.

The RMT results for the latter quantity are

$$K_{\text{GUE}}(\tau) = \tau, \quad \text{for } \tau \le 1$$

 $K_{\text{GUE}}(\tau) = 1, \quad \text{for } \tau > 1$ (2.68)

in the case of the Gaussian unitary ensemble and

$$K_{\text{GOE}}(\tau) = 2\tau - \tau \ln(1 + 2\tau) = 2\tau - 2\tau^2 + 2\tau^3 + \mathcal{O}\left(\tau^4\right), \text{ for } \tau \le 1$$

$$K_{\text{GOE}}(\tau) = 2 - \tau \ln\frac{(2\tau + 1)}{(2\tau - 1)}, \text{ for } \tau > 1$$
(2.69)

in the case of the Gaussian orthogonal ensemble.

A semiclassical expression for $K(\tau)$ can be obtained by inserting (2.66) in Eq. (2.67) and performing the ϵ -integral

$$K_{\rm sc}(\tau) = \left\langle \frac{1}{T_H} \sum_{\gamma, \gamma'} T_{\gamma}^{\rm prim} T_{\gamma'}^{\rm prim} C_{\gamma} C_{\gamma'} e^{(i/\hbar) \left(S_{\gamma} - S_{\gamma'} \right) - i(\pi/2) \left(\tau_{\gamma} - \tau_{\gamma'} \right)} \right.$$

$$\times \delta \left(\tau T_H - \frac{T_{\gamma} + T_{\gamma'}}{2} \right) \right\rangle_{\Delta k, \Delta \tau}. \tag{2.70}$$

As already in the last section we obtain a double sum over trajectories, however now periodic orbits are considered instead of lead-connecting paths like in the last section. We will now proceed with calculating the contributions to (2.70) surviving the averaging. In diagonal approximation we obtain the contribution $K_{\text{diag}}(\tau)$

$$K_{\text{diag}}(\tau) = \frac{1}{T_H} \sum_{\gamma} \left(T_{\gamma}^{\text{prim}} \right)^2 \left| C_{\gamma} \right|^2 \delta \left(\tau T_H - T_{\gamma} \right). \tag{2.71}$$

The sum over orbits in the last equation is performed with the Hannay and Ozorio de Almeida sum rule [42]

$$\sum_{\gamma} \left(T_{\gamma}^{\text{prim}} \right)^{2} \left| C_{\gamma} \right|^{2} \delta \left(\tau T_{H} - T_{\gamma} \right) \approx \tau T_{H}, \tag{2.72}$$

that can be derived in a similar way like (2.34) using ergodicity yielding finally [43]

$$K_{\text{diag}}(\tau) = \tau \tag{2.73}$$

and twice the latter contribution in the presence of time-reversal symmetry, because then we can additionally pair each orbit with its time-reversed counterpart.

We want to show now that the semiclassically calculated off-diagonal contributions to $K(\tau)$ are in accordance with the results (2.68, 2.69) from RMT. We will as for the introduction to the phase-space approach follow [6, 39, 40] and use the notation introduced there. The calculation is performed within the phase-space approach. We introduced for the transmission in the last section

- the duration of an encounter $t_{\text{enc}}(\boldsymbol{u}, \boldsymbol{s})$,
- the weight function $w(\mathbf{u}, \mathbf{s}, T)$ measuring the density of encounters,
- the action difference of the orbit and its partner ΔS ,
- the function $N(\mathbf{v})$ characterising the number of possible orbits for a vector \mathbf{v} .

Compared to the last section the only change in these quantities is that the weight function is altered due to the fact that here periodic orbits are considered. It is now given by

$$w(\boldsymbol{u}, \boldsymbol{s}, T) \approx \frac{T \left(T - \sum_{\alpha=1}^{V} l_{\alpha} t_{\text{enc}}^{\alpha} \right)^{L-1}}{(L-1)! \Omega^{L-V} \prod_{\alpha=1}^{V} t_{\text{enc}}^{\alpha}}.$$
 (2.74)

The factor T not appearing in the case of open trajectories, Eq. (2.56), results here from the possibility that the final point of the first encounter stretch can lie everywhere on a *periodic* orbit. This was not possible on an *open* orbit. With these quantities we obtain for the off-diagonal contributions to the spectral form factor $K(\tau)$ after applying the sum rule (2.72) [6, 39, 40]

$$K_{\text{off}}(\tau) = \frac{2}{\beta} \tau \left\langle \sum_{\mathbf{v}} \frac{N(\mathbf{v})}{L} \int_{-c}^{c} ds d\mathbf{u} w \left(\mathbf{u}, \mathbf{s}, \tau T_{H} \right) e^{(i/\hbar)\Delta S} \right\rangle_{\Delta k, \Delta \tau}$$
(2.75)

with $\beta=2$ in the unitary and $\beta=1$ in the orthogonal case. The factor $\frac{1}{L}$ avoids overcounting of equivalent diagrams: In contrast to an open orbit for a periodic orbit each encounter stretch can be singled out to be the first one. All these contributions lead however to the same contribution to (2.75) that should only be counted once. As already mentioned before Eq. (2.59) only terms of w (u, s, T) contribute to the s, u-integrals that are independent of $t_{\rm enc}$. We consider in (2.74) only those terms, we thus replace

$$w(\boldsymbol{u}, \boldsymbol{s}, T) \to \left(\frac{T}{\Omega}\right)^{L-V} \frac{(-1)^V \prod_{\alpha=1}^V l_\alpha}{(L-V-1)!},\tag{2.76}$$

where $\prod_{\alpha=1}^{V} l_{\alpha}$ can be transformed into $\prod_{l=2}^{\infty} l^{v_l}$ by noting that l_{α} depends only on the number l of encounter stretches in an encounter. This yields together with (2.59) for $K_{\text{off}}(\tau)$

$$K_{\text{off}}(\tau) = \frac{2}{\beta} \tau \sum_{\mathbf{v}} N(\mathbf{v}) \tau^{L-V} \frac{(-1)^{V} \prod_{l=2}^{\infty} l^{v_{l}}}{L(L-V-1)!} \equiv \frac{2}{\beta(n-2)!} \sum_{n=2}^{\infty} \sum_{\mathbf{v}}^{L-V+1=n} \widetilde{N}(\mathbf{v}) \tau^{n}$$
(2.77)

with

$$\widetilde{N}(\mathbf{v}) \equiv N(\mathbf{v}) \frac{(-1)^{V} \prod_{l=2}^{\infty} l^{\nu_{l}}}{L}.$$
(2.78)

The function $K_{\rm off}(\tau)$ can thus be expressed as

$$K_{\text{off}}(\tau) = \frac{2}{\beta} \sum_{n=2}^{\infty} K_n \tau^n$$
 (2.79)

with

$$K_n \equiv \frac{1}{(n-2)!} \sum_{\mathbf{v}}^{L-V+1=n} \widetilde{N}(\mathbf{v}). \tag{2.80}$$

The sum over \mathbf{v} is like in the case of the transmission in the last section performed with the help of recursion relations for the contributions for different n, for a derivation see e.g. [39, 40], in the unitary case this yields

$$K_n = 0 (2.81)$$

and in the orthogonal case

$$K_n = \frac{(-2)^{n-1}}{n-1}. (2.82)$$

Both results are consistent with the RMT predictions (2.68) and (2.69) for $\tau \leq 1$. This is obvious for the unitary case, while in the orthogonal case it is obtained by comparing the τ -expansions of the semiclassical and RMT result for $\tau \leq 1$. This semiclassical theory we have described is up to now however not able to explain the correlations that lead to the behaviour of $K(\tau)$ for $\tau > 1$; we will come back to this point in Chap. 5.

References

- 1. Sieber, M., Richter, K.: Phys. Scr. T 90, 128 (2001)
- 2. Sieber, M.: J. Phys. A 35, L613 (2002)
- 3. Turek, M., Richter, K.: J. Phys. A 36, L455 (2003)
- Turek, M.: Semiclassics beyond the diagonal approximation. Ph.D. thesis, Universität Regensburg (2004)
- 5. Spehner, D.: J. Phys. A 36, 7269 (2003)
- 6. Müller, S., Heusler, S., Braun, P., Haake, F., Altland, A.: Phys. Rev. Lett. 93, 014103 (2004)
- 7. Keppeler, S.: Spinning Particles-Semiclassics and Spectral Statistics, Springer Tracts in Modern Physics vol. 193, Berlin, Heidelberg (2003)
- Grosche, C., Steiner, F.: Handbook of Feynman Path Integrals, Springer Tracts in Modern Physics vol. 145, Berlin, Heidelberg (1998)
- Grigis, A., Sjöstrand, J.: Microlocal Analysis for Differential Operators. Cambridge University Press, Cambridge (1994)
- 10. van Vleck, J.H.: Proc. Natl. Acad. Sci. USA 14, 178 (1928)
- 11. Gutzwiller, M.: Chaos in Classical and Quantum Mechanics. Springer, New York (1990)
- 12. Choquard, P., Steiner, F.: Helv. Phys. Acta **69**, 637 (1996)
- 13. Berry, M.V., Tabor, M.: Proc. R. Soc. Lond. A **349**, 101 (1976)
- 14. Berry, M.V., Tabor, M.: J. Phys. A 10, 371 (1977)

References 39

- 15. Balian, R., Bloch, C.: Ann. Phys. **60**, 401 (1970)
- 16. Balian, R., Bloch, C.: Ann. Phys. 64, 271 (1971)
- 17. Balian, R., Bloch, C.: Ann. Phys. 69, 76 (1972)
- 18. Landauer, R.: IBM J. Res. Dev. 1, 223 (1957)
- 19. Landauer, R.: IBM J. Res. Dev. 32, 306 (1988)
- 20. Büttiker, M.: Phys. Rev. Lett. 57, 1761 (1986)
- 21. Fisher, D.S., Lee, P.A.: Phys. Rev. B 23, 6851(R) (1981)
- 22. Jalabert, R.A., Baranger, H.U., Stone, A.D.: Phys. Rev. Lett. 65, 2442 (1990)
- 23. Baranger, H.U., Jalabert, R.A., Stone, A.D.: Chaos 3, 665 (1993)
- 24. Richter, K., Sieber, M.: Phys. Rev. Lett. 89, 206801 (2002)
- 25. Sieber, M.: J. Phys. A 32, 7679 (1999)
- Waltner, D.: Spin-Bahn Kopplung in mesoskopischer Physik: Ein semiklassischer Zugang. VDM-Verlag Dr. Müller, Saarbrücken (2011)
- 27. Müller, S.: Eur. Phys. J. B 34, 305 (2003)
- 28. Beenakker, C.W.J.: Rev. Mod. Phys. 69, 731 (1997)
- Waltner, D., Richter, K.: Classical correlations and quantum interference in ballistic conductors.
 In: Radons, G., Schuster, H.G., Rumpf, B. (eds.) Nonlinear Dynamics of Nanosystems. Wiley-VCH, Berlin (2010)
- 30. Baranger, H.U., Jalabert, R.A., Stone, A.D.: Phys. Rev. Lett. 70, 3876 (1993)
- 31. Stone, A.D., Szafer, A.: IBM J. Res. Develop. 32, 384 (1988)
- 32. Creagh, S.C., Robbins, J.M., Littlejohn, R.G.: Phys. Rev. A 42, 1907 (1990)
- 33. Kuipers, J., Sieber, M.: Phys. Rev. E 77, 046219 (2008)
- 34. Brouwer, P.W., Rahav, S.: Phys. Rev. B 74, 075322 (2006)
- 35. Jensen, R.V.: Chaos 1, 101 (1991)
- 36. Doron, E., Smilansky, U., Frenkel, A.: Phys. D 50, 367 (1991)
- 37. Jacquod, P., Whitney, R.S.: Phys. Rev. B 73, 195115 (2006)
- 38. Heusler, S., Müller, S., Braun, P., Haake, F.: Phys. Rev. Lett. 96, 066804 (2006)
- 39. Müller, S., Heusler, S., Braun, P., Haake, F., Altland, A.: Phys. Rev. E 72, 046207 (2005)
- 40. Müller, S.: Periodic-Orbit Approach to Universality in Quantum Chaos. Ph.D. thesis, Universität Duisburg Essen (2005)
- 41. Gaspard, P.: Chaos, Scattering and Classical Mechanics. Cambridge University Press, Cambridge (1998)
- 42. Hannay, J., deAlmeida, A.O.: J. Phys. A 17, 3429 (1984)
- 43. Berry, M.V.: Proc. R. Soc. A 400, 229 (1985)

Chapter 3 Survival Probability and Fidelity Decay

Here we consider decay of open systems and the stability of closed systems under perturbations. For the quantities characterising these effects that can be treated semiclassically in a related manner we want to explain how to calculate for chaotic systems quantum corrections to the classical results in a similar way as shown in the last chapter. The corresponding calculations were published mainly in [1–4]. In the first section we define and introduce the relevant expressions. Afterwards we explain the unitarity problems occurring in a semiclassical calculation of quantum corrections presenting as an example the first quantum correction in the presence of time-reversal symmetry and how to remove those problems by considering additional diagrams. Then we extend our analysis to more complicated diagrams and explain the effect of spin-orbit interaction in this case. Afterwards we discuss how certain exact relations like the continuity equation are fulfilled in this semiclassical approach. Finally we explain the effect of quantum corrections in the regime of strong perturbations and for a time-dependent perturbation.

3.1 Survival Probability and Fidelity Within Diagonal Approximation

3.1.1 Survival Probability

We consider the quantum mechanical survival probability of a particle inside a cavity of an area A, i.e. the spatially integrated probability density

$$\rho_{\text{qm}}(t) = \int_{A} d\mathbf{r} \psi(\mathbf{r}, t) \psi^{*}(\mathbf{r}, t)$$
(3.1)

of the wave function $\psi(\mathbf{r},t)$. In the case of a closed system the probability to stay inside the system is conserved, $\rho_{\rm qm}(t)\equiv 1$. This fact is retained in the classical limit $\hbar\to 0$, since a classical particle also has to stay inside a closed system, i.e. the classical survival probability $\rho_{\rm cl}(t)$ is equal to the quantum one $\rho_{\rm qm}(t)$. Turning now

to an open system, $\rho_{\rm qm}$ (t) can deviate from its classical counterpart, $\rho_{\rm cl}$ (t). We can thus get access to quantum properties by opening up the system and comparing $\rho_{\rm cl}$ (t) and $\rho_{\rm qm}$ (t). As already given in the last chapter after Eq. (2.34), for an open system with completely chaotic dynamics, the classical survival probability is asymptotically given for long times by

$$\rho_{\rm cl}(t) \sim e^{-t/\tau_D} \tag{3.2}$$

with the classical dwell time $\tau_D = \Omega/(2\pi\hbar N)$ obtained in the case of N open channels.

We will study now $\rho_{\rm qm}(t)$, or more exactly quantum corrections to $\rho_{\rm cl}(t)$: Various methods were used to gain information about this quantity: Experimentally they have been studied either directly in atom billiards [5, 6], or indirectly in the spectral regime of Ericson fluctuations—i.e. when the average width of the resonances in the spectrum is much larger than their spacing—using electrons [7] or microwaves [8], and in atomic photoionisation [9]. Numerically they have been analysed by [10] for the kicked rotator. Furthermore $\rho_{\rm qm}(t)$ was also studied by supersymmetry techniques [11–13]. As several examples considered up to now showed, these results can be expected to be applicable to classically chaotic systems. It was found there that the quantum decay $\rho_{\rm qm}(t)$ follows $\rho_{\rm cl}(t)$ only up to a quantum relaxation time $t^* \sim \sqrt{\tau_D T_H}$, shorter than the Heisenberg time T_H . It was shown in Refs. [11–13] that $\rho(t)$ is given by a universal function depending only on τ_D and T_H . In contrast to the conductance and the spectral form factor in the last chapter the results do not possess a simple closed form. In the unitary case the first correction in t/T_H to (3.2) is given by

$$\rho_{\text{GUE}}(t) = e^{-t/\tau_D} \left(1 + \frac{t^4}{24\tau_D^2 T_H^2} + \cdots \right)$$
 (3.3)

and in the orthogonal case by

$$\rho_{\text{GOE}}(t) = e^{-t/\tau_D} \left(1 + \frac{t^2}{2\tau_D T_H} + \cdots \right)$$
(3.4)

with the dots indicating higher-order terms in t/T_H . For quantum graphs the given corrections were studied semiclassically and numerically in [14].

Here we want to calculate corrections to $\rho_{\rm cl}(t)$ by semiclassical methods for general classically chaotic quantum systems. In order to obtain a semiclassical approximation for the quantum survival probability we express

$$\psi(\mathbf{r},t) = \int_{A} d\mathbf{r}' K(\mathbf{r},\mathbf{r}',t) \psi_{0}(\mathbf{r}')$$
 (3.5)

with the initial state $\psi_0(\mathbf{r}')$ at t=0 and approximate the time-dependent propagator $K(\mathbf{r}, \mathbf{r}', t)$ semiclassically by (2.17). This yields the semiclassical expression for $\rho(t)$:

$$\rho_{\rm sc}(t) = \left(\frac{1}{2\pi\hbar}\right)^2 \int_A d\mathbf{r} \, d\mathbf{r}' \, d\mathbf{r}'' \, \psi_0(\mathbf{r}') \psi_0^*(\mathbf{r}'')$$

$$\times \sum_{\substack{\bar{\gamma} \ (\mathbf{r}' \to \mathbf{r}, t) \\ \bar{\gamma}' \ (\mathbf{r}'' \to \mathbf{r}, t)}} A_{\bar{\gamma}} A_{\bar{\gamma}'} e^{i\left(S_{\bar{\gamma}} - S_{\bar{\gamma}'}\right)/\hbar - i(\pi/2)\left(\mu_{\bar{\gamma}} - \mu_{\bar{\gamma}'}\right)}$$
(3.6)

with the trajectories denoted by $\bar{\gamma}$, $\bar{\gamma}'$. Similarly as in the last chapter we want to study now $\rho_{sc}(t)$ averaged over a classically small but quantum mechanically large time window Δt . Important contributions will thus again result from very similar trajectories. Therefore we first single out in the double sum in (3.6) all paths with similar starting points. We thus introduce midpoint coordinates $\mathbf{r}_0 = (\mathbf{r}' + \mathbf{r}'')/2$ and difference coordinates $\mathbf{q} = (\mathbf{r}' - \mathbf{r}'')$ and replace the original paths $\bar{\gamma}$, $\bar{\gamma}'$, by nearby trajectories γ and γ' connecting \mathbf{r}_0 and \mathbf{r} in time t. Then, upon expanding the action $S_{\bar{\gamma}}(\mathbf{r}, \mathbf{r}', t) \simeq S_{\gamma}(\mathbf{r}, \mathbf{r}_0, t) - \mathbf{q}\mathbf{p}_0^{\gamma}/2$ with \mathbf{p}_0^{γ} the initial momentum of path γ and expanding in the same way $S_{\bar{\gamma}'}$, we obtain

$$\rho_{\text{sc}}(t) = \frac{1}{(2\pi\hbar)^2} \int d\mathbf{r} \, d\mathbf{r}_0 \, d\mathbf{q} \, \psi_0 \left(\mathbf{r}_0 + \frac{\mathbf{q}}{2} \right) \psi_0^* \left(\mathbf{r}_0 - \frac{\mathbf{q}}{2} \right)$$

$$\times \sum_{\gamma, \gamma'(\mathbf{r}_0 \to \mathbf{r}, t)} A_{\gamma} A_{\gamma'} e^{(i/\hbar)[S_{\gamma} - S_{\gamma'} - (\mathbf{p}_0^{\gamma} + \mathbf{p}_0^{\gamma'})\mathbf{q}/2] - i(\pi/2) \left(\mu_{\gamma} - \mu_{\gamma'} \right)}. \tag{3.7}$$

The main contribution to $\rho_{sc}(t)$ in the semiclassical limit $\hbar \to 0$ arises from pairs $\gamma = \gamma'$, because they involve no action differences. We obtain

$$\rho_{\text{diag}}(t) = \frac{1}{(2\pi\hbar)^2} \int d\mathbf{r} \, d\mathbf{r}_0 \, d\mathbf{q} \, \psi_0 \left(\mathbf{r}_0 + \frac{\mathbf{q}}{2} \right) \psi_0^* \left(\mathbf{r}_0 - \frac{\mathbf{q}}{2} \right) \sum_{\gamma (\mathbf{r}_0 \to \mathbf{r}, t)} \left| A_{\gamma} \right|^2 e^{-(i/\hbar) \mathbf{p}_0^{\gamma} \mathbf{q}}.$$
(3.8)

Here $|A_{\gamma}|^2 = |\det(-\partial^2 S_{\gamma}/\partial \mathbf{r}\partial \mathbf{r}')| = |\det(\partial \mathbf{p}_0^{\gamma}/\partial \mathbf{r})|$ acts as a Jacobian for transforming the \mathbf{r} -integral into one with respect to the initial momentum \mathbf{p}_0^{γ} . This yields then the diagonal contribution [15]

$$\rho_{\text{diag}}(t) = \left\langle e^{-t/\tau_D} \right\rangle_{\mathbf{r}_0, \mathbf{p}_0}. \tag{3.9}$$

Here $\langle \ldots \rangle_{\mathbf{r}_0,\mathbf{p}_0}$ indicates the phase-space average,

$$\langle F \rangle_{\mathbf{r}_0, \mathbf{p}_0} = \frac{1}{(2\pi\hbar)^2} \int d\mathbf{r}_0 d\mathbf{p}_0 F(\mathbf{r}_0, \mathbf{p}_0) \rho_W(\mathbf{r}_0, \mathbf{p}_0), \tag{3.10}$$

where

$$\rho_W(\mathbf{r}_0, \mathbf{p}_0) = \int d\mathbf{q} \, \psi_0\left(\mathbf{r}_0 + \frac{\mathbf{q}}{2}\right) \psi_0^*\left(\mathbf{r}_0 - \frac{\mathbf{q}}{2}\right) \exp\left(-\frac{i}{\hbar}\mathbf{q}\mathbf{p}_0\right) \tag{3.11}$$

denotes the Wigner function of the initial wave packet ψ_0 . In the case that ψ_0 has a small energy dispersion around a mean energy E_0 , Eq. (3.9) can be approximated by

$$\rho_{\text{diag}}(t) = e^{-t/\tau_D},\tag{3.12}$$

with $\tau_D = \Omega(E_0) / (2\pi \hbar N(E_0))$.

3.1.2 Fidelity Amplitude and Fidelity

The fidelity M(t) was originally introduced by Peres [16] as a measure of the stability of a quantum system with respect to a perturbation, and has since then advanced to an important quantity characterising the sensitivity of a quantum system in the fields of quantum chaos and quantum information. It is given by the squared modulus of the fidelity amplitude, m(t), defined as the overlap integral of an initial state, e.g. a wave packet, with the state obtained upon forward and backward propagation governed by two Hamiltonians differing slightly by a perturbation, remember the right panel in Fig. 1.6. In terms of formulas we obtain

$$m(t) = \int_{A} d\mathbf{r} \, \psi^{*}(\mathbf{r}, t) \, \phi(\mathbf{r}, t)$$
(3.13)

and

$$M(t) = |m(t)|^2, (3.14)$$

with ψ (\mathbf{r} , t) obtained by propagating the initial state ψ_0 (\mathbf{r}') with the Hamiltonian H and ϕ (\mathbf{r} , t) by propagating the same initial state with the Hamiltonian $H' \equiv H + \Sigma$ with the perturbation Σ . As for the survival probability we represent ψ (\mathbf{r} , t) with the help of the quantum propagator K_H (\mathbf{r} , \mathbf{r}' , t) for the Hamiltonian H:

$$\psi\left(\mathbf{r},t\right) = \int_{A} d\mathbf{r}' K_{H}\left(\mathbf{r},\mathbf{r}',t\right) \psi_{0}\left(\mathbf{r}'\right). \tag{3.15}$$

A similar representation holds for Φ (\mathbf{r} , t), with K_H replaced by the propagator $K_{H'}$. Next we replace in Eq. (3.15) again the propagators by their semiclassical representations (2.17). We will assume that the perturbation Σ is classically small like the considered magnetic field in Sect. 2.3 such that only the actions, i.e. the phases, are affected while the classical trajectories $\bar{\gamma}$ remain unchanged. Under this assumption, after inserting Eqs. (2.17) and (3.15) into Eq. (3.13) we obtain the following semiclassical approximation [15] for m(t):

$$m_{\text{sc}}(t) = \left(\frac{1}{2\pi\hbar}\right)^{2} \int_{A} d\mathbf{r} \, d\mathbf{r}' \, d\mathbf{r}'' \, \psi_{0}\left(\mathbf{r}'\right) \, \psi_{0}^{*}\left(\mathbf{r}''\right)$$

$$\times \sum_{\substack{\bar{\gamma} \ (\mathbf{r}' \to \mathbf{r}, \, t) \\ \bar{\gamma}' \ (\mathbf{r}'' \to \mathbf{r}, \, t)}} A_{\bar{\gamma}} A_{\bar{\gamma}'} \exp\left(\frac{i}{\hbar} \left(S_{\bar{\gamma}} - S_{\bar{\gamma}'} + \Delta S_{\bar{\gamma}}^{\Sigma}\right) - i(\pi/2) \left(\mu_{\bar{\gamma}} - \mu_{\bar{\gamma}'}\right)\right),$$
(3.16)

where $\Delta S_{\bar{\gamma}}^{\Sigma}$ stands for the change in the action along the trajectory $\bar{\gamma}$ due to the perturbation Σ . Introducing again midpoint and difference coordinates like after Eq. (3.6) we obtain

$$m_{\rm sc}(t) = \left(\frac{1}{2\pi\hbar}\right)^{2} \int d\mathbf{r} \, d\mathbf{q} \, \psi_{0} \left(\mathbf{r}_{0} + \frac{\mathbf{q}}{2}\right) \psi_{0}^{*} \left(\mathbf{r}_{0} - \frac{\mathbf{q}}{2}\right)$$

$$\times \sum_{\gamma,\gamma'(\mathbf{r}_{0} \to \mathbf{r},t)} A_{\gamma} A_{\gamma'} \exp\left(\frac{i}{\hbar} \left(S_{\gamma} - S_{\gamma'}\right)\right)$$

$$\times \exp\left[\frac{i}{\hbar} \left(-\frac{\mathbf{q}}{2} \left(\mathbf{p}_{0}^{\gamma} + \mathbf{p}_{0}^{\gamma'}\right) + \Delta S_{\gamma}\right) - i\frac{\pi}{2} \left(\mu_{\gamma} - \mu_{\gamma'}\right)\right], \quad (3.17)$$

with \mathbf{r}_0 , \mathbf{q} , \mathbf{p}_0^{γ} and $\mathbf{p}_0^{\gamma'}$ defined after Eq. (3.6). To treat this quantity like the survival probability on the level of the diagonal approximation for chaotic systems we need to know more about the effect of the perturbation. We summarise here results from Refs. [15, 17, 18]. The perturbation is given by

$$\Delta S_{\gamma} = \int_{0}^{t} dt' L_{\gamma}^{\Sigma} \left(t' \right) \tag{3.18}$$

with the Lagrangian $L_{\gamma}^{\Sigma}\left(t'\right)$, i.e. the difference between the kinetic and potential energy of the perturbation Σ . In the case of a perturbation potential Σ , Eq. (3.18) simplifies to

$$\Delta S_{\gamma}(t) = -\int_{0}^{t} dt' \, \Sigma \left[\mathbf{q}_{\gamma} \left(t' \right), t' \right]. \tag{3.19}$$

We want to study now the average phase difference resulting from the perturbation. The average can be understood in this context as the average in the phase space over trajectories γ with different initial conditions like in the case of the crossing-angle distribution in the last chapter. Alternatively, one can fix γ and consider an average over an ensemble of different perturbations Σ . When the action difference results from a huge number of uncorrelated interactions of the particle with the disorder potential, $\Delta S_{\gamma}(t)/t$ is distributed according to the central limit theorem as Gaussian random variable and the variance of $\Delta S_{\gamma}(t)$ is given by $t\int_{-\infty}^{\infty} d\tau C(\tau)$, where $C(\tau) \equiv \langle L_{\gamma}^{\Sigma}(\tau) L_{\gamma}^{\Sigma}(0) \rangle$ is the time correlation of the perturbation. Assuming that the mean value of $\Delta S_{\gamma}(t)$ is zero, that the perturbation thus leads in average to no additional action difference, this implies

$$\left\langle \exp\left(\frac{i}{\hbar}\Delta S_{\gamma}\right)\right\rangle = \exp\left(-\frac{\left\langle \Delta S_{\gamma}^{2}\right\rangle}{2\hbar^{2}}\right) = \exp\left(-\frac{t}{2\tilde{t}}\right),$$
 (3.20)

where

$$\frac{1}{\tilde{t}} = \frac{1}{\hbar^2} \int_{-\infty}^{\infty} d\tau C(\tau). \tag{3.21}$$

To illustrate this treatment of the perturbation we consider a possible realisation by a quenched static disorder potential

$$\Sigma(\mathbf{r}) = \sum_{\alpha=1}^{N_i} \frac{u_{\alpha}}{2\pi \xi^2} \exp\left[-\frac{1}{2\xi^2} (\mathbf{r} - \mathbf{R}_{\alpha})^2\right].$$
 (3.22)

It is given by N_i random impurities in a cavity of an area A with the Gaussian profile characterised by a finite correlation length ξ , see [15, 18]. The independent impurities can be assumed to be uniformly distributed at positions \mathbf{R}_{α} with the densities $n_i = N_i/A$ and strengths u_{α} obeying $\langle u_{\alpha} u_{\beta} \rangle = u^2 \delta_{\alpha\beta}$.

The action differences ΔS_{γ} accumulated by segments of γ separated by distances larger than ξ are regarded for sufficiently small ξ as uncorrelated. Consequently the stochastic accumulation of ΔS_{γ} along γ can be described by a random process, resulting in a Gaussian distribution of the action difference ΔS_{γ} . This yields the previous result (3.20). Note that the average here is over the ensemble of the disorder potentials [15, 18]. For the potential in Eq. (3.22) the decay time \tilde{t} in Eq. (3.20) can be calculated explicitly. In this case the correlation function is given by

$$C_{\Sigma}\left(\left|\mathbf{r}-\mathbf{r}'\right|\right) = \left\langle \Sigma\left(\mathbf{r}(t)\right) \Sigma\left(\mathbf{r}(t')\right) \right\rangle = \frac{u^{2}n_{i}}{4\pi\xi^{2}} \exp\left[-\frac{1}{4\xi^{2}} \left(\mathbf{r}-\mathbf{r}'\right)^{2}\right], \quad (3.23)$$

and it depends only on the difference between $\mathbf{r} = \mathbf{r}(t)$ and $\mathbf{r}' = \mathbf{r}(t')$. Using then ergodicity of the classical flow and substituting time averages in Eq. (3.21) by the integration over the cavity domain we obtain for the decay time \tilde{t}_{ξ} the relation [18]

$$\tilde{t}_{\xi} = \sqrt{2\pi} \ k \tilde{\epsilon} \tilde{t}_{\delta}. \tag{3.24}$$

Here, $\tilde{t}_{\delta} = \hbar^3/(n_i u^2 m)$ is the quantum elastic scattering time for the white-noise case of δ -scatterers. Note that for $k\xi \gg 1$, \tilde{t}_{ξ} coincides with the elastic scattering time obtained quantum mechanically within the first Born approximation for the disorder potential (3.22). In the limit $k\xi \leq 1$, where the semiclassical treatment of disorder effects in terms of unperturbed trajectories is no longer valid, Eq. (3.20) can still be used but with \tilde{t}_{ξ} replaced by \tilde{t}_{δ} .

With (3.20) it is now possible to obtain $m_{\text{diag}}(t)$, i.e. m(t) in diagonal approximation. After inserting Eq. (3.20) into Eq. (3.17) we obtain [15]:

$$m_{\text{diag}}(t) = \left(\frac{1}{2\pi\hbar}\right)^{2} \int d\mathbf{r} d\mathbf{r}_{0} d\mathbf{q} \,\psi_{0}\left(\mathbf{r}_{0} + \frac{\mathbf{q}}{2}\right) \psi_{0}^{*}\left(\mathbf{r}_{0} - \frac{\mathbf{q}}{2}\right)$$

$$\sum_{\gamma(\mathbf{r}_{0} \to \mathbf{r}, t)} \left|A_{\gamma}\right|^{2} \exp\left(-\frac{i}{\hbar}\mathbf{q}\mathbf{p}_{0}^{\gamma}\right) \exp\left(-\frac{t}{2\tilde{t}}\right). \tag{3.25}$$

In the same way as for the survival probability, see Eqs. (3.9, 3.12), we obtain

$$m_{\text{diag}}(t) = \left\langle \exp\left(-\frac{t}{2\tilde{t}}\right) \right\rangle_{\mathbf{r}_0, \mathbf{p}_0},$$
 (3.26)

that again simplifies for small energy dispersion around E_0 to

$$m_{\text{diag}}(t) = \exp(-\Gamma t),$$
 (3.27)

with the decay rate $\Gamma \equiv 1/(2\tilde{t}(E_0))$. As our expressions for the fidelity amplitude depend on Γ , we will also use in the following the notation $m(t; \Gamma)$ instead of m(t). Equation (3.27) represents the exponential, so-called Fermi Golden Rule decay in the universal regime [15, 19, 20].

As we just introduced the Fermi Golden Rule decay we want to give here a brief overview of the decay regimes of the fidelity: Due to Eq. (3.17), the fidelity M(t), Eq. (3.14), can be expressed semiclassically as

$$\begin{split} M_{\rm sc}(t) &= \left(\frac{1}{2\pi\hbar}\right)^4 \left\langle \int d\mathbf{r} \, d\mathbf{q} \, d\mathbf{q} \, d\mathbf{\bar{r}} \, d\mathbf{q} \, d\mathbf{\bar{r}} \, d\mathbf{\bar{q}} \, \psi_0 \left(\mathbf{r}_0 + \frac{\mathbf{q}}{2}\right) \psi_0^* \left(\mathbf{r}_0 - \frac{\mathbf{q}}{2}\right) \psi_0^* \left(\mathbf{\bar{r}}_0 + \frac{\mathbf{\bar{q}}}{2}\right) \right. \\ &\times \psi_0 \left(\mathbf{\bar{r}}_0 - \frac{\mathbf{\bar{q}}}{2}\right) \sum_{\substack{\gamma_1 \ (\mathbf{r}_0 \to \mathbf{r}, \ t), \ \gamma_2 \ (\mathbf{\bar{r}}_0 \to \mathbf{\bar{r}}, \ t), \ \gamma_1' \ (\mathbf{r}_0 \to \mathbf{r}, \ t), \ \gamma_2' \ (\mathbf{\bar{r}}_0 \to \mathbf{\bar{r}}, \ t), \\ &\times \exp\left[\frac{i}{\hbar} \left(S_{\gamma_1} - S_{\gamma_1'} - S_{\gamma_2} + S_{\gamma_2'} - \frac{\mathbf{q}}{2} \left(\mathbf{p}_0^{\gamma_1} + \mathbf{p}_0^{\gamma_1'}\right) + \frac{\mathbf{\bar{q}}}{2} \left(\mathbf{p}_0^{\gamma_2} + \mathbf{p}_0^{\gamma_2'}\right)\right)\right] \\ &\times \exp\left[\frac{i}{\hbar} \left(\Delta S_{\gamma_1} - \Delta S_{\gamma_2}\right) - i\frac{\pi}{2} \left(\mu_{\gamma_1} - \mu_{\gamma_1'} - \mu_{\gamma_2} + \mu_{\gamma_2'}\right)\right]\right). \end{split} \tag{3.28}$$

Three main decay regimes for M(t) are distinguished, depending on the strength of the perturbation Σ : In the limit of a weak perturbation, i.e. if Σ is smaller than the quantum mean level spacing $\Delta(E)$, the fidelity decay is Gaussian characterising the perturbative regime [19–21]. As in this regime the perturbation dependence of M(t)has to be resolved on scales smaller than the mean level spacing the behaviour of M(t) cannot be yet predicted in this regime semiclassically. This regime can only be described by RMT within linear response with respect to the perturbation [22] and with supersymmetric techniques [23, 24]. For perturbations of the order of or larger than $\Delta(E)$, the decay is predominantly exponential, $M(t; \Gamma) \approx e^{-2\Gamma t}$, with a decay constant Γ that can be obtained by Fermi's golden rule [19]. The corresponding perturbation range is hence called the Fermi golden rule (FGR) regime [15, 19, 20]. For strong perturbations the decay is still exponential in time, but with a Σ -independent decay rate given by the Lyapunov exponent λ of the classically chaotic counterpart of the quantum system characterising the Lyapunov regime [15, 17]. The last two regimes were accessed semiclassically within diagonal approximation in the cited literature. For the first one additionally RMT results [22] and results from supersymmetry calculations exist [23, 24]. For a review of the extensive literature on fidelity decay see Ref. [25]. All the regimes given here refer usually to

global perturbations affecting the whole system. Recently the effect of local perturbations, e.g. local boundary deformations as in the right panel of Fig. 1.6 was studied, see for example [26, 27].

In this section we introduced semiclassical expressions for the survival probability and the fidelity and calculated both quantities in diagonal approximation. Now we want to turn to non-diagonal contributions to the double sums in Eqs. (3.7, 3.17).

3.2 Unitarity in Semiclassics

We now want to analyse quantum corrections to the survival probability and the fidelity amplitude. In this context we first explain the unitarity problems occurring when using previously developed techniques to calculate double sums considering as example the survival probability and afterwards show how to overcome them by introducing so-called one-leg-loops. As the corresponding calculation of the contributions to the fidelity amplitude is very similar we will afterwards just briefly explain the differences between the two cases and give the results. In order to simplify the presentation we restrict to localised wave packets. A generalisation to extended wave packets is straightforward by taking the phase-space average (3.10) of the results in the localised case, as explained in the last section.

As in the last chapter, for systems with time-reversal symmetry, leading-order quantum corrections to $\rho_{\rm diag}(t)$ arise from the double sum over orbits in Eq. (3.7), by considering correlated orbit pairs depicted as full and dashed line in Fig. 3.1a, The ingredients for determining the contribution of these pairs within the phase-space approach are given for general orbit pairs in Eqs. (2.54–2.56). We repeat them here for the orbit pair depicted in Fig. 3.1a: The duration of the encounter is $t_{\rm enc} = \lambda^{-1} \ln(c^2/|su|)$, the action difference $S_{\gamma} - S_{\gamma'} = su$ between orbit and its partner and the density of encounters

$$w_{2ll}(u, s, t) = \frac{(t - 2t_{enc})^2}{2\Omega(E)t_{enc}}.$$
 (3.29)

The index "2ll" is an abbreviation for "two-leg loops" because the configuration depicted in Fig. 3.1a possesses two links connecting the encounter to the initial and final point of the orbit.

We additionally take into account that the survival probability is, as discussed before Eq. (2.47), augmented by the factor $e^{t_{\rm enc}/\tau_D}$. Having characterised now the partner orbits of one orbit γ we perform the sum over γ by taking $|A_{\gamma}|^2$ as Jacobian like in Eq. (3.9) and get

$$\rho_{2ll}(t) = \int_{-c}^{c} ds \, du \, e^{(-t + t_{enc})/\tau_D} w_{2ll}(u, s, t) \, e^{(i/\hbar)us}. \tag{3.30}$$

Using the rules for performing the *s*, *u*-integrals explained before and in Eq. (2.59), we obtain the contribution from the configuration depicted in Fig. 3.1a to $\rho(t)$:

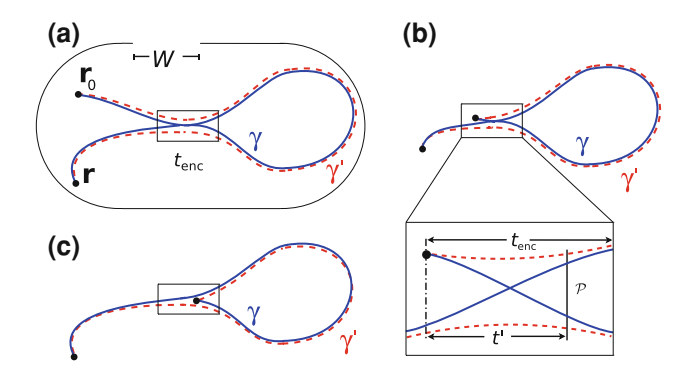


Fig. 3.1 Pairs of correlated classical trajectories γ (full line) and γ' (dashed) generating the leading quantum corrections to the classical decay probability. While in panel **a** the encounter region (box) connects a loop with two legs, the paths begin or end inside the encounter region (one-leg-loops) in **b** with and in **c** without a self-crossing in configuration space. The zoom into the encounter region in **b** depicts the position of the Poincaré surface of section used

$$\rho_{2ll}(t) = e^{-t/\tau_D} \left(-2\frac{t}{T_H} + \frac{t^2}{2\tau_D T_H} \right). \tag{3.31}$$

The term quadratic in t coincides with the first-order quantum correction found within supersymmetry in Refs. [11–13], see also (3.4). However, the linear term in Eq. (3.31) violates unitarity, since it does not vanish upon closing the system, i.e. as $\tau_D \to \infty$.

To cure this we have to consider a new type of diagrams. These orbit pairs, to which we refer as "one-leg-loops" (1ll), are characterised by an initial or final point inside the encounter region, see Fig. 3.1b, c. They are relevant for open orbits starting or ending *inside V* and hence have not arisen in conductance treatments based on lead-connecting paths in the last chapter, since for an encounter at the opening the exit of one encounter stretch implies the exit of the other one. They also could not occur when periodic orbits are involved.

To evaluate their contribution we consider as additional variable the time t' between the initial or final point of the trajectory and the Poincaré surface of section \mathcal{P} , defined in the zoom into Fig. 3.1b that is shorther than t_s . Then

$$\bar{t}_{\text{enc}}(t', u) = t' + \lambda^{-1} \ln(c/|u|)$$
 (3.32)

with $0 < t' < \lambda^{-1} \ln(c/|s|)$, i.e. $\bar{t}_{\rm enc}(t', u)$ is shorter than $t_{\rm enc}(u, s) = \lambda^{-1} \ln(c^2/|su|)$ considered before. The density of encounters is

$$w_{111}(u, s, t) = 2 \int_0^{\lambda^{-1} \ln(c/|s|)} dt' \frac{t - 2\bar{t}_{enc}(t', u)}{\Omega(E)\bar{t}_{enc}(t', u)}.$$
 (3.33)

The derivation of the last equation is analogous to the one described before Eq. (2.56): The prefactor 2 accounts for the two cases of the orbit beginning or ending in an encounter region. The factor $(t - 2\bar{t}_{enc}(t', u))$ accounts for the freedom where on the

orbits in Fig. 3.1b, c to put the encounter stretch that is not located at the beginning or end of the orbit and the additional time integral for the additional freedom to cut a part of the encounter stretch. The survival probability correction due to the proximity of the stretches is given by $e^{\bar{t}_{enc}/\tau_D}$. The sum over original orbits is again performed by considering $\left|A_{\gamma}\right|^2$ as Jacobian for the transformation from ${\bf r}$ to ${\bf p}_0^{\gamma}$ yielding ¹

$$\rho_{111}(t) = \int_{-c}^{c} ds \, du \, e^{(-t + \bar{t}_{enc})/\tau_D} w_{111}(u, s, t) e^{(i/\hbar)us}. \tag{3.34}$$

To evaluate the integrals we substitute [29] $t'' = t' + \lambda^{-1} \ln(c/|u|)$, $\sigma = c/u$ and $x = su/c^2$, with integration domains -1 < x < 1, $1 < \sigma < e^{\lambda t''}$ and $0 < t'' < \lambda^{-1} \ln(1/|x|)$. Note that the limits for t' include the case when the paths do not have a self-crossing in configuration space, for an example see Fig. 3.1c. At first we perform the σ -integral, its contribution cancels essentially the $\bar{t}_{enc}(t', u)$ in the denominator and we obtain

$$\rho_{111}(t) = \frac{4c^{2}\lambda}{\pi\hbar T_{H}} e^{-t/\tau_{D}} \int_{0}^{1} dx \cos\left(\frac{xc^{2}}{\hbar}\right) \int_{0}^{\frac{1}{\lambda}\ln(1/x)} dt''(t - 2t'') e^{t''/\tau_{D}}
= e^{-t/\tau_{D}} \left(t - 2\frac{d}{d\tau_{D}^{-1}}\right) \frac{4c^{2}\lambda\tau_{D}}{\pi\hbar T_{H}} \int_{0}^{1} dx \cos\left(\frac{xc^{2}}{\hbar}\right) \left(x^{-\frac{1}{\lambda\tau_{D}}} - 1\right). \quad (3.35)$$

The (-1) in the last curved bracket just yields as a function of t a highly oscillating contribution that is cancelled by the t-average. For the other term the integration over x can be performed by parts, neglecting again in the second step highly oscillating terms, yielding

$$\rho_{\text{III}}(t) = e^{-t/\tau_D} \left(t - 2 \frac{d}{d\tau_D^{-1}} \right) \frac{4c^2 \lambda \tau_D}{\pi \hbar T_H} \left(\frac{\sin c^2/\hbar}{c^2/\hbar} + \frac{1}{\lambda \tau_D} \int_0^1 dx \frac{\sin(c^2 x/\hbar)}{c^2 x/\hbar} \right) \\
= \frac{4t}{\pi T_H} e^{-t/\tau_D} \int_0^{c^2/\hbar} dy \frac{\sin y}{y} \approx \frac{4t}{\pi T_H} e^{-t/\tau_D} \int_0^\infty dy \frac{\sin y}{y} = \frac{2t}{T_H} e^{-t/\tau_D}. \tag{3.36}$$

It precisely cancels the linear term in $\rho_{2ll}(t)$, Eq. (3.31), i.e.

$$\rho_{2ll}(t) + \rho_{1ll}(t) = e^{-t/\tau_D} \frac{t^2}{2\tau_D T_H},$$
(3.37)

recovering unitarity! We recognise that this first quantum correction is positive, i.e. the survival probability is quantum mechanically enhanced compared to the classical one, again an effect of weak localisation resulting here from the survival probability enhancement during the encounter.

¹ The action difference depends [28] on the actual length of the encounter stretches $\bar{t}_{\rm enc}$ only by additional exponentially small summands $sue^{-n\lambda\bar{t}_{\rm enc}}$ with $n\in\mathbb{N}$, that can be shown to yield no further contribution by following the steps presented here for the leading contribution to the action difference.

After having calculated the first quantum correction to the survival probability we now want to consider the analogous quantum correction to the fidelity amplitude. As already mentioned quantum corrections to the classical result for the fidelity amplitude were studied by RMT and supersymmetrical approaches in the FGR-regime. For the GUE case, the result for the fidelity amplitude in the universal FGR regime takes the particularly compact form

$$m_{\text{GUE}}(\tau; \gamma) = \begin{cases} -\frac{\partial}{\partial \gamma} \left(\frac{e^{-\gamma}}{\gamma \tau} \sinh(\gamma \tau) \right) & \text{for } \tau \leq 1, \\ -\frac{\partial}{\partial \gamma} \left(\frac{e^{-\gamma \tau}}{\gamma \tau} \sinh(\gamma) \right) & \text{for } \tau > 1, \end{cases}$$
(3.38)

with $\gamma = \Gamma t$, $\tau = t/T_H$. In particular, these supersymmetrical calculations revealed a fidelity recovery at the Heisenberg time, that however cannot be completely understood semiclassically like all effects occurring beyond the Heisenberg time that we encountered up to now. In the orthogonal case a closed form of $m(t; \Gamma)$ cannot be obtained, the first quantum correction is given by

$$m_{\text{GOE}}^{q_1}(t; \Gamma) = -\frac{\Gamma t^2}{T_H} e^{-\Gamma t}.$$
 (3.39)

In the semiclassical calculation of quantum corrections to the classical result for the fidelity amplitude the only difference compared to the one for the survival probability results from the fact that the correction of the survival probability due to the fact that the two encounter stretches escape in a correlated manner is replaced by a correction due to the fact that the two encounter stretches traverse the disorder potential in a correlated way: As the stretches of a certain encounter are on classical scales very close together, one can assume that they traverse a region with the same disorder potential. The corrections for the survival probability and for the fidelity amplitude possess different functional forms. To calculate the phase difference induced by the disorder potential in the presence of encounters we here consider the orbit pair depicted in Fig. 3.1a. To this end we split the orbit into parts consisting of two encounter-stretches e(i) and three links l(i),

$$\left\langle \exp\left[\frac{i}{\hbar}\Delta S_{\gamma}\right]\right\rangle = \left\langle \exp\left[\frac{i}{\hbar}\left(\sum_{i=1}^{3}\Delta S_{l(i)} + \sum_{i=1}^{2}\Delta S_{e(i)}\right)\right]\right\rangle$$
$$= \left\langle \exp\left[\frac{i}{\hbar}\left(\sum_{i=1}^{3}\Delta S_{l(i)} + 2\Delta S_{e(1)}\right)\right]\right\rangle. \tag{3.40}$$

In the last line we assume that, in the semiclassical limit and for a fixed disorder correlation length ξ , the nearly parallel encounter stretches in the box are so close to each other (at a distance smaller than ξ) that they experience the same perturbation. Considering a Gaussian phase distribution for each orbit segment (encounter stretch and three links) and neglecting further correlations between the different segments we finally apply Eq. (3.20) to every part of the orbit individually and obtain

$$\left\langle \exp\left(\frac{i}{\hbar}\Delta S_{\gamma}\right)\right\rangle = \exp\left[-\left(\frac{\sum_{i=1}^{3}\left\langle\Delta S_{l(i)}^{2}\right\rangle}{2\hbar^{2}} + 4\frac{\left\langle\Delta S_{e(1)}^{2}\right\rangle}{2\hbar^{2}}\right)\right]$$

$$= \exp\left[-\Gamma\left(t + 2t_{\text{enc}}\right)\right]. \tag{3.41}$$

Note that the correction due to traversing correlated disorder is here given by $\exp(-2\Gamma t_{\rm enc})$ whereas it was given by $\exp(\Gamma t_{\rm enc})$ for the survival probability with $\Gamma = 1/\tau_D$.

Repeating now the steps of the calculation of the survival probability for two-legand one-leg-loops we indeed recover the first quantum correction given in (3.39) [4]. The corresponding contribution to the fidelity $M_{\rm GOE}(t)$ is, when including also the diagonal term, given by

$$M_{\text{GOE}}(t) = \exp(-2\Gamma t) \left(1 - 2\frac{\Gamma t^2}{T_H} \right). \tag{3.42}$$

Having treated the leading quantum correction in t/T_H in the orthogonal case, we want to generalise this in the next section to more complicated diagrams.

3.3 Higher-Order Contributions and the Effect of Spin-Orbit Interaction

Up to now we showed how to obtain semiclassically for chaotic systems the first quantum correction in t/T_H to the survival probability and the fidelity amplitude. As already explained in Chap. 2 further corrections result from orbit pairs differing in several encounter regions involving an arbitrary number of encounter stretches. In this section we show how to obtain general expressions for further quantum corrections to $\rho_{\rm cl}(t)$. Afterwards we explain how to reproduce semiclassically the results from the symplectic ensemble of RMT mentioned in the introduction. These results can be obtained semiclassically by including a classically weak spin-orbit-interaction term into the Hamiltonian describing the considered system. We will concentrate in this presentation on the survival probability. Similar results can however also be obtained in the case of the fidelity amplitude and are published in [4].

3.3.1 Higher-Order Contributions

The orbital configurations yielding non-diagonal contributions can then be separated into three classes:

A where the start and end points are outside of the encounters (211),

B where either the start or end point is inside an encounter (111) and

C where both the start and end point are inside different encounters (011).²

The cases A and B were introduced in the last section, while case C involves at least two independent encounters and thus could not occur there.

3.3.1.1 Case A

This contribution can be written as

$$\rho_{\mathbf{v},\mathbf{A}}(t) = N(\mathbf{v}) \int_{-c}^{c} d\mathbf{s} \, d\mathbf{u} \, w_{\mathbf{v},\mathbf{A}}(\mathbf{u},\mathbf{s},t) e^{-\mu t} e^{\sum_{\alpha=1}^{V} (l_{\alpha}-1)\mu t_{\text{enc}}^{\alpha}} e^{\frac{i}{\hbar} \mathbf{u} \mathbf{s}}, \qquad (3.43)$$

with $\mu \equiv 1/\tau_D$, the number of structures $N(\mathbf{v})$, the density of encounters for open orbits $w_{\mathbf{v},\mathbf{A}}(\mathbf{u},s,t)$, the action difference $\Delta S = \mathbf{u}s$ and the correction to the survival probability of the trajectories $\mathrm{e}^{\sum_{\alpha=1}^V (l_\alpha-1)\mu t_{\mathrm{enc}}^\alpha}$ due to the proximity of encounter stretches during the encounters. These quantities were introduced in the last chapter in Eqs. (2.54–2.56). To calculate the semiclassical contribution we will rewrite Eq. (3.43) as

$$\rho_{\mathbf{v},\mathbf{A}}(t) = N(\mathbf{v}) \int_{-c}^{c} d\mathbf{s} \, d\mathbf{u} \, z_{\mathbf{v},\mathbf{A}}(\mathbf{u},\mathbf{s},t) e^{-\mu t} e^{\frac{\mathrm{i}}{\hbar} \mathbf{u} \mathbf{s}}, \qquad (3.44)$$

where $z_{\mathbf{v},\mathbf{A}}(\mathbf{u},\mathbf{s},t)$ is an augmented weight including the term from the survival probability correction of the encounters

$$z_{\mathbf{v},\mathbf{A}}(\boldsymbol{u},\boldsymbol{s},t) = w_{\mathbf{v},\mathbf{A}}(\boldsymbol{u},\boldsymbol{s},t)e^{\sum_{\alpha}(l_{\alpha}-1)\mu t_{\text{enc}}^{\alpha}}$$

$$\approx \frac{\left(t - \sum_{\alpha=1}^{\infty} l_{\alpha}t_{\text{enc}}^{\alpha}\right)^{L} \prod_{\alpha=1}^{V} \left(1 + (l_{\alpha}-1)\mu t_{\text{enc}}^{\alpha}\right)}{L!\Omega^{L-V} \prod_{\alpha=1}^{V} t_{\text{enc}}^{\alpha}},$$
(3.45)

where we have expanded in the second line the exponent to first order in the encounter times. We can now use the fact that the semiclassical contribution comes from terms where the encounter times in the numerator cancel those in the denominator exactly, see the text before Eq. (2.59) in the last chapter. Keeping only those terms, we then get a factor of $(2\pi\hbar)^{L-V}$ from the integrals over s and u and obtain the result for trajectories described by the vector \mathbf{v} of interest. This implies that for obtaining contributions to the survival probability of the order \hbar^n we have to consider diagrams with n = L - V.

We want to study now as example the case n=2. We first consider one 3-encounter shown in Fig. 3.2a. The density for this type of encounter is

$$w_{(3)^{1},A}(\mathbf{u},\mathbf{s},t) = \frac{(t-3t_{\rm enc})^{3}}{6\Omega^{2}t_{\rm enc}},$$
(3.46)

² The case where start and end point are inside the same encounter is negligible here as it only contributes for classically very close initial and final points.

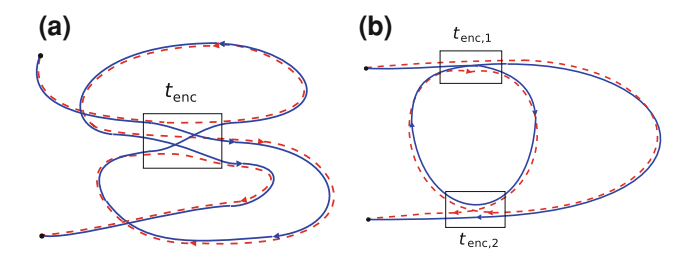


Fig. 3.2 Scheme of orbit pairs that do not require time-reversal symmetry and give higher-order corrections: **a** a single 3-encounter, **b** a double 2-encounter. The trajectories γ (*full line*) and γ' (*dashed*) connect the points \mathbf{r}_0 with \mathbf{r} in a time t, and they differ by the way they are connected in the encounter regions marked by boxes

where we use the notation $(l)^{v_l}$ to indicate that the trajectory has v_l *l*-encounters. We insert $w_{(3)^1,A}(\boldsymbol{u},\boldsymbol{s},t)$ in Eq. (3.43) and modify the classical survival probability by a factor $e^{2\mu t_{\rm enc}}$. In the case of time-reversal symmetry there are four possible structures in this case [30], and the final result is

$$\rho_{(3)^1,A}(t) = 4e^{-t/\tau_D} \left(-\frac{3t^2}{2T_H^2} + \frac{t^3}{3\tau_D T_H^2} \right), \tag{3.47}$$

which is four times the contribution obtained in the case of no time-reversal symmetry, where only one structure exists [30]. For a double 2-encounter shown in Fig. 3.2b, we define two encounter times: $t_{\text{enc},1} \approx \frac{1}{\lambda} \ln \frac{c^2}{|u_1s_1|}$ and $t_{\text{enc},2} \approx \frac{1}{\lambda} \ln \frac{c^2}{|u_2s_2|}$.

The density of such a double-encounter is given by

$$w_{(2)^2,A}(\mathbf{u}, \mathbf{s}, t) = \frac{(t - 2t_{\text{enc}})^4}{24\Omega^2 t_{\text{enc}, 1} t_{\text{enc}, 2}},$$
(3.48)

with $t_{\rm enc} = t_{\rm enc,1} + t_{\rm enc,2}$. In this case the number of possible structures for systems with time-reversal symmetry is 5. The contribution of such orbits to the survival probability is obtained by inserting everything into Eq. (3.43)

$$\rho_{(2)^2,A}(t) = 5e^{-t/\tau_D} \left(2\frac{t^2}{T_H^2} - \frac{2t^3}{3\tau_D T_H^2} + \frac{t^4}{24\tau_D^2 T_H^2} \right), \tag{3.49}$$

which is five times the contribution obtained in the case of no time-reversal symmetry, where only one structure exists [30].

The total contribution of structures with L-V=2 of 2ll's in the presence of time-reversal symmetry is then

$$\rho_{2,A}(t) = e^{-t/\tau_D} \left(4 \frac{t^2}{T_H^2} - \frac{2t^3}{\tau_D T_H^2} + \frac{5t^4}{24\tau_D^2 T_H^2} \right). \tag{3.50}$$

3.3.1.2 Case B

Now we consider the generalisation of the one-leg-loops introduced in the last section to orbit pairs differing in an arbitrary number of encounters with an arbitrary number of stretches involved. This contribution can be written as

$$\rho_{\mathbf{v},\mathbf{B}}(t) = N(\mathbf{v}) \int_{-c}^{c} d\mathbf{s} \, d\mathbf{u} \, z_{\mathbf{v},\mathbf{B}}(\mathbf{u},\mathbf{s},t) e^{-\mu t} e^{\frac{\mathrm{i}}{\hbar} \mathbf{u} \mathbf{s}}. \tag{3.51}$$

The augmented weight function $z_{\mathbf{v},\mathbf{B}}(\mathbf{u},s,t)$ is composed like for case A out of the weight function $w_{\mathbf{v},\mathbf{B}}(\mathbf{u},s,t)$ and the survival probability correction due to the proximity of the encounter stretches. To determine $w_{\mathbf{v},\mathbf{B}}(\mathbf{u},s,t)$ we note: Compared to case A one encounter overlaps with the start or end of the trajectory, we have thus like for one 2-encounter in the last section one link fewer (L in total) and an extra integral over the position of the encounter relative to the starting point of the trajectory like in Eq. (3.33). To determine the number of possible structures in this case we start with a closed periodic orbit, and divide by the overcounting factor of L, as in the case of the spectral form factor in the last chapter. We can then cut each of the L links in turn and move the encounter on either side of the cut to either the start or the end. In total we obtain $l_{\alpha'}$ copies of the same 1ll involving the encounter at the beginning or at the end of the trajectory. The augmented weight can then be expressed as a sum over the different possibilities, each of which involves an integral over the distance from the Poincaré surface of section to the initial or final point, $t_{\alpha'}$,

$$z_{\mathbf{v},\mathbf{B}}(\boldsymbol{u},\boldsymbol{s},t) = 2\sum_{\alpha'=1}^{V} l_{\alpha'} \int_{0}^{\frac{1}{\lambda} \ln \left(\frac{c}{\max_{j} |s_{\alpha',j}|}\right)} dt_{\alpha'} \frac{\left(t - \sum_{\alpha \neq \alpha'} l_{\alpha} t_{\text{enc}}^{\alpha} - l_{\alpha'} \bar{t}_{\text{enc}}^{\alpha'}\right)^{L-1}}{L! \Omega^{L-V} \prod_{\alpha \neq \alpha'} t_{\text{enc}}^{\alpha} \bar{t}_{\text{enc}}^{\alpha'}} \times e^{\sum_{\alpha=1,\alpha \neq \alpha'}^{V} (l_{\alpha}-1)\mu t_{\text{enc}}^{\alpha} + (l_{\alpha'}-1)\mu \bar{t}_{\text{enc}}^{\alpha'}},$$
(3.52)

where the time of encounter α' is related to the starting position via

$$\bar{t}_{\text{enc}}^{\alpha'} = t_{\alpha'} + \frac{1}{\lambda} \ln \left(\frac{c}{\max_j |u_{\alpha',j}|} \right). \tag{3.53}$$

Because of the integrals over the position of the encounter at the start or end of the trajectory, the semiclassical calculation of this contribution differs from the one in case A. It can be however shown that this additional integral can, when calculating the contribution to the survival probability, be effectively replaced by an additional factor $t_{\rm enc}^{\alpha'}$. In order to understand this one can perform the same substitution as in Eq. (3.35) for $s_{\alpha'}$, $u_{\alpha'}$ and $\bar{t}_{\rm enc}^{\alpha'}$. By comparing this with the recipe just given we see that the $t_{\alpha'}$ -integral yields effectively a $t_{\rm enc}^{\alpha'}$. This change of variables can be done for each $(u_{\alpha'}, s_{\alpha'}, t_{\alpha'})$, giving effectively a factor of $t_{\rm enc}^{\alpha'}$ for each integral over $t_{\alpha'}$, so that the augmented weight can be written as

$$z_{\mathbf{v},\mathbf{B}}(\mathbf{u},\mathbf{s},t) \approx \frac{2\left(\sum_{\alpha} l_{\alpha} t_{\text{enc}}^{\alpha}\right) \left(t - \sum_{\alpha} l_{\alpha} t_{\text{enc}}^{\alpha}\right)^{L-1}}{L!\Omega^{L-V} \prod_{\alpha=1}^{V} t_{\text{enc}}^{\alpha}} \prod_{\alpha=1}^{V} \left(1 + (l_{\alpha} - 1)\mu t_{\text{enc}}^{\alpha}\right), \quad (3.54)$$

and treated as before.

Returning to our example we find that for a single 3-encounter, Eq. (3.54) corresponds to

$$z_{(3)^{1},B}(\boldsymbol{u},\boldsymbol{s},t) \approx \frac{(t-3t_{\rm enc})^{2}}{\Omega^{2}} (1+2\mu t_{\rm enc}).$$
 (3.55)

Multiplying by the number of possible structures, the resulting contribution for systems with time-reversal symmetry (3.51) is

$$\rho_{(3)^1,B}(t) = 4e^{-t/\tau_D} \left(\frac{t^2}{T_H^2}\right). \tag{3.56}$$

For the double 2-encounter the corresponding augmented weight is given by

$$z_{(2)^2,B}(\boldsymbol{u}, \boldsymbol{s}, t) \approx \frac{1}{3} \frac{(t - 2t_{\rm enc})^3}{\Omega^2 t_{\rm enc}^1} (1 + \mu t_{\rm enc}),$$
 (3.57)

yielding for time-reversal symmetric systems

$$\rho_{(2)^2,B}(t) = 5e^{-t/\tau_D} \left(\frac{t^3}{3T_H^2 \tau_D} - 2\frac{t^2}{T_H^2} \right).$$
 (3.58)

The multiplicity factors present only for time-reversal symmetry are here the same as for case A. The total contribution of 11l's for L-V=2 for systems with time-reversal symmetry is

$$\rho_{2,B}(t) = e^{-t/\tau_D} \left(\frac{5t^3}{3T_H^2 \tau_D} - 6\frac{t^2}{T_H^2} \right). \tag{3.59}$$

3.3.1.3 Case C

This contribution can be written as

$$\rho_{\mathbf{v},\mathbf{C}}(t) = \int_{-c}^{c} d\mathbf{s} \ d\mathbf{u} \ z_{\mathbf{v},\mathbf{C}}(\mathbf{u},\mathbf{s},t) e^{-\mu t} e^{\frac{\mathrm{i}}{\hbar} \mathbf{u} \mathbf{s}}. \tag{3.60}$$

For determining $z_{v,C}(u,s,t)$ we note: As one encounter overlaps with the start of the trajectory, and a second (different) encounter with the end of the trajectory, there is again one link fewer (L-1) in total and now we have two extra integrals over the position of the start and end encounters relative to the start and end point.

Also the number of such structures is different. To explain how to obtain this number we start with a closed periodic orbit, we can cut each of the L links in turn and move the encounters on either side of the cut to both the start and the end, as long as the link joins two different encounters. We therefore need to count the number of ways that this is possible for the different sizes of encounters that are linked. We record these numbers in a matrix $\mathcal{N}(\mathbf{v})$, where the elements $\mathcal{N}_{\alpha,\beta}(\mathbf{v})$ record the number of links (divided by L) linking encounter α with encounter β . In this case it is convenient to include $\mathcal{N}_{\alpha,\beta}(\mathbf{v})$ in the augmented weight function. The augmented weight, including these possibilities, can then be expressed as the following sum over the Oll encounters

$$z_{\mathbf{v},C}(\mathbf{u},\mathbf{s},t) = \sum_{\alpha',\beta'=1}^{V} \mathcal{N}_{\alpha',\beta'}(\mathbf{v}) \int dt_{\alpha'} dt_{\beta'} \frac{\left(t - \sum_{\alpha \neq \alpha',\beta'} l_{\alpha} t_{\text{enc}}^{\alpha} - l_{\alpha'} \bar{t}_{\text{enc}}^{\alpha'} - l_{\beta'} \bar{t}_{\text{enc}}^{\beta'}\right)^{L-2}}{(L-2)! \Omega^{L-V} \prod_{\alpha \neq \alpha',\beta'} t_{\text{enc}}^{\alpha} \bar{t}_{\text{enc}}^{\alpha'} \bar{t}_{\text{enc}}^{\beta'}} \times e^{\sum_{\alpha=1,\alpha \neq \alpha',\beta'}^{V} (l_{\alpha}-1)\mu t_{\text{enc}}^{\alpha} + (l_{\alpha'}-1)\mu \bar{t}_{\text{enc}}^{\alpha'} + (l_{\beta'}-1)\mu \bar{t}_{\text{enc}}^{\beta'}}$$
(3.61)

with the same limits of the time integrals as in Eq. (3.52). Again we can expand the exponent to first order in the encounter times and replace the time integrals by $t_{\text{enc}}^{\alpha'}t_{\text{enc}}^{\beta'}$

$$z_{\mathbf{v},C}(\boldsymbol{u},\boldsymbol{s},t) \approx \left(\sum_{\alpha',\beta'=1}^{V} \mathcal{N}_{\alpha',\beta'}(\mathbf{v}) t_{\text{enc}}^{\alpha'} t_{\text{enc}}^{\beta'}\right) \left(t - \sum_{\alpha=1}^{V} l_{\alpha} t_{\text{enc}}^{\alpha}\right)^{L-2} \times \frac{\prod_{\alpha=1}^{V} \left(1 + (l_{\alpha} - 1)\mu t_{\text{enc}}^{\alpha}\right)}{(L-2)!\Omega^{L-V} \prod_{\alpha=1}^{V} t_{\text{enc}}^{\alpha}},$$
(3.62)

and treat it as before.

In our example, for a single 3-encounter there cannot be such a contribution, as two different encounters are needed. For a double 2-encounter the augmented weight function for systems with time-reversal symmetry is given by

$$z_{(2)^2,C}(\mathbf{u}, \mathbf{s}, t) \approx 2 \frac{(t - 2t_{\text{enc}})^2}{\Omega^2} (1 + \mu t_{\text{enc}}).$$
 (3.63)

This yields the following contribution to the survival probability (3.60) in the presence of time-reversal symmetry

$$\rho_{(2)^2,C}(t) = e^{-t/\tau_D} \left(\frac{2t^2}{T_H^2} \right), \tag{3.64}$$

which is four times the contribution in the absence of time-reversal symmetry as can be obtained by examining the diagrams considered in Refs. [30–32].

Summing the contributions from the three cases yields the overall contribution in the unitary case due to these diagrams

$$\rho_{(2)^2+(3)^1}^{\text{GUE}}(t) = e^{-t/\tau_D} \left(1 + \frac{t^4}{24\tau_D^2 T_H^2} \right)$$
 (3.65)

and in the orthogonal case

$$\rho_{(2)^{1}+(2)^{2}+(3)^{1}}^{GOE}(t) = e^{-t/\tau_{D}} \left(1 + \frac{t^{2}}{2\tau_{D}T_{H}} - \frac{t^{3}}{3\tau_{D}T_{H}^{2}} + \frac{5t^{4}}{24\tau_{D}^{2}T_{H}^{2}} \right), \quad (3.66)$$

including also the diagonal contribution and the first quantum correction in the presence of time-reversal symmetry discussed in the last section.

3.3.2 Unitary Case

With these general expressions at hand we can easily calculate the contribution for each vector v for each of the three cases, as long as we know the numbers of possible trajectory structures. For cases A and B, these numbers can be found in Refs. [31, 32] and are repeated in the first four columns of Table 3.1. For case C we will go up to the sixth-order correction, L - V = 6, and for this we have at most three different types of l-encounters together in one diagram. It is useful to rewrite the sum over α and β as a sum over the components of the vector \mathbf{v} . $\mathcal{N}_{\alpha,\beta}(\mathbf{v})$ records the number of ways of cutting links that connect encounter α and β , in the periodic orbit structures described by v. However the important quantities are the sizes of the encounters α and β . Instead we record in $\mathcal{N}_{k,l}(\mathbf{v})$ the number of links that join an encounter of size k to an encounter of size l. If we number the encounters from 1 to V in order of their size, then we only need to know the numbers $\mathcal{N}_{l_1,l_2}(\mathbf{v})$, $\mathcal{N}_{l_1,l_V}(\mathbf{v})$ and $\mathcal{N}_{l_{V-1},l_V}(\mathbf{v})$, as the maximal number of different sized encounters in one diagram is three. Moreover $\mathcal{N}_{k,l}$ is symmetric, therefore we include in Table 3.1 both $\mathcal{N}_{k,l}$ and $\mathcal{N}_{l,k}$ together. Using a program to count and classify the possible permutation matrices one obtains the remaining columns in Table 3.1 for systems without time-reversal symmetry. Note that $\mathcal{N}_{l_1,l_2}(\mathbf{v})$, $\mathcal{N}_{l_1,l_V}(\mathbf{v})$ and $\mathcal{N}_{l_{V-1},l_V}(\mathbf{v})$ might describe the same encounter combinations, in this case we record their number in the leftmost column.

Table 3.1 allows us to obtain the following results for the quantum corrections to the classical decay for the unitary case

$$\rho_2(t) = \frac{e^{-\frac{t}{\tau_D}}}{T_H^2} \frac{t^4}{24\tau_D^2},\tag{3.67}$$

$$\rho_4(t) = \frac{e^{-\frac{t}{\tau_D}}}{T_H^4} \frac{t^6}{\tau_D^2} \left(\frac{1}{90} - \frac{t}{180\tau_D} + \frac{t^2}{1920\tau_D^2} \right),\tag{3.68}$$

v	L	V	$N(\mathbf{v})$	$\mathcal{N}_{l_1,l_2}(\mathbf{v})$	$\mathcal{N}_{l_1,l_V}(\mathbf{v})$	$\mathcal{N}_{l_{V-1},l_V}(\mathbf{v})$
$(2)^2$	4	2	1	1	21,00	νγ =1,νγ · · ·
$(2)^2$ $(3)^1$	3	1	1			
$(2)^4$	8	4	21	21		
$(2)^2(3)^1$	7	3	49	12	32	
$(2)^{1}(4)^{1}$	6	2	24	16		
$(3)^2$	6	2	12	8		
$(5)^1$	5	1	8			
$(2)^6$	12	6	1,485	1,485		
$(2)^4(3)^1$	11	5	5,445	2,664	2,592	
$(2)^3(4)^1$	10	4	3,240	984	1,920	
$(2)^2(3)^2$	10	4	4,440	464	2,624	960
$(2)^2(5)^1$	9	3	1,728	228	1,080	
$(2)^{1}(3)^{1}(4)^{1}$	9	3	2,952	552	760	1,080
$(3)^3$	9	3	464	380		
$(2)^{1}(6)^{1}$	8	2	720	360		
$(3)^1(5)^1$	8	2	608	360		
$(4)^2$	8	2	276	180		
$(7)^1$	7	1	180			

Table 3.1 The number of trajectory pairs and the number linking certain encounters for systems without time-reversal symmetry, for details see text

$$\rho_6(t) = \frac{e^{-\frac{t}{\tau_D}}}{T_H^6} \frac{t^8}{\tau_D^2} \left(\frac{1}{224} - \frac{89t}{22680\tau_D} + \frac{31t^2}{30240\tau_D^2} - \frac{t^3}{10080\tau_D^3} + \frac{t^4}{322560\tau_D^4} \right). \tag{3.69}$$

These results enable us to calculate the decay up to 8th order in t, giving as the final result

$$\rho_{\text{GUE}}(t) = e^{-\frac{t}{\tau_D}} \left[1 + \frac{t^4}{24\tau_D^2 T_H^2} + \frac{t^6}{90\tau_D^2 T_H^4} - \frac{t^7}{180\tau_D^3 T_H^4} + \left(\frac{1}{1920\tau_D^4 T_H^4} + \frac{1}{224\tau_D^2 T_H^6} \right) t^8 + \cdots \right].$$
(3.70)

3.3.3 Orthogonal Case

Similarly, we can find all possible permutation matrices and obtain Table 3.2 for systems with time-reversal symmetry. This gives us the result up to 7th order in t

v	L	V	$N(\mathbf{v})$	$\mathcal{N}_{l_1,l_2}(\mathbf{v})$	$\mathcal{N}_{l_1,l_V}(\mathbf{v})$	$\mathcal{N}_{l_{V-1},l_V}(\mathbf{v})$
$(2)^1$	2	1	1			
$(2)^2$	4	2	5	4		
$(3)^1$	3	1	4			
$(2)^3$	6	3	41	36		
$(2)^{1}(3)^{1}$	5	2	60	40		
$(4)^1$	4	1	20			
$(2)^4$	8	4	509	468		
$(2)^2(3)^1$	7	3	1,092	228	672	
$(2)^{1}(4)^{1}$	6	2	504	296		
$(3)^2$	6	2	228	148		
$(5)^1$	5	1	148			
$(2)^5$	10	5	8,229	7,720		
$(2)^3(3)^1$	9	4	23,160	8,220	12,256	
$(2)^2(4)^1$	8	3	12,256	1,884	7,480	
$(2)^1(3)^2$	8	3	10,960	5,024		3,740
$(2)^{1}(5)^{1}$	7	2	5,236	2,696		
$(3)^1(4)^1$	7	2	4,396	2,696		
$(6)^1$	6	1	1,348			
$(2)^6$	12	6	1,66,377	1,58,148		
$(2)^4(3)^1$	11	5	5,79,876	2,66,040	2,65,056	
$(2)^3(4)^1$	10	4	3,31,320	93,456	1,86,160	
$(2)^2(3)^2$	10	4	4,43,400	41,792	2,49,216	93,080
$(2)^2(5)^1$	9	3	1,67,544	19,872	98,712	
$(2)^{1}(3)^{1}(4)^{1}$	9	3	2,80,368	49,576	66,240	98,712
$(3)^3$	9	3	41,792	33,120		
$(2)^{1}(6)^{1}$	8	2	65,808	30,208		
$(3)^1(5)^1$	8	2	52,992	30,208		
$(4)^2$	8	2	24,788	15,104		
$(7)^1$	7	1	15,104			

Table 3.2 The number of trajectory pairs and the number linking certain encounters for systems with time-reversal symmetry

$$\rho_{\text{GOE}}(t) = e^{-\frac{t}{\tau_D}} \left[1 + \frac{t^2}{2\tau_D T_H} - \frac{t^3}{3\tau_D T_H^2} + \left(\frac{5}{24\tau_D^2 T_H^2} + \frac{1}{3\tau_D T_H^3} \right) t^4 \right. \\
\left. - \left(\frac{11}{30\tau_D^2 T_H^3} + \frac{2}{5\tau_D T_H^4} \right) t^5 + \left(\frac{41}{720\tau_D^3 T_H^3} + \frac{7}{12\tau_D^2 T_H^4} + \frac{8}{15\tau_D T_H^5} \right) t^6 \\
\left. - \left(\frac{29}{168\tau_D^3 T_H^4} + \frac{14}{15\tau_D^2 T_H^5} + \frac{16}{21\tau_D T_H^6} \right) t^7 + \dots \right]. \tag{3.71}$$

We can now compare these results with the predictions for the decay obtained using supersymmetry [12, 13], after expanding the integrals appearing there in powers of t/T_H , following steps indicated for example in Ref. [33]. The results of these expansions agree with Eqs. (3.70) and (3.71). Along with the cases with and without time-reversal symmetry, there has recently been interest in a semiclassical treatment corresponding to the symplectic RMT ensemble in different contexts, such as in spectral statistics [31] and in the quantum transmission through mesoscopic conductors in the Landauer-Büttiker approach [34–36]. There the symplectic case is reproduced semiclassically by including in the Hamiltonian a classically weak spin-orbit interaction.

3.3.4 Spin-Orbit Interaction and the Symplectic Case

In the following we study the effect of spin-orbit interaction on the survival probability. The spin-orbit interaction is accounted for by replacing the Hamiltonian for the orbital dynamics, \hat{H}_0 considered up to now, by

$$\hat{H} = \hat{H}_0 + \hat{\mathbf{s}} \cdot \mathbf{C} \, (\hat{\mathbf{x}}, \hat{\mathbf{p}}), \tag{3.72}$$

with $C(\hat{\mathbf{x}}, \hat{\mathbf{p}})$ characterising the coupling of the translational degrees of freedom to the spin operator $\hat{\mathbf{s}}$.

For weak spin-orbit interaction and time-reversal symmetry, the semiclassical propagator is similar to Eq. (2.17), where the classical trajectories are the same as for the case without interaction [37] and presence of time-reversal symmetry. The only modification appears in the prefactor D_{γ} that contains now the additional factor $B_{\gamma}(\mathbf{x}', \mathbf{p}', t)$, which is the spin-s representation of the spin-1/2 propagator matrix $b_{\gamma}(\mathbf{x}', \mathbf{p}', t)$, defined as the solution of [37],

$$\frac{d}{dt}b_{\gamma}\left(\mathbf{x}',\mathbf{p}',t\right) + \frac{i}{2}\boldsymbol{\sigma}\cdot\mathbf{C}\left(\mathbf{X}(t),\mathbf{P}(t)\right)b_{\gamma}\left(\mathbf{x}',\mathbf{p}',t\right) = 0,$$
(3.73)

with the initial condition $b_{\gamma}\left(\mathbf{x}',\mathbf{p}',0\right)=\mathbb{1}_2$ and the vector $\boldsymbol{\sigma}$ containing the Pauli matrices. This propagator can be used now in the derivation of a modified semi-classical formula for the survival probability in the case of spin-orbit interaction. After replacing the initial state $|\psi_0\rangle$ introduced in Eq. (2.8) by $|\Psi_0\rangle \equiv |\psi_0\otimes \mathbf{s}_0\rangle$ containing additionally the initial spin state $|\mathbf{s}_0\rangle$, we obtain the matrix element $\left\langle \mathbf{s}_0 \left| B_{\gamma} B_{\gamma}^{\dagger} \right| \mathbf{s}_0 \right\rangle$ as an additional factor inside the double sum in Eq. (3.7). We are interested in the average behaviour of this quantity. Therefore, we analyse $\frac{1}{(2s+1)} \mathrm{Tr}(B_{\gamma} B_{\gamma}^{\dagger})$ with Tr denoting here the trace in the spin space. This quantity was already considered in Refs. [36, 38], where by assuming the mixing property of the combined spin and orbital dynamics, i.e. full spin relaxation, it was shown that we can effectively write

$$\frac{1}{(2s+1)}\operatorname{Tr}\left(B_{\gamma}B_{\gamma}^{\dagger}\right) \approx \left(\frac{(-1)^{2s}}{2s+1}\right)^{L-V} \tag{3.74}$$

with L and V defined as before. It is important to notice that the contribution from spin-orbit interaction depends, apart from the spin quantum number s, only on the difference L-V. The term (3.74) can now be inserted as prefactor into the expression (3.71) for the GOE case after choosing in each term the correct value of L-V. For s=1/2 this yields

$$\rho_{\text{GSE}}(t) = e^{-\frac{t}{\tau_D}} \left[1 - \frac{t^2}{4\tau_D T_H} - \frac{t^3}{12\tau_D T_H^2} + \left(\frac{5}{96\tau_D^2 T_H^2} - \frac{1}{24\tau_D T_H^3} \right) t^4 \right. \\
+ \left(\frac{11}{240\tau_D^2 T_H^3} - \frac{1}{40\tau_D T_H^4} \right) t^5 \\
- \left(\frac{41}{5760\tau_D^3 T_H^3} - \frac{7}{192\tau_D^2 T_H^4} + \frac{1}{60\tau_D T_H^5} \right) t^6 \\
- \left(\frac{29}{2688\tau_D^3 T_H^4} - \frac{7}{240\tau_D^2 T_H^5} + \frac{1}{84\tau_D T_H^6} \right) t^7 + \cdots \right].$$
(3.75)

This result is again consistent with supersymmetric results for the symplectic ensemble [11]. The second, negative term in (3.75) reflects weak-antilocalisation effects in the quantum decay, i.e. the quantum correction reduces the survival probability.

This section showed how to obtain semiclassically higher-order contributions to the survival probability. The quantities studied up to now, the survival probability and the fidelity amplitude, involved paths starting and ending inside the system. We now turn to the semiclassical expression for the current that contains paths starting in the system and ending on a cross section in the lead through that the particles can leave the system and connect it via the continuity equation to the semiclassical expression for the survival probability.

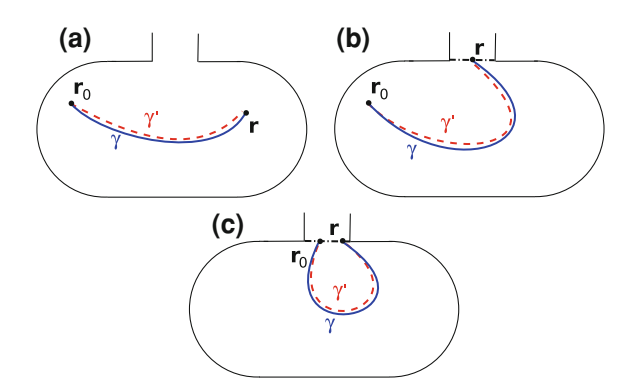
3.4 Continuity Equation

In order to see how the new kind of diagrams introduced in the last section preserve unitarity it is instructive to reformulate the decay problem in terms of paths reaching the opening. This connection will be made in this section in two steps:

- First we transform, by using a semiclassical version of the continuity equation, the sum over orbits starting *and* ending inside the system into a sum over orbits starting inside the system and ending at a cross section in the lead, for an illustration see Fig. 3.3a, b.
- Afterwards we use a continuity equation for the current to transform the sum over orbits starting inside the system and ending at a cross section in the lead into a sum over orbits starting *and* ending on a cross section in the lead, see Fig. 3.3c.

To this end we consider first the integrated version of the continuity equation for probability flow, $\partial \rho(\mathbf{r}, t)/\partial t + \nabla \cdot \mathbf{j}(\mathbf{r}, t) = 0$ with spatially resolved probability

Fig. 3.3 Illustration of the three scenarios considered in this section in diagonal approximation. In a the orbit pairs start and end inside the system, in b the orbits start inside the system and end on a cross section inside the lead, in c the orbits start and end on the cross section considered in b. The cross section is indicated by a dashed-dotted line



density $\rho(\mathbf{r}, t)$ yielding the survival probability $\rho(t)$ after a spatial integration over the area A, and the spatially resolved current density $\mathbf{j}(\mathbf{r}, t)$, namely

$$\frac{\partial}{\partial t}\rho(t) = -\int_{S} dx \,\mathbf{j}(\mathbf{r}, t) \cdot \hat{n}_{x},\tag{3.76}$$

where S is the cross section of the opening with a normal vector \hat{n}_x pointing to the outside of the system. In Eq. (3.76), the quantum mechanical current density

$$\mathbf{j}(\mathbf{r},t) = \frac{1}{m} \Re\left[\frac{\hbar}{i} \psi^*(\mathbf{r},t) \nabla \psi(\mathbf{r},t)\right]$$
 (3.77)

can be semiclassically expressed by Eq. (2.17) in terms of orbit pairs connecting points inside A with the opening yielding

$$\mathbf{j}_{sc}(\mathbf{r},t) = \frac{1}{8m\pi^{2}\hbar^{2}} \int_{A} d\mathbf{r}' d\mathbf{r}'' \psi_{0}(\mathbf{r}') \psi_{0}^{*}(\mathbf{r}'')$$

$$\times \sum_{\substack{\bar{\gamma}(\mathbf{r}' \to \mathbf{r},t) \\ \bar{\gamma}'(\mathbf{r}'' \to \mathbf{r},t)}} A_{\bar{\gamma}} A_{\bar{\gamma}'} e^{\frac{i}{\hbar}(S_{\bar{\gamma}} - S_{\bar{\gamma}'}) - i\frac{\pi}{2} \left(\mu_{\bar{\gamma}} - \mu_{\bar{\gamma}'}\right)} \left[\mathbf{p}_{\bar{\gamma},f} + \mathbf{p}_{\bar{\gamma}',f}\right], \qquad (3.78)$$

which involves a sum over pairs of trajectories $\bar{\gamma}$ and $\bar{\gamma}'$ with final momenta $\mathbf{p}_{\bar{\gamma},f}$ and $\mathbf{p}_{\bar{\gamma}',f}$ at \mathbf{r} . These result from differentiating the actions with respect to the final positions as required in Eq. (3.77). Again expanding the actions and the stability amplitudes of $\bar{\gamma}$ and $\bar{\gamma}'$ around the midpoint \mathbf{r}_0 , we obtain

$$\mathbf{j}_{sc}(\mathbf{r},t) = \frac{1}{4m\pi^2\hbar^2} \int d\mathbf{r}_0 \sum_{\gamma,\gamma'(\mathbf{r}_0 \to \mathbf{r},t)} A_{\gamma} A_{\gamma'} e^{\frac{i}{\hbar}(S_{\gamma} - S_{\gamma'}) - i\frac{\pi}{2} \left(\mu_{\gamma} - \mu_{\gamma'}\right)} \rho_{W}(\mathbf{r}_0, \mathbf{p}_{\gamma\gamma'}^0) \mathbf{p}_{\gamma\gamma'}^f,$$
(3.79)

where $\mathbf{p}_{\gamma\gamma'}^0$ and $\mathbf{p}_{\gamma\gamma'}^f$ are the average initial and final momenta of the trajectories γ and γ' , respectively and $\rho_{\mathrm{W}}(\mathbf{r}_0,\mathbf{p}_{\gamma\gamma'}^0)$ is defined in Eq. (3.11). We now want to consider the integrated current density obtained by inserting $\mathbf{j}(\mathbf{r},t)$ into

$$J(t) = \int_{S} dx \,\mathbf{j}(\mathbf{r}, t) \cdot \hat{n}_{x}.$$
 (3.80)

This is the quantity we wish to evaluate semiclassically now as it is related via a time integration to the survival probability, see Eq. (3.76). The integral over the cross section of the lead implies that we are interested in trajectory pairs that start inside the system and end in the lead.

The classical contribution results again from the diagonal approximation where we pair the trajectories with themselves, $\gamma = \gamma'$. Restricting ourselves to these pairs, (3.79) simplifies to

$$\mathbf{j}_{\text{diag}}(\mathbf{r},t) \cdot \hat{n}_{x} = \frac{1}{4m\pi^{2}\hbar^{2}} \int d\mathbf{r}_{0} \sum_{\gamma(\mathbf{r}_{0} \to \mathbf{r},t)} |A_{\gamma}|^{2} \rho_{\mathbf{W}}(\mathbf{r}_{0},\mathbf{p}_{\gamma,0}) p_{x,\gamma}^{\mathbf{f}}.$$
(3.81)

with the component of $\mathbf{p}_{\gamma\gamma'}^{\mathrm{f}}$ in the direction of \hat{n}_{x} , $p_{x,\gamma}^{\mathrm{f}}$ for $\gamma=\gamma'$. When Eq. (3.81) is inserted into Eq. (3.80), apart from the factor $p_{x,\gamma}^{\mathrm{f}}$ and the fact that the sum over final positions runs only over a cross section in the lead and not over the whole configuration space of the system, the resulting expression is the same as the one for the survival probability in Eq. (3.8), we can thus perform the sum over orbits in a similar manner.

Although it is possible to calculate the sum over orbits obtained when inserting (3.81) into (3.80) by using sum rules [3, 39–41] we want to give here a simple argument showing

$$J_{\text{diag}}(t) = \left\langle \mu e^{-\mu t} \right\rangle_{\mathbf{r}_0, \mathbf{p}_0} \tag{3.82}$$

with the average defined in Eq. (3.10). As we know how to perform the sum in the case of the survival probability we will transform the diagonal contribution to the current into that. As we assume that the considered trajectories are very long in order to become ergodic, their contribution to the survival probability can be assumed not to depend on the specific values of their final points but to be proportional to the number of possible final points of the orbits in phase space. Considering thus that the sum over orbits is proportional to phase-space area the particle trajectory is allowed to end in, we have to multiply our results for $\rho_{\text{diag}}(t)$ by $2pW/(2m\pi A)$. Here W/A results from the ratio of the possible endpoints in configuration space and the factor $2p/(2\pi)$ from the ratio of the possible final momenta in longitudinal direction in the lead and the possible momentum directions for the survival probability. The factor 1/m is due to the prefactor in (3.77). With the relation $W = N\pi\hbar/p$ it follows that $2pW/(2m\pi A) = \mu$ and by this Eq. (3.82).

By integrating Eq. (3.82) with respect to time and setting $\rho_{\text{diag}}(0) = 1$, we obtain

$$\rho_{\text{diag}}(t) = \left\langle e^{-\mu t} \right\rangle_{\mathbf{r}_0, \mathbf{p}_0},\tag{3.83}$$

i.e. in diagonal approximation the continuity equation is fulfilled.

For simplicity of presentation we again assume the initial wave function to possess a well defined energy and thus drop again the average in Eqs. (3.82, 3.83) from now on.

Next we want to consider off-diagonal contributions: In this case different diagrams are allowed in the case of the survival probability and the integrated current density, because the orbits have to end in the case of the integrated current density at the opening.

Before turning to the general case of orbit pairs differing in an arbitrary number of encounters we want as in the calculation of non-diagonal contributions to the survival probability present the calculation of the first quantum correction in the presence of time-reversal symmetry. Remember that for the survival probability the contributions came from encounters inside the orbit (case A) and from encounters situated at the beginning *or* at the end of the orbit (case B). For orbit pairs differing by several encounters different encounters can be situated additionally at the beginning *and* at the end of the orbit (case C). For the integrated current density we again have the possibility of encounters inside the orbit but only encounters at the beginning and *not* at the end of the orbit; thus only one half of this contribution in case B. An encounter at the end of the orbit obtained by shrinking the last link of the orbit is not possible here because then already the first encounter stretch has to touch the opening and the orbit has to exit already during traversing the first stretch. Thus a configuration containing one encounter at the beginning *and* one at the end of the orbit (case C) is also not possible for the integrated current density.

The contribution to the current from encounters inside the orbit is calculated in the same way as the corresponding contribution to the survival probability obtained in Sect. 3.2 with the modification of the sum rule discussed after Eq. (3.82). As for the survival probability we refer to this contributions as two-leg-loops (211), it is given by

$$J_{211}(t) = \frac{\left(t^2 \mu - 4t\right) \mu}{2T_H} e^{-\mu t}.$$
 (3.84)

In the same way we obtain the contribution from encounters at the beginning of the orbit, referred to as $J_{111}(t)$,

$$J_{111}(t) = \frac{t\mu}{T_H} e^{-\mu t}.$$
 (3.85)

Now it can be checked easily that $J_{2ll}(t) + J_{1ll}(t)$ is equal to $-\partial \left(\rho_{2ll}(t) + \rho_{1ll}(t)\right)/\partial t$. Thus also for these diagrams the continuity equation is fulfilled.

The latter relation shows that the first non-diagonal contributions to J(t) and $\rho(t)$ satisfy the following connection, which should hold in general: On one hand we can calculate the non-diagonal contributions to J(t). On the other hand we can also consider non-diagonal contributions to $-\rho(t)$ and differentiate afterwards the obtained result with respect to t. The result should be the same as for J(t). We now want to prove this nontrivial connection between the semiclassical contributions to $\rho(t)$ and

J(t) for orbit pairs differing in an arbitrary number of encounters. Therefore we first give general expressions for the contributions to J(t), then first prove the unitarity of the overall semiclassical contribution to $\rho(t)$, i.e. that the semiclassical expression for $\rho(t)$ yields one for a closed system. Finally we show that the semiclassical contributions to $\rho(t)$ and J(t) fulfil the continuity equation.

3.4.1 Higher-Order Contributions to the Integrated Current Density

3.4.1.1 Case A: Two-Leg-Loops

As for the survival probability, by again invoking the sum rule for the integrated current density we obtain here

$$J_{\mathbf{v},\mathbf{A}}(t) = \mu \rho_{\mathbf{v},\mathbf{A}}(t) = \mu N(\mathbf{v}) \int d\mathbf{s} \, d\mathbf{u} \, w_{\mathbf{v},\mathbf{A}}(\mathbf{u},\mathbf{s},t) e^{-\mu t} e^{\mu \sum_{\alpha=1}^{V} (l_{\alpha}-1) t_{\text{enc}}^{\alpha}} e^{\frac{i}{\hbar} \mathbf{u} \mathbf{s}},$$
(3.86)

with $\rho_{v,A}(t)$ defined in Eq. (3.43). There also the definition of the other quantities appearing after the second equality sign can be found.

This contribution can again be expressed in terms of the augmented weight function $z_{\mathbf{v},\mathbf{A}}(\boldsymbol{u},s,t)$ defined in Eq. (3.45).

3.4.1.2 Case B: One-Leg-Loops

We can write this contribution as

$$J_{\mathbf{v},B}(t) = \frac{1}{2}\mu \rho_{\mathbf{v},B}(t) = \mu N(\mathbf{v}) \int d\mathbf{s} \, d\mathbf{u} \, z_{\mathbf{v},B}(\mathbf{u},\mathbf{s},t) e^{-\mu t} e^{\frac{i}{\hbar}\mathbf{u}\mathbf{s}}.$$
 (3.87)

with $\rho_{\mathbf{v},\mathbf{B}}(t)$ defined in Eq. (3.51) and $z_{\mathbf{v},\mathbf{B}}(\mathbf{u},\mathbf{s},t)$ in Eq. (3.52).

3.4.2 Fourier Transforms

To show that the continuity equation holds to all orders it is simpler to make a Fourier transform rather than showing, for each L-V, that all terms sum to zero for each power of t.

For convenience we restrict ourselves to positive times, and we will consider the (one-sided) inverse Fourier transform of the current J(t)

$$\hat{J}(\omega) = \int_0^\infty d\tau \, J(\tau T_H) e^{2\pi i \omega \tau}, \qquad (3.88)$$

as well as of the survival probability $\rho(t)$

$$P(\omega) = \int_0^\infty d\tau \, \rho(\tau T_H) \mathrm{e}^{2\pi i \omega \tau}, \qquad (3.89)$$

where $\tau = t/T_H$. In the Fourier space the continuity Eq. (3.76) becomes

$$T_H \hat{J}(\omega) - (2\pi i\omega)P(\omega) = 1, \tag{3.90}$$

and this is the relation which we want to show semiclassically. We note that the 1 on the right hand side comes semiclassically from the diagonal terms given in (3.82) and (3.83).

3.4.2.1 Transformed Current Density

The semiclassical contribution for the current can be separated into a product of contributions over the encounters and the links of the trajectory, in a similar way as described for the conductance in Chap. 2. This means that we can obtain the semiclassical result very simply. For example for case A the contribution from trajectories with structures described by ${\bf v}$ is

$$\hat{J}_{\mathbf{v},A}(\omega) = \frac{\mu N(\mathbf{v})}{T_H} \left(\prod_{i=1}^{L+1} \int_0^\infty dt_i e^{-\left(\mu - \frac{2\pi i\omega}{T_H}\right)t_i} \right) \times \left(\int_{-c}^c ds \ d\mathbf{u} \prod_{\alpha=1}^V \frac{e^{-\left(\mu - \frac{2\pi i\omega l_\alpha}{T_H}\right)t_{\text{enc}}^\alpha} e^{\frac{i}{\hbar}\mathbf{u}_\alpha s_\alpha}}{\Omega^{l_\alpha - 1}t_{\text{enc}}^\alpha} \right). \tag{3.91}$$

We can perform these integrals as before, and because the Heisenberg times mutually cancel, we effectively get a factor of $(N-2\pi i\omega)^{-1}$ for each link and a factor of $-(N-2\pi i\omega l_{\alpha})$ for each encounter. The contribution therefore simplifies to

$$\hat{J}_{\mathbf{v},A}(\omega) = \mu N(\mathbf{v}) (-1)^{V} \frac{\prod_{\alpha=1}^{V} (N - 2\pi i \omega l_{\alpha})}{(N - 2\pi i \omega)^{L+1}}.$$
 (3.92)

Considering case B, we have one link fewer (L in total) and one encounter, α' at the start of the trajectory pair. We again replace the time integral in the augmented weight function by a $t_{\rm enc}^{\alpha'}$ like we did it in Eq. (3.54) and effectively obtain a factor of 1 from the integration with respect to $s_{\alpha'}$ and $u_{\alpha'}$. We also remember that to obtain the structures for this case we started from the corresponding closed orbits, so that we divide by the overcounting factor L, and note that the encounter α' occurs at the start $l_{\alpha'}$ times. Altogether, the contribution simplifies to

$$\hat{J}_{\mathbf{v},\mathbf{B}}(\omega) = \frac{\mu N(\mathbf{v})(-1)^{V-1}}{L} \sum_{\alpha'=1}^{V} l_{\alpha'} \frac{\prod_{\alpha \neq \alpha'} (N - 2\pi i \omega l_{\alpha})}{(N - 2\pi i \omega)^{L}}, \tag{3.93}$$

which we can also write as

$$\hat{J}_{\mathbf{v},\mathbf{B}}(\omega) = \frac{\mu N(\mathbf{v})(-1)^{V-1}}{L} \left(\sum_{\alpha'=1}^{V} \frac{l_{\alpha'}}{(N - 2\pi i \omega l_{\alpha'})} \right) \frac{\prod_{\alpha=1}^{V} (N - 2\pi i \omega l_{\alpha})}{(N - 2\pi i \omega)^{L}}, (3.94)$$

to remove the restriction on the product over α .

3.4.2.2 Transformed Survival Probability

The semiclassical contributions to the survival probability were given in the last section. Taking again the inverse Fourier transform we can also write them as a product of contributions from the links and encounters and for the first two cases we obtain very similar results as for the integrated current density in Eqs. (3.92) and (3.94). For case A we arrive due to Eq. (3.86) at

$$P_{\mathbf{v},A}(\omega) = \frac{\hat{J}_{\mathbf{v},A}(\omega)}{\mu}.$$
 (3.95)

For case B the result is due to Eq. (3.87)

$$P_{\mathbf{v},\mathbf{B}}(\omega) = 2\frac{\hat{J}_{\mathbf{v},\mathbf{B}}(\omega)}{\mu}.$$
 (3.96)

In case C the two encounters at the ends effectively give factors of 1 while the remaining encounters and links give their usual contributions. The number of possible structures is characterised again by $\mathcal{N}_{\alpha,\beta}(\mathbf{v})$ defined in the last section. Additionally we have again one link fewer leading us to the contribution

$$P_{\mathbf{v},\mathbf{C}}(\omega) = \left(\sum_{\alpha,\beta=1}^{V} \frac{\mathcal{N}_{\alpha,\beta}(\mathbf{v})}{(N - 2\pi i\omega l_{\alpha})(N - 2\pi i\omega l_{\beta})}\right) \frac{(-1)^{V-2} \prod_{\alpha=1}^{V} (N - 2\pi i\omega l_{\alpha})}{(N - 2\pi i\omega)^{L-1}}.$$
(3.97)

3.4.3 Recursion Relations

In the limit $\mu \to 0$ (or $\tau_D \to \infty$) the quantum wave packet remains inside the cavity and the survival probability is identically 1 for all times. This term comes from the diagonal approximation, which means that all higher-order terms from correlated trajectories should vanish. As we have shown in Sect. 3.2 for the survival probability, $\rho(t)$, one-leg-loops are necessary to ensure this unitarity and cancel the term from two-leg-loops which does not vanish when the system is closed. We first show that this holds to all orders by considering recursion relations between the different types of contribution.

3.4.3.1 Unitarity

Restricting the sum over vectors ${\bf v}$ to the ones that share the same value of L-V=m, and summing over the different cases, we will show that $P_m(\omega,\mu=0)$ vanishes for all m>0 and in the presence and absence of time-reversal symmetry. This is equivalent to showing that the lowest-order t terms in the polynomial multiplying $\exp(-\mu t)$ of the various $\rho_{\bf v}(t)$ also sum to zero, so that $\rho_m(t)$ involves a polynomial with lowest term proportional to t^{m+1} . We start with the semiclassical results for each case when $\mu=0$, and for case A we have

$$P_{\mathbf{v},A}(\omega,\mu=0) = N(\mathbf{v}) \frac{(-1)^{L+1} \prod_{\alpha=1}^{V} l_{\alpha}}{(2\pi i \omega)^{L-V+1}},$$
(3.98)

while similarly for case B, the result is

$$P_{\mathbf{v},\mathbf{B}}(\omega,\mu=0) = N(\mathbf{v}) \frac{2V}{L} \frac{(-1)^L \prod_{\alpha=1}^V l_\alpha}{(2\pi i \omega)^{L-V+1}},$$
(3.99)

because $\sum_{\alpha=1}^{V} 1 = V$. For case C we obtain

$$P_{\mathbf{v},\mathbf{C}}(\omega,\mu=0) = \left(\sum_{\alpha,\beta=1}^{V} \frac{\mathcal{N}_{\alpha,\beta}(\mathbf{v})}{l_{\alpha}l_{\beta}}\right) \frac{(-1)^{L-1} \prod_{\alpha=1}^{V} l_{\alpha}}{(2\pi i \omega)^{L-V+1}}.$$
 (3.100)

Replacing again $\mathcal{N}_{\alpha,\beta}(\mathbf{v})$ by $\mathcal{N}_{k,l}(\mathbf{v})$ defined in the last section before Eq. (3.67) we can replace the sum over α,β by a sum over k and l. With this in place we can sum the different types of contributions, and then sum over vectors \mathbf{v} with the same L-V=m

$$P_{m}(\omega, \mu = 0) = \frac{(-1)^{m+1}}{(2\pi i \omega)^{m+1}} \sum_{\mathbf{v}}^{L-V=m} (-1)^{V} \prod_{\alpha=1}^{V} l_{\alpha}$$

$$\times \left[\left(1 - \frac{2V}{L} \right) N(\mathbf{v}) + \sum_{k,l=2}^{\infty} \frac{\mathcal{N}_{k,l}(\mathbf{v})}{kl} \right]. \tag{3.101}$$

Let us first consider the third contribution

$$P_{m,C}(\omega, \mu = 0) = \frac{(-1)^{m+1}}{(2\pi i\omega)^{m+1}} \sum_{\mathbf{v}}^{L-V=m} (-1)^{V} \prod_{\alpha=1}^{V} l_{\alpha} \sum_{k,l=2}^{\infty} \frac{\mathcal{N}_{k,l}(\mathbf{v})}{kl}.$$
 (3.102)

To simplify this further we use the following recursion relation which can be deduced from [31,32]. We have that $\mathcal{N}_{k,l}(\mathbf{v})$ records the number of links that join a k-encounter to an l-encounter. Instead of cutting the link to make the trajectory structure, we imagine shrinking the link so that the k- and l-encounters merge to form a new

(k+l-1)-encounter. By considering the number of ways that it is possible to shrink the link and create a smaller periodic orbit structure, the following result is obtained [31, 32]

$$\mathcal{N}_{k,l}(\mathbf{v}) = \frac{(k+l-1)(v_{k+l-1}+1)}{L-1} N(\mathbf{v}^{[k,l\to k+l-1]}), \tag{3.103}$$

where v_{k+l-1} is the (k+l-1)-th component of \mathbf{v} and $\mathbf{v}^{[k,l\to k+l-1]}$ is the vector obtained by decreasing the components v_k and v_l by one and increasing the component v_{k+l-1} by one (so that $v_{k+l-1}+1=v_{k+l-1}^{[k,l\to k+l-1]}$). We also use the substitution

$$\tilde{N}(\mathbf{v}) = \frac{(-1)^V \prod_{\alpha=1}^V l_\alpha}{L} N(\mathbf{v}), \tag{3.104}$$

which allows us to rewrite (3.103) as

$$(-1)^{V} \prod_{\alpha=1}^{V} l_{\alpha} \frac{\mathcal{N}_{k,l}(\mathbf{v})}{kl} = -v_{k+l-1}^{[k,l\to k+l-1]} \tilde{N}(\mathbf{v}^{[k,l\to k+l-1]}), \tag{3.105}$$

so that (3.102) becomes

$$P_{m,C}(\omega,\mu=0) = -\frac{(-1)^{m+1}}{(2\pi i\omega)^{m+1}} \sum_{\mathbf{v}}^{L-V=m} \sum_{k,l=2}^{\infty} v_{k+l-1}^{[k,l\to k+l-1]} \tilde{N}(\mathbf{v}^{[k,l\to k+l-1]}).$$
(3.106)

As combining a k- and l-encounter reduces both L and V by one, the resulting vector $\mathbf{v}^{[k,l\to k+l-1]}$ still has the same value of L-V=m and by considering $\mathbf{v}^{[k,l\to k+l-1]}$ as a dummy variable \mathbf{v}' it can be shown [31, 32] that

$$\sum_{\mathbf{v}}^{L-V=m} v_{k+l-1}^{[k,l\to k+l-1]} \tilde{N}(\mathbf{v}^{[k,l\to k+l-1]}) = \sum_{\mathbf{v}'}^{L-V=m} v_{k+l-1}' \tilde{N}(\mathbf{v}').$$
(3.107)

By identifying this dummy vector \mathbf{v}' with \mathbf{v} and substituting into (3.106), the total contribution to $P_m(\omega, \mu = 0)$ in Eq. (3.101) simplifies to

$$P_m(\omega, \mu = 0) = \frac{(-1)^{m+1}}{(2\pi i\omega)^{m+1}} \sum_{\mathbf{v}}^{L-V=m} \left[(L - 2V) - \sum_{k,l=2}^{\infty} v_{k+l-1} \right] \tilde{N}(\mathbf{v}). \quad (3.108)$$

Concentrating on the sum over k and l, we define k' = k + l - 1 where k' > l because $k \ge 2$. The sum then becomes

$$\sum_{k,l=2}^{\infty} v_{k+l-1} = \sum_{l\geq 2} \sum_{k'>l} v_{k'} = \sum_{k'\geq 3} (k'-2)v_{k'} = \sum_{k'\geq 2} (k'-2)v_{k'}$$

$$= \sum_{k'\geq 2} k'v_{k'} - 2\sum_{k'\geq 2} v_{k'} = L - 2V, \tag{3.109}$$

and so the term in the square brackets in (3.108) is identically 0.

This result shows that $P_m(\omega, \mu = 0) = 0$ and hence that $\rho_m(t, \mu = 0) = 0$ for all m > 0, for both symmetry classes. This is consistent with the fact that the survival probability should be identically 1 for a closed system $(\mu = 0)$.

3.4.3.2 Continuity Equation

Building on this, we are now able to treat the full continuity equation in the Fourier space. Again this will require re-expressing the contribution from the third case, and we also need to sum over different vectors \mathbf{v} with the same value of L-V=m. If we define here

$$\hat{N}(\mathbf{v}, N) = \frac{(-1)^V}{L} \frac{\prod_{\alpha=1}^V (N - 2\pi i\omega l_\alpha)}{(N - 2\pi i\omega)^L} N(\mathbf{v}), \tag{3.110}$$

then the first two contributions to the transformed survival probability, see Eqs. (3.95) and (3.96), can be written as

$$P_{m,A}(\omega) = \sum_{\mathbf{v}}^{L-V=m} \frac{L}{(N-2\pi i\omega)} \hat{N}(\mathbf{v}, N)$$
(3.111)

and

$$P_{m,B}(\omega) = -\sum_{\mathbf{v}}^{L-V=m} \sum_{l=2}^{\infty} \frac{2lv_l}{(N-2\pi i\omega l)} \hat{N}(\mathbf{v}, N), \qquad (3.112)$$

where we have replaced the sum over α by a sum over the components of the vector \mathbf{v} . To simplify the third contribution from (3.97) we use a version of (3.105), modified for this situation to include the extra factors

$$\frac{(-1)^{V} \mathcal{N}_{k,l}(\mathbf{v})}{(N - 2\pi i\omega k)(N - 2\pi i\omega l)} \frac{\prod_{\alpha=1}^{V} (N - 2\pi i\omega l_{\alpha})}{(N - 2\pi i\omega)^{L-1}}
= -\frac{(k+l-1)v_{k+l-1}^{[k,l\to k+l-1]}}{(N - 2\pi i\omega(k+l-1))} \hat{N}(\mathbf{v}^{[k,l\to k+l-1]}, N).$$
(3.113)

We can then rewrite the sum over the dummy vector $\mathbf{v}' = \mathbf{v}^{[k,l \to k+l-1]}$ as a sum over \mathbf{v} and obtain

$$P_{m,C}(\omega) = -\sum_{\mathbf{v}}^{L-V=m} \sum_{k,l=2}^{\infty} \frac{(k+l-1)v_{k+l-1}}{(N-2\pi i\omega(k+l-1))} \hat{N}(\mathbf{v}, N).$$
(3.114)

We return to the continuity equation for the off-diagonal terms $(J_m(t) + \partial \rho_m(t) / \partial t = 0)$ in the Fourier space (3.90). To ensure that the continuity equation holds, we have to check that

$$N\left[P_{m,A}(\omega) + \frac{P_{m,B}(\omega)}{2}\right] - (2\pi i\omega)\left[P_{m,A}(\omega) + P_{m,B}(\omega) + P_{m,C}(\omega)\right] = 0.$$
(3.115)

Writing the left hand side in terms of the sum over vectors, we have to evaluate

$$\sum_{\mathbf{v}}^{L-V=m} \left[L - \sum_{l=2}^{\infty} \frac{l v_l (N - 4\pi i \omega)}{(N - 2\pi i \omega l)} + \sum_{l=2}^{\infty} \sum_{k'>l} \frac{2\pi i \omega k' v_{k'}}{(N - 2\pi i \omega k')} \right] \hat{N}(\mathbf{v}, N), \quad (3.116)$$

where k' = k + l - 1. Following similar reasoning to (3.109) we can simplify the double sum inside the square brackets as follows

$$\sum_{l=2}^{\infty} \sum_{k'>l} \frac{2\pi i\omega k' v_{k'}}{(N - 2\pi i\omega k')} = \sum_{l=2}^{\infty} \frac{2\pi i\omega (l-2)lv_l}{(N - 2\pi i\omega l)},$$
(3.117)

so that (3.116) becomes

$$\sum_{\mathbf{v}}^{L-V=m} \left[L - \sum_{l=2}^{\infty} \frac{lv_l(N - 4\pi i\omega - 2\pi i\omega(l-2))}{(N - 2\pi i\omega l)} \right] \hat{N}(\mathbf{v}, N)$$

$$= \sum_{\mathbf{v}}^{L-V=m} \left[L - \sum_{l=2}^{\infty} lv_l \right] \hat{N}(\mathbf{v}, N) = 0, \tag{3.118}$$

since $\sum_{l=2}^{\infty} lv_l = L$. This verifies Eq. (3.115) and shows that the semiclassical expansion satisfies the continuity equation for all m > 0. For the remaining diagonal terms (which can be thought of as corresponding to m = 0) this can be verified directly.

Both of these proofs rely on being able to re-express the contribution from case C in terms of a sum over vectors which has a similar form as in the other two cases. This relation is then responsible for the fact that we can shift from the survival probability to the current via the continuity equation and remove the possibility of having trajectories from case C (0ll).

3.4.4 Implications for Transport

We have seen how by differentiating $\rho(t)$, with respect to time, we obtain -J(t) in line with the continuity equation. For $\rho(t)$ we have a picture involving trajectories that start and end inside the cavity, and we have three cases to consider. When we differentiate $\rho(t)$, and shift to J(t), we arrive at a picture in terms of trajectories that start inside the cavity but end in the lead, effectively removing the third case (0ll) (and halving the contribution of 1ll). The next step is to repeat this process and differentiate again with respect to time. This will lead to the more usual transport picture involving trajectories that start and end in the leads, where we can only have case A (2ll).

We therefore consider the conservation of the current density, which has its own continuity equation. For systems with constant potentials, like billiards, this continuity equation has the simple form

$$\frac{\partial \mathbf{j}(\mathbf{r},t)}{\partial t} + \nabla f(\mathbf{r},t) = 0, \tag{3.119}$$

where $f(\mathbf{r}, t)$ is the second (antisymmetric spatial) derivative of the local density

$$f(\mathbf{r},t) = \frac{\hbar^2}{(2mi)^2} [\psi^*(\mathbf{r},t)\nabla^2\psi(\mathbf{r},t) - 2\nabla\psi^*(\mathbf{r},t)\nabla\psi(\mathbf{r},t) + \psi(\mathbf{r},t)\nabla^2\psi^*(\mathbf{r},t)].$$
(3.120)

To obtain a semiclassical approximation for this quantity, we express the wavefunction in terms of the semiclassical propagator using equations (2.17) and (3.5) and follow the same steps as at the beginning of this section

$$f_{\text{sc}}(\mathbf{r},t) = \frac{1}{4m^2\pi^2\hbar^2} \int d\mathbf{r}_0 \sum_{\gamma,\gamma'(\mathbf{r}_0 \to \mathbf{r},t)} A_{\gamma} A_{\gamma'} e^{\frac{i}{\hbar}(S_{\gamma} - S_{\gamma'}) - i\frac{\pi}{2} \left(\mu_{\gamma} - \mu_{\gamma'}\right)} \rho_{\mathbf{W}}(\mathbf{r}_0, \mathbf{p}_{\gamma\gamma'}^0) \times \left(\mathbf{p}_{\gamma\gamma'}^f\right)^2.$$
(3.121)

We are interested in the integrated version of this quantity

$$F(t) = \int_{A} d\mathbf{r} \nabla^{2} f(\mathbf{r}, t), \qquad (3.122)$$

which can be expressed in terms of trajectories starting and ending at the lead-cross section. Instead of using (3.121), which involves trajectories which start and end inside the cavity, we first insert (3.120) in Eq. (3.122). Note that F(t) equals $\partial^2 \rho(t)/(\partial t^2)$, in Eqs. (3.120), (3.122) these time derivatives are however replaced by spatial derivatives. We then replace all derivatives with respect to \mathbf{r} , originating from the derivative with respect to time of the current density (i.e. not the ones resulting from the first derivative of $\rho(t)$ with respect to t), by derivatives with respect to \mathbf{r}_0 . This replacement is justified semiclassically, it neglects changes in the slower varying amplitudes in Eq. (3.121). We can then rewrite the resulting expression as a divergence with respect to \mathbf{r} and \mathbf{r}_0 in a similar way as it is done with respect to \mathbf{r} to obtain the continuity equation itself. Upon applying Gauss' theorem for transforming the integrals with respect to \mathbf{r} and \mathbf{r}_0 to surface integrals, and again supposing that the initial wave function has a well defined energy, we arrive at the semiclassical expression

$$F(t) \approx \frac{1}{4m^2\pi^2\hbar^2} \int_{S} dx dx' \sum_{\gamma,\gamma'(x\to x',t)} A_{\gamma} A_{\gamma'} e^{\frac{i}{\hbar}(S_{\gamma} - S_{\gamma'}) - i\frac{\pi}{2} \left(\mu_{\gamma} - \mu_{\gamma'}\right)} p_{x,\gamma\gamma'} p_{x',\gamma\gamma'}$$

$$(3.123)$$

with the normal components of average initial and final momenta $p_{x,\gamma\gamma'}$ and $p_{x',\gamma\gamma'}$, respectively. The last formula expresses F(t) as a sum over trajectories travelling from the lead to itself. The connection to transport can be extended by projecting onto the channel basis and performing the sums over orbits with the sum rule (2.34). Alternatively the sum over orbits in (3.123) can be calculated in diagonal approximation in an analogous way as described before Eq. (3.83) by relating it to the calculation of the survival probability in diagonal approximation, that yielded e^{-t/τ_D} , see Eqs. (3.9, 3.12). The additional factor for the diagonal contribution to F(t) is $4p^2W^2/(4\pi^2m^2A^2) = \mu^2$, obtained in a similar way as for the current before Eq. (3.83).

Because in this situation encounters cannot occur in the leads we only have case A and the weight function $z_{\mathbf{v},\mathbf{A}}(\boldsymbol{u},s,t)$, Eq. (3.45), as before. However we have an additional contribution for systems with time-reversal symmetry due to coherent backscattering. As we briefly discussed before Eq. (2.46) when the start and end channels coincide (a=b), we can also compare the trajectory γ with the time reversal of its partner γ and we obtain a factor of 2 for this combination [42, 43]. The sum over channel combinations therefore gives a factor of $N(N+2/\beta-1)$. The diagonal contribution is

$$F_{\text{diag}}(t) = \mu^2 \left(1 + \frac{2/\beta - 1}{N} \right) e^{-\mu t},$$
 (3.124)

while we can simply express the contribution of trajectories described by a vector \mathbf{v} as

$$F_{\mathbf{v}}(t) = \mu \left(1 + \frac{2/\beta - 1}{N} \right) J_{\mathbf{v}, \mathbf{A}}(t).$$
 (3.125)

We again shift to the Fourier space, where because of (3.125), the integrated continuity equation

$$\frac{\partial}{\partial t}J(t) + F(t) = 0, (3.126)$$

becomes, for the off-diagonal terms

$$(N + 2/\beta - 1)\hat{J}_{A}(\omega) - (2\pi i\omega)\left[\hat{J}_{A}(\omega) + \hat{J}_{B}(\omega)\right] = -\frac{\mu(2/\beta - 1)}{(N - 2\pi i\omega)}, \quad (3.127)$$

where the term on the right is what is leftover from the diagonal approximation for the orthogonal case when pairing the orbits with their time reversed. Rewriting the left hand side in terms of a sum over vectors we have to see if the following holds (dividing through by μ)

$$\sum_{m=1}^{\infty} \sum_{\mathbf{v}}^{L-V=m} \left[L + \sum_{l=2}^{\infty} \frac{l v_l(2\pi i \omega)}{(N - 2\pi i \omega l)} + \frac{(2/\beta - 1)L}{(N - 2\pi i \omega)} \right] \hat{N}(\mathbf{v}, N) = -\frac{2/\beta - 1}{(N - 2\pi i \omega)}.$$
(3.128)

Focusing on the left hand side, we recall that $L = \sum_{l=2}^{\infty} lv_l$ and so we can rewrite the first term in square brackets as

$$L = \sum_{l=2}^{\infty} \frac{lv_l(N - 2\pi i\omega l)}{(N - 2\pi i\omega l)},$$
(3.129)

so that we can combine it with the second term. We also separate the third term to rewrite the left hand side of (3.128) as

$$\sum_{m=1}^{\infty} \sum_{\mathbf{v}}^{L-V=m} \sum_{l=2}^{\infty} \frac{l v_l (N - 2\pi i \omega (l-1))}{(N - 2\pi i \omega l)} \hat{N}(\mathbf{v}, N) + (2/\beta - 1) \sum_{m=1}^{\infty} \sum_{\mathbf{v}}^{L-V=m} \frac{L}{(N - 2\pi i \omega)} \hat{N}(\mathbf{v}, N).$$
(3.130)

For the unitary case, the second line vanishes, and because of the result (A.6) in Appendix A, we can see that the sum in (3.130) is identically zero for each m and so the continuity equation is satisfied. For the orthogonal case, using the result (A.9) in Appendix A, we can see that the terms in the sum in the first line for m = k cancel with the terms in the sum in the second line where m = k - 1. The only term remaining when we sum over all m is therefore the term from the first line where m = 1. This corresponds to a vector with a single 2-encounter for which we can easily evaluate

$$\sum_{\mathbf{v}}^{L-V=1} \sum_{l=2}^{\infty} \frac{l v_l (N - 2\pi i \omega (l-1))}{(N - 2\pi i \omega l)} \hat{N}(\mathbf{v}, N) = -\frac{1}{(N - 2\pi i \omega)}.$$
 (3.131)

as $N(\mathbf{v}) = 1$. This term cancels exactly with the remaining term from the diagonal approximation, and hence Eqs. (3.128) and (3.126) are verified for both symmetry classes.

3.4.5 Application of Recursion Relations to the Fidelity Amplitude

In this last part of the section we want to show how the recursion relations applied in this section can be used in the context of the fidelity amplitude. Therefore we first give general expressions for the contributions to the fidelity amplitude in the three cases A, B and C and their Laplace transforms, the (one sided) inverse Fourier transforms considered before in this section with imaginary arguments. Afterwards we first show the unitarity of the semiclassical expression for m(t), i.e. m(t) = 1 for $\Gamma = 0$ and a relation between m(t) and the spectral form factor, Eq. (2.67), first derived in the RMT framework in [44].

We start with giving the non-diagonal contributions to $m(t; \Gamma)$ in the three cases. As already explained for one 2-encounter after Eq. (3.39), the only change compared to the corresponding contributions to the survival probability (3.43, 3.51, 3.60) is that the survival probability correction for orbit pairs due to the proximity of encounters given after Eq. (3.43) is replaced by a correction caused by the fact that the encounter stretches of one encounter traverse regions of the same disorder. Compared to the correction to the survival probability the correction due to correlated disorder is smaller than one and has a different functional form, for an orbit with V encounters with each of them possessing I_{α} encounter stretches, it is given by

$$\left\langle \exp\left(\frac{i}{\hbar}\Delta S_{\gamma}\right)\right\rangle = \exp\left[-\Gamma\left(t + \sum_{\alpha=1}^{V} \left(l_{\alpha}^{2} - l_{\alpha}\right) t_{\text{enc}}^{\alpha}\right)\right].$$
 (3.132)

The last equation can be derived in an analogous way as shown for an orbit pair differing by a 2-encounter in Eqs. (3.40, 3.41); a derivation can also be found in [45, 46].

With this we obtain for encounters inside the orbit

$$m_{\mathbf{v},A}(t;\Gamma) = N(\mathbf{v}) \int_{-c}^{c} d\mathbf{s} \, d\mathbf{u} \frac{\left[t - \sum_{\alpha=1}^{V} l_{\alpha} t_{\text{enc}}^{\alpha}\right]^{L}}{L!\Omega^{L-V} \prod_{\alpha=1}^{V} t_{\text{enc}}^{\alpha}} e^{\frac{i}{\hbar} \mathbf{u} \mathbf{s}}$$

$$\times \exp\left[-\Gamma\left(t + \sum_{\alpha=1}^{V} \left(l_{\alpha}^{2} - l_{\alpha}\right) t_{\text{enc}}^{\alpha}\right)\right]. \tag{3.133}$$

Considering in Eq. (3.133) again the terms independent of t_{enc}^{α} , we get

$$m_{\mathbf{v},A}(t;\Gamma) = \left(\frac{1}{T_H \Gamma}\right)^{L-V} N(\mathbf{v}) \prod_{l=2}^{\infty} \left(-\frac{l}{t} \frac{\partial}{\partial \Gamma} - l^2\right)^{\nu_l} \frac{(\Gamma t)^L \exp(-\Gamma t)}{L!},$$
(3.134)

where we used the definition of the components v_l . In a similar way we can derive the contribution for the case B:

$$m_{\mathbf{v},B}(t;\Gamma) = 2\left(\frac{1}{T_H\Gamma}\right)^{L-V} N(\mathbf{v}) \sum_{l_1=2}^{\infty} \frac{l_1 v_{l_1}}{L} \left(-\frac{l_1}{t} \frac{\partial}{\partial \Gamma} - l_1^2\right)^{v_{l_1}-1}$$

$$\times \prod_{\substack{l=2\\l\neq l_1}}^{\infty} \left(-\frac{l}{t} \frac{\partial}{\partial \Gamma} - l^2\right)^{v_l} \frac{(t\Gamma)^{L-1} \exp(-\Gamma t)}{(L-1)!}, \tag{3.135}$$

with an l_1 -encounter at the beginning or end of the trajectory. Finally we obtain for the case C

$$m_{\mathbf{v},C}(t;\Gamma) = \left(\frac{1}{T_H \Gamma}\right)^{L-V} \sum_{l_1,l_2=2}^{\infty} \left(-\frac{l_1}{t} \frac{\partial}{\partial \Gamma} - l_1^2\right)^{v_{l_1}-1} \mathcal{N}_{l_1 l_2}(\mathbf{v}) \left(-\frac{l_2}{t} \frac{\partial}{\partial \Gamma} - l_2^2\right)^{v_{l_2}-1} \times \prod_{\substack{l=2\\l \neq l_1,l_2\\l \neq l_1,l_2}}^{\infty} \left(-\frac{l}{t} \frac{\partial}{\partial \Gamma} - l^2\right)^{v_l} \frac{(t\Gamma)^{L-2} \exp\left(-\Gamma t\right)}{(L-2)!},$$
(3.136)

with an l_1 -encounter and an l_2 -encounter at the beginning and at the end of the trajectory, respectively.

The entire contribution from orbit pairs to $m_{\rm sc}$ (t; Γ) is obtained from Eqs. (3.134–3.136) by summing over all possible vectors \mathbf{v} and finally adding up the three contributions together with the diagonal term (3.27):

$$m_{\text{sc}}(t; \Gamma) = m_{\text{diag}}(t; \Gamma) + \sum_{\mathbf{v}} \left[m_{\mathbf{v}, A}(t; \Gamma) + m_{\mathbf{v}, B}(t; \Gamma) + m_{\mathbf{v}, C}(t; \Gamma) \right]. \tag{3.137}$$

In the case of vanishing perturbation ($\Gamma = 0$) the fidelity amplitude m(t) should be equal to one by the unitarity of quantum evolution. In the following we will show that this property holds using the semiclassical form of m(t) obtained in Sect. 3.1 when $t < T_H$.

As one can immediately see from Eq. (3.27), $m_{\rm sc}(t; \Gamma=0)=1$ within the diagonal approximation. Hence one has to show that all further semiclassical loop contributions vanish for $\Gamma=0$. To this end we will demonstrate that the off-diagonal terms $m_{{\bf v},A}(t;0), m_{{\bf v},B}(t;0)$ and $m_{{\bf v},C}(t;0)$ cancel each other. According to Eqs. (3.134–3.136) they read:

$$m_{\mathbf{v},A}(t;0) = N(\mathbf{v})(-1)^{V} \left(\frac{t}{T_{H}}\right)^{L-V} \frac{\left(\prod_{\alpha=1}^{V} l_{\alpha}\right)}{(L-V)!},$$
 (3.138)

$$m_{\mathbf{v},B}(t;0) = 2N(\mathbf{v})(-1)^{V-1} \frac{V}{L} \left(\frac{t}{T_H}\right)^{L-V} \frac{\left(\prod_{\alpha=1}^{V} l_{\alpha}\right)}{(L-V)!},$$
 (3.139)

$$m_{\mathbf{v},C}(t;0) = \sum_{k,l=2}^{\infty} \frac{\mathcal{N}_{kl}(\mathbf{v})}{lk} (-1)^{V-2} \left(\frac{t}{T_H}\right)^{L-V} \frac{\left(\prod_{\alpha=1}^{V} l_{\alpha}\right)}{(L-V)!}.$$
 (3.140)

To simplify the notation we replaced the summation indices l_1 , l_2 by l, k. Adding these contributions, one can see that the off-diagonal corrections disappear if the following condition is satisfied:

$$\sum_{\mathbf{v}}^{L-V=m} (-1)^{V} \prod_{\alpha=1}^{V} l_{\alpha} \left[N(\mathbf{v}) - 2 \frac{V}{L} N(\mathbf{v}) + \sum_{k,l=2}^{\infty} \frac{\mathcal{N}_{kl}(\mathbf{v})}{kl} \right] = 0.$$
 (3.141)

Exactly this was shown to be fulfilled in the calculation following Eq. (3.101).

Next we want to semiclassically show a remarkable relation between the fidelity amplitude and the spectral form factor (2.67). The form factor $K(\tau; \Gamma)$ considered here now additionally depends parametrically on Γ : This additional dependence is included by allowing each of the two densities of states and by this also the actions of the classical orbits in the exponential contained in (2.70) to depend on an additional parameter. The effect of the phase resulting from this additional dependence is then calculated to obtain RMT results in a similar way as we did it for the fidelity in Eq. (3.20) by assuming that it is randomly accumulated. For more details on the definition of and the semiclassical expression for $K(\tau; \Gamma)$, see [45, 46]. The connection between the quantum fidelity amplitude and parametric spectral correlations was derived in Ref. [44] within an RMT approach. The idea was to use a certain invariance property of the integration measure for the ensemble of random matrices. A corresponding Ward identity [47] then led to

$$-\frac{T_H \beta}{2t^2} \frac{\partial K(t; \Gamma)}{\partial \Gamma} = m(t; \Gamma). \tag{3.142}$$

Here we show how this relationship can be obtained in the framework of our semiclassical approach for systems with and without time-reversal symmetry ($\beta = 1, 2$). To this end it is convenient to work with the Laplace transforms of the semiclassical expressions for the form factor and fidelity.

In order to reveal a systematic structure for the contribution of each encounter stretch and each link, it is instructive to take the Laplace transform of Eq. (3.137) with respect to $\gamma \equiv \Gamma t$ while keeping $\eta \equiv t/(T_H \gamma) = (T_H \Gamma)^{-1}$ fixed:

$$\tilde{F}(q,\eta) = \int_0^\infty d\gamma m_{\rm sc} \left(\eta T_H \gamma; (\eta T_H)^{-1} \right) \exp\left(-q\gamma \right). \tag{3.143}$$

Inserting the expressions for $m_{\rm sc}$ (t; Γ) and performing the Laplace transformation by partial integration gives rise to the perturbative expression (in powers of η)

$$\tilde{F}(q,\eta) = \sum_{n=0}^{\infty} \tilde{F}_n(q) \, \eta^n, \tag{3.144}$$

where the *n*-th term in this expansion originates from trajectory pairs with L-V=n. Explicitly, the terms $\tilde{F}_n(q)$ take the form

$$\tilde{F}_{n}(q) = \sum_{\mathbf{v}}^{L-V=n} \frac{\prod_{l=2}^{\infty} \left(-lq - l^{2}\right)^{v_{l}}}{(q+1)^{L+1}} \left[N\left(\mathbf{v}\right) + 2\sum_{l_{1}=2}^{\infty} N\left(\mathbf{v}\right) \frac{l_{1}v_{l_{1}}}{L} \left(\frac{q+1}{-l_{1}q - l_{1}^{2}}\right) + \sum_{l_{1}, l_{2}=2}^{\infty} \frac{\mathcal{N}_{l_{1}l_{2}}\left(\mathbf{v}\right) (q+1)^{2}}{\left(-l_{1}q - l_{1}^{2}\right) \left(-l_{2}q - l_{2}^{2}\right)} \right].$$
(3.145)

In Eq. (3.145) we again recognise a diagrammatic rule: Every link contributes to $\tilde{F}_n(q)$ a factor $(q+1)^{-1}$ and every *l*-encounter a factor -l(q+l).

Now we turn to the parametric spectral form factor for which we use the following semiclassical expression [45]:

$$K(t;\Gamma) = \frac{2}{\beta} \frac{\Gamma t^2}{T_H} \sum_{\mathbf{v}} \left(\frac{1}{\Gamma T_H} \right)^{L-V} \prod_{l=2}^{\infty} \left(-\frac{l}{t} \frac{\partial}{\partial \Gamma} - l^2 \right)^{v_l} N(\mathbf{v}) \frac{(\Gamma t)^{L-1} e^{-\Gamma t}}{L!}.$$
(3.146)

After taking the Laplace transform (3.143) of the left hand side of Eq. (3.142) we obtain for the *n*th term of the expansion (in powers of η)

$$\tilde{F}'_{n}(q) = \left(n + q \frac{\partial}{\partial q}\right) \sum_{\mathbf{v}}^{L-V=n} \frac{\tilde{N}(\mathbf{v}, q)}{L}, \tag{3.147}$$

where $\tilde{N}(\mathbf{v}, q)$ is defined as

$$\tilde{N}(\mathbf{v}, q) = \frac{N(\mathbf{v})(-1)^{V}}{(q+1)^{L}} \prod_{l=2}^{\infty} (l(q+l))^{v_{l}}.$$
(3.148)

Upon performing the derivatives in Eq. (3.147) we obtain

$$\tilde{F}'_{n}(q) = \sum_{\mathbf{v}}^{L-V=n} \frac{\tilde{N}(\mathbf{v}, q)}{L} \left[\frac{L}{(q+1)} - V + \sum_{l=2}^{\infty} \frac{qv_{l}}{(q+l)} \right]. \tag{3.149}$$

This must be compared with the $\tilde{F}_n(q)$ -term, Eq. (3.145), for the Laplace transform of the fidelity amplitude. Using Eq. (3.148) we can rewrite (3.145) as

$$\tilde{F}_{n}(q) = \sum_{\mathbf{v}}^{L-V=n} \frac{\tilde{N}(\mathbf{v}, q)}{L} \left[\frac{L}{(q+1)} - \sum_{l=2}^{\infty} \frac{2v_{l}}{(q+l)} \right] + (-1)^{V-2} \left(\sum_{k,l=2}^{\infty} \frac{\mathcal{N}_{kl}(\mathbf{v})}{k(q+k)l(q+l)} \right) \frac{\prod_{l=2}^{\infty} (l(q+l))^{v_{l}}}{(q+1)^{L-1}}.$$
 (3.150)

Furthermore, we can simplify this by expressing the matrix elements \mathcal{N}_{kl} (v) in terms of $\tilde{N}(\mathbf{v},q)$. Using Eq. (3.103) and taking into account the additional q-dependent factors we get for the terms in the second line in Eq. (3.150)

$$(-1)^{V-2} \frac{\mathcal{N}_{kl}(\mathbf{v})}{k(q+k)l(q+l)} \frac{\prod_{l=2}^{\infty} (l(q+l))^{v_l}}{(q+1)^{L-1}}$$

$$= -\frac{\tilde{N}(\mathbf{v}^{[k,l\to k+l-1]},q)}{(L-1)} \frac{v_{k+l-1}^{[k,l\to k+l-1]}}{(q+k+l-1)}.$$
(3.151)

We can then rewrite the sum over the dummy vectors, $\mathbf{v}' = \mathbf{v}^{[k,l \to k+l-1]}$, as a sum over \mathbf{v} which gives for the second line in Eq. (3.150):

$$-\sum_{\mathbf{v}}^{L-V=n} \frac{\tilde{N}(\mathbf{v}, q)}{L} \left(\sum_{k,l=2}^{\infty} \frac{v_{k+l-1}}{(q + (k+l-1))} \right). \tag{3.152}$$

By a similar calculation like in Eq. (3.109) we perform the sum over k

$$-\sum_{\mathbf{v}}^{L-V=n} \frac{\tilde{N}(\mathbf{v}, q)}{L} \left(\sum_{l=2}^{\infty} \frac{(l-2)v_l}{(q+l)} \right), \tag{3.153}$$

leading to the following expression for $\tilde{F}_n(q)$:

$$\tilde{F}_n(q) = \sum_{\mathbf{v}}^{L-V=n} \frac{\tilde{N}(\mathbf{v}, q)}{L} \left[\frac{L}{(q+1)} - \sum_{l=2}^{\infty} \frac{lv_l}{(q+l)} \right].$$
(3.154)

The final step is to show that Eq. (3.154) coincides with Eq. (3.149). This is indeed so, since the difference between the two expressions,

$$\sum_{\mathbf{v}}^{L-V=n} \frac{\tilde{N}(\mathbf{v}, q)}{L} \left[V - \sum_{l=2}^{\infty} \frac{qv_l}{(q+l)} - \sum_{l=2}^{\infty} \frac{lv_l}{(q+l)} \right]$$

$$= \sum_{\mathbf{v}}^{L-V=n} \frac{\tilde{N}(\mathbf{v}, q)}{L} \left[V - \sum_{l=2}^{\infty} v_l \right], \tag{3.155}$$

vanishes due to the fact that $V = \sum_{l=2}^{\infty} v_l$. This completes the prove of relationship (3.142) with semiclassical means. This result has the added bonus of showing that we recover the fidelity amplitude in Eq. (3.38) for $\tau \le 1$ for systems with broken time-reversal symmetry as we know that the semiclassical and RMT parametric form factor exactly agree in that regime [45, 46], when knowing the functional form of the parametric form factor.

To show semiclassically that Eq. (3.142) also holds in the symplectic case ($\beta=4$) we consider spin-orbit interaction for spin-1/2 particles. In this case the spectral form factor $K(\tau;\Gamma)$ on the left hand side of Eq. (3.142) is modified to $-\frac{1}{2}K_{\text{GOE}}(-\tau/2;\Gamma)$ [31] with $K_{\text{GOE}}(\tau;\Gamma)$ being the form factor in the GOE-case. The right hand side obtains with spin-orbit interaction the additional factor $(-1/2)^{L-V}$, see Eq. (3.74). A short calculation then shows that Eq. (3.142) also holds in the symplectic case. However, we note here that it is not true for general spin-s particles.

To conclude, in this section we introduced quantum mechanically exact continuity equations first for the time derivative of the survival probability and second for the time derivative of the current. Expressing the latter quantities semiclassically we showed that with these continuity equations we obtain formulas for the survival probability, expressed originally semiclassically in terms of orbits starting and ending inside the system, that express it first in terms of orbits starting inside the system and ending at the lead and second in terms of orbits starting and ending at the lead. Afterwards we showed within our approach, using recursion relations, that

the two continuity equations hold semiclassically to all orders in t/T_H . For the fidelity amplitude we finally proved the unitarity and a relation to the spectral form factor.

Up to now we concentrated mainly on explaining semiclassically results derived before by RMT methods. In the next section however we want to turn to results not calculated by the latter method.

3.5 Effects not Accessed by RMT

In this section we consider the effect of non-diagonal contributions to the fidelity in the Lyapunov regime. Finally we generalise the case of a time-independent perturbation considered up to now in this chapter to a time-dependent one. The orbits then feel different kinds of perturbations during the different traversals of the encounters.

3.5.1 Lyapunov Decay of the Fidelity

Up to now we always considered the case where the disorder average in the calculation of $M_{\rm sc}(t)$ can be performed independently for the trajectory pairs occurring in the calculation of each $m_{\rm sc}(t)$. However, already on the level of the diagonal approximation there is a further contribution originating from configurations where all four trajectories are too close together to perform the disorder average independently. The regime of large Γ where the FGR terms (3.38, 3.39) are rapidly decaying and this contribution becomes important is referred to as the Lyapunov regime, because it decays as $e^{-\lambda t}$ [15].

Here we examine whether additional contributions may arise in this regime from loop diagrams. To this end we briefly review the semiclassical calculation of the diagonal contribution to the fidelity in the Lyapunov regime [15] and consider afterwards the role of trajectories differing at encounters.

Starting from Eq. (3.28), one performs the disorder average along the trajectories no longer independently for both action differences ΔS_{γ_1} and ΔS_{γ_2} . For two nearby trajectories γ_1 , γ_2 , one instead linearises the motion of one trajectory around the other to obtain

$$\Delta S_{\gamma_1} - \Delta S_{\gamma_2} = \int_0^t dt' \, \nabla L_{\gamma_1}^{\Sigma} \left(t' \right) \left[\mathbf{q}_{\gamma_1} \left(t' \right) - \mathbf{q}_{\gamma_2} \left(t' \right) \right], \tag{3.156}$$

where $L_{\gamma_1}^{\Sigma}(t')$ is the Lagrangian associated with the disorder, see Eq. (3.18), and $\mathbf{q}_{\gamma_i}(t')$ denote the coordinates of the trajectories γ_i at time t'. The difference $\mathbf{q}_{\gamma_1}(t') - \mathbf{q}_{\gamma_2}(t')$ can then be expressed by the difference of the final points \mathbf{r} and $\overline{\mathbf{r}}$ of γ_1 and γ_2 , respectively, using the possible exponential separation of long neighboring trajectories in the chaotic case. Assuming again that the action difference is

accumulated during a large number of uncorrelated events leading to a Gaussian distribution of $\Delta S_{\gamma_1} - \Delta S_{\gamma_2}$, as in the FGR regime for ΔS_{γ} in Eq. (3.20), one obtains

$$\left\langle \exp\left[\frac{i}{\hbar} \left(\Delta S_{\gamma_1} - \Delta S_{\gamma_2}\right)\right]\right\rangle$$

$$= \exp\left[-\frac{1}{2\hbar^2} \int_0^t dt' \int_0^t dt'' e^{\lambda(t'+t''-2t)} C_{\nabla \Sigma} \left(\mathbf{r}_1 - \mathbf{r}_2\right)^2\right]$$
(3.157)

with the force correlator $C_{\nabla \Sigma} \equiv \langle \nabla L_{\gamma_1}^{\Sigma} (t') \nabla L_{\gamma_2}^{\Sigma} (t'') \rangle$ and the final positions of two trajectory pairs \mathbf{r}_1 and \mathbf{r}_2 .

Replacing in Eq. (3.157) the second time integral by one with respect to t'-t'' and taking into account the short range behaviour of the force correlator (it vanishes on scales larger than the correlation length ξ) one can perform the (t'-t'')-integral in the range from $-\infty$ to ∞ . Further evaluation of the t'-integral, where one neglects contributions from the lower limit because they are damped by a factor $e^{-\lambda t}$, eventually gives

$$\left\langle \exp\left[\frac{i}{\hbar}\left(\Delta S_{\gamma_1} - \Delta S_{\gamma_2}\right)\right]\right\rangle = \exp\left[-\frac{A}{2\hbar^2}\left(\mathbf{r}_1 - \mathbf{r}_2\right)^2\right].$$
 (3.158)

Here the constant A depends on ξ and the disorder strength. Equation (3.158) is afterwards inserted into the full expression for the fidelity (3.28) finally yielding a contribution proportional to $e^{-\lambda t}$ within the diagonal approximation [15]. We note that when performing the two time integrals in Eq. (3.157), only contributions from t' and t'' close to t (a time of the order $1/\lambda$ apart) mattered. All further contributions are exponentially damped due to the factor $e^{\lambda(t'+t''-2t)}$.

We now consider a possible effect of non-diagonal loop contributions. The basic contribution of this kind would originate from trajectories γ_1 and γ_1' forming pairs as depicted in Fig. 3.1 and two nearly identical trajectories γ_2 and γ_2' . When calculating $C_{\nabla \Sigma}$, correlations between points of γ_1 traversed at different times could get important as the latter quantity depends on the difference of the positions along γ_1 at two different times. However, as we noted below Eq. (3.158), correlations in the Lyapunov regime only matter between points at the end of the orbit, that are a time of the order $1/\lambda$ apart. Compared to that distance, an encounter stretch is exceedingly long, so that correlations between *different* encounter stretches cannot play an important role for this contribution. This implies that there is no significant effect of such orbit pairs in the Lyapunov regime, because there exists, apart from the action difference and the weight function, no further relevant phase change induced by the encounter (depending on the (s, u)-coordinates).

The same reasoning can be directly carried over to correlated orbits differing by an arbitrary number of encounters, and hence no off-diagonal interference contributions from orbits differing in encounters can be obtained in the Lyapunov regime. This constitutes another distinct difference between FGR- and Lyapunov decay.

3.5.2 Effect of a Time-Dependent Perturbation

Many physical situations require a generalisation of fidelity decay to systems with a time-varying perturbation. This is relevant if a subsystem evolves under the influence of a time-dependent external environment or may arise if one models fidelity decay for a many-body system in terms of single-particle dynamics exposed to an external fluctuating potential mimicking the mutual interactions. Fidelity decay for time-dependent perturbations has been addressed in Refs. [48, 49] in numerical studies of periodically kicked systems and in Ref. [50] in the context of decoherence. Coupling to an external environment and its connection to fidelity decay has semiclassically been treated in [51, 52] and in Ref. [53], which represents a direct extension of the semiclassical approach of Refs. [15, 17] to a spatially and time-varying random potential.

In Ref. [53], both a finite disorder correlation length ξ (and associated time ξ/v_0 with v_0 the particle velocity) as well as a finite correlation time τ_0 characterising temporal fluctuations were introduced. It was shown semiclassically on the level of the diagonal approximation, how the FGR decay is governed by a decay rate Γ into which both time scales generally enter and which is predominantly determined by the shorther of the two times, ξ/v_0 or τ_0 , if they strongly differ.

In this subsection we will use the perturbation model of Ref. [53] and illustrate the effect of a spatially and time-dependent perturbation for the representative case of the first quantum correction, $m_{\text{GOE}}^{q_1}(t; \Gamma)$, see Eq. (3.39) for the static case. Since this interference contribution is based on the mechanism that the same (static) perturbation exists along the two encounter stretches traversed at different times we can compute how finite correlation times τ_0 will reduce this effect.

We will consider the interesting case where $\xi/v_0 \ll \tau_0$ so that Γ depends only on the spatial fluctuations and not on τ_0 . (For pure temporal fluctuations or $\xi/v_0 \gg \tau_0$, the spatial proximity of the encounter stretches cannot have an important effect. A change in τ_0 will thus alter the exponential decay rate Γ and thereby mask the effect of τ_0 on quantum fidelity contributions.) We assume that the time dependence and the spatial dependence of the perturbation can be separated, i.e.

$$\Delta S_{\gamma} = \int_0^t dt' V\left(\mathbf{q}(t')\right) W(t'), \tag{3.159}$$

which allows for further analytical treatment. We first calculate the averaged phase difference for this perturbation similar as in Eqs. (3.40, 3.41)

$$\left\langle \exp\left(\frac{i}{\hbar}\Delta S_{\gamma}\right)\right\rangle = \exp\left(-\frac{2}{\hbar^{2}}\left\langle\int_{0}^{t_{\text{enc}}}dt\,dt'V\left(\mathbf{q}(t)\right)W(t)\right.$$

$$\left.\times V\left(\mathbf{q}(t_{l}+2t_{\text{enc}}-t')\right)W(t_{l}+2t_{\text{enc}}-t')\right\rangle\right)\exp\left(-\Gamma t\right)$$

(3.160)

with a loop of length t_l connecting the two encounter stretches. The last contribution in the second line of this equation is the overall exponential decay, not taking into account the correlated way the perturbation acts during the encounter. The additional effects of this correlation are included in the first exponential in the equation above, and yielded a contribution proportional to $e^{-2\Gamma t_{enc}}$ for an explicitly time-independent perturbation. However we now have to analyse this contribution in more detail: First we again use that the two stretches during the encounter are very close together implying $\mathbf{q}(t_l + 2t_{enc} - t') \approx \mathbf{q}(t')$. Furthermore, we assume in this subsection, as in Ref. [53], a Gaussian form of the spatial and the time-dependent perturbation

$$\left\langle V\left(\mathbf{q}(t)\right) W(t) V\left(\mathbf{q}(t_l + 2t_{\text{enc}} - t')\right) W(t_l + 2t_{\text{enc}} - t')\right\rangle \\
= \frac{\Gamma v_0 \hbar^2}{\xi \sqrt{\pi}} \exp\left(-\frac{\left|\mathbf{q}(t) - \mathbf{q}(t')\right|^2}{\xi^2}\right) \exp\left(-\frac{\left(t_l + 2t_{\text{enc}} - t' - t\right)^2}{\tau_0^2}\right).$$
(3.161)

The two time integrals in Eq. (3.160) are transformed into one integral with respect to $\tau = t - t'$ and one with respect to $\tau' = (t + t')/2$. The integral with respect to τ is performed from $-\infty$ to ∞ . Here our assumption that the correlation length of the spatial part, $V(\mathbf{q}(t))$, is much shorter than the one of the time-dependent part W(t), $\xi \ll v_0 \tau_0$ enters. The integral with respect to τ' is from 0 to $t_{\rm enc}$, and we thus obtain from Eq. (3.160)

$$\left\langle \exp\left(\frac{i}{\hbar}\Delta S_{\gamma}\right)\right\rangle = \exp\left(-\frac{2\Gamma v_{0}}{\xi\sqrt{\pi}}\left\langle \int_{0}^{t_{\text{enc}}} d\tau' \int_{-\infty}^{\infty} d\tau \exp\left(-\frac{v_{0}^{2}\tau^{2}}{\xi^{2}}\right)\right.\right.$$

$$\left. \times \exp\left(-\frac{\left(t_{l} + 2t_{\text{enc}} - 2\tau'\right)^{2}}{\tau_{0}^{2}}\right)\right\rangle \exp\left(-\Gamma t\right). \tag{3.162}$$

We perform the two time integrals taking into account that only terms linear in $t_{\rm enc}$ will give a contribution when performing the s, u-integrals. This finally yields for the action difference due to the perturbation

$$\left\langle \exp\left(\frac{i}{\hbar}\Delta S_{\gamma}\right)\right\rangle = \left[1 - 2\Gamma \exp\left(-\frac{t_{l}^{2}}{\tau_{0}^{2}}\right)t_{\text{enc}} + \mathcal{O}\left(t_{\text{enc}}^{2}\right)\right] \exp\left(-\Gamma t\right). \quad (3.163)$$

The first term in the square bracket gives a contribution independent of the perturbation and is cancelled by the contribution coming from one-leg-loops. We insert the remaining term into our expression for $m_{\text{GOE}}^{q_1}(t; \Gamma, \tau_0)$, evaluated as in the first two sections of this chapter, but that it now depends additionally on the correlation time τ_0 of the explicitly time-dependent part of the potential:

$$m_{\text{GOE}}^{q_1}(t; \Gamma, \tau_0) = \int_{-c}^{c} ds \, du \int_{0}^{t-2t_{\text{enc}}} \frac{(t - 2t_{\text{enc}} - t_l)}{\Omega} (-2\Gamma) \, e^{\frac{i}{\hbar}us} \exp\left(-\Gamma t - \frac{t_l^2}{\tau_0^2}\right).$$
(3.164)

After performing the remaining integrals we finally obtain the leading quantum correction in the presence of an explicitly time-dependent perturbation

$$m_{\text{GOE}}^{q_1}(t; \Gamma, \tau_0) = -\frac{2\Gamma}{T_H} \left[\frac{\sqrt{\pi}}{2} \tau_0 t \text{Erf}\left(\frac{t}{\tau_0}\right) - \frac{\tau_0^2}{2} \left(1 - \exp\left(-\frac{t^2}{\tau_0^2}\right)\right) \right] \exp\left(-\Gamma t\right), \tag{3.165}$$

with the error function $\operatorname{Erf}(x) = \frac{2}{\sqrt{\pi}} \int_0^x dt \exp\left(-t^2\right)$. By expanding $\operatorname{Erf}(x)$ we obtain in the limit $t \ll \tau_0$:

$$m_{\text{GOE}}^{q_1}(t \ll \tau_0; \Gamma, \tau_0) \simeq -\frac{\Gamma t^2}{T_H} e^{-\Gamma t} \left[1 - \frac{1}{6} \left(\frac{t}{\tau_0} \right)^2 \right],$$
 (3.166)

indicating a small reduction of the interference term (3.39), $-(\Gamma t^2/T_H) \exp(-\Gamma t)$ of the static case.

Much more interesting and relevant is the opposite limit, $t \gg \tau_0$, where we find

$$m_{\text{GOE}}^{q_1}(t \gg \tau_0; \Gamma, \tau_0) \simeq -\frac{\Gamma t^2}{T_H} e^{-\Gamma t} \left[\sqrt{\pi} \frac{\tau_0}{t} - \left(\frac{\tau_0}{t}\right)^2 \right].$$
 (3.167)

Quantum fidelity corrections (3.39) in the static case arise at time scales t given by the geometrical mean, $(\tilde{t}_\xi T_H)^{1/2}$, of the Heisenberg time and the decay time $\tilde{t}_\xi = 1/(2\Gamma)$ from Eq. (3.24). Equation (3.167) hence implies, in view of the hierarchy of timescales, that the quantum fidelity contributions are suppressed (by τ_0/t) compared to the static case, if τ_0 is much smaller than the above mentioned geometrical mean that usually represents a large time scale. Together with the initial assumption, $\xi/v_0 \ll \tau_0$, we can conclude that quantum fidelity contributions are suppressed for time-varying perturbations with $\xi/v_0 \ll \tau_0 \ll (\tilde{t}_\xi T_H)^{1/2}$. Furthermore, such a suppression of this negative quantum correction implies that upon reducing τ_0 , that is introducing faster time variations, the overall fidelity amplitude increases in the FGR regime and approaches $\exp(-\Gamma t)$.

Finally we mention that we treated besides fidelity decay and the survival probability in [2, 54] also another example of decay: molecular photodissociation [55, 56] and atomic photoionisation [9, 57], where the molecule or atom absorbs one or several photons such that the system is (highly) excited to an intermediate configuration, which subsequently allows for decay, i.e. dissociation or ionisation of the system. If this decay is sufficiently slow, a large portion of the complex, presumably chaotic phase space of the excited system can be explored and the statistics of such processes are assumed to show universal behaviour. In semiclassical approaches in this case usually the autocorrelation function of photodissociation-cross sections is studied. Previous approaches were limited to the diagonal approximation [58, 59]. We extended this calculation also to non-diagonal contributions.

To summarise, we presented in this chapter semiclassical results for timedependent processes: The calculation of quantum corrections to the survival probability and the fidelity decay was explained in detail. It was checked that the obtained results are unitary and that they fulfil the continuity equation in the case of the survival probability and a relation between the fidelity amplitude and the parametric spectral form factor. Finally also effects not accessed by RMT are discussed.

In the next chapter we return mainly to the stationary transport process introduced in Chap. 2 and consider there especially the effect of a non-vanishing Ehrenfest-time.

References

- 1. Waltner, D., Gutiérrez, M., Goussev, A., Richter, K.: Phys. Rev. Lett. 101, 174101 (2008)
- 2. Gutiérrez, M., Waltner, D., Kuipers, J., Richter, K.: Phys. Rev. E 79, 046212 (2009)
- 3. Kuipers, J., Waltner, D., Gutiérrez, M., Richter, K.: Nonlinearity 22, 1945 (2009)
- 4. Gutkin, B., Waltner, D., Gutiérrez, M., Kuipers, J., Richter, K.: Phys. Rev. E 81, 036222 (2010)
- 5. Milner, V., Hanssen, J.L., Campbell, W.C., Raizen, M.G.: Phys. Rev. Lett. 86, 1514 (2001)
- 6. Friedman, N., Kaplan, A., Carasso, D., Davidson, N.: Phys. Rev. Lett. 86, 1518 (2001)
- Marcus, C.M., Rimberg, A.J., Westervelt, R.M., Hopkins, P.F., Gossard, A.C.: Phys. Rev. Lett. 69, 506 (1992)
- 8. Doron, E., Smilansky, U., Frenkel, A.: Phys. Rev. Lett. 65, 3072 (1990)
- 9. Stania, G., Walther, H.: Phys. Rev. Lett. 95, 194101 (2005)
- 10. Casati, G., Maspero, G., Shepelyansky, D.L.: Phys. Rev. E 56, 6233(R) (1997)
- 11. Frahm, K.: Phys. Rev. E **56**, 6237(R) (1997)
- 12. Savin, D.V., Sokolov, V.V.: Phys. Rev. E 56, 4911(R) (1997)
- 13. Savin, D.V., Sommers, H.-J.: Phys. Rev. E 68, 036211 (2003)
- 14. Puhlmann, M., Schanz, H., Kottos, T., Geisel, T.: Europhys. Lett. 69, 313 (2005)
- 15. Jalabert, R.A., Pastawski, H.M.: Phys. Rev. Lett. **86**, 2490 (2001)
- 16. Peres, A.: Phys. Rev. A 30, 1610 (1984)
- 17. Cucchietti, F.M., Pastawski, H.M., Jalabert, R.A.: Phys. Rev. B 70, 035311 (2004)
- 18. Richter, K., Ullmo, D., Jalabert, R.A.: J. Math. Phys. 37, 5087 (1996)
- 19. Jacquod, P., Silvestrov, P.G., Beenakker, C.W.J.: Phys. Rev. E 64, 055203(R) (2001)
- 20. Cerruti, N.R., Tomsovic, S.: Phys. Rev. Lett. 88, 054103 (2002)
- 21. Prosen, T., Seligman, T.H., Žnidarič, M.: Prog. Theor. Phys. Suppl. 150, 200 (2003)
- 22. Gorin, T., Prosen, T., Seligman, T.: New J. Phys. 6, 20 (2004)
- 23. Stöckmann, H.-J., Schäfer, R.: New J. Phys. 6, 199 (2004)
- 24. Stöckmann, H.-J., Schäfer, R.: Phys. Rev. Lett. 94, 244101 (2005)
- 25. Gorin, T., Prosen, T., Seligman, T.H., Žnidarič, M.: Phys. Rep. 435, 33 (2006)
- 26. Goussev, A., Richter, K.: Phys. Rev. E 75, 015201(R) (2007)
- 27. Goussey, A., Waltner, D., Richter, K., Jalabert, R.A.: New J. Phys. 10, 093010 (2008)
- 28. Braun, P.A., Heusler, S., Müller, S., Haake, F.: Eur. Phys. J. B 30, 189 (2002)
- 29. Brouwer, P.W., Rahav, S.: Phys. Rev. B 74, 075322 (2006)
- 30. Heusler, S., Müller, S., Braun, P., Haake, F.: Phys. Rev. Lett. 96, 066804 (2006)
- 31. Müller, S., Heusler, S., Braun, P., Haake, F., Altland, A.: Phys. Rev. E 72, 046207 (2005)
- 32. Müller, S.: Periodic-orbit approach to universality in quantum Chaos, Ph.D. thesis, Universität Duisburg Essen (2005)
- 33. Kuipers, J., Sieber, M.: Nonlinearity 20, 909 (2007)
- 34. Zaitsev, O., Frustaglia, D., Richter, K.: Phys. Rev. Lett. 94, 026809 (2005)
- 35. Zaitsev, O., Frustaglia, D., Richter, K.: Phys. Rev. B 72, 155325 (2005)
- 36. Bolte, J., Waltner, D.: Phys. Rev. B 76, 075330 (2007)
- 37. Bolte, J., Keppeler, S.: Ann. Phys. 274, 125 (1999)
- Waltner, D.: Spin-Bahn Kopplung in mesoskopischer Physik: Ein semiklassischer Zugang, VDM-Verlag Dr. Müller, Saarbrücken, 2011
- 39. Richter, K., Sieber, M.: Phys. Rev. Lett. 89, 206801 (2002)

References 87

- 40. Sieber, M.: J. Phys. A 32, 7679 (1999)
- 41. Hannay, J., de Almeida, A.O.: J. Phys. A 17, 3429 (1984)
- 42. Baranger, H.U., Jalabert, R.A., Stone, A.D.: Phys. Rev. Lett. 70, 3876 (1993)
- 43. Baranger, H.U., Jalabert, R.A., Stone, A.D.: Chaos 3, 665 (1993)
- 44. Kohler, H., Smolyarenko, I.E., Pineda, C., Guhr, T., Leyvraz, F., Seligman, T.H.: Phys. Rev. Lett. **100**, 190404 (2008)
- 45. Nagao, T., Braun, P., Müller, S., Saito, K., Heusler, S., Haake, F.: J. Phys. A 40, 47 (2007)
- 46. Kuipers, J., Sieber, M.: J. Phys. A 40, 935 (2007)
- 47. Ward, J.C.: Phys. Rev. 78, 182 (1950)
- 48. Jacquod, P., Silvestrov, P.G., Beenakker, C.W.J.: Phys. Rev. E 64, 055203(R) (2001)
- 49. Benenti, G., Casati, G.: Phys. Rev. E **65**, 066205 (2002)
- 50. Cucchietti, F.M., Dalvit, D.A.R., Paz, J.P., Zurek, W.H.: Phys. Rev. Lett. 91, 210403 (2003)
- 51. Petitjean, C., Jacquod, P.: Phys. Rev. Lett. 97, 124103 (2006)
- 52. Petitjean, C., Jacquod, P.: Phys. Rev. Lett. 97, 194103 (2006)
- 53. Cucchietti, F.M., Lewenkopf, C.H., Pastawski, H.M.: Phys. Rev. E 74, 026207 (2006)
- 54. Gutiérrez, M.: From spectral statistics to decay in quantum chaotic systems: a semiclassical analysis beyond Random Matrix Theory, Ph.D. thesis, Universität Regensburg, (2008)
- 55. Baumert, T., Grosser, M., Thalweiser, R., Gerber, G.: Phys. Rev. Lett. 67, 3753 (1991)
- 56. Schinke, R.: Photodissociation Dynamics. Cambridge University Press, Cambridge (1993)
- 57. Lawley, K.P.: Photodissociation and Photoionization. Wiley, New York (1995)
- 58. Agam, O.: Phys. Rev. E 61, 1285 (2000)
- 59. Eckhardt, B., Fishman, S., Varga, I.: Phys. Rev. E 62, 7867 (2000)

Chapter 4 Ehrenfest-Time Effects in Mesoscopic Systems

This chapter is devoted to the most prominent universal effect in ballistic systems beyond RMT that can be accessed by semiclassical methods: the effect of a non-zero Ehrenfest-time. The Ehrenfest-time [1] provides a separation between the timescales when the dynamics of an initially spatially localised wave packet can be described by classical mechanics on the one hand and when it is dominated by wave interference on the other hand, for an illustration of this transition see Fig. 1.1. For an estimate we consider two points inside the wave packet a distance λ_F apart and calculate the time until they feel the effect of the boundary, i.e. until they are a distance of the order of the system size $\mathcal L$ apart taking into account the possible exponential separation of neighbouring trajectories in chaotic systems. This yields for the Ehrenfest-time τ_E

$$e^{\lambda \tau_E} \approx \frac{\mathcal{L}}{\lambda_F}, \quad \tau_E \approx \frac{1}{\lambda} \ln \left(\frac{\mathcal{L}}{\lambda_F} \right).$$
 (4.1)

Usually a more general definition is applied: The Ehrenfest-time is given by a time logarithmically diverging with \hbar in the semiclassical limit defined only up to a classical constant inside the logarithm. That this time can lead to corrections to the RMT result for the conductance was first noticed by Aleiner and Larkin [2]: Modelling the scattering off the curved walls in ballistic systems by a small amount of disorder they took into account that orbits scattered under a small angle need special consideration as the motion of the outgoing orbit can be obtained for long times in linearised approximation around the motion of the incoming orbit. This was then generalised to ballistic systems in [3]. We review this calculation in the first section of this chapter. Afterwards we analyse the effect of a non-zero Ehrenfest-time on the fidelity amplitude and the survival probability, the latter result is supported by numerical simulations. We then consider additionally tunnel barriers in the leads and describe the dependence of the variance of the conductance for non-zero Ehrenfest-time on the tunnel probability. Returning to the transmission and reflection for perfectly transmitting barriers we calculate the Ehrenfest-time dependence in one order lower in N

We will often refer to this calculation as field-theoretical approach to describe Ehrenfest-time effects.

than in first section of this chapter. Afterwards we apply the gained insight on possible orbital configurations to the calculation of the Ehrenfest-time dependence of the spectral form factor. Our result differs from a previous semiclassical result [4] but agrees with the field-theoretical prediction of [5]. In the fifth section we calculate the dependence on the Ehrenfest-time of correlation functions of arbitrarily many pairs of scattering matrices at different energies to leading order in *N*. Finally we show an application of the last result: We determine in the last section the spectral density of a chaotic Andreev billiard for non-zero Ehrenfest-time, recall the discussion in Sect. 1.1. The corresponding results were published in [6–11].

4.1 Leading-Order Quantum Correction to the Conductance

In this section we want to explain how the contributions to the transmission calculated in Sect. 2.3 are influenced by a non-zero Ehrenfest-time. The diagonal (classical) contribution, see Sect. 2.3, is independent of the Ehrenfest-time as the orbit pairs do not differ in encounters and thus involve no dependence on \hbar . To explain how the leading-order quantum correction in N is changed by a non-zero Ehrenfest-time for clean chaotic systems we follow the pioneering work [3] that has later been extended to the reflection [12–14], including a distinction between different Ehrenfest-times. To this end, we directly start from Eq. (2.48); however, we have to be more careful when evaluating the ϵ -integral: In our former calculation we assumed $\mathrm{e}^{-\tau_E/\tau_D} = \left(2m\lambda\hbar/p^2\right)^{\frac{1}{\lambda\tau_D}} \approx 1$, requiring $\tau_E \ll \tau_D$. Lifting however, this strong restriction for τ_D , but still keeping it large enough to fulfil our assumption of chaotic dynamics, we obtain

$$\left|t_{\alpha,\beta}(k,\tau_E)\right|_{\mathcal{L}}^2 = -\frac{1}{(N_1 + N_2)^2} e^{-\tau_E/\tau_D},$$
 (4.2)

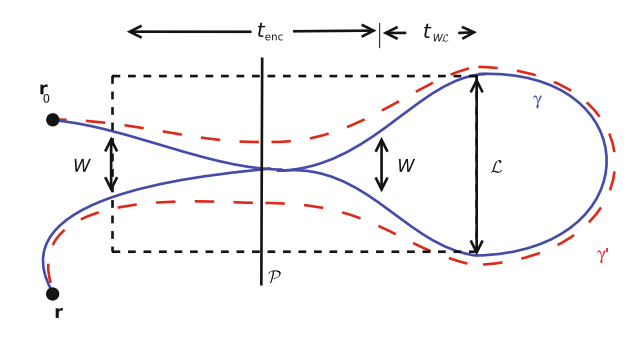
i.e. an exponential suppression of the non-diagonal contribution due to the Ehrenfest-time. This dependence has been confirmed in numerical simulations for chaotic maps [13, 15]. Experimentally Ehrenfest-time signatures were found in antidot lattices in [16] probing the effect of weak localisation. The same dependence as in Eq. (4.2) holds for the reflection and coherent backscattering contribution [12, 13] implying that the current conservation relation (2.46) is also fulfilled at this order in *N*.

4.2 Non-zero Ehrenfest-Time for Time-Dependent Processes

In the last section we explained how Ehrenfest-time effects appear in stationary processes considering the conductance. Signatures of the Ehrenfest-time τ_E were however, also studied in the time domain [4, 17, 18]. Here we semiclassically compute

² Using the estimate that $1/\lambda$ is of the order of the free flight time, $\lambda \approx p/(m\mathcal{L})$, we obtain $2m\lambda\hbar/p^2 \approx \lambda_F/\mathcal{L}$ and by this consistency with Eq. (4.1).

Fig. 4.1 Sketch of trajectories γ and γ' with a 2-encounter illustrating the length restrictions in the case of non-vanishing Ehrenfest-time



the τ_E -dependence of the first quantum correction to $\rho(t)$ given in Eq. (3.37) in the presence of time-reversal symmetry.

We start with deriving the Ehrenfest-time dependence of $\rho_{2ll}(t)$, for the underlying trajectories, see Figs. 3.1, 4.1. We show here the explicit dependence of the constant c introduced in Eq. (2.44) and approximated by one in the last section on system parameters [18]. This also opens the possibility to compare our analytical results with the numerics presented below.

Note that the different encounter stretches escape in an uncorrelated manner when their spatial distance becomes of the order of the size of the opening *W* or larger, because then the fact that one encounter stretch touches the opening does not imply that the other also has to touch the opening. We thus require that inside of an encounter two segments of the trajectory are separated by distances less than *W*, see Fig. 4.1. This leads to the following definition of the duration of the encounter³

$$t_{\rm enc} \approx \frac{1}{\lambda} \ln \left(\frac{W^2 \hbar}{\mathcal{L} \lambda_F |su|} \right),$$
 (4.3)

where \mathcal{L} is of the order of the system size. Specifically, on the right hand side of the encounter, depicted in Fig. 4.1, the stretches should be separated by a distance of the order of \mathcal{L} in order to close themselves and form a loop.⁴ On the left side, however, the encounter stretches have to be separated only by the distance W as we first consider loops with two legs (2ll). This means the minimal time of the trajectory is $2t_{\text{enc}} + 2t_{W\mathcal{L}}$, where

$$t_{WL} \approx \lambda^{-1} \ln(\mathcal{L}/W)$$
 (4.4)

³ The reason for the special choice of c in Eq. (4.3) can be best seen within the configuration-space approach introduced in Chap. 2. One therefore needs the monodromy matrix element $M_{12} \approx (m\lambda)^{-1} \exp(\lambda t/2)$ determining the position difference of two orbits at time t, given by W, as a function of the initial angle difference ϵ and the approximation $\lambda \approx p/(m\mathcal{L})$. This yields $t_{\rm enc} \approx 2/\lambda \ln [W/(\mathcal{L}\epsilon)]$ in the configuration-space approach. For a detailed derivation see [13]. Comparing then the constants c in the configuration and in the phase-space approach one finally arrives at Eq. (4.3).

⁴ This condition for the minimal loop duration is equivalent to the one in the last section. Note here that setting $W=\mathcal{L}$ in $t_{\rm enc}\approx 2/\lambda \ln \left[W/(\mathcal{L}\epsilon)\right]$ obtained in the last footnote yields the same expression for $t_{\rm enc}$ as setting c=1 in Eq. (2.45) as done in the last section.

is the time it at least takes for the stretches to be separated by the distance \mathcal{L} when they are initially separated by the distance W. The density $w_{2ll}(\boldsymbol{u}, \boldsymbol{s}, \boldsymbol{t})$ in (3.29) and later also $w_{1ll}(\boldsymbol{u}, \boldsymbol{s}, \boldsymbol{t})$ (3.33) should be multiplied by a Heaviside theta function $\Theta(x)$ in time ensuring that a contribution exists only if the trajectory time \boldsymbol{t} is sufficiently long to enable a closed path. Accordingly, the weight function (3.29) is slightly modified by introducing these minimal times and takes the form

$$w_{2ll}(u, s, t) = \frac{[t - 2(t_{enc} + t_{WL})]^2}{2\Omega t_{enc}} \Theta(t - 2(t_{enc} + t_{WL})).$$
(4.5)

To account for the proximity correction to the survival probability explained before Eq. (3.30) we again multiply by e^{t_{enc}/τ_D} with t_{enc} defined in Eq. (4.3) as the encounter stretches escape in a correlated manner if they are less than a distance W apart. Now we are in the position to calculate the Ehrenfest-time dependence of $\rho_{2ll}(t)$. In order to avoid performing the integrals resulting finally from the phase-space integrals over a finite range we will study the Ehrenfest-time dependence of the inverse Fourier transform of the corresponding contribution to the survival probability and finally transform this back to the survival probability. We thus define

$$\rho_{2ll}(\omega) = \int_0^\infty dt \, \rho_{2ll}(t) e^{2i\pi\omega t}
= \frac{1}{2T_H} \int_0^\infty dt \, I^{2ll}(\omega) t^2 e^{-(1-2i\pi\omega\tau_D)(t+2t_{WL})/\tau_D}$$
(4.6)

with $I^{2ll}(t)$ defined as

$$I^{211}(\omega) \equiv \frac{1}{\pi \hbar} \int_{-W\sqrt{\hbar}/\sqrt{\mathcal{L}\lambda_F}}^{W\sqrt{\hbar}/\sqrt{\mathcal{L}\lambda_F}} du \int_{0}^{W\sqrt{\hbar}/\sqrt{\mathcal{L}\lambda_F}} ds \frac{e^{(i/\hbar)us}}{t_{\text{enc}}} e^{-t_{\text{enc}}/\tau_D + 4i\pi\omega t_{\text{enc}}}, \quad (4.7)$$

again using $c = W\sqrt{\hbar}/\sqrt{\mathcal{L}\lambda_F}$, compare Eqs. (2.54) and (4.3). The s, u-integrals are best performed by the substitutions $x = us\mathcal{L}\lambda_F/\left(\hbar W^2\right)$ and $\sigma = W\sqrt{\hbar}/\left(\sqrt{\mathcal{L}\lambda_F}u\right)$ with the limits -1 < x < 1 and $1 < \sigma < 1/|x|$. Calculating now the σ -integral, that essentially cancels the $t_{\rm enc}$ in the denominator, yields

$$I^{2ll}(\omega) = \frac{W^2 \lambda}{\pi \mathcal{L} \lambda_F} \int_{-1}^1 dx \cos\left(\frac{W^2 x}{\mathcal{L} \lambda_F}\right) |x|^{(1 - 4i\pi\omega\tau_D)/(\lambda\tau_D)}.$$
 (4.8)

Next we perform the *x*-integral by partial integration neglecting again rapidly oscillating terms that are cancelled by the time average to obtain

$$I^{2ll}(\omega) = -\frac{1 - 4i\pi\omega\tau_D}{\tau_D} e^{-(1 - 4i\pi\omega\tau_D)\tau_E^0/\tau_D}$$
(4.9)

with the open Ehrenfest-time $\tau_E^0 = \lambda^{-1} \ln \left[W^2 / (\mathcal{L}\lambda_F) \right]$ [18]. We now insert this expression in Eq. (4.6) to transform the resulting expression back to the survival probability contribution $\rho_{2ll}(t)$:

$$\rho_{2ll}(t) = \int_{-\infty}^{\infty} d\omega \, \rho_{2ll}(\omega) e^{-2i\pi\omega t}
= \frac{\left(t - 2\tau_E^{e}\right)^2}{2\tau_D T_H} e^{-(t - \tau_E^{o})/\tau_D} \Theta(t - 2\tau_E^{e})
- 2\frac{\left(t - 2\tau_E^{e}\right)}{T_H} e^{-(t - \tau_E^{o})/\tau_D} \Theta(t - 2\tau_E^{e}).$$
(4.10)

Here we additionally introduced the escape Ehrenfest-time $2\tau_E^e = \tau_E^o + \tau_E^c$ with the closed Ehrenfest-time $\tau_E^c = \lambda^{-1} \ln(\mathcal{L}/\lambda_F)$ [18]. The same procedure we now perform for the one-leg-loops, we thus consider the Fourier transform of $\rho_{III}(t)$

$$\rho_{111}(\omega) = \frac{2}{T_H} \int_0^\infty dt \, I^{111}(\omega) \, t \, e^{-(1 - 2i\pi\omega\tau_D)(t + 2t_{WL})/\tau_D}$$
 (4.11)

with

$$I^{111}(\omega) = \frac{1}{\pi\hbar} \int_{-W\sqrt{\hbar}/\sqrt{L\lambda_F}}^{W\sqrt{\hbar}/\sqrt{L\lambda_F}} du \int_{0}^{W\sqrt{\hbar}/\sqrt{L\lambda_F}} ds \int_{0}^{\lambda^{-1} \ln\left[W\sqrt{\hbar}/\left(\sqrt{\lambda_F \mathcal{L}}|s|\right)\right]} dt' \frac{e^{(i/\hbar)us}}{\bar{t}_{enc}}$$

$$\times e^{-\bar{t}_{enc}/\tau_D + 4i\pi\omega\bar{t}_{enc}}$$

$$= e^{-(1-4i\pi\omega\tau_D)\tau_E^0/\tau_D}$$

$$(4.12)$$

with $\bar{t}_{\rm enc} \equiv t' + \lambda^{-1} \ln \left[W \sqrt{\hbar} / (\sqrt{\mathcal{L} \lambda_F} |u|) \right]$. The integrals in the last equation are performed by the substitutions given after Eq. (3.34). Inserting afterwards $I^{111}(\omega)$ in $\rho_{111}(\omega)$ and performing the inverse Fourier transform like for $\rho_{211}(t)$ in Eq. (4.10) this yields

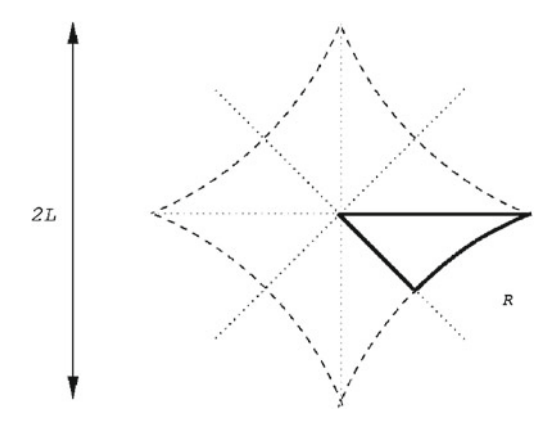
$$\rho_{111}(t) = 2 \frac{\left(t - 2\tau_E^{\text{e}}\right)}{T_H} e^{-(t - \tau_E^{\text{o}})/\tau_D} \Theta(t - 2\tau_E^{\text{e}}). \tag{4.13}$$

Finally we thus obtain the overall contribution from orbit pairs differing in one encounter for non-zero Ehrenfest-time

$$\rho_{2ll}(t) + \rho_{1ll}(t) = e^{-(t - \tau_E^0)/\tau_D} \frac{(t - 2\tau_E^0)^2}{2\tau_D T_H} \Theta(t - 2\tau_E^0). \tag{4.14}$$

For an intuitive interpretation of the last formula we remark that the length of the encounter (box in Fig. 3.1) is of the order of the Ehrenfest-time. This can be seen by noting that $t_{\rm enc}$ in Eq. (4.3) is logarithmically dependent on |su|. When substituting in the calculation above $|su| = y\hbar$ to cancel the \hbar in the phases, we obtain $t_{\rm enc} = \lambda^{-1} \left(\ln \hbar^{-1} + \mathcal{O}(1) \right)$. With this in mind, we recognise two competitive effects of the Ehrenfest-time occurring in (4.14): On one hand the quantum corrections in (4.14) can occur only for orbits longer than $2\tau_E^e$, because otherwise the orbits cannot complete the encounter. This fact is taken into account by the Θ -function in (4.14) which decreases this quantum correction. On the other hand, after the orbit has

Fig. 4.2 Construction of the DD billiard: It is defined as the fundamental domain of the area confined by four intersecting disks of radius R centred at the vertices of a square of length 2L (taken from [20]). In the numerical simulations described here L = 100 and R = 131 are considered



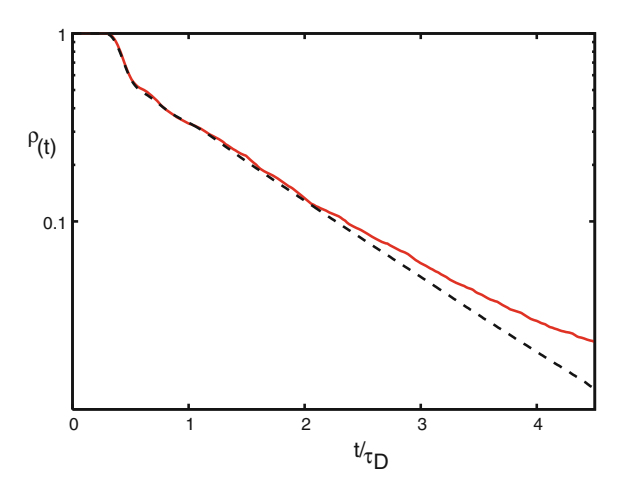
traversed an encounter, this quantum correction is enhanced by the Ehrenfest-time, because of the enhanced survival probability due to the fact that the orbit cannot escape during the second encounter stretch, if it did not escape during the first one.

After the analytical calculations of quantum corrections to the survival probability, we want to compare now our semiclassical predictions with quantum calculations of $\rho(t)$ based on the numerical propagation of Gaussian wave packets inside a billiard. We consider the open DD billiard depicted on the left in Fig. 1.6—we already encountered this billiard in Fig. 1.1—that is classically chaotic. This billiard is defined as the fundamental domain of the area confined by four intersecting disks of radius R centred at the vertices of a square of length 2L, for the construction see also Fig. 4.2. More details about the simulations performed by A. Goussev can also be found in [19]. We express our system parameters used in the simulations in terms of the mean free flight time τ_f , i.e. the average time between two bounces of the particle with the wall: We obtain for the Lyapunov exponent $\lambda^{-1} \simeq 3\tau_f$, for the dwell time $\tau_D \simeq 15\tau_f$, for the Heisenberg time $T_H \simeq 159\tau_f$. We furthermore consider $\mathcal{L} = \sqrt{A}$ with A the area of the system, $\lambda_F = 3$, L and R as given in the caption of Fig. 4.2, an opening of width W = 16 and N = 10 open channels. Its position is indicated in the left diagram of Fig. 1.6. We then obtain $\tau_E^0 = 2.55\tau_f$ and $\tau_E^c = 8.25\tau_f$. In Fig. 4.3 we compare the decay $\rho_{\rm am}^{sim}(t)$ (full line) for a representative wave-packet simulation with the corresponding classical decay, $\rho_{cl}^{sim}(t)$ (dashed line), obtained from an ensemble of trajectories with the same phase-space distribution as the Wigner function of the initial quantum state. The function $\rho_{\rm cl}^{sim}(t)$ merges into the exponential decay $\exp(-t/\tau_D)$ and deviations between $\rho_{\rm qm}^{sim}(t)$ and $\rho_{\rm cl}^{sim}(t)$ are visible.

We proceed with a more detailed analysis of the quantum deviations from $\rho_{\rm cl}^{sim}(t)$, therefore we consider now the ratio

$$R(t) \equiv \frac{\rho_{\text{cl}}^{sim}(t) - \rho_{\text{cl}}^{sim}(t)}{\rho_{\text{cl}}^{sim}(t)},$$
(4.15)

Fig. 4.3 Survival probability obtained from the numerical simulations in the classical (dashed line) and in the quantum case (full line). Up to $t/\tau_D \approx 0.5$ non universal effects resulting from a finite time the trajectories need to become ergodic in good approximation are observed (from [6])



shown in Fig. 4.4. The dots there represent an average of R(t) over 27 different opening positions and initial momentum directions. The full curve depicts the semi-classical prediction

$$R(t) \simeq \frac{t^2}{2\tau_D T_H},\tag{4.16}$$

based on Eq. (3.37), that is dominant for the t/τ_D -range displayed. We note that our semiclassical result (4.16) shows, compared to the numerical data, mainly a shift in time. We try to explain this now by considering the influence of a non-vanishing Ehrenfest-time. A comparison between the numerical results and our semiclassical results including a non-zero Ehrenfest-time for R(t) is shown in Fig. 4.5. We find a much better agreement of the numerical results with our semiclassical ones including the Ehrenfest-time than with the ones without Ehrenfest-time. This leads us to the interpretation, that the shift observed in Fig. 4.4 is indeed caused by the Ehrenfesttime. We note, however, that in order to rule out other effects than the Ehrenfest-time, we would have to be able to plot the quantum correction (4.14) for a range of τ_E instead of t to check if the analytically obtained Ehrenfest-time dependence is correct. This seems impossible to date for wave packets evolved in billiards, because \mathcal{L} cannot be varied over a sufficiently wide range in these simulations (the Ehrenfest-time depends logarithmically on \mathcal{L}). Furthermore we have to note, that the individual numerical results for $\rho(t)$ exhibit strong fluctuations, which are reflected in a large standard deviation shown by the error bars in Figs. 4.4 and 4.5.

We remark at the end of this section that an analogous calculation can also be performed for the leading quantum correction to the fidelity amplitude in the presence of time-reversal symmetry. For the survival probability the stretches escaped in an uncorrelated manner when they were more than a distance W away from each other. Now the different encounter stretches are subject to uncorrelated disorder when their spatial distance becomes larger than ξ . We thus require that inside of an encounter

Fig. 4.4 The *dots* mark the results for R(t) obtained from numerical simulations, the *bars* correspond to the standard deviation after averaging (see text), compared with the corresponding semiclassical prediction [Eq. (4.16)] (*full line*) (from [6])

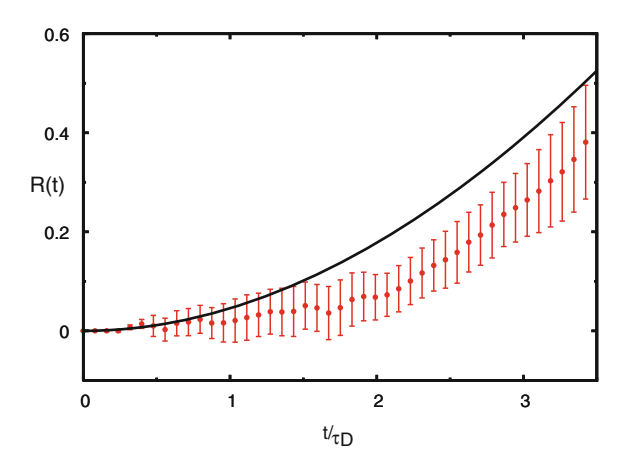
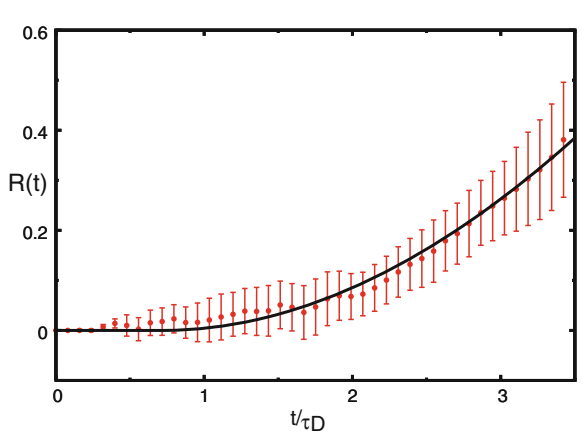


Fig. 4.5 The *dots* mark again the results for R(t) obtained from numerical simulations and the *bars* the standard deviation, compared with the corresponding semiclassical prediction now *with* Ehrenfest-time [Eq. (4.14)] (full line) (from [6])



two segments of the trajectory are separated by distances less than ξ on the left end of the encounter in Fig. 4.1 and less than \mathcal{L} on the right as before. Performing then an analogous calculation to the one for the survival probability we find

$$m_{\rm sc}^{q_1}(t;\Gamma) = -\frac{\Gamma}{T_H}(t - 2\tau_E^{\rm d})^2 e^{-\Gamma(t + 2\tau_E^{\xi})}\Theta(t - 2\tau_E^{\rm d}),$$
 (4.17)

where we defined analogously like after Eqs. (4.9, 4.10) $\tau_E^{\xi} = \lambda^{-1} \ln(\xi^2/(\mathcal{L}\lambda_B))$ and $2\tau_E^d = \tau_E^c + \tau_E^{\xi}$. Equation (4.17) reveals the role of Ehrenfest-time corrections in this case: They lead first to a time shift such that the quantum corrections set in later, i.e. for short times the system behaves "classically" due to the theta function. Second they lead to a stronger exponential decay as the disorder is accumulated coherently during the encounter stretches.

After this excursion to time-dependent processes we now return stationary ones and study now the variance of the conductance.

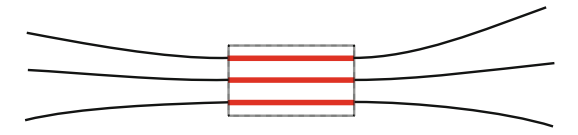


Fig. 4.6 A 3-encounter as it can be approximated in the semiclassical treatment to reproduce RMT results. The encounter stretches are marked by a *box* (shown *red*)

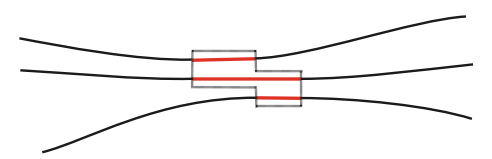


Fig. 4.7 A 3-encounter as previously treated with Ehrenfest-time [12, 26]. The encounter stretches are marked by a *box* (shown *red*)

4.3 Variance of the Conductance

In Fig. 2.3 we observed large (universal) fluctuations of the conductance around its mean value. Its variance can also be obtained by RMT [21] that can be reproduced semiclassically [22]. When calculating the leading order in *N* contribution to the variance of the conductance in [12] for non-zero Ehrenfest-time, two main difficulties were noticed:

- when considering encounters containing more than two stretches it was shown to be sufficient [22–25] to obtain the RMT results semiclassically (as considered in the Chap. 2) to take into account only encounters where all orbits are linearisable up to the *same* point, see for an example Fig. 4.6. Generalising this to non-zero Ehrenfest-time, for 2-encounters considered in the first section of this chapter, this is naturally fulfilled. When taking into account the Ehrenfest-time dependence of more general encounter diagrams this is no longer sufficient as was first shown in [12, 26], see Fig. 4.7 for an example of an additional diagram analysed in this case. Here also correlations between *some parts* of the stretches need to be taken into account, we will refer to these regions as encounter fringes.
- when studying encounter diagrams involving surrounded periodic orbits, for example see Fig. 4.8, it was shown [22–25] that RMT results can be obtained by restricting the diagrams to those where the encounter stretches do not wind around the periodic orbit, i.e. where the encounter stretches are shorter than the periodic orbit. Also this restriction cannot be made for non-zero Ehrenfest-time. We mention that also these encounter diagrams could not occur for a single 2-encounter or coherent backscattering.

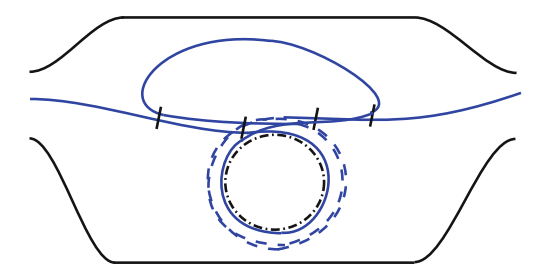


Fig. 4.8 Diagram studied in the calculation of the first quantum correction to the transmission and reflection in the absence of time-reversal symmetry. Here the orbit traverses the central periodic orbit (dashed-dotted line) once during its first encounter and twice during its second encounter. We draw the parts of the orbit during the second encounter dashed to distinguish them from the first. The partner orbit (not shown) has one traversal of the central periodic orbit exchanged between its first and the second encounter with the periodic orbit (i.e. it goes around twice then once). The fringes where the two orbits approaching the dashed-dotted orbit are correlated with each other but not with the dashed-dotted orbit are marked by black vertical lines perpendicular to the trajectories

The first calculation taking into account both effects was performed in [12]. This calculation showed that the leading-order contribution to the variance of the conductance is independent of the Ehrenfest-time. The averaged conductance variance or more precisely the variance of the transmission T (without the factor $2e^2/h$) is defined as

$$\operatorname{var} T = \left\langle \operatorname{Tr} \left(t t^{\dagger} \right)^{2} \right\rangle_{\Delta k} - \left\langle \operatorname{Tr} \left(t t^{\dagger} \right) \right\rangle_{\Delta k}^{2}. \tag{4.18}$$

From the first summand we obtain semiclassically a fourfold sum over orbits, contributions that lead pairwise to small action differences (i.e. by only considering the two double sums independently) are subtracted by the second summand. Only quadruplets of orbits that interact through encounters in a way that does not lead to a small action difference in the second term are then left to give a contribution. In [12] it was shown that var T can be semiclassically also obtained by considering instead the covariance of the reflection cov RR', that is defined as

$$\operatorname{cov} RR' = \left\langle \operatorname{Tr} \left(rr^{\dagger} \right) \operatorname{Tr} \left(r'r'^{\dagger} \right) \right\rangle_{\Delta k} - \left\langle \operatorname{Tr} \left(rr^{\dagger} \right) \right\rangle_{\Delta k} \left\langle \operatorname{Tr} \left(r'r'^{\dagger} \right) \right\rangle_{\Delta k} \tag{4.19}$$

with $R \equiv \text{Tr}(rr^{\dagger})$ and $R' \equiv \text{Tr}(r'r^{\dagger})$. Due to the unitarity relation (2.46) this quantity is equal to var T. Considering the covariance leads however, to the technical simplification in the semiclassical calculation that no encounters touching the opening need to be considered, because the two pairs of trajectories start and end in different leads. In this case two different diagrammatic contributions are identified:

• two independent 2-encounters, see Fig. 4.9. The contribution of this diagram is given by the square of the first quantum correction to the transmission [12], as can be seen easily by expressing it in terms of link and encounter contributions:

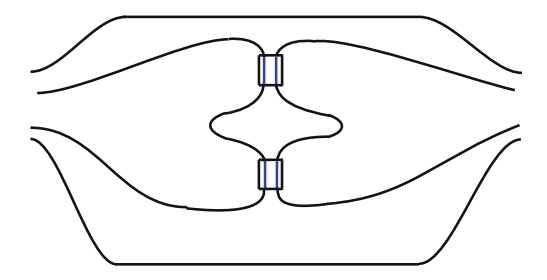


Fig. 4.9 Diagram occurring in the calculation of the reflection covariance (or the conductance variance) containing two orbits possessing two independent encounters. The encounters of the two orbits are marked by a *box* (shown *blue*). At the encounters the partners (not shown) differ by crossing over to the other orbit

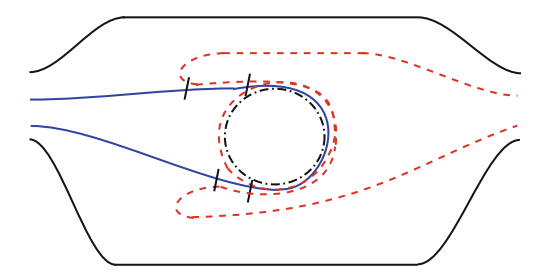


Fig. 4.10 Diagram occurring in the calculation of the reflection covariance (or the conductance variance) containing two orbits surrounding a central periodic orbit. The fringes are marked by *black vertical lines* perpendicular to the trajectories. Partner orbits are not shown

$$(\operatorname{cov} RR')^{4.9} = \frac{N_1^2 N_2^2}{(N_1 + N_2)^4} e^{-2\tau_E/\tau_D}$$
(4.20)

with the superscript referring to the number of the figure.

• two trajectories (one from either lead) approach a trapped periodic orbit with one winding around it an extra time, see Fig. 4.10. Partner trajectories (not shown) can be found which follow those trajectories almost exactly but where one winding is exchanged between the two trajectories leading to a quadruplet of trajectories with a small action difference and a contribution in the semiclassical limit given by⁵

$$(\cos RR')^{4.10} = \frac{N_1^2 N_2^2}{(N_1 + N_2)^4} \left(1 - e^{-2\tau_E/\tau_D} \right). \tag{4.21}$$

Such a contribution vanishes when the Ehrenfest-time goes to zero and can be seen to contain the discrete diagram types considered without Ehrenfest-time [22], i.e. two 2-encounters and one 3-encounter (the contributions from these diagrams sum

⁵ As the calculation in [12] shows, this contribution is actually only non-zero due to taking into account the encounter fringes shown in Fig. 4.10.

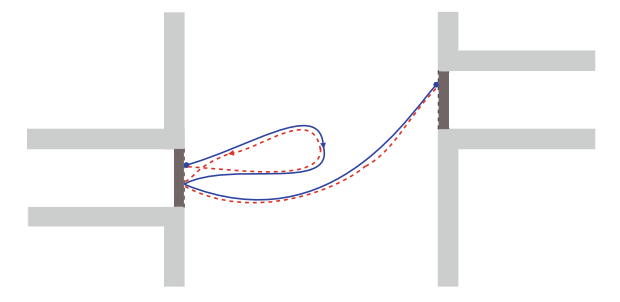


Fig. 4.11 Schematic drawing of an additional pair of orbits to be considered when calculating the first non-diagonal contribution to the transmission in the presence of tunnel barriers. This diagram is obtained from the configuration containing an encounter inside the system, see Fig. 2.2, by cutting the *left* link short. An analogous configuration touching the *right* lead can be obtained by cutting the *right* link short

to zero in a similar way as for the conductance in the unitary case in Sect. 2.3). In contrast to the Ehrenfest-time dependencies considered above a simple intuitive explanation for the last dependence is not yet available.

In order to show that a non-zero Ehrenfest-time can lead to further interesting effects, that are however, not easy to access intuitively, we now consider the variance for a system containing additional tunnel barriers in the leads through that the particles can tunnel with a probability Γ . We first describe the general changes induced by including tunnel barriers and afterwards explain the dependence of the variance on Γ and introduce the most relevant diagrams leading semiclassically to this dependence.

The inclusion of tunnel barriers leads to some changes in the transport calculations presented up to now that were originally described in [27]: First the dwell time τ_D defined after Eq. (2.34) is usually replaced by τ_D/Γ . Without tunnel barriers every particle that hit the lead left the system, now only the ratio Γ of the particles hitting the lead leaves the cavity, if the corresponding trajectory part is not correlated with an other during an encounter at that time. If such a correlation is present when hitting the lead, the whole configuration is lost if one stretch of the encounter leaves the system. This happens with a probability $1-(1-\Gamma)^n$ for n correlated stretches. The dwell time is in such a situation thus replaced by $\tau_D/\left[1-(1-\Gamma)^n\right]$. A further change is that additional encounter diagrams become possible where encounters touch a lead but the orbit does not exit the system each time it hits the opening, for an example see Fig. 4.11.

After these explanations of the effects of tunnel barriers in general we now turn to the variance of the transmission introduced in Eq. (4.18) for arbitrary tunnel probability and non-zero Ehrenfest-time. As just explained the variance is to leading order in N for $\Gamma=1$ independent of the Ehrenfest-time. For arbitrary Γ this is no longer the case: To linear order in the ratio τ_E/τ_D , to that we restrict here, we obtain that the variance increases with increasing Ehrenfest-time up to $\Gamma\approx0.5$ and then decreases with increasing Ehrenfest-time. We predicted this behaviour—more exactly the curve in Fig. 4.12—semiclassically. We also compared this analytical

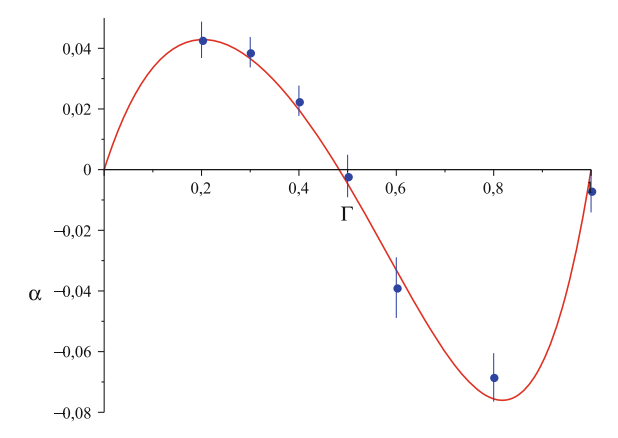


Fig. 4.12 Concentrating on the linear dependence of the variance of the transmission var T on τ_E/τ_D ; var $T \approx \text{var}\,T_{\text{RMT}} + \alpha\tau_E/\tau_D$ with the RMT contribution to the variance var T_{RMT} ; we obtain for the dependence of α on Γ the depicted (red) line in the presence of time-reversal symmetry. The (blue) dots and $error\ bars$ indicate the corresponding results from numerical simulations performed for the kicked rotator by Jacquod (from [28])

prediction with numerical data obtained by Jacquod using a kicked rotator in the chaotic regime [28]. We find fairly good agreement between the numerical results, see the blue dots in Fig. 4.12 and the analytical prediction, see the red curve: The analytical curve always lies within the error bars of the numerical results. As the calculation of the complete set of contributions leading to this curve is rather involved due to the large number of diagrams and the complicated dependence of the dwell time on Γ we show the diagrams causing the main contributions here and give all contributions leading to the curve in Fig. 4.12 in Appendix C. At first we remember that in the absence of tunnel barriers the contributions resulted from orbit pairs depicted in Figs. 4.9 and 4.10. For $\Gamma \neq 1$ we first need to take into account these configurations using the modified survival probability introduced above and second additional diagrams obtained when encounters touch the opening similar to the one depicted in Fig. 4.11. When neglecting the effect of encounter fringes, we can concentrate on configurations where the encounter stretches are longer than the encountered periodic orbit: This can be understood by taking into account that there are in this case no contributions for $\Gamma = 1$ from surrounded periodic orbits and by noticing that for most of the contributions the number n of traversals of the periodic orbit is quite large implying $1 - (1 - \Gamma)^n \to 1$, i.e. the results obtained for $\Gamma = 1$ still remain valid for these diagrams for $\Gamma \neq 1$. Now we analyse the diagrams leading to the two peaks: The first positive peak lies in a region of small Γ . In this case there exists for the contributions from most of the diagrams the following approximate cancellation mechanism: The contributions from diagrams containing encounters inside the orbits (i.e. the ones depicted in Figs. 4.9 and 4.10) are cancelled by the ones obtained when one and two links are cut short. This cancellation however, does not hold for 3-encounters with the periodic orbit, see the leftmost diagram in Fig. 4.13. In this case

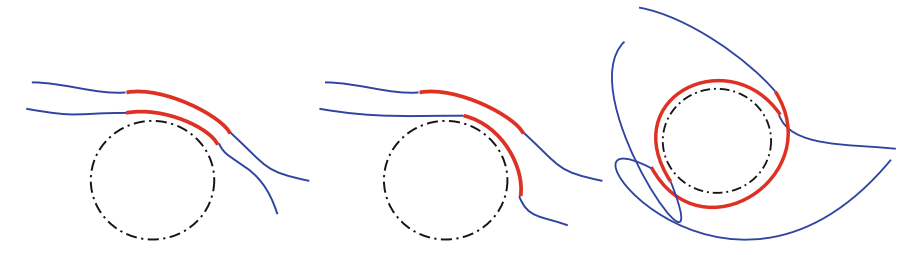


Fig. 4.13 Diagrams contributing to the variance of the conductance. The links are marked by *thin* (*blue*) *lines*, the encounter stretches by *fat* (*red*) *lines*, the encountered periodic orbit is shown dashed dotted. The partners (not shown) traverse the encountered periodic orbit once more than the depicted orbits. In the *left* diagram the two orbits encountering form together with the periodic orbit a 3-encounter, in the *middle* the encounter stretches overlap partially and on the *right* they overlap at both ends. For the importance of these diagrams for different values of Γ , see main text

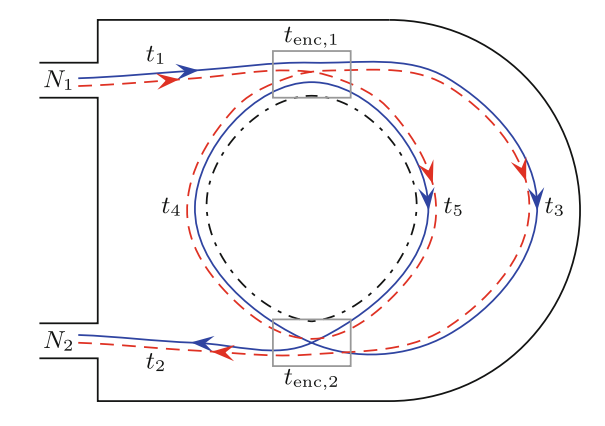
we have two possibilities: First that the encounter lies inside the system or touches the lead at one end. This leads in dependence of the Ehrenfest-time to an exponentially decaying contribution proportional to $e^{-[1-(1-\Gamma)^3]\tau_E/\tau_D}$. Additionally for non-zero Ehrenfest-time we also need to take into account the contributions from encounters touching the leads at both sides leading to an increasing contribution proportional to $1-e^{-[1-(1-\Gamma)^3]\tau_E/\tau_D}$ with a larger prefactor than the first one. This causes the first peak in Fig. 4.12. In the case of the second peak the factor $(1-\Gamma)$, i.e. the probability for the particle to be back reflected at the opening, is quite small. This implies that we get the main contributions from diagrams with encounters inside the system, i.e. the ones also obtained for $\Gamma=1$. The first important diagram in this case is obtained from the one depicted in Fig. 4.14 by cutting the link of duration t_3 open and the others are shown in Figs. 4.9, 4.10, 4.13, which yield altogether a negative contribution.

4.4 Next-to-Leading Order Quantum Corrections

After these results for the Γ -dependence of the variance of the transmission we now return to the case of transparent barriers $\Gamma=1$. All the approaches for calculating conductance or spectral properties for non-vanishing Ehrenfest-time are up to now restricted to very low order in the inverse channel number for the transmission and in $1/\epsilon$ or τ for the spectral autocorrelation function or form factor. A calculation of the corrections to infinite order, as it has been performed in the case of vanishing Ehrenfest-time $\tau_E/\tau_D \to 0$ (see Chap. 2), is still lacking. In this section we want to make a step towards filling this gap. More precisely we consider in the first subsection the next-to-leading order quantum correction to the transmission and reflection in the case of the dc transport without and with time-reversal symmetry (the contribution

⁶ For a detailed explanation how such contributions increasing with increasing Ehrenfest-time arise see Sect. 4.5.2.

Fig. 4.14 Example of an orbit (and its partner shown *dashed*), considered in [29], that contributes to the transmission for systems without time-reversal symmetry. A central periodic orbit (*dashed-dotted*) can be identified



one order lower in N than in the first section of this chapter). We then check the unitarity of our result, i.e. that T and R add up to a constant (N_1) at the considered order. In the next subsection we extend these results to ac transport and then check that corrections to the closely related Wigner time delay are indeed zero at the order considered.

4.4.1 Transmission and Reflection for dc Transport

We start in this subsection calculating the Ehrenfest-time dependence of the next-to-leading order quantum corrections (of order 1/N) with the simpler case where the scattering system does not have time-reversal symmetry.

4.4.1.1 No Time-Reversal Symmetry

Without Ehrenfest-time the 1/N-order contribution results from orbits with two encounters with itself [29], see Fig. 4.14 (and additionally an orbit with a single 3-encounter). We can see that there is a central periodic orbit through the two encounters. This fact is essential for the Ehrenfest-time dependence and simplifies treating the different cases. Depending on how much these encounters overlap (i.e. depending on the lengths of the links t_4 and t_5 in Fig. 4.14), one distinguishes in the case of no overlap two independent 2-encounters (i.e. encounters involving 2 orbit stretches) as in Fig. 4.14, in the case the two 2-encounters overlap at one of their ends (shrinking t_4 or t_5 say) a 3-encounter (the other discrete diagram) and in the case the two 2-encounters overlap at both ends (shrinking t_4 and t_5) an encounter fully surrounding the periodic orbit (a possibility which has only to be treated for non-zero Ehrenfest-time).

We first want to describe the length restriction for the considered orbits in this case. Although we mentioned up to now only one contained periodic orbit shown dashed dotted in Fig. 4.14, there are two in total: one built up by t_4 and t_5 , the other by t_3 and t_4 . In the following calculations we could choose either as we actually treat this configuration as an orbit meeting a central periodic orbit twice, see Fig. 4.8. The two encounters of the orbit with the central periodic orbit have to be independent, because otherwise there exists no connected partner with a small but non-zero action difference. That means the orbit has to decorrelate from the central periodic orbit. Then this orbit has to become ergodic before returning, therefore an encounter time, which is of the order of the Ehrenfest-time is required, so the stretch outside the encounter in Fig. 4.14 must be of positive length. The total orbit has thus to be longer than the sum of the two durations of the encounters with the central periodic orbit, $t_{\rm enc.1} + t_{\rm enc.2}$.

As just explained these orbital configurations also occurred in the calculation of the covariance of the reflection coefficients [12]. In fact, by cutting the top loop in Fig. 4.8 and moving the ends to the correct places we can see we recreate Fig. 4.10. Reversing this cutting though, to return to the transmission and reflection, we create the second periodic orbit which is the top loop in Fig. 4.8 and travels through t_3 and the encounters in Fig. 4.14. We will see that this changes the orbital configurations compared to the case of the reflection covariance, changing also the resulting contribution: For the covariance of the reflection coefficients it turned out to be essential [12] to note that apart from the orbit being longer than the encounter stretches (where both orbits in Fig. 4.10 are correlated with the central dashed–dotted periodic orbit) additionally that the orbit is longer than the encounter fringes, where the orbits are correlated with each other **but** where they are no longer correlated to the periodic orbit. We marked the places where correlations between fringes occur in Fig. 4.10 by black vertical lines. The duration of the fringes before the orbits get correlated to the central periodic orbit is denoted by t_s and after the orbits leave the central periodic orbit by t_u . Note that these times possess here another meaning than in Eqs. (2.39, 2.54).

These fringes are the key to the difference between the possible orbital configurations for the covariance of the reflection coefficients on the one hand and the transmission and reflection on the other hand: In the case of the covariance of the reflection these fringes need to have a non-vanishing length, because the two orbits (see Fig. 4.10) which are correlated during the fringes have to end at two different leads where they necessarily must be uncorrelated. The orbits away from the central periodic orbit must be long enough for the chaotic dynamics to allow this to happen. When we join one end of the dashed and one of the solid orbit in Fig. 4.10 say to return to the transmission (or reflection) as in Fig. 4.8 then it is no longer necessary that the upper periodic orbit (in Fig. 4.8) thereby created has to be longer than the fringe times. These fringes can now start to overlap as depicted in Fig. 4.15; compared to Fig. 4.14 we let the fringes grow till they overlap in the link t_3 . The stretches of the orbit that connect to the leads must though still be longer than the duration of the fringes as they must decorrelate from the upper periodic orbit to exit the system.

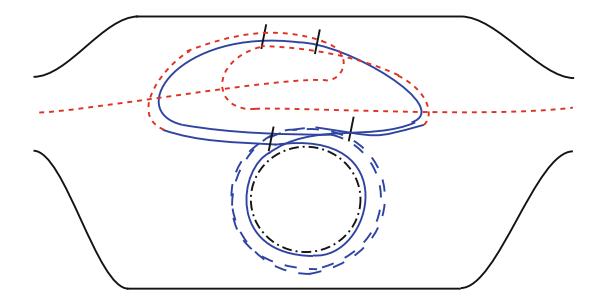


Fig. 4.15 Example of a diagram, that has to be considered in the calculation of the transmission, however, not when the upper periodic orbit is cut open in the calculation of the conductance fluctuations. The parts of the orbit that were changed in comparison to Fig. 4.8 are shown *dotted* (*red*)

Now we can explain the effect of the possible orbital configurations on the resulting contributions. Applying the sum rule (2.34) in Eq. (2.57), we obtain the following contribution to T resulting from the diagrams shown in Figs. 4.8 and 4.15, which we denote $T^{4.8,4.15}$

$$T^{4.8,4.15} = \left\langle \frac{N_1 N_2}{T_H} \int_0^\infty dT \int_{-c}^c ds \, d\mathbf{u} \, w(\mathbf{u}, \mathbf{s}, T) e^{(i/\hbar)\Delta S} p'(T) \right\rangle_{\Delta k}. \tag{4.22}$$

We defined here the modified survival probability in the presence of encounters p'(T) taking into account the modification explained before Eq. (2.47) for encounters with the fringes and periodic orbits: When the encounters surround the periodic orbit the parts of the encounter stretches traversing a certain point of the periodic orbit are so close to each other that they either leave the cavity during the first traversal or do not leave at all [12, 29] leading to

$$p'(T) = p(T)e^{(t_{\text{enc},1} + t_{\text{enc},2} + t_s + t_u)/\tau_D} = e^{-(t_1 + t_2 + t_3 + \tau_p)/\tau_D},$$
 (4.23)

assuming that t_4 and t_5 form the surrounded periodic orbit. Note that although we are in contrast to Chap. 2 considering now encounters that are not only allowed to touch but also to surround periodic orbits the functional form of the action difference remains unchanged [12, 30] $\Delta S = \sum_{i=1}^{2} u_i s_i$. Now however, the coordinates s_i and u_i are the stable and unstable coordinate differences between the central periodic orbit and the ith encounter stretch. The weight function w(u, s, T) derived in an analogous way like before Eq. (2.56) is given by

$$w(\boldsymbol{u}, \boldsymbol{s}, T) = \frac{1}{\Omega^2 t_{\text{enc}, 1} t_{\text{enc}, 2}} \left(\prod_{i=1}^2 \int dt_i \right) \int d\tau_p \int_0^{\tau_p} dt', \tag{4.24}$$

where t_i denotes the duration of two of the three links away from the periodic orbit (two connecting the opening to the central periodic orbit and one the periodic orbit to itself), τ_p is the duration of the central periodic orbit and t' the time difference

between the two points (in the different encounters) where each of the two encounter stretches reaches a phase-space difference c with respect to the periodic orbit. The limits of the time integrals in (4.24) are determined by the fact that the duration of the links, the periodic orbit and the encounters have to be positive. This differs from the treatment of Fig. 4.14 in Chap. 2 as it was assumed there that all five links have to have positive duration, but here we allow some of them to overlap. This automatically includes the other cases described at the start of this section as part of a continuous deformation of Fig. 4.8 or 4.14. In particular we allow t_4 and t_5 to shrink and instead just assume that τ_p is positive, so we therefore use this variable in (4.24) instead of t_4 and t_5 .

This expression can be again transformed, using (4.24) and converting the integral over the full duration of the orbit T into one over the link t_3 , into

$$T^{4.8,4.15} = \left\langle \frac{N_1 N_2}{T_H} \left(\prod_{i=1}^3 \int_0^\infty dt_i \exp\left(-\frac{t_i}{\tau_D}\right) \right) \int_{-c}^c ds \, d\mathbf{u} \int_0^\infty d\tau_p \int_0^{\tau_p} dt' \right.$$

$$\times \exp\left(-\frac{\tau_p}{\tau_D}\right) \frac{1}{\Omega^2 t_{\text{enc},1} t_{\text{enc},2}} \exp\left(\frac{i}{\hbar} \sum_{i=1}^2 u_i s_i\right) \right\rangle_{\Delta k}, \tag{4.25}$$

where we also used the explicit form of the survival probability and the action difference ΔS . To understand that the expression in (4.25) yields zero, we perform the integrals with respect to s_i , u_i , like in [12]

$$\int_{-c}^{c} ds_i du_i e^{(i/\hbar)u_i s_i} \frac{1}{t_{\text{enc},i}} = 4c^2 \int_0^1 dx_i \int_1^{1/x_i} d\sigma_i \cos\left(\frac{c^2 x_i}{\hbar}\right) \frac{1}{\sigma_i t_{\text{enc},i}}$$
$$= 4c^2 \lambda \int_0^1 dx_i \cos\left(\frac{c^2 x_i}{\hbar}\right)$$
(4.26)

with the substitution $u_i = c/\sigma_i$ and $s_i = cx_i\sigma_i$. The integral in the last line in (4.26) rapidly oscillates as a function of energy in the limit $\hbar \to 0$ and thus yields no contribution due to the energy average in (4.25). We want to note that in the case of the conductance variance or reflectance covariance the expression determining its contribution additionally contains compared to Eq. (4.25) a factor $e^{-(t_s+t_u)/\tau_D}$ because of the different length restrictions of the links in that case. As t_s and t_u depend on s_i , u_i and t', this thus yields a non-vanishing contribution [12].

We thus obtain that there are no quantum corrections (at least to this order) to the transmission when time-reversal symmetry is absent

$$T^{4.8,4.15} = 0, (4.27)$$

and a similar calculation shows that this also holds for the reflection *R*. Coherent backscattering, i.e. having encounters at the opening that additionally have to be taken into account for reflection, is also not possible. First this requires the encounter to be

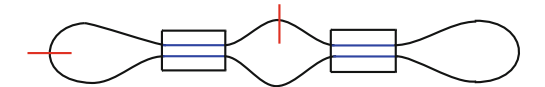


Fig. 4.16 Periodic orbit with two independent 2-encounters. The different positions, where it can be cut to obtain an open orbit contributing to the transmission are indicated by (*red*) *perpendicular lines*, the position of the (*blue*) encounter stretches are indicated by a *box*

traversed in opposite direction on both traversals, which can only occur with time-reversal symmetry. Second, even with time-reversal symmetry, when the trajectory returns to the encounter the second time it would necessarily escape the systems, and not be able to complete the rest of the semiclassical diagram.

To summarise, we saw in the first part of this section how, despite their close similarities, the two different orbital configurations appearing in the case of the covariance of the reflection on one hand and the transmission and reflection coefficients on the other lead to two different results: in the case of the covariance of the reflection to a term proportional to $(1 - e^{-2\tau_E/\tau_D})$, in the case of the transmission and reflection coefficients to zero contribution.

4.4.1.2 With Time-Reversal Symmetry

We now turn to the calculations in the case with time-reversal symmetry. In this case we also have to consider diagrams where the encounters are traversed in different directions by the orbit. As their contributions are quite different we will study them individually. We start with two independent encounters with no central periodic orbit involved, referred to as two 2-encounters, shown in Fig. 4.16. We first cut the periodic orbit during one of the middle links and refer to the corresponding contribution as $T^{4.16(a)}$. Expressing the corresponding contribution again as in Sect. 2.3 in terms of products of link and encounter contributions the two s, u-integrals for the two different encounters factorise and can be evaluated for each encounter separately, as was done in [12] for the case of the reflection covariance (obtained by cutting both the leftmost and rightmost links in the periodic orbit in Fig. 4.16). Each encounter provides a factor $-Ne^{-\tau_E/\tau_D}$, the five links factors N^{-1} and the leads the factor N_1N_2 so that we obtain for the contribution $T^{4.16(a)}$,

$$T^{4.16(a)} = \frac{N_1 N_2}{(N_1 + N_2)^3} e^{-2\tau_E/\tau_D}.$$
 (4.28)

with $\tau_E = \lambda^{-1} \ln \left(c^2/\hbar\right)$. The corresponding contribution to the reflection $R^{4.16(a)}$ is obtained by multiplying $T^{4.16(a)}$ by N_1/N_2 to take into account that the orbit leaves through the lead 1 instead of lead 2. When cutting the left link of the periodic orbit in Fig. 4.16, whose contribution we denote $T^{4.16(b)}$, we obtain for the transmission the same result as $T^{4.16(a)}$. However, for the reflection in this case it is also possible to obtain a coherent backscattering contribution, i.e. a contribution from an encounter touching the lead, by shrinking the length of both links on the left in Fig. 4.16 to

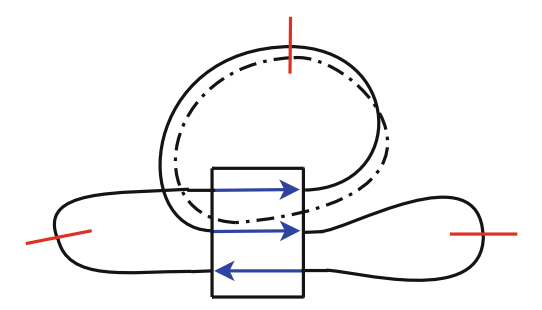


Fig. 4.17 A periodic orbit encounter only existing in the case of time-reversal symmetry. The central periodic orbit is drawn with a *dashed–dotted line*, the position of the (*blue*) encounter stretches are marked by a *box*. The (*red*) lines perpendicular to the orbit mark the places where it can be cut open

zero (or we cut the diagram in Fig. 4.16 at the leftmost encounter and move this to the lead). For this contribution we have, compared to the corresponding one for all encounters inside the cavity, two links less and as already in Eq. (3.33) an additional integral measuring the length of the encounter stretch that was not cut. Additionally the lead provides a factor N_1 as the orbit has to start and end in this case in the same channel as we saw in the last chapter. We finally obtain

$$R^{4.16(b)} = \frac{N_1^2}{(N_1 + N_2)^3} e^{-2\tau_E/\tau_D} - \frac{N_1}{(N_1 + N_2)^2} e^{-2\tau_E/\tau_D}, \tag{4.29}$$

where the first term is the same as $R^{4.16(a)}$ and the second comes from the coherent backscattering.

Next we consider, as for the case of no time-reversal symmetry, the situation of two 2-encounters near a periodic orbit. The configuration where the encounter stretches are parallel (in the same direction) was treated in the last subsection so, as we have now the freedom to traverse the two encounter stretches in opposite directions, we now turn to configurations where some of the stretches are antiparallel to each other. Starting with the periodic orbit configuration in Fig. 4.17 there are three possible places to cut this orbit open as shown by the red lines perpendicular to the orbit. By opening the parts not enclosing the central periodic orbit, we obtain a configuration shown in Fig. 4.18.

Unlike the case without time-reversal symmetry, we can see that some of the fringes must have non-vanishing length like considered in [12] for the contribution to the conductance fluctuations: The two fringes marked by dotted boxes in Fig. 4.18 on the right hand side of the encounter cannot have vanishing length, because as long as the two parts are correlated, the corresponding loop they form cannot close. The two fringes in Fig. 4.18 on the left hand side of the encounter can only vanish in the case of coherent backscattering, i.e. if the orbit starts and ends in a correlated manner in the same lead. Note that in the left fringe (defined where stretches are correlated with each other away from the central periodic orbit) we only have the two stretches which connect to the leads and that the remaining encounter stretch in

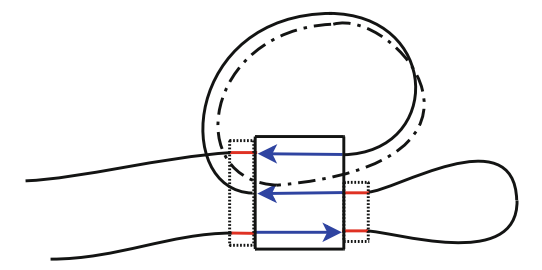


Fig. 4.18 A periodic orbit encounter only existing in the case of time-reversal symmetry. The position of the (*blue*) encounter stretches are marked by a *box*, the position of the fringes by small *dotted boxes* (are marked *red*)

Fig. 4.18 which follows the central periodic orbit has already decorrelated from the others so it does not also need to escape. To evaluate the contribution we first need to determine the values of the prefactors a, b, d in the exponential in J in the Appendix in Eq. (B.1) in front of $t_{\rm enc,1}+t_{\rm enc,2}$, t_s+t_u and τ_p , respectively. As the survival probability along the periodic orbit depends only on τ_p and not on $t_{\rm enc,1},t_{\rm enc,2}$, we obtain a=0 and $d=1/\tau_D$. During the fringes we have two correlated stretches with the survival probability determined by one of them, thus yielding $b=-1/\tau_D$. When multiplying the resulting contribution for J by the factors resulting from the links and the channel factors due to the leads we obtain the contribution $T^{4.18}$ originating from Fig. 4.18 to the transmission

$$T^{4.18} = \frac{N_1 N_2}{2 (N_1 + N_2)^3} \left(1 - e^{-2\tau_E/\tau_D} \right)$$
 (4.30)

and to the reflection

$$R^{4.18} = \frac{N_1^2}{2(N_1 + N_2)^3} \left(1 - e^{-2\tau_E/\tau_D} \right) - \frac{N_1}{2(N_1 + N_2)^2} \left(1 - e^{-2\tau_E/\tau_D} \right), \quad (4.31)$$

with the second term resulting again from coherent backscattering.

The last case, depicted in Fig. 4.19, is obtained by opening along the central periodic orbit in Fig. 4.17. In general any two of the three stretches on either side of the encounter could remain correlated in the fringes away from the main encounter where all three stretches are close and correlated. The duration of the fringes, i.e. here in general the orbital parts where only two of the three encounter stretches are correlated, is denoted before and after where all three orbits are correlated by t_s and t_u , respectively as in [26]. On each side, fringe correlations become important if the two orbital parts containing the fringes are connected to each other, referred to as case A, but not if one orbital part of them is connected to the opening, referred to as case B. The reason why we have to take into account fringe correlations in case A is that namely the loop cannot close as long as the two parts of the orbit are still correlated. In case B the part of the orbit connected to the opening still has to be longer than the fringes so that when it escapes it does not force the rest of the orbit to also escape.

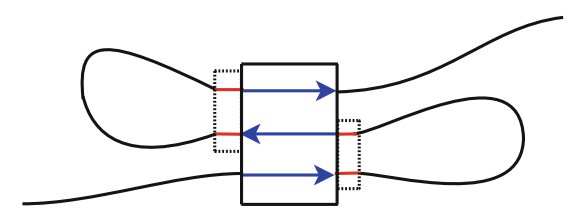


Fig. 4.19 A 3-encounter involving no periodic orbits. The (*blue*) encounter stretches are again marked by *boxes*, the places where fringe correlations can occur indicated by smaller *dotted boxes* (are marked *red*)

However, the other fringe which lies on the orbit that is not connected to the opening in Fig. 4.19 has no length restriction: If the length of that fringe tends to zero, the orbital part connected to the opening will just follow the first one for the time t_s or t_u . The latter part then also contains the survival probability contribution due to the fringes. The fact, that only the part of the orbit connected to the opening has a length restriction due to the fringes together with the enhancement of the survival probability during the fringe parts lets, as already in Eq. (4.25), the t_s and the t_u drop from the resulting expressions for the contribution $T^{4.19}$ from these diagrams in case B.

With these remarks in mind we evaluate the contribution $T^{4.19}$ in Fig. 4.19 by making use of the results obtained in [26], that we review in Appendix B as contributions K_1 and K_2 . The overall contribution K is split into two parts K_1 and K_2 : K_1 contains the contribution resulting from the 3-encounter without fringes and K_2 the contribution resulting from the difference between the 3-encounter with fringes and a 3-encounter without fringes. In all the cases considered here we have the first part K_1 where as for the survival probability during encounters we only need to count one encounter stretch we get $f = -1/\tau_D$ in K_1 in the Appendix. To obtain the contribution K_2 in this case we first note that it was shown in [26] to be sufficient to only consider certain encounter diagrams: Only one stretch contains two fringes, for an example of a not contributing diagram in this context see Fig. 4.20a, the other two fringes lie on the other stretches in one distinct way. Furthermore by setting $g_1 = 0$ or $g_2 = 0$ to study the case that only t_s or t_u is non-zero we obtain zero contribution, see Eq. (B.7). Thus three different possibilities remain: one from each of the three stretches containing two fringes, one belonging to case A and two to case B. For a contributing diagram see Fig. 4.20b, the others are obtained by cyclic permutations of the fringes along the stretches. As already explained there is no t_s , t_u -dependence in case B and thus in this case no contribution to K_2 . As in K_2 in Appendix B a non-zero prefactor of t_s and t_u is assumed in the cases A and B, we obtain 1/3 of the contribution K_2 in Eq. (B.6), we set $f = g = -1/\tau_D$ to take into account that only one stretch of the encounter is taken into account in the survival probability. For the overall contribution $T^{4.19}$ we therefore have

$$T^{4.19} = -\frac{N_1 N_2}{(N_1 + N_2)^3} e^{-2\tau_E/\tau_D}.$$
 (4.32)

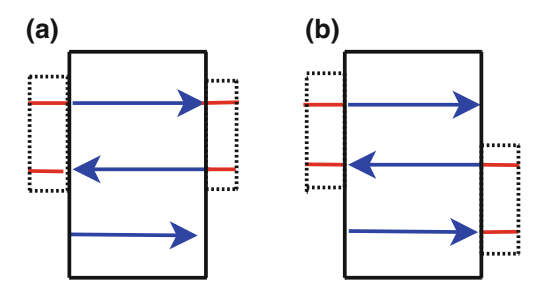


Fig. 4.20 Illustration of the contributing encounters in the case of the diagram in Fig. 4.19. The (*blue*) encounter stretches are again marked by *boxes*, the places where fringe correlations can occur (are marked *red*) indicated by smaller *dotted boxes*. The encounter in (**a**) does not contribute to K_2 , the encounter shown in (**b**) and the encounters obtained by cyclic permutations of the fringes along the stretches yield a non-zero contribution to K_2

The same contribution times the factor N_1/N_2 is obtained for the reflection.

To calculate the overall quantum correction to the transmission at the considered order T_{2nd} in the case of time-reversal symmetry we sum twice (to account for diagrams related by symmetry) the contributions from (4.28) and (4.30) and the contribution from (4.32) yielding

$$T_{\text{2nd}} = \frac{N_1 N_2}{(N_1 + N_2)^3}. (4.33)$$

Note that this quantum correction is independent of the Ehrenfest-time. This also holds for the corresponding contribution to the reflection R_{2nd} , which we obtain here by adding the contribution from (4.29) to twice the contribution from (4.31) and to the related contributions from (4.28) and (4.32) multiplied by N_1/N_2

$$R_{2\text{nd}} = \frac{N_1^2}{(N_1 + N_2)^3} - \frac{N_1}{(N_1 + N_2)^2}.$$
 (4.34)

4.4.1.3 Current Conservation

Having calculated all contributions to the transmission and reflection we now want to check if current conservation is fulfilled, i.e. if the transmission and the reflection calculated for one lead add up to the number of open channels in that lead. As without time-reversal symmetry there are no contributions at the order 1/N considered here, current conservation, already fulfilled at the diagonal level, is thus not violated. In the case of time-reversal symmetry the contributions to T and R at the considered order are given in (4.33) and (4.34) and sum to zero. Current conservation is thus again fulfilled. We want to emphasise here that correlations between encounter fringes, first treated in [12], were important to obtain this result: Forgetting for a moment the effect of fringe correlations, the contribution (4.32) would possess the Ehrenfest-time

dependence $e^{-\tau_E/\tau_D}$ and the contributions (4.30, 4.31) would be zero leading to a non current conserving result for T_{2nd} and R_{2nd} .

4.4.2 Frequency Dependence of Transmission and Reflection

In this subsection we want to generalise the results obtained for dc transport to the ac case. Therefore we consider

$$T(\omega) = \langle \text{Tr}(t(E + \hbar\omega/2)t^{\dagger}(E - \hbar\omega/2)) \rangle_{\Delta k}$$
 (4.35)

and a correspondingly defined $R(\omega)$ for an incoming wave in lead 1. The corresponding quantities in the case of an incoming wave in lead 2 are denoted by $T'(\omega)$, $R'(\omega)$. In general adding a frequency dependence means including into the formulas in the last subsection a factor $e^{i\omega T}$ in linearised approximation of the action with T again the overall duration of the orbit.

For the dc conductance $T(\omega=0)$ was directly proportional to the conductance, remember Eq. (2.25). For the ac conductance this is usually no longer a good approximation. The time-dependent voltage can lead to a temporary pile up of charge carriers in the system. An important effect is then the screening of the electric field of the system by the environment. To model this one introduces an additional gate capacitively coupled to the cavity [31, 32]. This leads, when taking into account all leads (i.e. also the capacitively coupled gate) to a configuration where the condition that the sum of the incoming currents equals the sum of the outgoing currents is fulfilled. Then the Landauer-Büttiker formalism can be applied yielding the connection between the transmission $T(\omega)$ defined in Eq. (4.35) and the transmission determining the admittance, i.e. the (complex) conductance, denoted by $T^{C}(\omega)$ [31]

$$T^{C}(\omega) = T(\omega) + \frac{[R(\omega) + T(\omega)][T(\omega) + R'(\omega)]}{i\omega Ch/(2e^{2}) - [R(\omega) + T(\omega) + R'(\omega) + T'(\omega)]}$$
(4.36)

with $R(\omega)$, $R'(\omega)$ and $T'(\omega)$ introduced after Eq. (4.35). The capacitance C of the capacitor formed by the cavity and the capacitively coupled gate is determined by the Coulomb interaction between system and environment.

We now want to show the effect of the transformation $T(\omega) \to T^C(\omega)$ considering the diagonal and the weak-localisation contribution to the conductance in the presence of tunnel barriers for non-zero Ehrenfest-time [33]. Therefore we first analyse the expression (4.35) in this case and obtain the overall contribution

$$T_{\text{D+WL}}(\omega) = \frac{\Gamma N_1 N_2}{(N_1 + N_2) (1 - i\omega \tau_D / \Gamma)} - \frac{N_1 N_2}{(N_1 + N_2)^2 (1 - i\omega \tau_D / \Gamma)^2} \times \left[\frac{2 - \Gamma - 2i\omega \tau_D / \Gamma}{1 - i\omega \tau_D / \Gamma} - 2 (1 - \Gamma) \right] e^{-[1 - (1 - \Gamma)^2]\tau_E / \tau_D} e^{2i\omega \tau_E}.$$
(4.37)

The first summand, i.e. the diagonal contribution, is as for the dc case independent of the Ehrenfest-time. Its form is obtained by taking into account that the particles enter and exit the system with the probability Γ yielding a factor Γ^2 . The additional factor $(\Gamma - i\omega\tau_D)$ is obtained by taking into account in the time integral in Eq. (2.34) additionally the factor $e^{i\omega T}$ and the modified dwell time τ_D/Γ introduced after Eq. (4.21). The overall Ehrenfest-time dependence of the second term contains as in Eq. (4.2) a term exponentially decaying with increasing Ehrenfest-time now containing the dwell time of two correlated orbits. The term $e^{i\omega T}$ leads now additionally to an oscillating dependence on the Ehrenfest-time. Both dependencies follow from a straightforward extension of the integrals performed in Eqs. (2.47, 2.48) to the present situation. The form of the prefactors of the exponentials follows directly by including the Γ - and the ω -dependent factors into the diagrammatic rules presented in Chap. 2: Each link then yields a factor $(\Gamma - i\omega\tau_D)$ and a 2-encounter a factor $-(1-(1-\Gamma)^2-2i\omega\tau_D)$. The first summand in the curved brackets in Eq. (4.37) results from encounters inside the system possessing three links and one 2-encounter. The second summand is due to the diagram depicted in Fig. 4.11 obtained from the corresponding pair with an encounter inside the system, Fig. 2.2, by cutting the left link and a corresponding diagram obtained by cutting the right link. This configuration has one link less, an additional integral over the duration of the part of the encounter remaining inside the system that cancels as for coherent backscattering the factor $-(1-(1-\Gamma)^2-2i\omega\tau_D)$. The additional factor $(1-\Gamma)$ in this case is the probability for the orbit being back reflected at the opening.

Inserting now Eq. (4.37) in Eq. (4.36), we obtain for the corresponding contribution $T_{\rm D+WL}^{C}(\omega)$

$$T_{\rm D+WL}^{C}(\omega) = \frac{\Gamma N_1 N_2}{(N_1 + N_2) (1 - i\omega\tau/\Gamma)} - \frac{N_1 N_2}{(N_1 + N_2)^2 (1 - i\omega\tau/\Gamma) (1 - i\omega\tau_D/\Gamma)} \times \left[\frac{2 - \Gamma - 2i\omega\tau/\Gamma}{1 - i\omega\tau/\Gamma} - 2 (1 - \Gamma) \right] e^{-[1 - (1 - \Gamma)^2]\tau_E/\tau_D} e^{2i\omega\tau_E}.$$
(4.38)

This means the only change compared to Eq. (4.37) is that the dwell time τ_D is replaced in some cases by a time τ defined as

$$\frac{1}{\tau} = \frac{1}{\tau_D} + \frac{2e^2N}{Ch}.\tag{4.39}$$

Expression (4.38) generalises the result derived for zero Ehrenfest-time and $\Gamma=1$ in [34]. Note that for $\omega=0$ the Eqs. (4.37) and (4.38) are identical.

We now return to the second-order quantum corrections to $T(\omega)$ and $R(\omega)$. As the calculation leading to this generalisation is straightforward we only briefly explain the difference to the calculation before and then show the results. In the case of no time-reversal symmetry we get in terms of the notation of Eq. (4.25) an additional factor $e^{i\omega(\tau_p+t_{\text{enc},1}+t_{\text{enc},2})}\prod_{i=1}^3 e^{i\omega t_i}$. To include this factor when performing the

s,u-integrals we take a,b,d for $\omega=0$ from the last subsection and include the ω -dependent exponential factor given in the last sentence to obtain $a=i\omega, b=0$ and $d=1/\tau_D-i\omega$. Inserting this in J in Appendix B and taking into account the factors from the links and the leads we obtain

$$T^{4.8,4.15}(\omega) = \frac{N_2}{N_1} R^{4.8,4.15}(\omega) = \frac{-N_1 N_2}{(N_1 + N_2)^3} \frac{(\omega \tau_D)^2}{(1 - i\omega \tau_D)^5} e^{2i\omega \tau_E}.$$
 (4.40)

In the orthogonal case, including a frequency dependence into Eq. (4.28) adds an additional factor $e^{i\omega(2t_{\text{enc},1}+2t_{\text{enc},2})}\prod_{i=1}^{5}e^{i\omega t_i}$ yielding finally

$$T^{4.16(a)}(\omega) = T^{4.16(b)}(\omega) = \frac{N_2}{N_1} R^{4.16(a)}(\omega)$$
$$= \frac{N_1 N_2}{(N_1 + N_2)^3} \frac{(1 - 2i\omega\tau_D)^2}{(1 - i\omega\tau_D)^5} e^{-2\tau_E/\tau_D + 4i\omega\tau_E}. \tag{4.41}$$

The first term of Eq. (4.29) is modified in the same way as the expression in Eq. (4.41) while for the second we have three links instead of five, reducing the power of $(1 - i\omega\tau_D)$ in the denominator by two, and an additional integral over the duration of the encounter reducing the power of $(1 - 2i\omega\tau_D)$ by one compared to the first term. We thus obtain

$$R^{4.16(b)}(\omega) = \frac{N_1^2}{(N_1 + N_2)^3} \frac{(1 - 2i\omega\tau_D)^2}{(1 - i\omega\tau_D)^5} e^{-2\tau_E/\tau_D + 4i\omega\tau_E} - \frac{N_1}{(N_1 + N_2)^2} \frac{(1 - 2i\omega\tau_D)}{(1 - i\omega\tau_D)^3} e^{-2\tau_E/\tau_D + 4i\omega\tau_E}.$$
 (4.42)

In Eq. (4.30) the additional factor $e^{i\omega(\tau_p+t_{\rm enc,1}+t_{\rm enc,2}+2t_s+2t_u)}\prod_{i=1}^3 e^{i\omega t_i}$ occurs, the equation is thus replaced by

$$T^{4.18}(\omega) = \frac{N_1 N_2}{2 (N_1 + N_2)^3} \left[\left(e^{2i\omega \tau_E} - e^{-2\tau_E/\tau_D + 4i\omega \tau_E} \right) \times \frac{(1 - 2i\omega \tau_D)^2}{(1 - i\omega \tau_D)^5} - \frac{2\omega^2 \tau_D^2}{(1 - i\omega \tau_D)^5} e^{2i\omega \tau_E} \right].$$
(4.43)

The latter equation can be obtained from J in the Appendix by setting $a = i\omega$, $b = -1/\tau_D + 2i\omega$ and $d = 1/\tau_D - i\omega$, again considering the additional terms from the ω -dependent exponentials. The additional frequency in the first term in Eq. (4.31) has the same effect as in Eq. (4.30), in the second term we again have one instead of three link times t_i and an additional integral over t_s or t_u

$$R^{4.18}(\omega) = \frac{N_1^2}{2(N_1 + N_2)^3} \left[\left(e^{2i\omega\tau_E} - e^{-2\tau_E/\tau_D + 4i\omega\tau_E} \right) \times \frac{(1 - 2i\omega\tau_D)^2}{(1 - i\omega\tau_D)^5} - \frac{2\omega^2\tau_D^2}{(1 - i\omega\tau_D)^5} e^{2i\omega\tau_E} \right] - \frac{N_1}{2(N_1 + N_2)^2} \left[\left(e^{2i\omega\tau_E} - e^{-2\tau_E/\tau_D + 4i\omega\tau_E} \right) \frac{(1 - 2i\omega\tau_D)}{(1 - i\omega\tau_D)^3} \right].$$
(4.44)

In case of Eq. (4.32) we get by taking the corresponding contribution of the encounter again from the Appendix with $f = -1/\tau_D + 3i\omega$ and $g = -1/\tau_D + 2i\omega$ in K_1 and K_2 since $t_{\rm enc}$ is traversed three times and the fringes two times

$$T^{4.19}(\omega) = -\frac{N_1 N_2}{(N_1 + N_2)^3} \left[\frac{(1 - 2i\omega\tau_D)^2}{(1 - i\omega\tau_D)^5} e^{-2\tau_E/\tau_D + 4i\omega\tau_E} + \frac{\omega^2 \tau_D^2}{(1 - i\omega\tau_D)^5} e^{-\tau_E/\tau_D + 3i\omega\tau_E} \right]$$
(4.45)

and a corresponding contribution for the reflection.

After obtaining these results it is now possible to check if they fulfil the relation

$$\frac{d}{d\tau_E} \frac{d}{d\omega} \text{Tr} \left[S \left(E + \hbar \omega \right) S^{\dagger} \left(E - \hbar \omega \right) \right] \Big|_{\omega = 0} = 0 \tag{4.46}$$

with the scattering matrix at the energy E, S(E) defined in Eq. (2.24). Up to now we only considered the reflection and transmission for an incoming wave in the lead 1, i.e. only the correlators of elements of r(E) and t(E). The corresponding results for the correlators of r'(E) and t'(E) are obtained by swapping N_1 and N_2 .

In order to see why relation (4.46) is fulfilled we rewrite it in terms of the Wigner time delay [35, 36], measuring the additional time spend in the scattering process compared to the free motion, $\tau_W \equiv \frac{d}{d\omega} \text{Tr} \left[S \left(E + \hbar \omega \right) S^{\dagger} \left(E - \hbar \omega \right) \right] \Big|_{\omega=0}$. Equation (4.46) is then

$$\frac{d}{d\tau_E}\tau_W = 0. (4.47)$$

That this relation has to hold can be obtained by comparing the two equivalent representations of the Wigner time delay given in [35–37]; their semiclassical equivalence is discussed in [30]. The first representation in terms of the density of states involves a single sum over trapped periodic orbits, the second representation in terms of transmission coefficients involves a double sum over lead-connecting paths. As the first representation yields, after taking an energy average, an Ehrenfest-time-independent result—we cannot identify any Ehrenfest-time-dependent contributions in a single sum over periodic orbits— τ_W has to be Ehrenfest-time independent.

Using the splitting of S(E) into subblocks introduced in Eq. (2.24), τ_W can be expressed as

$$\tau_W = \frac{d}{d\omega} \left[T(\omega) + R(\omega) + T'(\omega) + R'(\omega) \right] \bigg|_{\omega=0}. \tag{4.48}$$

The quantities on the right hand side of the equation above were defined in and after Eq. (4.35). We start our further analysis with the first two terms: In order to check if our results for $T(\omega)$ and $R(\omega)$ given above Eq. (4.46) fulfil relation (4.47), we first consider the sum of the contributions to τ_W which decrease with increasing Ehrenfest-time. The contribution proportional to $e^{-\tau_E/\tau_D}$ is obtained by considering the corresponding term in (4.45) yielding

$$\frac{d}{d\omega} \left[-\frac{N_1}{(N_1 + N_2)^2} \frac{\omega^2 \tau_D^2}{(1 - i\omega \tau_D)^5} e^{-\tau_E/\tau_D + 3i\omega \tau_E} \right]_{\omega = 0}.$$
 (4.49)

For calculating the contribution proportional to $e^{-2\tau_E/\tau_D}$ we sum the corresponding terms from (4.41, 4.42) and (4.45)

$$\frac{d}{d\omega} \left[\frac{N_1 \omega^2 \tau_D^2}{(N_1 + N_2)^2} \frac{(1 - 2i\omega \tau_D)}{(1 - i\omega \tau_D)^5} e^{-2\tau_E/\tau_D + 4i\omega \tau_E} \right]_{\omega = 0}.$$
 (4.50)

In the case of the contributions increasing or oscillating with increasing Ehrenfesttime we obtain from (4.43) and (4.44)

$$\frac{d}{d\omega} \left\{ \frac{-N_1}{2(N_1 + N_2)^2} \frac{\omega^2 \tau_D^2}{(1 - i\omega \tau_D)^5} \left[2e^{2i\omega \tau_E} - (1 - 2i\omega \tau_D) \left(e^{2i\omega \tau_E} - e^{-2\tau_E/\tau_D + 4i\omega \tau_E} \right) \right] \right\}_{\omega = 0}$$
(4.51)

and from (4.40)

$$\frac{d}{d\omega} \left[-\frac{N_1}{(N_1 + N_2)^2} \frac{(\omega \tau_D)^2}{(1 - i\omega \tau_D)^5} e^{2i\omega \tau_E} \right]_{\alpha = 0}, \tag{4.52}$$

which is the only contribution also existing in the absence of time-reversal symmetry. The results in (4.49-4.52) fulfil Eq. (4.47), because all are proportional to ω^2 and thus are equal to zero after differentiating them with respect to ω and setting $\omega = 0$.

The results obtained from the two last terms in Eq. (4.48) differ from the first ones by a factor N_2/N_1 and thus also yield zero contribution to τ_W .

4.4.3 Spectral Form Factor

In this subsection we want to apply our knowledge gained up to now in this section about the orbital configurations which contribute to the conductance to calculate the

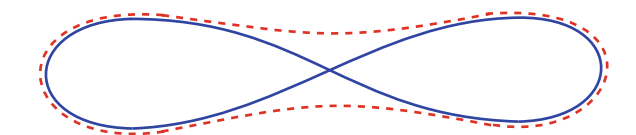


Fig. 4.21 The correlated orbit pair first analysed by Sieber and Richter [38, 39] where the orbit and its partner differ in an encounter. This pair leads to the first off-diagonal correction to the spectral form factor for time-reversal symmetric systems

first off-diagonal quantum correction to the correlation function $R(\epsilon)$, defined in Eq. (2.65), in the absence of time-reversal symmetry. We first want to briefly review the contributions to the spectral form factor (2.67) calculated in [4]. So we will use a similar notation as there and for further details refer the reader to that paper. The diagonal contribution is, as for the conductance, independent of the Ehrenfest-time. In the presence of time-reversal symmetry the next-to-leading order contribution results from the periodic orbit in Fig. 4.21. We studied its open orbit analogue in Sect. 2.3. Its contribution to the form factor contains an additional factor $\Theta(t - 2\tau_E)$ for non-vanishing Ehrenfest-time [4].

For systems without time-reversal symmetry however, we have for the leading order in $1/\epsilon$ non-diagonal contributions diagrams starting like in Fig. 4.14 but with the orbits in the leads connected together so that t_1 and t_2 join to a single link. Note that we can then identify four periodic orbits in the picture, one central orbit, one through t_3 as before and two through the newly joined links and t_3 and t_5 , respectively. From there we can allow the encounters to overlap to create a 3-encounter and then finally to wind around the central periodic orbit, as described at the start of Sect. 4.4.1. As we saw for the transmission there are further possibilities compared to the covariance of the reflection (or we can relax more restrictions) and likewise here there are additional contributions. We will see how they lead semiclassically to the field-theoretical result for the first off-diagonal quantum correction to the spectral form factor [5], but first we recall the results of the diagrams covered in [4].

Also the contributions to $\delta R_2(\epsilon)$, i.e. to $R(\epsilon)$ at the considered order in $1/\epsilon$, can be in a similar way, as the ones to the conductance, expressed for an orbit of duration T as product over contributions from links and encounters

$$\delta R_2(\epsilon) \propto \frac{1}{4} \frac{\partial^2}{\partial \epsilon^2} \int dt_1 \int dt_2 \int_{-c}^{c} ds \, d\mathbf{u} \int d\tau_p \int dt' \frac{\mathrm{e}^{(i/\hbar)\Delta S} \mathrm{e}^{2i\epsilon T/T_H}}{\Omega^2 t_{\mathrm{enc},1} t_{\mathrm{enc},2}}$$
(4.53)

with the overall duration T of the orbit, τ_p and t' defined after Eq. (4.24) and the two links of durations t_1 and t_2 decorrelated from the central periodic orbit. The choice of the limits of the time integrals depends on the considered diagram. We thus observe that the integrand of the s, u-integrals has the same structure as the one for the transmission considered in this section up to now. The periodic orbit contributions to $\delta R_2(\epsilon)$ differ from the corresponding open orbit contributions on the right hand side of Eq. (4.53) however, by symmetry factors. For this reason the last equation contains a proportionality sign. We will return to this point soon.

The contribution of two independent 2-encounters (c.f. Fig. 4.14), denoted by $\delta R_{2b}(\epsilon)$, is given by

$$\delta R_{2b}(\epsilon) = \frac{1}{16} \frac{\partial^2}{\partial \epsilon^2} \frac{e^{8i\epsilon \tau_E/T_H}}{\epsilon^2}.$$
 (4.54)

Compared to the open orbit contribution it is divided by four because each of the four links can be chosen as the first yielding each time an identical configuration. The contribution of one 3-encounter, $\delta R_{2c}(\epsilon)$, obtained by allowing the encounter stretches to overlap along one enclosed periodic orbit in Fig. 4.14 at one end, is obtained in [4] using [26] to be

$$\delta R_{2c}(\epsilon) = \frac{1}{16} \frac{\partial^2}{\partial \epsilon^2} \frac{1}{\epsilon^2} \left(3e^{6i\epsilon\tau_E/T_H} - 4e^{8i\epsilon\tau_E/T_H} \right). \tag{4.55}$$

As each of the three contained periodic orbits can be chosen as the first yielding identical configurations this contribution is divided by a factor three compared to the open orbit contribution obtained from (4.53). A further diagram results from encounter overlap along one enclosed periodic orbit at both ends, see Fig. 4.22. The overall contribution I containing the contribution from the latter diagram and the contributions $\delta R_{2b}(\epsilon)$ and $\delta R_{2c}(\epsilon)$ is obtained [4] by considering J in the Appendix with $a=i\epsilon$, $b=2i\epsilon$ and $d=-i\epsilon$, because the orbit is assumed to be longer than $t_{\text{enc},1}+t_{\text{enc},2}+2t_s+2t_u+\tau_p$, and multiplying it by factors resulting from the links not surrounding the central periodic orbit. A technical complication is that the contribution from this diagram contains three copies of the contribution with a 3-encounter and four copies of the contribution with two 2-encounters, because I is constructed for open instead of periodic orbits. To take this into account we subtract them here with the right multiplicity factors. All told, the contribution resulting from the periodic orbit encounters, $\delta R_{2d}(\epsilon)$ was calculated in [4] to be

$$\delta R_{2d}(\epsilon) = I - 4\delta R_{2b}(\epsilon) - 3\delta R_{2c}(\epsilon)
= \frac{1}{16} \frac{\partial^2}{\partial \epsilon^2} \frac{1}{\epsilon^2} \left(3e^{4i\epsilon\tau_E/T_H} - 9e^{6i\epsilon\tau_E/T_H} + 6e^{8i\epsilon\tau_E/T_H} \right).$$
(4.56)

However, as already explained above, this is only the complete set of contributions in the case when the two orbits approaching and leaving the periodic orbit are open like in the case of the reflection covariance as in Fig. 4.10, otherwise the corresponding orbital parts can get shorter than the duration of the fringes, like moving from Figs. 4.8 to 4.15. To take into account this additional configuration we replace $\delta R_{2d}(\epsilon)$ studied in [4] by another contribution denoted by $\delta R_{2e}(\epsilon)$. Up to now we only allowed the orbital parts decorrelated from the central periodic orbit, to be altogether longer than $2t_s + 2t_u$. However, the contribution considered now results like for the conductance from an orbital configuration where the two other links, those decorrelated from the central periodic orbit in Fig. 4.22, get shorter than $t_s + t_u$ each. The bottom and the top loop in Fig. 4.22 outside of the encounter with the central

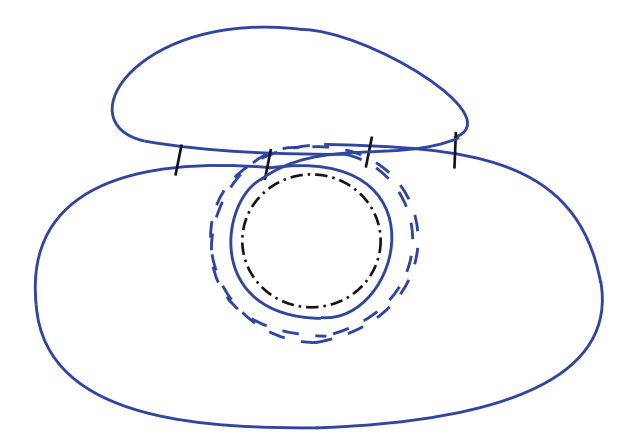


Fig. 4.22 A diagram accounted for in the contribution $\delta R_{2d}(\epsilon)$ to the spectral form factor. A central dashed–dotted periodic orbit is encountered two times. Fringe correlations are marked by black vertical lines. For the partner (not shown) one traversal of the central periodic orbit is exchanged between the first and the second encounter

periodic orbit must again have positive length, i.e. must decorrelate from the central periodic orbit, but do not necessarily need to be longer than the fringes. In order to calculate this contribution we first consider J in the Appendix with $a=i\epsilon$, b=0 and $d=-i\epsilon$, because the orbit has a minimal length of $t_{\rm enc,1}+t_{\rm enc,2}+\tau_p$ as in Eq. (4.40), together with the factors resulting from the links not surrounding the central periodic orbit and subtract from this contribution like in Eq. (4.56) $\delta R_{2b}(\epsilon)$ and $\delta R_{2c}(\epsilon)$ with the right multiplicity factors. The corresponding contribution denoted by $\delta R_{2e,1}(\epsilon)$ is

$$\delta R_{2e,1}(\epsilon) = \frac{1}{16} \frac{\partial^2}{\partial \epsilon^2} \frac{1}{\epsilon^2} e^{4i\epsilon \tau_E/T_H} - 4\delta R_{2b}(\epsilon) - 3\delta R_{2c}(\epsilon)
= \frac{1}{16} \frac{\partial^2}{\partial \epsilon^2} \frac{1}{\epsilon^2} \left(e^{4i\epsilon \tau_E/T_H} - 9e^{6i\epsilon \tau_E/T_H} + 8e^{8i\epsilon \tau_E/T_H} \right).$$
(4.57)

This procedure however, counts some configurations containing a surrounded periodic orbit twice: Shrinking in Fig. 4.22 the length of the upper periodic orbit to zero we again obtain a contribution containing one surrounded periodic orbit. A configuration containing one surrounded periodic orbit was however, already taken into account in $\delta R_{2e,1}(\epsilon)$ when shrinking the length of the central periodic orbit to zero. We thus subtract the latter contribution. This contribution referred to as $\delta R_{2e,2}(\epsilon)$ is calculated by again making use of K_1 and K_2 in the Appendix: We therefore consider a 3-encounter, i.e. $f=3i\epsilon$, with fringes with duration between t_s+t_u and $2t_s+2t_u$. We thus consider once the prefactor $g=2i\epsilon$ and once $g=i\epsilon$ in front of t_s+t_u and take the difference of the two results obtained for K in the Appendix yielding for the contribution $\delta R_{2e,2}(\epsilon)$

$$\delta R_{2e,2}(\epsilon) = \frac{1}{16} \frac{\partial^2}{\partial \epsilon^2} \frac{1}{\epsilon^2} \left[4 \left(e^{8i\epsilon \tau_E/T_H} - e^{6i\epsilon \tau_E/T_H} \right) - \left(e^{6i\epsilon \tau_E/T_H} - e^{4i\epsilon \tau_E/T_H} \right) \right]. \tag{4.58}$$

Subtracting $\delta R_{2e,2}(\epsilon)$ from $\delta R_{2e,1}(\epsilon)$ we obtain $\delta R_{2e}(\epsilon)$

$$\delta R_{2e}(\epsilon) = \delta R_{2e,1}(\epsilon) - \delta R_{2e,2}(\epsilon) = \frac{1}{16} \frac{\partial^2}{\partial \epsilon^2} \frac{4}{\epsilon^2} \left(e^{8i\epsilon \tau_E/T_H} - e^{6i\epsilon \tau_E/T_H} \right). \quad (4.59)$$

Summing now the quantum corrections in the absence of time-reversal symmetry given in (4.54, 4.55) and (4.59) we obtain for the overall quantum correction at the considered order $\delta R_2(\epsilon)$

$$\delta R_2(\epsilon) = \frac{1}{16} \frac{\partial^2}{\partial \epsilon^2} \frac{\left(e^{8i\epsilon \tau_E/T_H} - e^{6i\epsilon \tau_E/T_H} \right)}{\epsilon^2}.$$
 (4.60)

This yields then after the Fourier transform (2.67) for the corresponding correction to the spectral form factor $\delta K_2(\tau)$

$$\delta K_2(\tau) = -\frac{\tau^2}{T_H} \left[\Upsilon \left(\tau T_H - 3\tau_E \right) - \Upsilon \left(\tau T_H - 4\tau_E \right) \right] \tag{4.61}$$

with $\Upsilon(x) \equiv \int_0^x dx' \Theta(x') = x \Theta(x)$. Expression (4.61) was also obtained in [5] by field-theoretical methods.

As already noted for the conductance, we also emphasise here that these results for the spectral correlation function could not be obtained without considering fringes: Not doing so we would only get the contribution (4.54) with a multiplicity factor four along with the contribution from a 3-encounter with three equally long encounter stretches, given by

$$-\frac{1}{16}\frac{\partial^2}{\partial \epsilon^2} \frac{e^{6i\epsilon\tau_E/T_H}}{\epsilon^2} \tag{4.62}$$

with a multiplicity factor three and the overall contribution resulting from all possible encounter configurations given by

$$\frac{1}{16} \frac{\partial^2}{\partial \epsilon^2} \frac{e^{4i\epsilon \tau_E/T_H}}{\epsilon^2} \tag{4.63}$$

with a multiplicity factor one. As one can easily see it is not possible to obtain the field-theoretical result from just these semiclassical contributions.

In this chapter we have so far calculated the Ehrenfest-time dependence of the next-to-leading order quantum corrections to the transmission through open systems and the first quantum correction to the spectral form factor of closed systems in the absence of time-reversal symmetry. For the transmission and reflection the key step was that we can relax one of the restrictions compared to the calculation of the reflection covariance in [12]. Namely, because of the slightly different topology

formed by rejoining some of the links (previously cut open to get to the reflection covariance) the fringes were allowed to overlap and surround the second periodic orbit formed. For closed systems without time-reversal symmetry we then rejoined one more link and created a third (and fourth) periodic orbit. This also allows to relax a similar restriction and leads to a modification of the results obtained for the spectral form factor in [4]. By including all possibilities we showed that our semiclassical result agrees with the field-theoretical prediction from [5].

When considering in this section the ac conductance we treated the correlation function of the trace of one pair of scattering matrices with Ehrenfest-time. We want to generalise this now to n pairs of scattering matrices, however, only treating the leading order in N contributions.

4.5 Correlation Function of an Arbitrary Number of Pairs of Scattering Matrices

To be precise we will consider the correlation function of 2n scattering matrices at alternating energies defined as

$$C(\epsilon, \tau, n) = \frac{1}{N} \left\langle \text{Tr} \left[S \left(E + \frac{\epsilon \hbar}{2\tau_{\text{D}}} \right) S^{\dagger} \left(E - \frac{\epsilon \hbar}{2\tau_{\text{D}}} \right) \right]^{n} \right\rangle_{\Delta k}, \tag{4.64}$$

where the energy ϵ is measured with respect to the (Fermi) energy E and in units of the so-called Thouless energy $E_T = \hbar/2\tau_D$. We defined $\tau \equiv \tau_E/\tau_D$. We want to show that $C(\epsilon, \tau, n)$ possesses to leading order in N the following form

$$C(\epsilon, \tau, n) = C_1(\epsilon, \tau, n) + C_2(\epsilon, \tau, n), \tag{4.65}$$

$$C_1(\epsilon, \tau, n) = C(\epsilon, n)e^{-\tau(1-in\epsilon)},$$
 (4.66)

$$C_2(\epsilon, \tau, n) = \frac{1 - e^{-\tau(1 - in\epsilon)}}{1 - in\epsilon},$$
(4.67)

with the RMT (i.e. $\tau=0$) part of this correlation function denoted by $C(\epsilon,n)$. This form is predicted by effective RMT [26, 40] So far Ref. [26] calculated $C(\epsilon,\tau,n)$ within the trajectory based approach used here for n=1,2,3 while [13, 41] showed the separation into two terms in (4.65) to be a consequence of the preservation under time evolution of a phase-space volume of the system. Moreover they also calculated the explicit form we give in (4.67) for the second term and that the first term in (4.66) is proportional to the factor $e^{-\tau(1-in\epsilon)}$.

In this book we already compared several times our results for non-zero Ehrenfest-time with the ones obtained by field-theoretical methods. In these approaches the fact that nearby trajectories are linearisable was taken into account in the presence of a small amount of disorder: In the last paragraph we mentioned another method to describe the effect of the Ehrenfest-time, effective RMT [40]. It splits the phase space and thereby also the underlying scattering matrix of the considered system

into two independent parts. A classical and a quantum part, where the first one is determined by all trajectories shorter than τ_E and the second one by all trajectories longer than τ_E . The scattering matrix of the system can thus be expressed as

$$S(E) = \begin{pmatrix} S_{\rm cl}(E) & 0\\ 0 & S_{\rm qm}(E) \end{pmatrix}. \tag{4.68}$$

The classical part $S_{\rm cl}(E)$ is treated by considering the motion along classical trajectories. For $S_{\rm qm}(E)$ at first an energy dependence is factored out $S_{\rm qm}(E) = {\rm e}^{iE\tau_E/\hbar}\tilde{S}_{\rm qm}(E)$, that takes into account that the minimal dwell time of the trajectories is τ_E [26]. Afterwards $\tilde{S}_{\rm qm}(E)$ is assumed to be distributed according to RMT. Effective RMT proved successful for describing effects at leading order in N like shot noise [42–45], that is determined by the n=2 term in (4.64) or the gap in the density of states of a chaotic Andreev billiard [46, 47] However, this phenomenological theory does not provide a dynamical justification of the obtained results.

Using Eqs. (2.29, 2.31, 2.32), the correlation function can be written semiclassically in terms of 2n scattering trajectories connecting certain channels in the opening like shown for n = 3 in Fig. 4.23a. Including the energy dependence in linearised approximation, the correlation function becomes semiclassically

$$C^{\text{sc}}(\epsilon, \tau, n) = \frac{1}{N} \left\langle \left(\frac{\pi \hbar}{2W^2} \right)^n \prod_{j=1}^n \sum_{i_j, o_j} \sum_{\substack{\gamma_j (i_j \to o_j) \\ \gamma'_j (i_{j+1} \to o_j)}} D_{\gamma_j} D_{\gamma'_j} \right\rangle_{Ak}, \tag{4.69}$$

 T_{γ} are the times trajectories γ spend inside the system, and we identify the channels $i_{n+1} = i_1$ due to the trace in (4.64).

For n=1 the leading order contribution in N results from the diagonal approximation, that yields an Ehrenfest-time-independent result. This changes for n>1: The trajectories connect channels along a closed cycle as shown in Fig. 4.23a and need then to be collapsed onto each other as shown in the other diagrams in Fig. 4.23 to create orbit pairs with small action difference.

As we are only considering leading order in N contributions we can restrict for a certain n to orbital configurations containing (n-1) encounters with every orbit involved in at least one encounter. These encounters are allowed to overlap, like when moving from Fig. 4.23b to c, or allowed to be moved into the lead, for examples see Fig. 4.23d–h. Keeping n constant and including one more encounter into these diagrams always creates diagrams with at least two more links as can be easily checked. Following then the diagrammatic rule that each encounter leads to a factor -N and each link to a factor N^{-1} (see Chap. 2) we obtain a contribution one order lower in N.

In this section we want to show how (4.65–4.67) can be obtained by identifying systematically correlated orbits and calculating their contributions. In Sect. 4.5.1 we

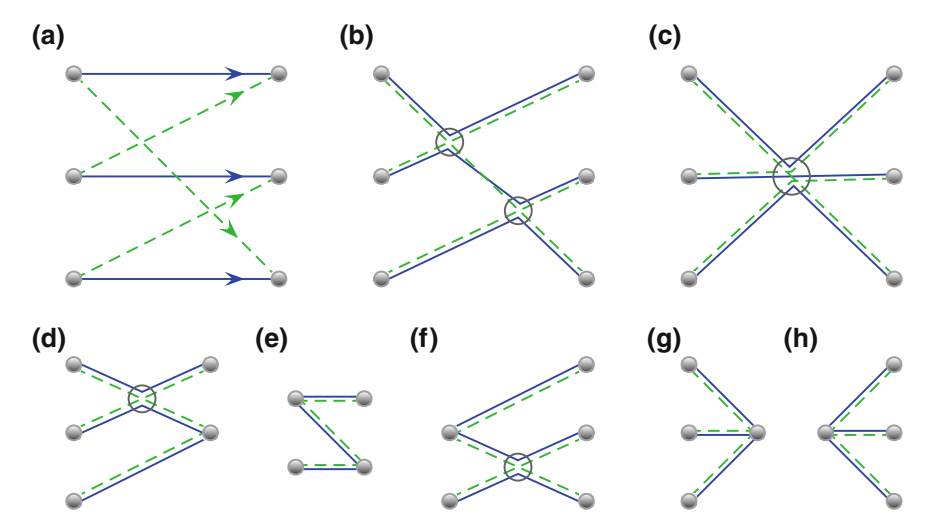


Fig. 4.23 The trajectory sets with encounters that contribute to the 3rd correlation function $C(\epsilon, 3)$

consider the first term in (4.65): We show that the prefactor $C(\epsilon, n)$ of the exponential is indeed given by the RMT expression obtained semiclassically in [48] and that this is multiplied by the exponential given in (4.66). The underlying diagrams considered here are the same as the ones occurring also in the semiclassical calculation of the RMT contribution. In Sect. 4.5.2 we treat the second term in (4.65) and show how this contribution arises from trajectories that are always correlated. Furthermore we show in Sect. 4.5.3 that there exist no mixed terms between the first and the second term in (4.65), that could result—expressed in terms of the considered diagrams—from correlations between trajectories always correlated with each other on the one hand and trajectories only correlated with each other during encounters on the other hand.

4.5.1 Influence of the Ehrenfest-Time on Orbits with Encounters

The main idea in this subsection is to split our diagrams in a different way compared to the semiclassical analysis without Ehrenfest-time (referred to as the RMT treatment) and the analysis of the Ehrenfest-time dependence of the cases n=1,2,3 in [26]: In the semiclassical calculation one considers a certain number of orbits encountering each other. It turns out in the RMT treatment to be sufficient to consider only encounters where all orbits are linearisable up to the *same* point, see for an example Fig. 4.6. As already explained in the last sections when taking into account the Ehrenfest-time dependence this is no longer sufficient as was first shown in [12], see Fig. 4.7 for an example of an additional diagram analysed in this case. The main complication arising in [26] to calculate $C(\epsilon, \tau, n)$ is then to treat these encounters. In order to simplify the calculation we imagine these encounters being built up out

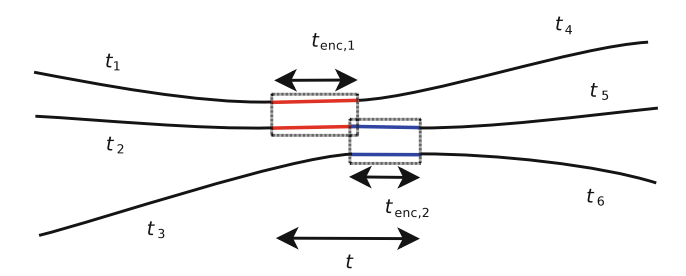


Fig. 4.24 A diagram with two 2-encounters as we treat it with Ehrenfest-time. The encounter stretches of the two 2-encounters are marked by *boxes* (shown *red* and *blue*)

of several encounters which each consist of two encounter stretches, we have distinguished these 2-encounters by different boxes in Fig. 4.24. In this way it is much easier to consider encounter diagrams for arbitrary n for non-zero Ehrenfest-time, which appeared not feasible in the formalism used in [26].

We first illustrate our procedure by considering three correlated orbits with two 2-encounters as in Fig. 4.24 and show how the result given in [26] can be obtained in this case and then treat the general case of n orbits with (n-1) independent or overlapping 2-encounters.

4.5.1.1 Explanation of Our Procedure for n = 3

In the treatment of the RMT-type contribution (4.66) we first consider the case where all the encounters occur inside the system. For n=3 we have the two semiclassical diagrams in Fig. 4.23b, c which include a trajectory set (of three original trajectories and three partners) with two 2-encounters in Fig. 4.23b and a single 3-encounter in Fig. 4.23c. By shrinking the link connecting the two encounters in Fig. 4.23b we can see how we deform them into the diagram in Fig. 4.23c and we use this idea in our Ehrenfest-time treatment.

Two 2-Encounters

In our treatment, the overall contribution $C^{4.24}(\epsilon, \tau, 3)$ of the two 2-encounters (depicted in more detail in Fig. 4.24) is obtained by allowing the upper trajectory to possess a minimal length of the first 2-encounter and the lowest one a minimal length of the second 2-encounter. The middle trajectory, which passes through both encounters has a minimal length given by the maximum of the two encounter times as we allow the encounters to overlap. However, we do not yet allow one encounter to be subsumed into the other so we also set the time t between the start of the first encounter and the end of the second to be longer than the maximum encounter time. To write down the semiclassical contribution of the diagram in Fig. 4.24 we use the sum rule (2.34) and the expected number of times the classical trajectories would

approach and form such encounters calculated in an analogous way as before, for details see for example [22], which gives when transformed again into a product of link and encounter contributions

$$C^{4.24}(\epsilon, \tau, 3) = \frac{N^2}{\tau_{\rm D}^3} \Biggl(\prod_{i=1}^6 \int_0^\infty dt_i e^{-t_i (1 - i\epsilon)/\tau_{\rm D}} \Biggr) \int_{-c}^c ds \, du \frac{e^{i\epsilon (t_{\rm enc, 1} + t_{\rm enc, 2})/\tau_{\rm D}}}{\Omega^2 t_{\rm enc, 1} t_{\rm enc, 2}} \times \int_{\max\{t_{\rm enc, 1}, t_{\rm enc, 2}\}}^\infty dt \, e^{(i/\hbar)\Delta S} e^{-t(1 - i\epsilon)/\tau_{\rm D}},$$
(4.70)

where the superscript refers to Fig. 4.24. We have summed over the possible channels, and t_i with i = 1, ..., 6 label the links from the channels to the encounters. The action difference of three orbits encountering each other is when the (s'_i, u'_i) coordinates are measured in one Poincaré surface of section given by [24, 25] $\Delta S = u_1' s_1' + u_2' s_2' - u_2' s_1'$. If we measure the coordinates in two different sections, we denote the corresponding coordinates by s_i , u_i , it is given due to the exponential increase and decrease of (s'_i, u'_i) -coordinates with time by $\Delta S =$ $u_1s_1 + u_2s_2 - u_2s_1 \exp(-\lambda \Delta t)$, where the time Δt denotes the time the particle needs to travel between the two sections. By expanding the part of the exponential $e^{(i/\hbar)\Delta S}$ containing this Δt -dependent part into a Taylor series one obtains apart from the leading one terms rapidly decaying with Δt because of the factor $e^{-\lambda \Delta t}$ to some power. One verifies easily that contributions from higher-order terms than the leading (time-independent) one lead to contributions of higher order in $1/(\lambda \tau_D)$ and can be neglected. The quantity $1/(\lambda \tau_D)$ can be considered as small in this context because first $1/\lambda$ is a time related to the underlying classical system, given by the time between a few number of bounces, second τ_D however, has to assumed to be of the order of the Ehrenfest-time τ_E in order to observe exponential factors like $e^{-\tau_E/\tau_D}$, i.e. τ_D is assumed to be classically large.

In the first line of (4.70) we can see that each integral over the links is weighted by its classical probability to remain inside the system for the time t_i . As the time t (between the two outer ends of the encounter stretches on the middle trajectory shown in Fig. 4.24) passes through both encounters their survival probability is included in the t-dependent factor in the last line of (4.70) taking into account the survival probability correction for encounters explained before Eq. (2.47).

Performing the time integrals in the first line of (4.70) we have

$$C^{4.24}(\epsilon, \tau, 3) = \frac{\tau_{\rm D} T_{\rm H}^2}{(1 - i\epsilon)^6} F^{4.24}(\tau), \tag{4.71}$$

where we have moved all Ehrenfest-time-dependent parts into the factor $F^{4.24}(\tau)$ with the superscript again referring to Fig. 4.24,

$$F^{4.24}(\tau) = \int_{-c}^{c} ds \, du \frac{e^{(i/\hbar)\Delta S} e^{i\epsilon (t_{\text{enc},1} + t_{\text{enc},2})/\tau_{\text{D}}}}{\Omega^{2} t_{\text{enc},1} t_{\text{enc},2}} \int_{\max\{t_{\text{enc},1},t_{\text{enc},2}\}}^{\infty} dt \, e^{-t(1-i\epsilon)/\tau_{\text{D}}}.$$
(4.72)

Here we can also see the connection with the previous Ehrenfest-time treatment of such a diagram. When $t > t_{\text{enc},1} + t_{\text{enc},2}$ the two encounters separate (the integrals can then be further broken down into products) and this is the case where the trajectories can be considered to have two independent 2-encounters as in [26]. Because we choose a different lower limit though, the contribution above also includes some of the diagrams previously treated as 3-encounters in [26]. The reason for our choice becomes clear in the following steps. We first substitute $t' = t - \max\{t_{\text{enc},1}, t_{\text{enc},2}\}$,

$$F^{4.24}(\tau) = \int_{-c}^{c} ds \, du \frac{e^{(i/\hbar)\Delta S} e^{i\epsilon (t_{\text{enc},1} + t_{\text{enc},2})/\tau_{\text{D}}}}{\Omega^{2} t_{\text{enc},1} t_{\text{enc},2}} \times \int_{0}^{\infty} dt' \, e^{-(t' + \max\{t_{\text{enc},1}, t_{\text{enc},2}\})(1 - i\epsilon)/\tau_{\text{D}}}, \tag{4.73}$$

and then substitute like in Eq. (4.26) $u_i = c/\sigma_i$, $s_i = cx_i\sigma_i$ and perform the σ_i -integrals using the explicit form of the $t_{\text{enc},i} \equiv \frac{1}{\lambda} \ln \left(c^2/|s_i u_i| \right)$. This results in

$$F^{4.24}(\tau) = 16 \int_0^1 d\mathbf{x} \frac{\lambda^2 c^4}{\Omega^2} \cos\left(\frac{c^2}{\hbar} x_1\right) \cos\left(\frac{c^2}{\hbar} x_2\right) e^{-i\epsilon(\ln x_1 + \ln x_2)/(\lambda \tau_D)}$$

$$\times \int_0^\infty dt' e^{-(t' + \max\{-\ln x_1, -\ln x_2\}/\lambda)(1 - i\epsilon)/\tau_D}.$$
(4.74)

Now we substitute $x_i' = x_i c^2/\hbar$ and obtain

$$F^{4.24}(\tau) = 16 \int_0^\infty d\mathbf{x}' \frac{\lambda^2 \hbar^2}{\Omega^2} \cos(x_1') \cos(x_2') e^{-i\epsilon(\ln x_1' + \ln x_2')/(\lambda \tau_D)}$$

$$\times \int_0^\infty dt' e^{-(t' + \max\{-\ln x_1', -\ln x_2'\}/\lambda)(1 - i\epsilon)/\tau_D} e^{-\tau(1 - 3i\epsilon)}.$$
 (4.75)

Here we split the resulting expression into an \hbar -independent integral (or more exactly trivially dependent on \hbar), that exists due to the energy average contained in Eq. (4.64), and an Ehrenfest-time or \hbar -dependent part with $\tau_E \equiv 1/\lambda \ln \left(c^2/\hbar\right)$. This contains the Ehrenfest-time dependence that is expected from (4.66), so (4.75) already shows that the diagrams considered here yield the correct Ehrenfest-time dependence.

A 3-Encounter

Now we consider the case that one of the two 2-encounters lies fully inside the other one, which we will refer to as a generalised version of a 3-encounter, as depicted in Fig. 4.25.

For the Ehrenfest-time-dependent part we have a similar contribution as in (4.72) with two differences: First t is here best defined as the distance between the midpoints of the two different encounter stretches and so can vary between

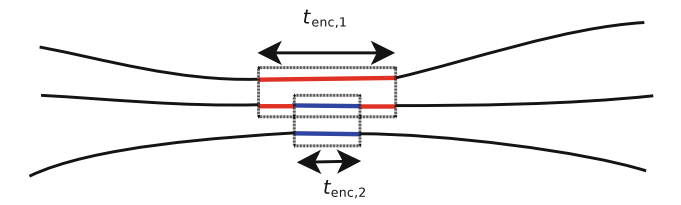


Fig. 4.25 One 2-encounter is located fully inside the other, corresponding to our treatment of a generalised version of a 3-encounter. The two 2-encounters are marked by *boxes* (indicated by different colours)

$$|t| \le \frac{1}{2} \left(\max \left\{ t_{\text{enc},1}, t_{\text{enc},2} \right\} - \min \left\{ t_{\text{enc},1}, t_{\text{enc},2} \right\} \right),$$

$$|t| \le \frac{1}{2} |t_{\text{enc},1} - t_{\text{enc},2}|. \tag{4.76}$$

Second the survival probability of the encounters is determined by the longest encounter stretch and is independent of t. The Ehrenfest-time-dependent part can then be written as

$$F^{4.25}(\tau) = \int_{-c}^{c} ds \, du \frac{e^{(i/\hbar)\Delta S} e^{i\epsilon (t_{\text{enc},1} + t_{\text{enc},2})/\tau_{\text{D}}}}{\Omega^{2} t_{\text{enc},1} t_{\text{enc},2}} \times \int_{-\frac{1}{2}|t_{\text{enc},1} - t_{\text{enc},2}|}^{\frac{1}{2}|t_{\text{enc},1} - t_{\text{enc},2}|} dt \, e^{-(\max\{t_{\text{enc},1},t_{\text{enc},2}\}\})(1-i\epsilon)/\tau_{\text{D}}}.$$
(4.77)

Performing the t-integral and following the same steps like for (4.74, 4.75), we find

$$F^{4.25}(\tau) = 16 \int_0^\infty d\mathbf{x}' \frac{\lambda^2 \hbar^2}{\Omega^2} \frac{|\ln x_1' - \ln x_2'|}{\lambda} \cos(x_1') e^{-i\epsilon (\ln x_1' + \ln x_2')/(\lambda \tau_D)} \times \cos(x_2') e^{-(\max\{-\ln x_1', -\ln x_2'\})(1 - i\epsilon)/(\lambda \tau_D)} e^{-\tau (1 - 3i\epsilon)}. \tag{4.78}$$

Also this part shows an Ehrenfest-time dependence as expected from (4.66). Note that when performing the *t*-integral the result in this case is of course proportional to $|t_{\text{enc},1} - t_{\text{enc},2}|$ which contains, after the substitution from *x* to x', two times the same terms linear in τ_E with different signs that thus cancel each other.

Touching the Lead

Up to now we concentrated on encounters inside the system, but apart from these diagrams we also need to consider diagrams where the encounters touch the opening as in Fig. 4.23d—h. We will, as above, start with considering encounters built up out of two 2-encounters and focus here on how the calculation of the contribution when encounters move into the lead is changed compared to the treatment of encounters

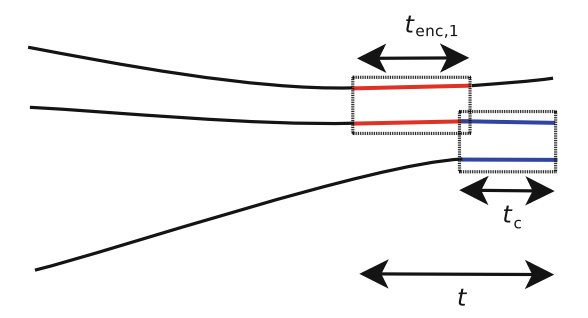


Fig. 4.26 The second of two 2-encounters now enters the lead so that only t_c of it remains inside the system

inside the system. As already explained in the last section when encounters touch the lead we have two links less and one includes an additional time integral running between zero and the corresponding encounter time, which characterises the duration of the part of the encounter stretch that has not yet been moved into the lead.

We consider two encounters with durations $t_{\rm enc,1}$ and $t_{\rm enc,2}$ with the second encounter touching the opening as in Fig. 4.23d and drawn in more detail in Fig. 4.26. As the second encounter enters the lead we now define the time t to be from the start of the first encounter until the lead and introduce the time t_c which measures the part of the second encounter that has not yet been moved into the lead. We also distinguish for the Ehrenfest-time relevant contribution $F^{4.26}(\tau)$ two cases: In the first case (A), $t_{\rm enc,2} \leq t_{\rm enc,1}$, we have $F_{\rm A}^{4.26}(\tau)$ with the additional integral over the time t_c

$$F_{\rm A}^{4.26}(\tau) = \int_{-c}^{c} ds \, du \frac{e^{(i/\hbar)\Delta S} e^{i\epsilon t_{\rm enc,1}/\tau_{\rm D}}}{\Omega^{2} t_{\rm enc,1} t_{\rm enc,2}} \int_{0}^{t_{\rm enc,2}} dt_{c} \, e^{i\epsilon t_{c}/\tau_{\rm D}} \int_{t_{\rm enc,1}}^{\infty} dt \, e^{-t(1-i\epsilon)/\tau_{\rm D}},$$
(4.79)

where the limits on the time integrals derive from the fact that the first encounter is not allowed to touch the lead (this would be included as a 3-encounter) and that the second must. Performing the time integrals this is

$$F_{\rm A}^{4.26}(\tau) = \int_{-c}^{c} ds \, du \, \frac{\mathrm{e}^{(i/\hbar)\Delta S}}{\Omega^{2} t_{\rm enc,1} t_{\rm enc,2}} \frac{\tau_{\rm D}^{2}}{i\epsilon(1-i\epsilon)} \left[\mathrm{e}^{i\epsilon t_{\rm enc,2}/\tau_{\rm D}} - 1 \right] \mathrm{e}^{-t_{\rm enc,1}(1-2i\epsilon)/\tau_{\rm D}}, \tag{4.80}$$

with the first and second term in the square brackets resulting from the upper and lower limit of the t_c -integration. In the second case (B), $t_{\text{enc},2} > t_{\text{enc},1}$, we obtain

$$F_{\rm B}^{4.26}(\tau) = \int_{t_{\rm enc,2} > t_{\rm enc,1}}^{c} ds \, du \frac{{\rm e}^{(i/\hbar)\Delta S} {\rm e}^{i\epsilon t_{\rm enc,1}/\tau_{\rm D}}}{\Omega^{2} t_{\rm enc,1} t_{\rm enc,2}} \left[\int_{0}^{t_{\rm enc,1}} dt_{c} \, {\rm e}^{i\epsilon t_{c}/\tau_{\rm D}} \right] \times \int_{t_{\rm enc,1}}^{\infty} dt \, {\rm e}^{-t(1-i\epsilon)/\tau_{\rm D}} + \int_{t_{\rm enc,1}}^{t_{\rm enc,2}} dt_{c} \, {\rm e}^{i\epsilon t_{c}/\tau_{\rm D}} \int_{t_{c}}^{\infty} dt \, {\rm e}^{-t(1-i\epsilon)/\tau_{\rm D}} \right],$$

$$(4.81)$$

where the more complicated limits derive from not allowing the second encounter to move further left than the first. After integrating we have

$$\begin{split} F_{\rm B}^{4.26}(\tau) &= \int_{t_{\rm enc,2} > t_{\rm enc,1}}^{c} ds \, du \, \frac{{\rm e}^{(i/\hbar)\Delta S}}{\varOmega^{2} t_{\rm enc,1} t_{\rm enc,2}} \frac{\tau_{\rm D}^{2}}{(1-i\epsilon)} \left[\frac{1}{i\epsilon} \left[{\rm e}^{i\epsilon t_{\rm enc,1}/\tau_{\rm D}} - 1 \right] \right. \\ &\times {\rm e}^{-t_{\rm enc,1}(1-2i\epsilon)/\tau_{\rm D}} + \frac{1}{(1-2i\epsilon)} {\rm e}^{-t_{\rm enc,1}(1-3i\epsilon)/\tau_{\rm D}} \\ &- \frac{1}{(1-2i\epsilon)} {\rm e}^{i\epsilon t_{\rm enc,1}/\tau_{\rm D}} {\rm e}^{-t_{\rm enc,2}(1-2i\epsilon)/\tau_{\rm D}} \right]. \end{split} \tag{4.82}$$

The last line comes from the upper limit of the second t_c -integral and has the same Ehrenfest-time dependence as before and in line with (4.66). Likewise the upper t_c -time limit for case A in (4.79) leads to the same dependence and we can conclude that the upper limits of the t_c -integrations yield contributions similar to when the encounters are inside the system and with the same Ehrenfest-time dependence. The remaining (lower) limits of the time integrations in (4.79, 4.81) give contributions possessing a different Ehrenfest-time dependence which however, always yield zero in the semiclassical limit due to the fact that the corresponding terms contain no $t_{\rm enc,2}$ in the exponentials containing $\tau_{\rm D}$. Apart from the action difference, the only term depending on s_2 , u_2 is the $1/t_{\rm enc,2}$. The resulting expression is rapidly oscillating as a function of the energy as shown in Eq. (4.26) and thus cancelled by the energy average.

We can repeat this procedure for the remaining diagrams in Fig. 4.23 and see that the contributions are determined by the upper limits of the corresponding t_c -integrals. For the diagrams with a generalised 3-encounter (Fig. 4.23g, h) this follows like for the 3-encounter inside the system but for Fig. 4.23e where the two 2-encounters enter different channels (and possibly different leads) there is an additional subtlety. The two encounters are still allowed to overlap, so that during the time t the stretch now connecting both channels can always be inside encounters but the individual encounters are not allowed to connect leads at both ends. These additional possibilities are considered later, where if both encounters connect to the leads at both ends we actually have a band of correlated trajectories (treated in Sect. 4.5.2) and if only one does we have a mixed term (treated in Sect. 4.5.3). With this organisation of the encounters we see that each diagram has the same Ehrenfest-time dependence as when the encounters are inside the system and hence in line with (4.66).

Intermediate Summary

The reasoning so far in this subsection proves the form of (4.66) for n=3. First we know that the resulting contribution from the diagrams analysed contains an overall factor $e^{-\tau(1-3i\epsilon)}$, second the remaining integrals are independent of \hbar and thus independent of the Ehrenfest-time and third the diagrams we analyse are the same as the ones analysed in the RMT case in the first part of [8]. As in the limit $\tau_E \to 0$ we must recover that previous result, this implies that $C(\epsilon, \tau, 3)$ in (4.66) is indeed given by the RMT expression.

Full Contributions

Before proceeding to the general case, we first however, want to illustrate how our calculation can be used to obtain, apart from just the Ehrenfest-time dependence, the complete dependence on τ_D and ϵ .

We therefore start for the two 2-encounters from Fig. 4.24 from the last expression in (4.75) and perform first the t'-integral

$$F^{4.24}(\tau) = \frac{16\tau_D}{(1 - i\epsilon)} \int_0^\infty d\mathbf{x}' \frac{\lambda^2 \hbar^2}{\Omega^2} \cos(x_1') \cos(x_2') e^{\min\{-\ln x_1', -\ln x_2'\} i\epsilon/(\lambda \tau_D)}$$

$$\times e^{-\max\{-\ln x_1', -\ln x_2'\} (1 - 2i\epsilon)/(\lambda \tau_D)} e^{-\tau(1 - 3i\epsilon)}, \tag{4.83}$$

where it is simpler to rewrite the result in terms of the maximum and minimum value of $\ln x_i'$. For calculating the x_i' -integrals we perform partial integrations (integrating each time the cos functions) and then perform the resulting integrals from zero to infinity

$$F^{4.24}(\tau) = -\frac{16i\epsilon}{\tau_D} \frac{(1 - 2i\epsilon)}{(1 - i\epsilon)} \int_0^\infty d\mathbf{x}' \frac{\hbar^2}{\Omega^2} \frac{\sin(x_1')}{x_1'} \frac{\sin(x_2')}{x_2'} e^{\min\{-\ln x_1', -\ln x_2'\}i\epsilon/(\lambda\tau_D)}$$

$$\times e^{-\max\{-\ln x_1', -\ln x_2'\}(1 - 2i\epsilon)/(\lambda\tau_D)} e^{-\tau(1 - 3i\epsilon)}$$

$$= -\frac{i\epsilon}{\tau_D T_H^2} \frac{(1 - 2i\epsilon)}{(1 - i\epsilon)} e^{-\tau(1 - 3i\epsilon)}.$$
(4.84)

In the first line the further terms due the partial integration are either zero or cancel due to the energy average. The final result in the last line of (4.84) is also obtained when replacing max $\left\{-\ln x_1', -\ln x_2'\right\}/\lambda = y_1$ and min $\left\{-\ln x_1', -\ln x_2'\right\}/\lambda = y_2$ and performing the integrals with respect to y_i from zero to infinity.

To evaluate the contribution from the generalised 3-encounter in Fig. 4.25 we again perform two partial integrations in (4.78) and obtain

$$F^{4.25}(\tau) = \frac{16}{\tau_D} (1 - i\epsilon) \int_0^\infty d\mathbf{x}' \frac{\hbar^2}{\Omega^2} \frac{\sin(x_1')}{x_1'} \frac{\sin(x_2')}{x_2'} e^{\min\{-\ln x_1', -\ln x_2'\}i\epsilon/(\lambda \tau_D)}$$

$$\times e^{-\max\{-\ln x_1', -\ln x_2'\}(1 - 2i\epsilon)/(\lambda \tau_D)} e^{-\tau(1 - 3i\epsilon)}$$

$$= \frac{(1 - i\epsilon)}{\tau_D T_H^2} e^{-\tau(1 - 3i\epsilon)},$$
(4.85)

where we have also left out the terms from the partial integrations which cancel due to the energy average.

With these results we can now show how they connect to the RMT-type results. For this we split our diagrams differently and first need the result for an ideal 3-encounter as depicted in Fig. 4.6 whose contribution was calculated [26] to be

$$F^{4.6}(\tau) = -\frac{(1 - 3i\epsilon)}{\tau_D T_H^2} e^{-\tau(1 - 3i\epsilon)}.$$
 (4.86)

With the extra factors in (4.71) it is clear how in the limit $\tau_E = 0$ this reduces to the RMT-type result for a 3-encounter as in [8]. All the remaining contributions should be collected together as two 2-encounters, and as the ideal 3-encounter is included in our generalised 3-encounter we first subtract (4.86) from (4.85)

$$F^{4.25}(\tau) - F^{4.6}(\tau) = 2 \frac{(1 - 2i\epsilon)}{\tau_D T_H^2} e^{-\tau (1 - 3i\epsilon)}.$$
 (4.87)

Before we add the result from our separation of two 2-encounters in (4.84) we remember that in the treatment we enforce that the first encounter is to the left of the second. The result in (4.87) does not have this restriction so we divide by 2 to ensure compatibility and then add the result in (4.84) to obtain

$$F^{4.7}(\tau) = \frac{1}{\tau_D T_H^2} \frac{(1 - 2i\epsilon)^2}{(1 - i\epsilon)} e^{-\tau(1 - 3i\epsilon)}.$$
 (4.88)

This then reduces to the RMT-type result for trajectories with two 2-encounters when $\tau_E=0$ as in [8]. The agreement of these results with the previous Ehrenfest-time treatment [26] can be seen as the result in (4.88) includes both the result from two independent 2-encounters as well as a part of the contribution of the diagram referred to as a 3-encounter in [26]. When splitting the contribution in a different way like in [26] this leads to terms in both classes that contain different Ehrenfest-time dependencies which only cancel when summed together.

4.5.1.2 All Orders

Although up to now we have just reproduced results from [26], the procedure used here has the advantage that it yields a simple algorithm for determining the Ehrenfest-time dependence of the corresponding contributions to $C_1(\epsilon, \tau, n)$ at arbitrary order.

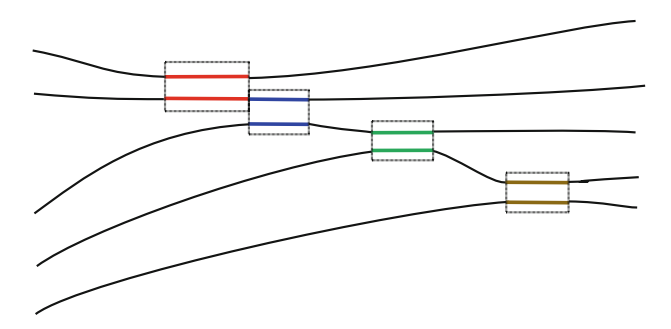


Fig. 4.27 A ladder of consecutive 2-encounters. The encounter stretches are marked by *boxes* (shown in different colours)

For our example of n=3 we showed how it was possible to split the diagrams into two classes that both showed the Ehrenfest-time dependence as expected from (4.66). We want to now show how to generalise our way of splitting considered for 3 trajectories to diagrams containing n trajectories.

Ladder Diagrams

We start again with the situation where all of the encounters are inside the system and by considering a case analogous to Fig. 4.24 involving now however, n instead of 3 trajectories. We first take a diagram that consists of a ladder of (n-1) 2-encounters so that the central n-2 trajectories each contain two encounter stretches while the two outside trajectories only contain one encounter stretch each. This situation is depicted in Fig. 4.27 and the encounters are thus characterised by (n-1) (s, u)-coordinates.

In this case we obtain for the Ehrenfest-time relevant contribution $F^{4.27}(\tau)$ that the t-integral measuring the time difference between the end points of the two encounter stretches on the middle orbit in (4.72) is replaced by n-2 integrals over times t_i with the same meaning as t; they measure the time difference between the outer end points of the two (consecutive) encounter stretches on the central trajectories containing 2-encounter stretches. These times likewise run from the maximum of the corresponding encounter times to infinity. The survival probability is determined by a single (artificial) stretch that runs through all the encounters so that the exponential term describing the τ_D - and ϵ -dependence is now given by

$$e^{-\sum_{i=1}^{n-2} t_i (1-i\epsilon)/\tau_D} e^{\sum_{i=2}^{n-2} t_{\text{enc},i}/\tau_D} e^{i\epsilon (t_{\text{enc},1} + t_{\text{enc},n-1})/\tau_D}.$$
 (4.89)

where $t_{\text{enc},i}$ are the durations of the (n-1) individual 2-encounters and the middle exponential compensates for the fact that the middle encounters are traversed by two t_i and that only one traversal should contribute to the survival probability. Setting $t_i' = t_i - \max\{t_{\text{enc},i}, t_{\text{enc},i+1}\}$ and repeating now the steps of (4.74, 4.75) we find the Ehrenfest-time-dependent factor in this case to be

$$F^{4.27}(\tau) = \left(\frac{4\lambda\hbar}{\Omega}\right)^{n-1} \prod_{j=1}^{n-1} \int_{0}^{\infty} dx'_{j} \cos\left(x'_{j}\right) \prod_{i=1}^{n-2} \int_{0}^{\infty} dt'_{i} e^{-i\epsilon\left(\ln x'_{1} + \ln x'_{n-1}\right)/(\lambda\tau_{D})}$$

$$\times e^{-\sum_{i=1}^{n-2} (t'_{i} + \max\left\{-\ln x'_{i}, -\ln x'_{i+1}\right\}/\lambda\right)(1-i\epsilon)/\tau_{D}} e^{-\sum_{i=2}^{n-2} \ln x'_{i}/(\lambda\tau_{D})} e^{-\tau(1-in\epsilon)},$$
(4.90)

again confirming the Ehrenfest-time dependence of (4.66).

Single Encounter

Along with the case where none of the encounters in the ladder can move completely inside another we can look at the opposite extreme where all the encounter stretches lie inside of the encounter k with the longest duration $t_{\text{enc},k} = \max_i \left\{ t_{\text{enc},i} \right\}$ where $t_{\text{enc},i}$ are again the durations of the (n-1) individual 2-encounters. This situation is like a generalisation of the diagram in Fig. 4.25 and we similarly now define the times t_i to be measured between the centres of encounter i and the encounter i of maximum length (with $i \neq k$). Here the same Ehrenfest-time dependence $e^{-\tau(1-in\epsilon)}$ follows by taking into account that each time t_i has a range of variation of size $t_{\text{enc},k} - t_{\text{enc},i}$ and that the τ_D - and ϵ -dependent exponential in this case is

$$e^{-t_{\text{enc},k}(1-i\epsilon)/\tau_D}e^{i\epsilon\sum_{i=1}^{n-1}t_{\text{enc},i}/\tau_D}.$$
(4.91)

This yields for the Ehrenfest-time-dependent factor

$$F^{4.27'}(\tau) = \left(\frac{4\lambda\hbar}{\Omega}\right)^{n-1} \prod_{j=1}^{n-1} \int_{0}^{\infty} dx'_{j} \cos\left(x'_{j}\right) e^{(1-i\epsilon)\ln x'_{k}/(\lambda\tau_{D})} e^{-i\epsilon \sum_{i=1}^{n-1} \ln x'_{i}/(\lambda\tau_{D})}$$

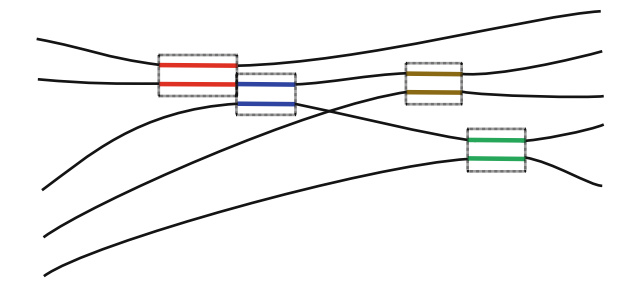
$$\times \prod_{\substack{i=1\\i\neq k}}^{n-1} \frac{(\ln x'_{i} - \ln x'_{k})}{\lambda} e^{-\tau(1-in\epsilon)},$$
(4.92)

confirming again the Ehrenfest-time dependence predicted by (4.66).

Mixture

Of course it is additionally possible to have a mixed form between these two extreme cases. This means that some 2-encounters only overlap like in the case of a ladder diagram the others form a single encounter. This however, just means that some t_i -integrals behave like in the first (ladder) case and some like in the second (single encounter) case. A verification of the predicted Ehrenfest-time dependence is then straightforward.

Fig. 4.28 A general diagram containing encounters marked by *boxes* (shown in different colours)



General Encounters

Up to now we restricted our discussion to diagrams where each trajectory is involved in one or two encounters. This is however, not yet the most general case where the only restriction is that each trajectory contains at least one encounter stretch, so that some trajectories can also contain more than two encounter stretches. Note that the situation where two trajectories interact (pass through the same 2-encounter block) more than once cannot occur at first order in inverse channel number. An example of a diagram that is possible is depicted in Fig. 4.28. In the most general case we define the times t_i slightly different: First we separate the $k \geq 2$ trajectories that have one encounter stretch from the remaining n-k that have more than one. Then we number our encounters accordingly, first those along the trajectories with one encounter stretch with duration $t_{\text{enc},i}$, $i=1,\ldots,k$ then the remaining encounters with duration $t_{\text{enc},i}$, $i=k+1,\ldots,n-1$. For the n-k trajectories with two or more encounter stretches we now define t_i , $i=1,\ldots,n-k$, to be the time difference between the outer edges of the outermost encounters along those trajectories.

For any trajectories with more than two encounter stretches we will need additional time differences to fully fix the positions of the encounters. Because we defined the times t_i to go through the outermost encounters, importantly the exponential factor with the survival probability and the energy dependence does not depend on these additional time differences and is given by

$$e^{-\sum_{i=1}^{n-k} t_i (1-i\epsilon)/\tau_D} e^{\sum_{i=k+1}^{n-1} t_{\text{enc},i}/\tau_D} e^{i\epsilon \sum_{i=1}^k t_{\text{enc},i}/\tau_D}.$$
 (4.93)

where the middle term ensures that the survival probability only includes one copy of each encounter and the energy dependence involves all traversals of all the encounters.

For the remaining times we notice that, starting with the ladder system with 2 trajectories containing one encounter stretch and n-2 trajectories containing two stretches, every time we increase the number of trajectories with one encounter stretch we simultaneously increase the number of stretches on the orbits with two. Therefore there are k-2 additional time differences needed to fix the positions of the central encounters along trajectories with more than two and we define times \tilde{t}_i for $i=1,\ldots,k-2$ from the left hand side of one encounter stretch to the right hand side of the next encounter stretch following on the right on those trajectories, see

also Fig. 4.29. As the encounters are ordered, they are not allowed to be pushed past the outside encounters and each other. The ranges of the times \tilde{t}_i are then given by these restrictions. Using $M[i, j] = \max \{t_{\text{enc},i}, t_{\text{enc},j}\}$ in the following to make the notation more compact, we obtain for a trajectory containing m encounter stretches of durations $t_{\text{enc},i}$, $i=1,\ldots,m$, as illustrated in Fig. 4.29, the time integrals accounting for their different positions

$$\int_{M(1,2)}^{t_{i}} d\tilde{t}_{1} \dots \int_{M[m-2,m-1]}^{t_{i}-\sum_{o=1}^{m-3} (\tilde{t}_{o}-M[o,o+1])} d\tilde{t}_{m-2}
= \int_{0}^{t_{i}-M[1,2]} d\tilde{t}'_{1} \dots \int_{0}^{t_{i}-\sum_{o=1}^{m-3} \tilde{t}'_{o}-M[m-2,m-1]} d\tilde{t}'_{m-2}.$$
(4.94)

In the second line we substituted $\tilde{t}'_j = \tilde{t}_j - M[j, j+1]$. The time differences t_i , which are more important for the Ehrenfest-time dependence, must instead be longer than the maximal length of the encounter stretches lying on the considered trajectory. In general the numbering of the encounters and time differences can be more complicated than in Fig. 4.29 as the two encounter stretches of one encounter do not necessarily lie on all orbits in such a way that their number increases from left to right. Then we define l(i) to be a list of length m(i) of the encounters enclosed by the time t_i (including the outer encounters) and L(i) a list of the corresponding m(i)-1 times \tilde{t} between the ends of those encounters. Now we can make the substitution $t'_i=t_i-\max_{j\in l(i)}\left\{t_{\mathrm{enc},j}\right\}$. After this substitution we recognise that (4.94) has become independent of \hbar or the Ehrenfest-time. Following then the steps in (4.74, 4.75) we obtain

$$F^{4.28}(\tau) = \left(\frac{4\lambda\hbar}{\Omega}\right)^{n-1} \prod_{j=1}^{n-1} \int_{0}^{\infty} dx'_{j} \cos\left(x'_{j}\right) \prod_{i=1}^{n-k} \int_{0}^{\infty} dt'_{i} e^{-i\epsilon \sum_{i=1}^{k} \ln x'_{i}/(\lambda \tau_{D})}$$

$$\times \int_{0}^{t'_{i} - \left(\ln x'_{\max,i} + \hat{M}[l_{1}, l_{2}]\right)/\lambda} d\tilde{t}'_{L_{1}} \dots$$

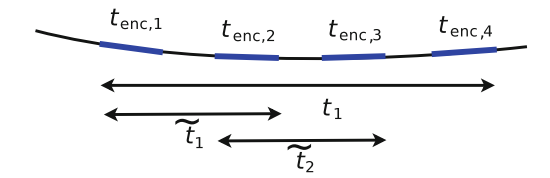
$$\times \int_{0}^{t'_{i} - \sum_{o=1}^{m-3} \tilde{t}'_{L_{o}} - \left(\ln x'_{\max,i} + \hat{M}[l_{m-2}, l_{m-1}]\right)/\lambda} d\tilde{t}'_{L_{m-2}}$$

$$\times e^{-\sum_{i=1}^{n-k} \left(t'_{i} - \ln x'_{\max,i}/\lambda\right)(1 - i\epsilon)/\tau_{D}} e^{-\sum_{i=k+1}^{n-1} \ln x'_{i}/(\lambda \tau_{D})} e^{-\tau(1 - in\epsilon)},$$
(4.95)

with $-\ln x'_{\max,i} = \max_{j \in l(i)} \{-\ln x'_j\}$ linked to the duration of the longest encounter stretch contained within t_i . We defined $\hat{M}[i,j] = \max\{-\ln x'_i, -\ln x'_j\}$ and dropped the explicit i-dependence of l, L and m above. Again we obtain the Ehrenfest-time dependence predicted by (4.66).

As in the case of the ladder diagram above, we can also have the possibility of some encounter stretches being contained in larger encounter stretches and some separated from those larger encounters. This just implies that some of the t_i -integrals

Fig. 4.29 Definition of the times \tilde{t}_i in the case of more than two encounter stretches on one orbit. The encounter stretches are shown *thicker*



have to be treated as was done in the case of the configuration shown in Fig. 4.25, and the Ehrenfest-time dependence predicted by (4.66) also follows in this case.

Touching the Lead

When the encounters are allowed to enter the lead we again have to consider times representing how far each encounter has moved into the lead (actually how much of the encounter remains inside the system). For the case treated in detail for n=3 it is only the upper limit (namely the full encounter time) of these time integrals which have the necessary encounter time dependence to contribute in the semiclassical limit. The reasoning for n=3 can be carried over directly to the more general cases as first also here there is only a contribution from the upper limits: For all other contributions we get at least for one $t_{\text{enc},i}$ an integral containing only $\exp(is_iu_i/\hbar)/t_{\text{enc},i}$ as only s_i , u_i -dependent factors that yield zero as was shown in Eq. (4.26). Second the upper limits of these integrations yield contributions that are (up to Ehrenfest-time-independent factors) the same as the ones obtained when the encounters are inside the system. We thus obtain the same Ehrenfest-time dependence from encounters moved into the leads.

4.5.1.3 Summary

The separate diagrams considered in the RMT-type semiclassical treatment [48] can be created from the original collapse of trajectories onto each other and by sliding the individual encounters together or into the leads. The Ehrenfest-time treatment however, suggests treating all of these possibilities instead as part of continuous families. What we have shown above in this subsection is that, if we partition this family in a particular way, for any partition we can find a suitable set of coordinates which allows us to transform the semiclassical contribution so that we can extract the overall Ehrenfest-time dependence. Though the exact details of this transformation depend on the structures of the partition, the algorithmic routines described above all lead to the same Ehrenfest-time dependence. Each partition and hence family then has the factor $e^{-\tau(1-in\epsilon)}$ and no other Ehrenfest-time or \hbar -dependence. As we know that we must recover the RMT-type result $C(\epsilon, n)$ in (4.66) when $\tau_E = 0$ (since we treat the same diagrams) and have no further Ehrenfest-time dependence apart from $e^{-\tau(1-in\epsilon)}$, we then obtain the full result in (4.66) and hence provide a semiclassical justification of the first part of the effective RMT ansatz.

4.5.2 Trajectories Always Correlated

In this subsection we determine the so-called classical contribution in (4.67). To obtain this contribution $C_2(\epsilon, \tau, n)$ semiclassically we consider a band of n trajectories which are correlated (inside the same encounter) for their entire duration between entering and leaving the system as in Fig. 4.30. This implies that all the trajectories have the same length t and that the maximum of the differences s_i, u_i between their stable and unstable coordinates lies below the constant c (related to the Ehrenfest-time). For the case n=2 this configuration was first considered in [45], the calculation was then extended to n=3 in [26]. For our calculation we follow [26] and place a Poincaré surface of section at a distance t_1 from the left end of the trajectories while the remaining time on the right of the section is denoted by $t_2=t-t_1$. The semiclassical contribution $C_2(\epsilon, \tau, n)$ can be written as

$$C_{2}(\epsilon, \tau, n) = \frac{1}{\tau_{D}} \int_{0}^{\infty} dt_{1} \int_{0}^{\infty} dt_{2} \frac{e^{-t(1-in\epsilon)/\tau_{D}}}{(2\pi\hbar)^{n-1} (t_{1} + t_{2})} \times \int_{|s| < ce^{-\lambda t_{1}}} ds^{n-1} \int_{|u| < ce^{-\lambda t_{2}}} du^{n-1} e^{(i/\hbar)\Delta S},$$
(4.96)

where we only include one traversal of the band in the survival probability and the restrictions on the s- and u-integrals ensure that the band always remains together under the exponential divergence of the trajectories due to the chaotic dynamics. Performing an integral over $t_1 - t_2$ and the u_i -integrals, this gives

$$C_2(\epsilon, \tau, n) = \frac{4^{n-1}}{\tau_D} \int_0^\infty dt \, \frac{e^{-t(1-in\epsilon)/\tau_D}}{(2\pi\hbar)^{n-1}} \int_0^{e^{-\lambda t}} dx^{n-1} \prod_{i=1}^{n-1} \frac{\hbar}{x_i} \sin\left(\frac{c^2 x_i}{\hbar}\right),\tag{4.97}$$

where $x_i = e^{-\lambda t_2} s_i / c$. Using that in the semiclassical limit

$$\int_{0}^{e^{-\lambda t}} dx \frac{\hbar}{x} \sin\left(\frac{c^{2}x}{\hbar}\right) = \frac{\pi \hbar}{2} \Theta\left(\tau_{E} - t\right),\tag{4.98}$$

we finally obtain

$$C_2(\epsilon, \tau, n) = \frac{1 - e^{-\tau(1 - in\epsilon)}}{1 - in\epsilon},\tag{4.99}$$

proving the Ehrenfest-time dependence of the $C_2(\epsilon, \tau, n)$ in (4.67).

4.5.3 Mixed Terms

Finally we want to consider possible correlations between trajectory structures giving the RMT-type contribution and those giving the classical part, i.e. contributions from correlations between bands of trajectories (that are always correlated with each



Fig. 4.30 Band of n=3 correlated trajectories. The length of the orbits is marked by a *box*; the duration of the encounter $t_{\text{enc}} = 1/\lambda \ln \left[c^2 / \left(\max_i |s_i| \max_j |u_j| \right) \right]$ is marked by a *dotted box*

other) and trajectories that are only correlated with each other during encounters. In particular we want to show that diagrams that have a correlated band which has any encounter with other trajectory structures (with encounters) give no contribution in the semiclassical limit. This, once generalised, then excludes the existence of mixed terms in (4.65) so that (4.65) is complete. First we consider the case that n-1 of the trajectories form a correlated band with the remaining trajectory meeting the band in an encounter inside the system as depicted in Fig. 4.31. This contribution $C^{4.31}(\epsilon, \tau, n)$ to the correlation function $C(\epsilon, \tau, n)$ can be written by treating the correlated band as before and introducing the times t_3 and t_4 to represent the durations of the parts of the trajectory that encounter the band on the left and on the right of the Poincaré surface of section. It reads

$$C^{4.31}(\epsilon, \tau, n) = \frac{1}{\tau_D^3} \int_0^\infty \prod_{i=1}^4 dt_i \frac{e^{-\sum_{i=1}^4 t_i (1 - i\epsilon)/\tau_D}}{(2\pi\hbar)^{n-1}} \int_{|s| \le ce^{-\lambda t_1}} ds^{n-2} \int_{|u| \le ce^{-\lambda t_2}} du^{n-2} \times \int_{ce^{-\lambda t_1} < |s| \le c} ds \int_{ce^{-\lambda t_2} < |u| \le c} du \frac{e^{(i/\hbar)\Delta S} e^{i\epsilon(t_{\text{enc}} + (n-2)(t_1 + t_2))/\tau_D}}{(t_1 + t_2)},$$
(4.100)

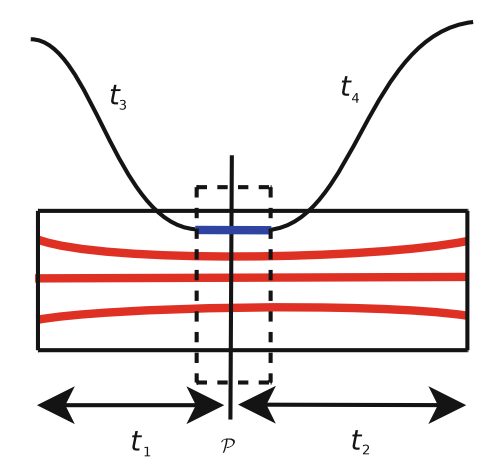
where $t_{\rm enc}$ is the time during which the remaining trajectory encounters the band. Performing the integrals as in (4.97, 4.98) we obtain the Heaviside function $\Theta(\tau_E - t)$ from the integral in (4.100) over the stable and unstable distances s_i , u_i in the band in the same way as in Eq. (4.98). The integral in (4.100) over the difference s_i , u_i between the coordinates of a band trajectory and the trajectory encountering is given by

$$\int_{Ce^{-\lambda t_1} < |s| \le c} ds \int_{Ce^{-\lambda t_2} < |u| \le c} du e^{(i/\hbar)us} e^{i\epsilon t_{enc}/\tau_D}. \tag{4.101}$$

We obtain the upper limit $|su| < c^2 e^{-\lambda t}$, this implies when performing similar steps as in Eqs. (4.97, 4.98) that the overall duration of the band has to be at least longer than τ_E to give a contribution. As $C^{4.31}(\epsilon, \tau, n)$ contains additionally the function $\Theta(\tau_E - t)$, such a contribution vanishes. If we move more trajectories from the band (composed of at least two trajectories) to the trajectory structure with encounters we still obtain these opposing Heaviside functions and hence no contribution.

A similar reasoning can be applied if the encounter of a trajectory (or part of a trajectory structure) with a band does not happen inside the system but enters the

Fig. 4.31 An example of a band of 3 trajectories that possesses an encounter with another trajectory. The band is marked by a *thicker box* (*red* stretches) and the encounter of the other trajectory with the band by a *dotted box* (*blue* stretch). The duration of the links is denoted by t_3 and t_4 , the duration of the band on the *left* and on the *right* of the Poincaré surface \mathcal{P} of section by t_1 and t_2 , respectively



lead at the beginning or the end. In this case we obtain an additional time integral with respect to the time of the encounter that remains inside the system but, as the s, u-integrals still yield the same Heaviside functions, this contribution also vanishes. Note that if we move both ends of the encounter into the leads then the encountering trajectory can be considered as part of the band and treated as above in Sect. 4.5.2.

The reasoning in this subsection applies to an arbitrary number of bands of correlated trajectories connected by trajectories that are only correlated in encounters. Therefore all such mixed terms vanish and this completes our argument showing the validity of Eq. (4.65).

Now we want to present an application of the form of $C(\epsilon, \tau, n)$ given in Eqs. (4.65–4.67): We want to calculate the density of states of a chaotic Andreev billiard for arbitrary Ehrenfest-time.

4.6 The Density of States of Chaotic Andreev Billiards

Although we presented in Fig. 1.5 the density of states of Andreev billiards showing a gap above the Fermi energy in the chaotic case, we have not yet said anything about its microscopic origin: If a superconductor (S) is brought in contact with a normal conductor (N) its spectral density of quasiparticle excitations is considerably changed due to Andreev reflection [49] at the NS interface: When an electron from the vicinity of the Fermi energy surface of the normal conductor hits the superconductor, the bulk energy gap Δ of the superconductor prevents the negative charge from entering, unless a Cooper pair is formed in the superconductor. Since a Cooper pair is composed of two electrons, an extra electron has to be taken from the Fermi sea, thus creating a hole in the conduction band of the normal metal. The Andreev reflection therefore leads to a retroreflection of the particle, where Andreev reflected electrons (or holes) retrace their trajectories as holes (or electrons), i.e. an incoming electron (hole) is not specularly reflected, but is replaced a hole (electron) flying in the direction of the

incoming electron. This leads then to a suppression of the density of states (DoS) directly above the Fermi energy E_F . This proximity effect is also expected for an Andreev billiard [50], an impurity-free quantum dot attached to a superconductor [51, 52], and has attracted considerable theoretical attention during the last decade (see [47] for a review).

As we have seen in the introduction in Fig. 1.5, an Andreev billiard has the interesting peculiarity that the suppression of its (mean) DoS crucially depends on whether the dynamics of its classical counterpart is integrable or chaotic: While the DoS vanishes linearly in energy for the considered integrable system, the spectrum of a chaotic billiard is expected to exhibit a true universal gap above E_F [53]. Based on RMT this gap was predicted to scale with the Thouless energy, $E_T = \hbar/2\tau_D$ [53]. On the contrary, semiclassics based on the Bohr-Sommerfeld (BS) quantisation yields only an exponential suppression of the DoS [54–56], a discrepancy that has attracted much theoretical interest [40, 57–60]. Lodder and Nazarov [54] pointed out that these seemingly contradictory predictions are valid in different limits, governed by the ratio τ . In the RMT regime, $\tau = 0$, the Thouless gap (from RMT) is clearly established [53, 57], while the BS approximation describes the classical limit $\tau \to \infty$.

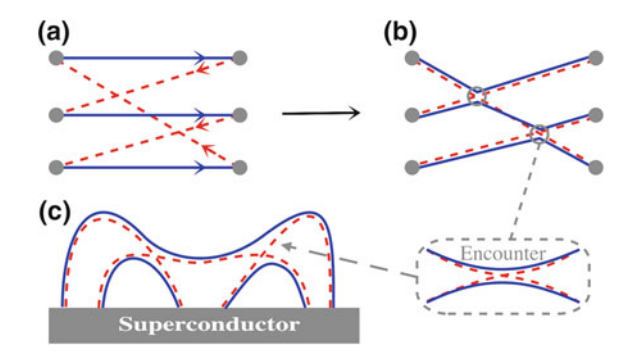
Various approaches have been used to better understand the crossover from the Thouless to the Ehrenfest regime of large τ , where RMT loses its applicability [57]. These include effective RMT [40], predicting a gap size scaling with the Ehrenfest energy $E_E = \hbar/2\tau_E$, as well as stochastic [59] and perturbative [58] methods. Recently the gap at πE_E was confirmed for $\tau \gg 1$ in a quasiclassical approach based on the Eilenberger equation [60].

In this section we first, after introducing the scattering approach [61], briefly demonstrate that the DoS can be evaluated semiclassically for $\tau_E=0$ by using an energy-dependent extension of the work [62] on the moments of the transmission eigenvalues. This semiclassically computed DoS yields a hard gap, in agreement with RMT. Secondly we address the whole crossover regime of $\tau>0$, by incorporating the τ_E -dependence. In the limit $\tau\gg1$, the width of the gap approaches $\pi\,E_E$, eventually recovering the BS prediction for $\tau\to\infty$. More interestingly in the intermediate regime $\tau\geq1$ we predict the appearance of a second Ehrenfest gap at $\pi\,E_E$.

4.6.1 Scattering Approach for the Andreev Billiard and the RMT Density of States

In the scattering approach the superconductor is represented by, or can rather be thought of as replaced by, a lead that carries N scattering channels, and the excitation spectrum can be entirely expressed in terms of the (electron) scattering matrix S [61]. The average DoS $d(\epsilon, \tau)$ reads [56] (when divided by twice the average density of the isolated billiard),

Fig. 4.32 a Schematic picture of the trajectory structures for n = 3. The (blue) solid lines represent electrons which are retroreflected as holes [dashed (red) lines]. b Collapsing the trajectories onto each other leads to encounters. c The end result, i.e. correlated Andreev reflected paths. (Figures from [8])



$$d(\epsilon, \tau) = 1 + 2\sum_{n=1}^{\infty} \frac{(-1)^n}{n} \Im\left(\frac{\partial C(\epsilon, \tau, n)}{\partial \epsilon}\right),\tag{4.102}$$

in terms of correlation functions of 2n scattering matrices, defined in Eq. (4.64). To obtain a semiclassical expression for $d(\epsilon, \tau)$ containing multiple sums over trajectories we can insert in Eq. (4.102) for $C(\epsilon, \tau, n)$ the expression (4.69). This of course leads to the same trajectory pairs as considered before in this section, see Fig. 4.32a, b. They can be interpreted here in the following way, see Fig. 4.32c: Each summand of the n-summation is given by trajectory pairs that hit the superconductor or the lead in the scattering picture 2n times. Each time an electron is transformed into a hole and vice versa.

In order to determine the overall contribution to $d(\epsilon) \equiv d(\epsilon,0)$ of these trajectories, the diagrams contributing to $C(\epsilon,0,n)$ are constructed recursively with respect to n. For this the diagrams are redrawn as rooted plane trees [11, 48]. The name derives from the fact that the channel of the first incoming trajectory is chosen as the root (hence rooted trees) and the remaining channels are placed in order around an anticlockwise loop (hence plane). The factors resulting from a certain tree can be obtained recursively by analysing in which ways it can be split into its subtrees. The contributions of the links and the encounters in these subtrees or diagrams is determined by diagrammatic rules that we encountered already several times in this book: Each link gives a factor of $[N(1-i\epsilon)]^{-1}$, while each l-encounter contributes $-N(1-il\epsilon)$ when the encounter stretches all remain inside the cavity. If the encounter touches the lead the latter contribution is again replaced by a 1, because of the additional integration over the length of the encounter stretch that has not been moved into the lead.

When summing the contributions of the trees we additionally have to take into account that no diagram contribution is overcounted. If the top encounter enters both leads (which can only happen if the diagram involves a single encounter) we have to ensure that it does not enter the lead at both ends at the same time [11].

Introducing now a generating function of the correlation functions $C(\epsilon, n)$

$$G(\epsilon, r) = \sum_{n=1}^{\infty} r^{n-1} C(\epsilon, n), \tag{4.103}$$

where all possible encounter configurations are allowed and an auxiliary generating function $g(\epsilon, r)$ including all possibilities apart from where the top encounter enters the lead at one end of the trajectory, it can be shown that both generating functions are related by [11]

$$G(\epsilon, r) = \frac{g}{1 - rq} \tag{4.104}$$

and that g fulfils the equation

$$g(1 - i\epsilon) - 1 = rg^2(g - 1 - i\epsilon),$$
 (4.105)

obtained as an extension of the corresponding equation for $\epsilon = 0$ in [62]. By inverting Eq. (4.104) we can see that G is given implicitly by the cubic equation

$$r(r-1)^2 G^3 + r(3r+i\epsilon-3)G^2 + (3r+i\epsilon-1)G = -1.$$
 (4.106)

Expanding G (or g) as a power series in r, we can obtain recursively the first couple of correlation functions (which can also be checked by considering the semiclassical diagrams explicitly) as:

$$C(\epsilon, 1) = \frac{1}{(1 - i\epsilon)}, \quad C(\epsilon, 2) = \frac{1 - 2i\epsilon - 2\epsilon^2}{(1 - i\epsilon)^4}, \tag{4.107}$$

To obtain now the RMT result for the density of states it might seem most straightforword to solve (4.106) and afterwards insert the solution into Eq. (4.102), perform an integration with respect to r and set r=-1 to obtain the factor $(-1)^n/n$ and finally differentiate with respect to ϵ . As the solutions of the cubic equation (4.106) are already quite involved, performing the r-integration is not an easy task. For that reason one instead tries to find the generating function $H(\epsilon, r)$ of the terms that appear in the density of states

$$H(\epsilon, r) = \frac{1}{ir} \frac{\partial}{\partial \epsilon} \int dr \, G(\epsilon, r) = \sum_{n=1}^{\infty} \frac{r^{n-1}}{in} \frac{\partial C(\epsilon, n)}{\partial \epsilon},$$

$$d(\epsilon) = 1 - 2\Re H(\epsilon, -1). \tag{4.108}$$

Using a computer aided search over cubic equations with low order polynomial coefficients one obtains the equation fulfilled by $H(\epsilon, r)$ [11]

$$(\epsilon r)^{2} (1 - r) H^{3} + i \epsilon r \left[r(i\epsilon - 2) + 2(1 - i\epsilon) \right] H^{2}$$

$$+ \left[r(1 - 2i\epsilon) - (1 - i\epsilon)^{2} \right] H + 1 = 0.$$
(4.109)

As G and H are algebraic generating functions, i.e. solutions of algebraic equations, so too must be their derivatives. One then proves the result in Eq. (4.109) by differentiating G with respect to ϵ and irH with respect to r—these quantities are equal by their definitions in Eqs. (4.103) and (4.108)—and demonstrating that these derivatives satisfy the same algebraic equation starting once from Eq. (4.106) and once from Eq. (4.109), for details see [11].

Taking the solution of Eq. (4.109) whose expansion agrees with Eq. (4.107), the DoS then follows from Eq. (4.108) as

$$d(\epsilon) = \frac{\sqrt{3}}{6\epsilon} \left[Q_{+}(\epsilon) - Q_{-}(\epsilon) \right], \quad \epsilon > 2 \left[\frac{\sqrt{5} - 1}{2} \right]^{\frac{5}{2}}, \tag{4.110}$$

where $Q_{\pm}(\epsilon) = \left[8 - 36\epsilon^2 \pm 3\epsilon\sqrt{3\epsilon^4 + 132\epsilon^2 - 48}\right]^{\frac{1}{3}}$. This is exactly the RMT result [53] (dotted line in Fig. 4.33).

4.6.2 Density of States for Non-vanishing Ehrenfest-Time

We now want to generalise the results for $\tau=0$ obtained up to now to non-zero Ehrenfest-time using Eqs. (4.65–4.67). It is clear that in the limit $\tau=0$ (4.65–4.67) reduces to the previous (and hence RMT) results while in the opposite limit, $\tau=\infty$, substituting (4.67) into (4.102) and performing a Poisson summation we obtain the BS result [55]

$$d_{\rm BS}(\epsilon) = \left(\frac{\pi}{\epsilon}\right)^2 \frac{\cosh(\pi/\epsilon)}{\sinh^2(\pi/\epsilon)}.\tag{4.111}$$

This result was previously found semiclassically studying trajectory correlations by [56] and corresponds to the classical limit where only bands of correlated trajectories contribute.

For arbitrary Ehrenfest-time dependence we simply substitute the two terms in (4.65) into Eq. (4.102). With the second term we include $1-(1+\tau)e^{-\tau}$ from the constant term (this turns out to simplify the expressions) and again perform a Poisson summation to obtain for its contribution to $d(\epsilon, \tau)$

$$d_{2}(\epsilon, \tau) = 1 - (1+\tau)e^{-\tau} + 2\Im \sum_{n=1}^{\infty} \frac{(-1)^{n}}{n} \frac{\partial}{\partial \epsilon} \left(\frac{1 - e^{-(1-in\epsilon)\tau}}{1 - in\epsilon} \right)$$
$$= d_{BS}(\epsilon) - \exp\left(-\frac{2\pi k}{\epsilon}\right) \left(d_{BS}(\epsilon) + \frac{2k(\pi/\epsilon)^{2}}{\sinh(\pi/\epsilon)} \right), \tag{4.112}$$

where $k = \lfloor (\epsilon \tau + \pi)/(2\pi) \rfloor$ involves the floor function, and we see that this function is zero for $\epsilon \tau < \pi$.

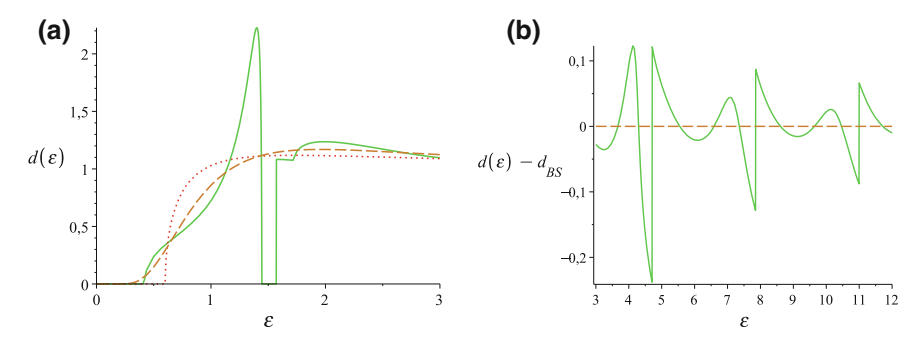


Fig. 4.33 a Density of states for $\tau = \tau_E/\tau_D = 2$ (solid line), along with the BS (dashed) limit $\tau \to \infty$ and the RMT (dotted) limit $\tau = 0$, showing a second gap just below $\epsilon \tau = \pi$. b Ehrenfest-time related $2\pi/\tau$ -periodic oscillations in the density of states after subtracting the BS curve (from [11])

Of course the first term in (4.65) also contributes and when we substitute into (4.102) we obtain two further terms from the energy differential. These however, may be written, using the semiclassical generating functions, as

$$d_1(\epsilon, \tau) = e^{-\tau} [1 - 2\Re e^{i\epsilon\tau} H(\epsilon, -e^{i\epsilon\tau})] + \tau e^{-\tau} [1 - 2\Re e^{i\epsilon\tau} G(\epsilon, -e^{i\epsilon\tau})].$$
(4.113)

Because G and H are given by cubic equations, we can write this result explicitly as

$$d_{1}(\epsilon, \tau) = \frac{\sqrt{3}e^{-\tau}}{6\epsilon} \Re \left[Q_{+}(\epsilon, \tau) - Q_{-}(\epsilon, \tau) \right] + \frac{\sqrt{3}\tau e^{-\tau}}{6} \Re \left[P_{+}(\epsilon, \tau) - P_{-}(\epsilon, \tau) \right], \tag{4.114}$$

where

$$Q_{\pm}(\epsilon,\tau) = \left[8 - \frac{24\epsilon \left(1 - \cos(\epsilon\tau)\right)}{\sin(\epsilon\tau)} - 24\epsilon^2 - \frac{24\epsilon^2 \left(1 - \cos(\epsilon\tau)\right)}{\sin^2(\epsilon\tau)} + \frac{6\epsilon^3 \left(1 - \cos(\epsilon\tau)\right)}{\sin(\epsilon\tau)} + \frac{2\epsilon^3 \left(2 - 3\cos(\epsilon\tau) + \cos^3(\epsilon\tau)\right)}{\sin^3(\epsilon\tau)} \pm \frac{6\epsilon\sqrt{3D} \left(1 - \cos(\epsilon\tau)\right)}{\sin^2(\epsilon\tau)}\right]^{\frac{1}{3}},$$

$$(4.115)$$

$$P_{\pm}(\epsilon,\tau) = \left[\frac{36\epsilon}{(1+\cos(\epsilon\tau))^2} - \frac{9\epsilon^2 \sin(\epsilon\tau)}{(1+\cos(\epsilon\tau))^3} + \frac{\epsilon^3}{(1+\cos(\epsilon\tau))^3} \pm \frac{3\sqrt{3D}}{(1+\cos(\epsilon\tau))^2} \right]^{\frac{1}{3}}.$$
(4.116)

These all involve the same discriminant D and so the differences in (4.114) are only real (and hence $d_1(\epsilon, \tau)$ itself is non-zero) when

$$D(\epsilon, \tau) = \epsilon^4 - 8\epsilon^3 \sin(\epsilon \tau) + 4\epsilon^2 [5 + 6\cos(\epsilon \tau)] + 24\epsilon \sin(\epsilon \tau) - 8[1 + \cos(\epsilon \tau)]$$
(4.117)

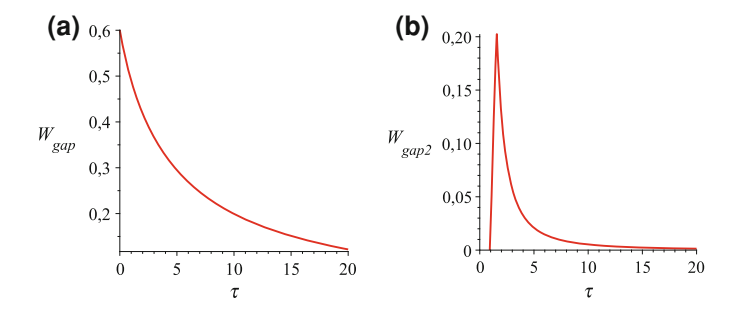


Fig. 4.34 a Width (and end point) of the first gap and b width of the second gap as a function of τ (from [11])

is positive. Recalling that the second contribution is zero up to $\epsilon \tau = \pi$, the complete density of states is therefore zero up to the first root of $D(\epsilon, \tau)$ as it lies below $\epsilon \tau = \pi$. The width of this gap is then solely determined by the contribution from quantum interference terms given by the trajectories with encounters. The hard gap up to the first root shrinks as τ increases, see Fig. 4.34a. When taking the limit $\tau \to \infty$ while keeping the product $\epsilon \tau$ constant (4.117) reduces to $-8 \left[1 + \cos(\epsilon \tau)\right]$ which has its first root at $\epsilon \tau = \pi$. The gap then approaches $E = \pi E_E$ for $\tau \gg 1$, where $E_E = \hbar/2\tau_E$ is the Ehrenfest energy. So one indeed observes a hard gap up to πE_E in the limit $\tau \to \infty$ at fixed $\epsilon \tau$ in agreement with the quasiclassical result of [60].

Alongside this reduction in size of the first gap, which was predicted by effective RMT [47], when $\tau \geq 0.916$ the discriminant (4.117) has additional roots. Between the second and third root $D(\epsilon, \tau)$ is also negative and a second gap appears. As τ increases the roots spread apart so the gap widens. For example, the complete density of states for $\tau = 2$ is shown in Fig. 4.33a along with the oscillatory behaviour visible at larger energies (with period $2\pi/\tau$) in Fig. 4.33b. There the second gap is clearly visible and only ends when the second contribution $d_2(\epsilon, \tau)$ becomes non-zero at $\epsilon \tau = \pi$. In fact for $\tau > \pi/2$ the third root of $D(\epsilon, \tau)$ is beyond $\epsilon \tau = \pi$ so the second gap is cut short by the jump in the contribution $d_2(\epsilon, \tau)$. Since the second root also increases with increasing τ the gap shrinks again, as can be seen in Fig. 4.34b.

To illustrate this behaviour further, we show the density of states for different values of τ in Fig. 4.35. One observes first the formation and then the shrinking of the second gap. As can be seen in the inset of Fig. 4.35b the second gap persists even for large values of τ and the size of the first hard gap slowly approaches $\epsilon \tau = \pi$. The plot for $\tau = 20$ also shows how the density of states converges to the BS result.

Having presented the application of Eqs. (4.65-4.67) to calculate the gap in chaotic Andreev billiards we want to emphasise here that the derived result for $C(\epsilon, \tau, n)$ possesses a much wider range of applications to all situations where correlators of pairs of scattering matrices need to be analysed, examples are the moments of

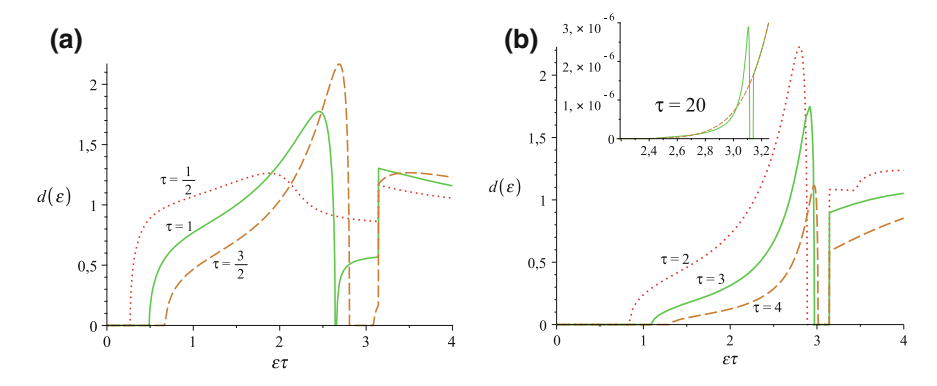


Fig. 4.35 Density of states as a function of $\epsilon \tau = E/E_{\rm E}$ for various values of τ showing the appearance of a second gap below $\epsilon \tau = \pi$. *Inset*: Density of states for $\tau = 20$ (*solid line*) together with the BS limit (*dashed*) (from [11])

the transmission and of the Wigner delay times; their Ehrenfest-time dependence is determined in [10].

To summarise, in this chapter we presented different effects of a non-zero Ehrenfest-time in chaotic systems: We calculated its impact on the transmission and reflection, the conductance variance, the spectral form factor and the correlation function of n pairs of scattering matrices. The last result opened up the possibility to determine the Ehrenfest-time dependence of the energy gap of chaotic Andreev billiards.

In the next chapter we will return to the case of zero Ehrenfest-time and study the semiclassical analogues of certain field-theoretical or RMT effects.

References

- 1. Chirikov, B.V., Izrailev, F.M., Shepelyansky, D.L.: Sov. Sci. Rev. Sect. C 2, 209 (1981)
- 2. Aleiner, I.L., Larkin, A.I.: Phys. Rev. B 54, 14423 (1996)
- 3. Adagideli, İ.: Phys. Rev. B 68, 233308 (2003)
- 4. Brouwer, P.W., Rahav, S., Tian, C.: Phys. Rev. E 74, 066208 (2006)
- 5. Tian, C., Larkin, A.I.: Phys. Rev. B 70, 035305 (2004)
- 6. Waltner, D., Gutiérrez, M., Goussev, A., Richter, K.: Phys. Rev. Lett. 101, 174101 (2008)
- 7. Gutkin, B., Waltner, D., Gutiérrez, M., Kuipers, J., Richter, K.: Phys. Rev. E 81, 036222 (2010)
- Kuipers, J., Waltner, D., Petitjean, C., Berkolaiko, G., Richter, K.: Phys. Rev. Lett. 104, 027001 (2011)
- 9. Waltner, D., Kuipers, J.: Phys. Rev. E 82, 066205 (2010)
- 10. Waltner, D., Kuipers, J., Richter, K.: Phys. Rev. B **83**, 195315 (2011)
- Kuipers, J., Engl, T., Berkolaiko, G., Petitjean, C., Waltner, D., Richter, K.: Phys. Rev. B 83, 195316 (2011)
- 12. Brouwer, P.W., Rahav, S.: Phys. Rev. B 74, 075322 (2006)
- 13. Jacquod, P., Whitney, R.S.: Phys. Rev. B 73, 195115 (2006)
- 14. Rahav, S., Brouwer, P.W.: Phys. Rev. Lett. 96, 196804 (2006)

References 147

- 15. Rahav, S., Brouwer, P.W.: Phys. Rev. Lett. 95, 056806 (2005)
- 16. Yevtushenko, O., Lütjering, G., Weiss, D., Richter, K.: Phys. Rev. Lett. 84, 542 (2000)
- 17. Schomerus, H., Tworzydło, J.: Phys. Rev. Lett. 93, 154102 (2004)
- 18. Schomerus, H., Jacquod, P.: J. Phys. A 38, 10663 (2005)
- 19. Goussev, A., Richter, K.: Phys. Rev. E 75, 015201(R) (2007)
- 20. Goussev, A., Waltner, D., Richter, K., Jalabert, R.A.: New J. Phys. 10, 093010 (2008)
- 21. Beenakker, C.W.J.: Rev. Mod. Phys. 69, 731 (1997)
- 22. Müller, S., Heusler, S., Braun, P., Haake, F.: New J. Phys. 9, 12 (2007)
- 23. Müller, S., Heusler, S., Braun, P., Haake, F., Altland, A.: Phys. Rev. Lett. 93, 014103 (2004)
- 24. Müller, S., Heusler, S., Braun, P., Haake, F., Altland, A.: Phys. Rev. E 72, 046207 (2005)
- 25. Müller, S.: Periodic-orbit approach to universality in quantum chaos. Ph.D. thesis, Universität Duisburg, Essen (2005)
- 26. Brouwer, P.W., Rahav, S.: Phys. Rev. B 74, 085313 (2006)
- 27. Whitney, R.S.: Phys. Rev. B 75, 235404 (2007)
- 28. Waltner, D., Kuipers, J., Jacquod, P., Richter, K.: arXiv: 1108.5091, unpublished (2011)
- 29. Heusler, S., Müller, S., Braun, P., Haake, F.: Phys. Rev. Lett. 96, 066804 (2006)
- 30. Kuipers, J., Sieber, M.: Phys. Rev. E 77, 046219 (2008)
- 31. Büttiker, M., Prêtre, A., Thomas, H.: Phys. Rev. Lett. 70, 4114 (1993)
- 32. Büttiker, M.: . J. Phys.: Condens. Matter 5, 9361 (1993)
- 33. Petitjean, C., Waltner, D., Kuipers, J., Adagideli, İ., Richter, K.: Phys. Rev. B 80, 115310 (2009)
- 34. Brouwer, P.W., Büttiker, M.: Europhys. Lett. **37**, 441 (1997)
- 35. Wigner, E.P.: Phys. Rev. 98, 145 (1955)
- 36. Smith, F.T.: Phys. Rev. 118, 349 (1960)
- 37. Friedel, J.: Phil. Mag. 43, 153 (1952)
- 38. Sieber, M., Richter, K.: Phys. Scr. T. 90, 128 (2001)
- 39. Sieber, M.: J. Phys. A **35**, L613 (2002)
- 40. Silvestrov, P.G., Goorden, M.C., Beenakker, C.W.J.: Phys. Rev. Lett. 90, 116801 (2003)
- 41. Whitney, R.S., Jacquod, P.: Phys. Rev. Lett. 94, 116801 (2005)
- 42. Agam, O., Aleiner, I., Larkin, A.: Phys. Rev. Lett. 85, 3153 (2000)
- 43. Silvestrov, P.G., Goorden, M.C., Beenakker, C.W.J.: Phys. Rev. B 67, 241301(R) (2003)
- 44. Tworzydło, J., Tajic, A., Schomerus, H., Beenakker, C.W.J.: Phys. Rev. B 68, 115313 (2003)
- 45. Whitney, R.S., Jacquod, P.: Phys. Rev. Lett. 96, 206804 (2006)
- 46. Goorden, M.C., Jacquod, P., Beenakker, C.W.J.: Phys. Rev. B 72, 064526 (2005)
- 47. Beenakker, C.W.J.: Lect. Notes Phys. **667**, 131 (2005)
- 48. Berkolaiko, G., Kuipers, J.: J. Phys. A 43, 035101 (2010)
- 49. Andreev, A.F.: Sov. Phys. JETP 19, 1228 (1964)
- 50. Kosztin, I., Maslov, D.L., Goldbart, P.M.: Phys. Rev. Lett. 75, 1735 (1995)
- Morpurgo, A.F., Holl, S., van Wees, B.J., Klapwijk, T.M., Borghs, G.: Phys. Rev. Lett. 78, 2636 (1997)
- 52. Jakob, M., Stahl, H., Knoch, J., Appenzeller, J., Lengeler, B., Hardtdegen, H., Lüth, H.: Appl. Phys. Lett. 76, 1152 (2000)
- 53. Melsen, J.A., Brouwer, P.W., Frahm, K.M., Beenakker, C.W.J.: Europhys. Lett. 35, 7 (1996)
- 54. Lodder, A., Nazarov, Y.V.: Phys. Rev. B 58, 5783 (1998)
- 55. Schomerus, H., Beenakker, C.W.J.: Phys. Rev. Lett. 82, 2951 (1999)
- 56. Ihra, W., Leadbeater, M., Vega, J.L., Richter, K.: Eur. Phys. J. B 21, 425 (2001)
- 57. Taras-Semchuk, D., Altland, A.: Phys. Rev. B 64, 014512 (2001)
- 58. Adagideli, İ., Beenakker, C.W.J.: Phys. Rev. Lett. 89, 237002 (2002)
- 59. Vavilov, M.G., Larkin, A.I.: Phys. Rev. B 67, 115335 (2003)
- 60. Micklitz, T., Altland, A.: Phys. Rev. Lett. 103, 080403 (2009)
- 61. Beenakker, C.W.J.: Phys. Rev. Lett. 67, 3836 (1991)
- 62. Berkolaiko, G., Harrison, J.M., Novaes, M.: J. Phys. A 41, 365102 (2008)

Chapter 5 Semiclassical Analogues to Field-Theoretical Effects

In this chapter we want to present analogues of field-theoretical or RMT effects in semiclassics: In the first section we study the connection between the unitarity of the semiclassical time evolution and the functional form of the spectral form factor for $\tau \equiv t/T_H > 1$ predicted by RMT, remember Eqs. (2.68, 2.69). It differs from the one for $\tau \leq 1$. We start here with presenting a recipe for obtaining the form factor as predicted by RMT for $\tau \equiv t/T_H > 1$ published in [1]. We then explain how this method can be connected with semiclassical unitarity. Although the corresponding result was published in [2], it was found independently during the research carried out for this book. In the second section we show that the semiclassical analogues of field-theoretical curvature terms are pairs involving multiply traversed periodic orbits when considering the two-point correlator of spectral determinants. This result was published as Fast Track Communication in [3].

5.1 Spectral Form Factor for $\tau > 1$ and Unitarity in Semiclassics

5.1.1 Semiclassical Approximations for the Spectral Determinant

In Chap. 2 we showed how to approximate the density of states d(E) semiclassically by the Gutzwiller trace formula in (2.23). This formula however has the drawback that it is divergent, as it contains an infinite sum over an exponentially proliferating number of periodic orbits. This can qualitatively be understood by taking into account that in chaotic systems a certain number K of primitive segments of average duration T_0 exists from that all periodic orbits can be constructed. Orbits of duration T can be constructed by gluing the primitive segments together in almost arbitrary succession yielding K^{T/T_0} possibilities. For a rigorous proof of this exponential increase for surfaces of constant negative curvature, see for example [4]. In the Hannay and

Ozorio de Almeida sum rule (2.72) this exponential increase is cancelled by the square of the stability amplitude. As the semiclassical approximation for the density of states contains however the stability amplitude itself it grows exponentially with time.

This problem of the trace formula had renewed the interest in the semiclassical theory of spectral determinants. The quantum spectral determinant is defined as

$$\Delta(E) = \det\left[\Omega(E, \hat{H})(E - \hat{H})\right] = \prod_{n=1}^{\infty} \Omega(E, E_n)(E - E_n), \tag{5.1}$$

where $\Omega(E, E_n)$ is a regularisation factor making the infinite product convergent. It can be chosen real for real E and everywhere non-zero, for details see [5]. By definition $\Delta(E)$ is real for real E as the Hamiltonian is Hermitian and thus possesses real eigenvalues E_n . Usually $\Delta(E)$ is regularised by dividing it by its value at a certain energy E_0 , then it is related to the trace of the Green function introduced in Eq. (2.21) by

$$\Delta(E) = \exp\left(\int_{E_0}^{E[\mu+1]} dE' \text{Tr} G^{[\mu]}(E')\right),$$
 (5.2)

where $[\mu + 1]$ and $[\mu]$ in the exponent denote the $[\mu + 1]$ -fold integration and the $[\mu]$ -th derivative, respectively. The curved brackets denote the integer part of μ , that is given by the power of energy to that the smooth part of the level counting function (i.e. the energy integral of the spectral density) is proportional to leading order [5]. The expression in the exponent on the right hand side of the last equation is regularised by extracting its finite part, for details and the choice of E_0 , see again [5]. Note that an alternative shorter derivation of this formula was given in [6]. An expression containing periodic-orbit contributions is given by an infinite product over the periodic orbits γ occurring in the Gutzwiller trace formula, the corresponding quantity will be indexed here by G. The resulting expression is obtained by inserting in Eq. (5.2) the semiclassical approximation for TrG(E'), Eq. (2.22). Equivalently, by expanding the exponential in (5.2), $\Delta^{G}(E)$ can be written as an infinite sum over composite orbits, so-called pseudo orbits A with overall actions and Maslov phases given by the sum of the corresponding quantities of the subsets of periodic orbits with n_A elements. The stability prefactor is obtained as product of the prefactors of the contained orbits yielding finally $[7]^2$

The real part of TrG(E') only contributes to B(E) defined after Eq. (5.3) [5].

² This form is strictly speaking only correct when neglecting repetitions of periodic orbits, for an expression taking them into account, see [8]. The contributions of repeated pairs are however damped exponentially like $e^{-\lambda T/2}$ with their overall duration T compared to ones from pseudo orbits traversed once, as the number is the same in both cases, however the stability factors of the repeated ones are reduced. We can thus neglect them anyway when calculating the contributions of pseudo-orbit pairs.

$$\Delta^{G}(E) = B(E)e^{-i\pi\bar{N}(E)} \prod_{\gamma} \exp\{-C_{\gamma}e^{iS_{\gamma}(E)/\hbar - i\pi\tau_{\gamma}/2}\}$$

$$= B(E)e^{-i\pi\bar{N}(E)} \sum_{A} (-1)^{n_{A}} F_{A}(E)e^{iS_{A}(E)/\hbar - i\pi\tau_{A}/2}.$$
(5.3)

Here, $\bar{N}(E)$ is the mean number of states up to energy E, i.e. the energy integral of the mean spectral density given in Eq. (2.23), and B(E) again a regularisation factor, that is real and non-zero for real E [5]. As already noted in the introduction, the periodic-orbit representation of the trace of the Green function diverges for real energies, i.e. in the physical region. The same holds true for the spectral determinant built up by periodic-orbit contributions. We emphasise that this divergence is not related to the semiclassical approximation, it also occurs in cases where the periodic-orbit representation is exact as for the Selberg trace formula for surfaces of constant negative curvature. These expressions converge, however, for sufficiently large imaginary parts of the energy (beyond the so called entropy barrier) and need to be extended to real energies by analytic continuation. Further problems are encountered in (5.3) for systems where semiclassics is not exact. Here it is not even clear, if the last formula yields zeros on the real axis at the eigenenergies of the system.

However, by directly imposing that the spectral determinant is real for real energies, an expression containing a truncated sum over pseudo orbits can be obtained. Such an approach was developed by Keating and Berry [8] and derived by Georgeot and Prange using Fredholm theory [9]. Thereby an improved semiclassical approximation to the quantum spectral determinant is obtained. It is given by³

$$\Delta^{R_1}(E) = \Delta^{G}_{T_H/2}(E) + \Delta^{G*}_{T_H/2}(E), \tag{5.4}$$

where $\Delta_{T_H/2}^{\rm G}(E)$ is obtained from $\Delta^{\rm G}(E)$ by including only pseudo orbits with periods smaller than $T_H/2$. Comparing (5.3) with (5.4) one can expect that the pseudo orbits with overall durations longer than $T_H/2$ contribute to $\Delta(E)$ just the complex conjugate of the pseudo orbits with durations shorter than $T_H/2$. We want to emphasise that such a relation is semiclassically highly nontrivial: To our knowledge it can neither be seen to hold based on (5.3) nor on any other semiclassical expression. Adding the complex conjugate in Eq. (5.4) assures that $\Delta^{\rm R_1}(E)$ is real for real energies and including a cut off in the sum over pseudo orbits makes it finite. Another approach by Sieber and Steiner [10] considers the following periodic-orbit representation of the spectral determinant

$$\Delta^{\mathbf{R}_2}(E) = \Delta^{\mathbf{G}}(E) + \Delta^{\mathbf{G}*}(E), \tag{5.5}$$

imposing only the spectral determinant to be real.

³ An improved version considers a smooth classically small cut off at $T_H/2$.

5.1.2 Spectral Form Factor for $\tau > 1$

Having introduced semiclassical expressions for spectral determinants, we now want to explain the recipe for obtaining using (5.3) the spectral form factor as predicted by RMT for τ larger and smaller than 1. In Chap. 2 only the regime $\tau \leq 1$ could be accessed semiclassically. The latter calculation was first published in [1]; we will mainly follow this article in our presentation. We introduce a generating function Z(E) containing in the numerator and in the denominator two spectral determinants at in total four different energies

$$Z(E) \equiv \left\langle \frac{\det(E_C^+ - H) \det(E_D^- - H)}{\det(E_A^+ - H) \det(E_B^- - H)}, \right\rangle_{\Delta k},$$
 (5.6)

where $E^\pm_{A,B,C,D}$ are energies nearby to E defined as $E^\pm_{A,B,C,D} = E + \epsilon^\pm_{A,B,C,D}/(2\pi\bar{d})$ with the \pm in the exponent determining the sign of the imaginary part γ of $\epsilon_{A,B,C,D}$.

As we have already seen in Sect. 3.4 obtaining diagrammatic rules for the contributions of links and encounters is straightforward in the energy domain. We will thus consider here the spectral correlation function $R(\epsilon)$, Eq. (2.65), instead of the spectral form factor $K(\tau)$, Eq. (2.67), studied semiclassically in Chap. 2. For $R(\epsilon)$, RMT predicts in the unitary case:

$$R_{\text{GUE}}(\epsilon) = \frac{1}{4(i\epsilon)^2} - \frac{e^{2i\epsilon}}{4(i\epsilon)^2}$$
 (5.7)

and in the orthogonal case

$$R_{\text{GOE}}(\epsilon) = \frac{1}{2(i\epsilon)^2} + \sum_{n=3}^{\infty} \frac{(n-3)!(n-1)}{4(i\epsilon)^n} + e^{2i\epsilon} \sum_{n=4}^{\infty} \frac{(n-3)!(n-3)}{4(i\epsilon)^n}$$
(5.8)

When transforming back to the spectral form factor via the relation (2.67) the nonoscillating terms in (5.7, 5.8) lead to the contributions to $K(\tau)$ for $\tau \le 1$ obtained semiclassically in Sect. 2.4, and the oscillating terms correct the contributions to $K(\tau)$ for $\tau < 1$ to the ones for $\tau > 1$.

To proceed with our semiclassical analysis we approximate $\Delta(E)$ by Eq. (5.3) and use the following formula for the inverse spectral determinant

$$\Delta^{G}(E)^{-1} = B(E)^{-1} e^{i\pi \bar{N}(E)} \prod_{\gamma} \exp\{C_{\gamma} e^{iS_{\gamma}(E)/\hbar - i\pi \tau_{\gamma}/2}\}$$

$$= B(E)^{-1} e^{i\pi \bar{N}(E)} \sum_{A} F_{A}(E) e^{iS_{A}(E)/\hbar - i\pi \tau_{A}/2}.$$
(5.9)

yielding the semiclassical expression for Z(E), Eq. (5.6),

$$\begin{split} Z^{G}(E) &= \mathrm{e}^{\frac{i}{2}(\epsilon_{A}^{+} - \epsilon_{B}^{-} - \epsilon_{C}^{+} + \epsilon_{D}^{-})} \\ &\times \big\langle \exp\big(\sum_{\gamma} C_{\gamma} \mathrm{e}^{\frac{i}{\hbar} S_{\gamma}(E) + i \frac{T_{\gamma}}{T_{H}} \epsilon_{A}^{+} - i \pi^{\frac{\tau_{\gamma}}{2}}} + \sum_{\gamma'} C_{\gamma'} \mathrm{e}^{-\frac{i}{\hbar} S_{\gamma'}(E) - i \frac{T_{\gamma'}}{T_{H}} \epsilon_{B}^{-} - i \pi^{\frac{\tau_{\gamma'}}{2}}} \\ &- \sum_{\bar{\gamma}} C_{\bar{\gamma}} \mathrm{e}^{\frac{i}{\hbar} S_{\bar{\gamma}}(E) + i \frac{T_{\bar{\gamma}}}{T_{H}} \epsilon_{C}^{+} - i \pi^{\frac{\tau_{\bar{\gamma}}}{2}}} - \sum_{\bar{\gamma}} C_{\bar{\gamma}} \mathrm{e}^{-\frac{i}{\hbar} S_{\bar{\gamma}}(E) - i \frac{T_{\bar{\gamma}}}{T_{H}} \epsilon_{D}^{-} - i \pi^{\frac{\tau_{\bar{\gamma}}}{2}}} \big) \big\rangle_{\Delta k} \\ &= \mathrm{e}^{\frac{i}{2}(\epsilon_{A}^{+} - \epsilon_{B}^{-} - \epsilon_{C}^{+} + \epsilon_{D}^{-})} \big\langle \sum_{A,B,C,D} F_{A} F_{B} F_{C} F_{D}(-1)^{n_{C} + n_{D}} \mathrm{e}^{-i \pi (\tau_{A} - \tau_{B} + \tau_{C} - \tau_{D})/2} \\ &\times \mathrm{e}^{i(S_{A}(E) - S_{B}(E) + S_{C}(E) - S_{D}(E))/\hbar} \mathrm{e}^{i(T_{A} \epsilon_{A}^{+} - T_{B} \epsilon_{B}^{-} + T_{C} \epsilon_{C}^{+} - T_{D} \epsilon_{D}^{-})/T_{H}} \big\rangle_{\Delta k}, \end{split} \tag{5.10}$$

where we expanded the actions in the exponentials in the same way like before Eq. (2.64).

The correlation function $R(\epsilon)$, Eq. (2.65), can be obtained by differentiating Z(E) in Eq. (5.6) two times with respective to ϵ , see Eq. (5.2), and identifying afterwards the two energies in the numerator with the two energies in the denominator in a way that Z(E) approaches 1:

$$R(\epsilon) = -\frac{1}{4} + \lim_{\gamma \to 0} \frac{\partial^2 Z}{\partial \epsilon_A^+ \partial \epsilon_B^-} \Big|_{\parallel, \times}.$$
 (5.11)

The subscripts $\|, \times$ in the last equation refer to the two possible ways used in [1] of identifying the energies in Z(E) after having performed the differentiations in the last equation. The so-called parallel identification $\|$ sets $\epsilon_A^+ = \epsilon_C^+ = \epsilon^+, \ \epsilon_B^- = \epsilon_D^- = -\epsilon^+$ and the so-called crosswise identification \times sets $\epsilon_A^+ = \epsilon^+, \ \epsilon_B^- = -\epsilon^+, \ \epsilon_C^+ = -\epsilon^-, \ \epsilon_D^- = \epsilon^-$. For both identifications Z(E) approaches unity, in the second case additionally the limit $\gamma \to 0$ is required. The observation made in [1, 11] is that the complete result for the spectral correlation function predicted by RMT can only be obtained by adding the contributions from the two different identifications in (5.11). The parallel identification leads together with the (-1/4) in Eq. (5.11) to the nonoscillating contributions to $R(\epsilon)$ and the crosswise identification leads to the as a function of ϵ oscillating contributions to the spectral correlation function $R(\epsilon)$.

This procedure can be connected with the fact that the semiclassical expression for the spectral determinant has to be real that led to Eq. (5.5). To explain this, we consider $\Delta^{R_2}(E + \epsilon/(2\pi \bar{d}))$, Eq. (5.5), and expand the action like in (5.10):

$$\Delta^{R_{2}}\left(E + \frac{\epsilon}{2\pi\bar{d}}\right) = B(E)e^{-i\pi\bar{d}(E + \frac{\epsilon}{2\pi\bar{d}})} \sum_{A} (-1)^{n_{A}} F_{A} e^{\frac{i}{\hbar}S_{A}(E) + i\epsilon\frac{T_{A}}{T_{H}} - i\pi\frac{\tau_{A}}{2}} + B(E)e^{i\pi\bar{d}(E + \frac{\epsilon}{2\pi\bar{d}})} \sum_{A} (-1)^{n_{A}} F_{A} e^{-\frac{i}{\hbar}S_{A}(E) - i\epsilon\frac{T_{A}}{T_{H}} + i\pi\frac{\tau_{A}}{2}}.$$
(5.12)

This we insert instead of the expression $\Delta^{\rm G}(E)$, Eq. (5.3), in Z(E) in the numerator and approximate the determinants in the denominator again by the expression given in Eq. (5.9). Performing now only the parallel identification \parallel , we obtain due to the

second summand in each determinant in the numerator three further contributions. Two of them contain a rapidly oscillating phase factor with the argument proportional to $\bar{d}E$ and drop when performing the energy average. The last further contribution, that is not fully cancelled by the energy average, is obtained by pairing the two additional terms; i.e. the ones in the second line in Eq. (5.12) for the two determinants in the numerator with the ones in the denominator. When comparing the second and the first summand in Eq. (5.12) we see that all essential terms finally contained in Z(E) originating from the second summand can be obtained from the first by replacing ϵ by $-\epsilon$. The same replacement is also made when replacing the parallel by the crosswise identification, showing that these two procedures are identical: It is thus possible to use the representation (5.5) for the spectral determinant instead of $\Delta^{G}(E)$ in Z(E), but to consider only *one* identification of the energies. This connection between the condition that the spectral determinant is real for real energies and the RMT prediction for $K(\tau)$ for $\tau > 1$ leaves however also several open questions: The semiclassical formula for the determinant derived in [8, 9] involves additionally a truncation of the pseudo-orbit sum at $T_H/2$, see Eq. (5.4). Taking this into account by including an upper cut off when applying the sum rule (2.72) in the calculation of contributions from pseudo-orbit pairs below, this would lead to further terms, as can easily be checked, that do not obviously cancel. We want to emphasise in this context that the method presented in [2] for showing that contributions from the upper cut off vanish in diagonal approximation does not work in general. Furthermore only the determinants in the numerator are made real. Claiming the same for the determinants in the denominator would again lead to additional unwanted contributions. We will return to these problems in the conclusions.

We now study the diagonal contribution to $Z^G(E)$. As the overall action difference has to vanish in this case only orbital configurations where all orbits contained in the A- and C-sum in Eq. (5.10) are repeated in the B- and D-sum can contribute. As the stability prefactors of the exponentials for long orbits are dominated by $e^{-\lambda T/2}$ with the overall duration of the pseudo orbit T, consider their explicit form given after Eq. (2.23), they are approximately multiplicative. We thus obtain for their contribution in diagonal approximation $|F_A|^2|F_C|^2$. For the time-dependent exponentials we obtain the contribution of the ϵ_A^+ - and ϵ_C^+ -dependent factor to be given by $e^{i(T_A\epsilon_A^++T_C\epsilon_C^+)/T_H}$. Denoting the set of N orbits contained in the pseudo orbit taken as A as $\left\{a_i\right\}_{j=1}^N$ and the set taken as C as $\left\{c_i\right\}_{i=1}^M$ we can express the ϵ_B^- - and ϵ_D^- -dependent factor together with the $(-1)^{n_D}$ as

$$\prod_{j=1}^{N} \left(e^{-iT_{a_{j}}\epsilon_{B}^{-}/T_{H}} - e^{-iT_{a_{j}}\epsilon_{D}^{-}/T_{H}} \right) \prod_{i=1}^{M} \left(e^{-iT_{c_{i}}\epsilon_{B}^{-}/T_{H}} - e^{-iT_{c_{i}}\epsilon_{D}^{-}/T_{H}} \right).$$
 (5.13)

Reexponentiating this factor together with the other contributions to $Z_{\text{diag}}(E)$, we obtain

⁴ As we are considering positive as well as negative action differences in the s, u-integrals, the sign change of the actions is not important.

$$Z_{\text{diag}}(E) = \exp\left[\sum_{\gamma} |C_{\gamma}|^{2} \left(e^{i\frac{T_{\gamma}}{T_{H}}(\epsilon_{A}^{+} - \epsilon_{B}^{-})} - e^{i\frac{T_{\gamma}}{T_{H}}(\epsilon_{A}^{+} - \epsilon_{D}^{-})}\right) - \sum_{\gamma'} |C_{\gamma'}|^{2} \left(e^{i\frac{T_{\gamma'}}{T_{H}}(\epsilon_{C}^{+} - \epsilon_{B}^{-})} - e^{i\frac{T_{\gamma'}}{T_{H}}(\epsilon_{C}^{+} - \epsilon_{D}^{-})}\right)\right].$$
(5.14)

The sums over orbits are calculated by the Hannay and Ozorio de Almeida sum rule (2.72): It implies that $\sum_{\gamma} |C_{\gamma}|^2$ (...) can be replaced by $\int_{T_0}^{\infty} \frac{dT}{T}$ (...) with a minimal period of the orbits T_0 from which on the orbits behave ergodically in good approximation, justifying the application of the sum rule. The T_0 will drop out in the final result for $Z_{\text{diag}}(E)$. Performing the T-integrals we obtain exponential integrals that can be expanded for small arguments yielding to leading order in \hbar

$$Z_{\text{diag}}(E) = e^{\frac{i}{2}(\epsilon_A^+ - \epsilon_B^- - \epsilon_C^+ + \epsilon_D^-)} \left(\frac{(\epsilon_A^+ - \epsilon_D^-)(\epsilon_C^+ - \epsilon_B^-)}{(\epsilon_A^+ - \epsilon_B^-)(\epsilon_C^+ - \epsilon_D^-)} \right)^{2/\beta}.$$
 (5.15)

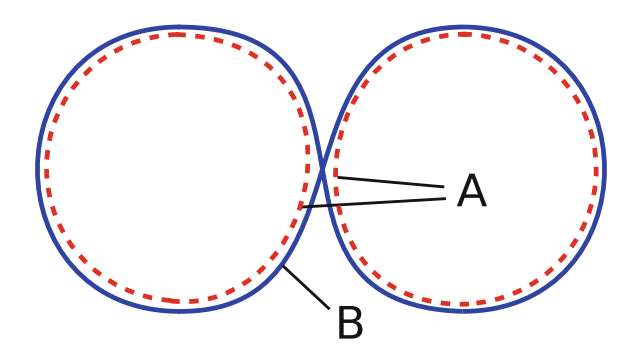
As we need to consider in the presence of time-reversal symmetry also for each orbit its time reversed as partner, each sum in Eq. (5.14) must be multiplied by 2 yielding a factor 2 in the exponent in (5.15). As described around Eq. (5.11), one now proceeds with taking derivatives, performing identifications of the $\epsilon_{A,B,C,D}$ and adding the resulting contributions. This yields in the absence of time-reversal symmetry the nonoscillating contribution in (5.7) in the case of the parallel identification \parallel and the oscillating contribution in the case of the crosswise identification \times [1]. In the presence of time-reversal symmetry with the parallel identification \parallel the first order in $1/\epsilon$ of the nonoscillating contribution in (5.8) is obtained and the crosswise identification \times yields zero.

Turning now to non-diagonal terms, the semiclassical contributions to Z(E) can be expressed as we have seen already several times as product of link and encounter contributions with each link contributing a factor given by a certain linear combination of the different $\epsilon_{A,B,C,D}$ in the denominator and each encounter a certain linear combination of the different $\epsilon_{A,B,C,D}$ in the numerator. For the next-to-leading order in $1/\epsilon$ we thus need to consider a pair where the pseudo orbit and its partner differ in one encounter and possess two links. Like for pure orbits, i.e. no pseudo orbits, we will again take into account the configuration depicted in Fig. 4.21, in the following we will refer to it as " ∞ ". As we are now treating pseudo orbits we have the additional possibility that two independent orbits encounter each other. As partner we can then consider one long orbit following the two short orbits and encountering itself at the

⁵ The T_0 could have been introduced always when evaluating sums over orbits by sum rules, but in all cases considered up to now the semiclassical limit $\hbar \to 0$ and the limit $T_0 \to 0$ commuted. This is not the case here, the resulting integrals do not exist for $T_0 = 0$.

⁶ As can be easily checked it is not possible to construct diagrams with a larger number of links where the number of links and of (s, u)-coordinates needed to characterise the encounter configuration differs by one.

Fig. 5.1 Sketch of an eight diagram, an example of correlated pseudo orbits [1]



encounter of the two short partner orbits. Both components are exponentially close to each other up to deviations in the encounter region, for an illustration see Fig. 5.1, we will refer to this pseudo-orbit pair as eight orbit "8".

When calculating the non-diagonal pseudo-orbit contributions we consider these non-diagonal pairs just in one sum of the pseudo-orbit sums in (5.10) and perform diagonal approximation in the others. Each non-diagonal contribution $Z_{\rm off}(E)$ to Z(E) thus possesses the form

$$Z_{\text{off}}(E) = Z_{\text{diag}}(E) G(E)$$
(5.16)

with $Z_{\text{diag}}(E)$ given in Eq. (5.15) and G(E) the contribution from a non-diagonal pair as for example " ∞ " or "8" to Z(E). The contribution to G(E) from the orbit pair " ∞ " depicted in Fig. 4.21 can be obtained by using the explicit form of the sum rule, weight function, the encounter duration and action difference given in Sect. 2.4. We then obtain when one of the two orbits is included in the A-sum and the other in the B-sum in Eq. (5.10) [1]

$$G_{\infty}(E) = \int_{0}^{\infty} dt_{1} dt_{2} \int_{-c}^{c} ds du \frac{1}{\Omega t_{\text{enc}}} e^{(i/\hbar)su} e^{i(t_{1}+t_{2}+2t_{\text{enc}})\left(\epsilon_{A}^{+}-\epsilon_{B}^{-}\right)/T_{H}}$$

$$= \frac{2}{i\left(\epsilon_{A}^{+}-\epsilon_{B}^{-}\right)}$$
(5.17)

with the duration of the left and the right link t_1 and t_2 , respectively. Analogous contributions are also obtained by distributing the two orbits among the other of the four sums over A, B, C and D. Taking finally the overall contribution to (5.16) and performing the steps explained around Eq. (5.11), this contribution reproduces the nonoscillatory second-order contribution in $1/\epsilon$ in (5.8) given by $1/[2(i\epsilon)^3]$.

Considering now the pseudo-orbit pair "8" depicted in Fig. 5.1, we obtain, if we do not allow encounters to overlap as we did in the last chapter when studying the effect of a non-zero Ehrenfest-time, again contributions as in Eq. (5.17) with the only difference that we can allow now the two short orbits to be contained also in two different pseudo-orbit sums. This leads to the following cancellation mechanism [1]: consider the long orbit of the "8"-pair to be contained in the A-sum, then the two

short orbits can be contained either both in the B-sum or both in the D-sum or one in the B-sum and one in the D-sum. Calculating those contributions in an analogous manner as in (5.17) we obtain for their sum

$$\frac{1}{i\left(\epsilon_{A}^{+}-\epsilon_{B}^{-}\right)}-\frac{i\left(2\epsilon_{A}^{+}-\epsilon_{B}^{-}-\epsilon_{D}^{-}\right)}{i\left(\epsilon_{A}^{+}-\epsilon_{B}^{-}\right)i\left(\epsilon_{A}^{+}-\epsilon_{D}^{-}\right)}+\frac{1}{i\left(\epsilon_{A}^{+}-\epsilon_{D}^{-}\right)}=0\tag{5.18}$$

and an analogous cancellation of the other terms. That this cancellation mechanism is however not yet fully general we will show in the next section.

The arguments given here can again be generalised to orbits differing in an arbitrary number of encounters leading again to the result predicted by field theory. This connection was analysed in detail in [11]: First it was used that there is a one-to-one correspondence between the contributions from semiclassical diagrams and the field-theoretical contributions for the nonoscillatory contributions to $R(\epsilon)$ shown in [12, 13]. Second by comparing the contributions from the two saddle points in the field-theoretical calculation—the one yielding the nonoscillatory and the other the oscillatory contributions to $R(\epsilon)$ —it was shown that they are connected in the same way like the parallel and the crosswise identification of energies in Z(E) in the semiclassical calculation. This shows that the field-theoretical and the semiclassical contributions to $R(\epsilon)$ indeed are identical.

To summarise, in this first section we explained following [1] a procedure to calculate the contributions to the spectral form factor consistent with RMT for all τ values and discussed the current status of a semiclassical understanding of this procedure. In the next section we will present another problem where a field-theoretical effect needs to be understood semiclassically: the integration over a curved manifold in field theory.

5.2 Curvature and Multiple Traversals of Periodic Orbits

We start our analysis with the question, how to obtain semiclassically the RMT results for the energy-averaged two-point correlator of spectral determinants,

$$C_{\beta}(\epsilon) = \frac{\langle \Delta \left(E + \epsilon / \left(2\pi \bar{d} \right) \right) \Delta \left(E - \epsilon / \left(2\pi \bar{d} \right) \right) \rangle_{\Delta k}}{\langle \Delta \left(E \right)^{2} \rangle_{\Delta k}}, \tag{5.19}$$

starting from the semiclassical representation $\Delta^{R_2}(E)$ and using the knowledge about action correlations between orbits and pseudo orbits. This problem was first addressed by Kettemann et al. [14] in the context of maps using diagonal approximation. The quantity $C_{\beta=2}(\epsilon)$ was then reconsidered in diagonal approximation in [2] for continuous flows applying the methods of [1]. In both cases the calculations show perfect agreement with the universal RMT results for the unitary case

$$C_{\beta=2}^{\rm RMT}(\epsilon) \propto \frac{\sin \epsilon}{\epsilon}.$$
 (5.20)

Here the proportionality sign indicates that we focus on the universal part of $C_{\beta}(\epsilon)$ and do not consider the semiclassical calculation of the prefactor, that contains for example the contribution from multiply traversed orbits. To understand this, consider the first representation of $\Delta^{G}(E)$ in Eq. (5.3).

In the case of time-reversal symmetry, however, Ref. [14] could not obtain semi-classically the RMT result [14]

$$C_{\beta=1}^{\rm RMT}(\epsilon) \propto \left(\frac{\cos \epsilon}{\epsilon^2} - \frac{\sin \epsilon}{\epsilon^3}\right).$$
 (5.21)

In this section we evaluate $C_{\beta}(\epsilon)$ beyond the diagonal approximation. We demonstrate in the first subsection that the contributions from the "8"-pseudo-orbit pair, shown to cancel in Eq. (5.18) for $R(\epsilon)$, do *not* vanish when one considers the simplest non-rational function of spectral determinants, i.e. Eq. (5.19). The next subsection is devoted to a corresponding field-theoretical analysis of $C_{\beta}(\epsilon)$, showing that the additional terms we find in our semiclassical analysis are cancelled in field theory by so-called curvature contributions. In the third subsection we then provide the type of correlations between pseudo orbits that allows us to semiclassically recover the RMT result in the unitary and, for the first time, also in the orthogonal case. We finally discuss of the consistency of our results with previous results.

5.2.1 Semiclassical Calculation

We now semiclassically evaluate the correlator $C_{\beta}(\epsilon)$ by means of $\Delta^{R_2}(E)$. Upon substituting Eqs. (5.3) and (5.5) into the numerator of Eq. (5.19), this leads to

$$\left\langle \Delta^{\mathrm{R}_2} \left(E + \frac{\epsilon}{2\pi \bar{d}} \right) \Delta^{\mathrm{R}_2} \left(E - \frac{\epsilon}{2\pi \bar{d}} \right) \right\rangle_{\Delta k}$$

$$\approx 2B^2(E) \Re \mathrm{e}^{-i\epsilon} \left\langle \sum_{A,B} F_A F_B^* (-1)^{n_A + n_B} \, \mathrm{e}^{(i/\hbar)(S_A - S_B)} \mathrm{e}^{i\epsilon(T_A + T_B)/T_H} \right\rangle_{\Delta k},$$
(5.22)

where we already neglected terms highly oscillatory in the energy. We also expanded the actions of the pseudo orbits around E.

We start with calculating contributions that survive the energy average in an analogous way as in the last section. In diagonal approximation, we can write the resulting sum over pseudo orbits as an exponentiated sum over orbits γ . The Hannay and Ozorio de Almeida sum rule is afterwards used in the form given after Eq. (5.14) to yield the first term in the square brackets in

$$C_{\beta}(\epsilon) \propto -\Re \frac{\mathrm{e}^{-i\epsilon}}{(i\epsilon)^{2/\beta}} \left[1 + \tilde{C}_{\beta}(\epsilon) \right].$$
 (5.23)

The function $\tilde{C}_{\beta}(\epsilon)$ contains all universal effects beyond the diagonal approximation, consisting of both orbit and pseudo-orbit correlations. In the following we compute $\tilde{C}_{\beta}(\epsilon)$ to leading order in $1/\epsilon$.

In the *unitary case*, the leading order in $1/\epsilon$ contribution to $\tilde{C}_{\beta=2}(\epsilon)$ comes only from the first pseudo-orbit correlations, namely, the "8"-diagrams, see Fig. 5.1.

Similar to the last section, we include in A a pseudo orbit of order n and in B a pseudo orbit of order n+1 and vice versa. All orbits contained in A and B are assumed to be equal except for the ones forming an "8"-orbit. As calculated in the last section in Eq. (5.18), we obtain

$$\tilde{C}_{\beta=2}^{\text{eight}}(\epsilon) = -\frac{1}{i\epsilon},$$
(5.24)

where an additional factor 2 accounts for the possibility to include the two short orbits in the A- or B-sum in Eq. (5.22). Using the expression obtained for $\tilde{C}_{\beta=2}^{\text{eight}}(\epsilon)$ in Eq. (5.24) now in Eq. (5.23) gives a result which is inconsistent with the RMT prediction (5.20).

In the *orthogonal case* we must consider also the contribution $\tilde{C}_{\beta=1}^{\infty}(\epsilon)$ from the " ∞ "-shaped orbit pair sketched in Fig. 4.21, apart from the eight-shaped contribution. Furthermore, for the latter diagram the possible time-reversal operation leaving invariant each of the orbits must be taken into account. The calculations follow the same lines as for the unitary case, consider Eq. (5.17). We finally obtain

$$\tilde{C}_{\beta=1}^{\text{eight}}(\epsilon) = -\frac{4}{i\epsilon},$$
 (5.25)

$$\tilde{C}_{\beta=1}^{\infty}(\epsilon) = \frac{1}{i\epsilon}.$$
(5.26)

Again this result contains extra terms resulting from the "8"-diagram when compared with the corresponding RMT result (5.21). We note that the contribution $\tilde{C}_{\beta=1}^{\infty}(\epsilon)$ alone yields a result consistent with the RMT prediction.

We can conclude that, although the analysis based on the semiclassical representation $\Delta^{R_2}(E)$ of the spectral determinant produces the same structure as the RMT results (both are naturally ordered in powers in $1/\epsilon$), the terms (5.24, 5.25) following from semiclassical loop contributions are not consistent with RMT and spoil the agreement found between RMT and the results in [2, 14] based on the diagonal approximation. Moreover, using the same methods we also obtain non-vanishing contributions of higher order in $1/\epsilon$ [15, 16].

As we will see, the problem requires a better insight into possible pseudo-orbit correlations. Such an insight is gained here through the comparison with a corresponding field-theoretical approach.

5.2.2 Field-Theoretical Calculation: The Curvature Contribution

In order to better understand the difference between the semiclassical and the RMT results, we calculate $C_{\beta}(\epsilon)$ by field-theoretical methods [17]. Our approach consists of transforming the non-perturbative field-theoretical expression for $C_{\beta}(\epsilon)$ into a perturbative expansion. As we will see, the difference between the previous semi-classical and the RMT results has a direct correspondence in the field theory.

We start with the non-perturbative evaluation of the integral following from field-theoretical considerations, which is given by [16]

$$C_{\beta}(\epsilon) \propto \frac{1}{4\pi} \int_{S} d\mu (S) e^{-i\frac{\beta\epsilon}{4} \text{TrS}},$$
 (5.27)

with $S \in Sp(4)/(Sp(2)*Sp(2))$ in the orthogonal and $S \in U(2)/(U(1)*U(1))$ in the unitary case. The group of the n-dimensional symplectic matrices is denoted in this context by Sp(n) and the group of n-dimensional unitary matrices by U(n). Parameterising U(2)/(U(1)*U(1)) in terms of angles θ and ϕ , we calculate in the unitary case

$$C_{\beta=2}(\epsilon) \propto \frac{1}{4\pi} \int_0^{2\pi} d\phi \int_{-1}^1 d\cos\theta e^{-i\epsilon\cos\theta} = \frac{\sin\epsilon}{\epsilon}$$
 (5.28)

In a similar way one obtains in the orthogonal case Eq. (5.21) [16].

To obtain a perturbative evaluation of the field-theoretical expressions, in the form of a power-series in $1/\epsilon$ that is comparable to semiclassics, we perform the following procedure in the unitary case: We replace the integration variables on the sphere by stereographic projection variables in the complex plane. In this parametrisation we rewrite S as

$$S = \begin{pmatrix} \mathbb{1}_{2/\beta} & 0\\ 0 & -\mathbb{1}_{2/\beta} \end{pmatrix} T \begin{pmatrix} \mathbb{1}_{2/\beta} & 0\\ 0 & -\mathbb{1}_{2/\beta} \end{pmatrix} T^{-1}$$
 (5.29)

with

$$T = \begin{pmatrix} \mathbb{1}_{2/\beta} - B^{\dagger} \\ B & \mathbb{1}_{2/\beta} \end{pmatrix} \tag{5.30}$$

and the stereographic projection variable $B \in \mathbb{C}$ in the unitary case. An analogous procedure yields in the orthogonal case

$$B = \begin{pmatrix} B_1 - B_2 \\ B_2^* B_1^* \end{pmatrix} \tag{5.31}$$

with $B_1, B_2 \in \mathbb{C}$. We used here the dagger to indicate the Hermitian conjugate of a matrix and the power -1 for its inverse. Using this parametrisation a one-to-one correspondence between the field-theoretical and the semiclassical contributions was shown to hold in the case of the spectral form factor [12, 13].

The effect of this parameterisation is twofold: On the one hand this variable transformation has a nontrivial Jacobian corresponding to a curved measure,

$$d\mu(S) = \frac{4[dB]}{(1+B^2)^{4/\beta}}$$
 (5.32)

with $\mathcal{B} = |B|$, $[dB] = dBdB^*$ in the unitary and $\mathcal{B} = \sqrt{|B_1|^2 + |B_2|^2}$, $[dB] = dB_1dB_2dB_1^*dB_2^*$ in the orthogonal case. On the other hand it leads to a particular form of the phase in the exponential

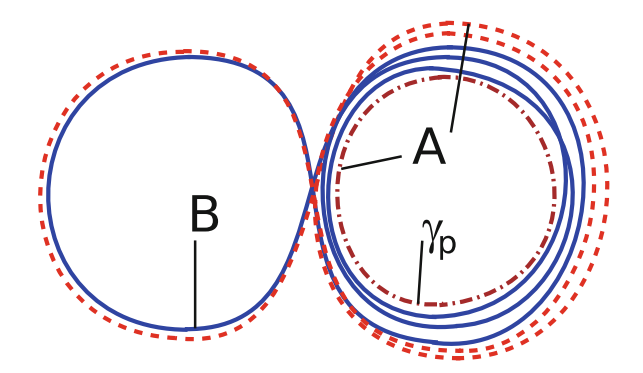
$$\operatorname{Tr} S = \frac{4}{\beta} \left(1 + 2 \sum_{k=1}^{\infty} (-1)^k \, \mathcal{B}^{2k} \right). \tag{5.33}$$

For this particular parameterisation of the integral in Eq. (5.27), we can unambiguously identify two kinds of terms in the $1/\epsilon$ expansion of the correlator obtained by using in the unitary case $\int_0^\infty dB \, |B|^{2k} \, \mathrm{e}^{-2i\epsilon|B|^2} \propto (1/\epsilon)^{k+1} \, (k \in \mathbb{N}_0)$ and the corresponding relation for B_1 and B_2 in the orthogonal case. We will call these terms simply phase contributions if the factor in front of the exponential in the last integral (i.e. in front of the k=1-term in (5.33)) results from expanding the right hand side of Eq. (5.33) and curvature contributions if it results from expanding the right hand side of Eq. (5.32) in powers of \mathcal{B} .

For the spectral form factor a one-to-one correspondence between the field-theoretical phase contributions and the contributions from semiclassical diagrams was shown in [12, 13]. In this case the evaluation was performed applying the replica trick [18]. Here a parameter r contained in the considered quantities, that is allowed to take positive integer values is at the end of the calculation extrapolated to $r \to 0$. Although this is mathematically not justified—analytic continuation would need the functional values on a finite compact region and not just for isolated points—it mostly leads to reasonable results, although there are also counterexamples where it leads to wrong conclusions [19]. As the integration in the case of the spectral form factor is performed with respect to a manifold with a dimension proportional to r, the curvature vanishes in the replica limit $r \to 0$. In the case of the spectral form factor curvature contributions can thus be neglected and phase contributions and contributions from semiclassical diagrams are equal. We can thus expect agreement between the phase contributions and the contributions from the semiclassical diagrams also for the correlator of two determinants.

As can be easily checked, we indeed find agreement between the field-theoretical and the semiclassical results (5.24–5.26), by evaluating Eq. (5.27) and ignoring the terms originating from the curvature of the measure, i.e. replacing $(1+\mathcal{B}^2)^{-4/\beta}$ in Eq. (5.32) by a constant. Clearly, what we are missing in the semiclassical calculation are the analogues of the terms that can be derived from curvature. This means that a new kind of pseudo-orbit correlation is lacking which corresponds to the curvature effects.

Fig. 5.2 Sketch of a pair of pseudo orbits A, B correlated in a way that one of the orbits (*dashed-dotted*) has a period smaller than the encounter time. The two long orbits (*dashed* and *full line*) differ in the number of traversals around the short periodic orbit γ_p by one



5.2.3 Semiclassical Interpretation of Curvature Effects

In this subsection we present the missing pseudo-orbit correlations which provide the curvature effects in the integration over the curved manifold in the field-theoretical approach and thereby consistency with RMT. The essential step is to lift the constraint that one of the short periodic orbits does not surround the other one more than once. This assumption is implicit in the calculation of the eight-shaped diagrams in Ref. [1] presented in the last section when one assumes that both short orbits have periods larger than the encounter time.

To be precise, we consider as components of a pseudo orbit two periodic orbits, (dashed and full line in Fig. 5.2) which include several traversals around a common short periodic orbit γ_p and differ in the number of repetitions by one. In order to find further contributions to Eq. (5.22), we have to look for pseudo-orbit pairs possessing almost equal actions: We thus pair the short periodic orbit γ_p and the orbit surrounding it (k-1) times with the orbit surrounding it k times. In terms of symbolic dynamics, i.e. when representing every orbit by the sequence of primitive traversed orbits, this way of pairing can be described in the following way: We consider an orbit traversing a loop γ_1 once and a short periodic orbit γ_p k times possessing the symbolic notation $\gamma_1 \gamma_p^k$. This orbit is paired with a pseudo orbit consisting of the orbit γ_p and an orbit traversing γ_1 once and γ_p k-1 times; this pair has the symbolic code (γ_p) $(\gamma_1 \gamma_p^{k-1})$. This situation occurs in the case, when the encounter time t_{enc} is longer than the shortest of the periodic orbits, i.e. when the encounters overlap.

For the evaluation of this contribution, we again need the action difference between the two orbits, obtained as $\Delta S = us$ as discussed before Eq. (4.24) and the weight function as a function of s, u that is obtained in analogous manner as before to be given by $w_{T,T_p}(u,s) = \frac{TT_p}{2\Omega(E)t_{\rm gnc}}$ expressed through the periods of the two short periodic orbits, T and T_p . The winding number n of the orbit with duration T around the one with duration T_p is then $n = \frac{t_{\rm enc}}{T_p}$. This implies, that the integration over T_p for fixed s, u contains a summation over all possible winding numbers. Using the action difference and the weight function given above and applying the Hannay and Ozorio sum rule with respect to T and T_p , we find for $\tilde{C}_{\beta=2}(\epsilon)$ the additional "curvature"

contribution

$$\tilde{C}_{\beta=2}^{\text{curv}}(\epsilon) = -4 \left\langle \int_{-c}^{c} ds \, du \int_{t_{\text{enc}}}^{\infty} \frac{dT}{T} \int_{0}^{t_{\text{enc}}} \frac{dT_{\text{p}}}{T_{\text{p}}} e^{(i/\hbar)us} e^{2i\epsilon(T+T_{\text{p}})/T_{H}} w_{T,T_{\text{p}}}(u,s) \right\rangle_{\Delta k}$$

$$= \frac{1}{i\epsilon}.$$
(5.34)

To obtain the second line in Eq. (5.34) we perform first the time integrals exactly and afterwards do the s, u-integrals using that only terms linear in $t_{\rm enc}$ contribute and the result given in Eq. (2.59). The expression for $\tilde{C}_{\beta=2}^{\rm curv}(\epsilon)$ thus precisely cancels the undesired term (5.24) coming from the eight-shaped diagram, and allows for the full explanation of the RMT result (5.20) in purely semiclassical terms. In the orthogonal case, one obtains in a similar way

$$\tilde{C}_{\beta=1}^{\text{curv}}(\epsilon) = \frac{4}{i\epsilon},$$
(5.35)

cancelling again the extra term (5.25) and yielding the universal RMT result (5.21).

We could thus identify the semiclassical analogue of the field-theoretical curvature contributions. As in the field-theoretical case the splitting between the two diagrams analysed in the semiclassical calculation in first and third subsection is completely arbitrary; the final result, the sum of the two, is however always the same. This can be taken into account in the semiclassical calculation by considering as reference orbits in the calculation of the weight function always the two short orbits as we did above Eq. (5.34) and by allowing for an arbitrary length of one of the two periodic orbits as long as the other one is longer than the duration of the encounter. This yields

$$\begin{split} \tilde{C}_{\beta=2}^{\text{eight}}(\epsilon) + \tilde{C}_{\beta=2}^{\text{curv}}(\epsilon) \\ &= -2 \left\langle \int_{-c}^{c} ds \, du \int_{0}^{\infty} \frac{dT}{T} \int_{0}^{\infty} \frac{dT_{\text{p}}}{T_{\text{p}}} \mathrm{e}^{(i/\hbar)us} \mathrm{e}^{2i\epsilon(T+T_{\text{p}})/T_{H}} w_{T,T_{\text{p}}}(u,s) \right. \\ &+ 2 \int_{-c}^{c} ds \, du \int_{0}^{t_{\text{enc}}} \frac{dT}{T} \int_{0}^{t_{\text{enc}}} \frac{dT_{\text{p}}}{T_{\text{p}}} \mathrm{e}^{(i/\hbar)us} \mathrm{e}^{2i\epsilon(T+T_{\text{p}})/T_{H}} w_{T,T_{\text{p}}}(u,s) \right\rangle_{\Delta k} \\ &= 0, \end{split}$$

$$(5.36)$$

i.e. the sum of the two contributions calculated in the first and third subsection. The final result in the last equation is obtained by taking into account that the expression before contains no terms linear in $t_{\rm enc}$. The splitting of the two contributions in our semiclassical calculation presented before showed however the one-to-one correspondence to the corresponding field-theoretical contributions after the stereographic projection.

We want to emphasise here the different behaviour of an eight orbit in Fig. 5.1 and the " ∞ "-orbit pair in Fig. 4.21: For an "8"-orbit with overlapping encounter stretches, one of the short orbits winds around the other and thus yields another nontrivial contribution, that is not yet contained in the diagonal terms. In the case

of an "\infty"-orbit pair with overlapping encounter stretches, however, the orbit and its partner traverse the whole orbit in the same direction [20, 21], which is already contained in the diagonal contribution.

By this calculation we demonstrated that overlapping encounter regions, usually only considered when taking into account the effect of a non-zero Ehrenfest-time as we did in the last chapter, can lead to non-vanishing contributions even for vanishing Ehrenfest-time. One question, however, has to be addressed at this point: When are effects of encounter overlap important and when can they be neglected for zero Ehrenfest-time? This point will be treated in the following subsection.

5.2.4 Consistency with Former Results

Also in former semiclassical calculations to reproduce RMT results, diagrams involving orbits surrounding a short periodic orbit occurred. However the contributions from (approximate) multiple traversals needed never to be taken into account to reproduce RMT results. Here we discuss the consistency of our results with those approaches. We distinguish in this context two different situations: first approaches involving orbits and second the approaches involving pseudo orbits.

In the case of orbit pairs the diagram analysed in the last subsection cannot occur as two partner orbits are needed for the original trajectory to obtain a pair possessing small action difference. One simple example for a possible diagram in the case of orbit pairs, where a longer orbit surrounds a short periodic orbit, is shown in Fig. 5.3. We treated this orbit pair also in the last chapter, when studying the effect of nonzero Ehrenfest-time, see for one orbit of the pair Fig. 4.22. In this case a central dashed-dotted periodic orbit is encountered twice by an orbit and its partner. The partner is obtained from the original orbit by exchanging one traversal of the dashed-dotted orbit between the first and the second encounter with it. For orbit correlations, i.e. no pseudo orbits, it was shown in the case of spectral statistics [12, 13] and the case of quantities related to the conductance [22, 23], as already mentioned in Chap. 4, that RMT results can be reproduced when neglecting contributions from multiply traversed periodic orbits.

This fact can also be obtained independently for the spectral form factor and the conductance for orbit pairs encountering one periodic orbit twice, see Fig. 5.3, by considering our Ehrenfest-time calculation in the last chapter and studying the limit $\tau_E \to 0$. As can be easily checked, just the configurations of two independent encounters with the periodic orbit, see Fig. 4.14, and one encounter of three stretches with one of them lying on the periodic orbit, see Fig. 4.6, yield a non-zero contribution for $\tau_E = 0$. In particular, this means that we do not find a different result by neglecting configurations where a periodic orbit is surrounded by a longer one many times. Generalising this calculation to more complicated diagrams would provide also in these cases the cancellation mechanism and by this show that there are no contributions from multiply surrounded periodic orbits.

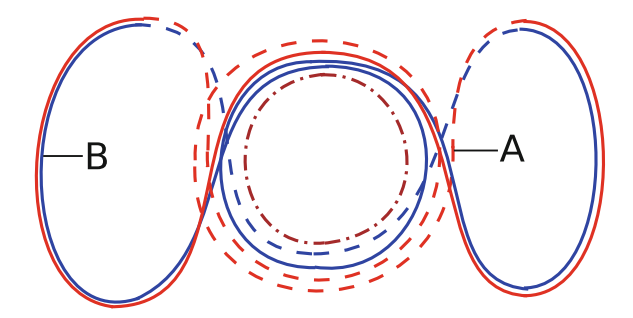


Fig. 5.3 Encounter overlap for different encounters. We consider an orbit (*blue*) and its partner (*red*), that differ by one traversal during the encounter with the central *dashed-dotted* periodic orbit (*brown*). The stretches of one encounter of the orbit and its partner with the central periodic orbit are indicated by *full lines*, the others for distinction by *dashed lines*. We calculated the contribution of this configuration to the spectral form factor for non-zero Ehrenfest-time in the last chapter

Next we consider the consistency with other approaches involving pseudo orbits. Correlation functions of spectral densities can be obtained by considering semiclassical expressions for homogeneous ratios of spectral determinants, as explained in the last section. The contributions from eight-shaped orbits containing surrounded periodic orbits, see Fig. 5.2, and related diagrams did not need to be considered to obtain RMT results [1, 11], because they apparently all cancel each other. In the case of the eight-shaped diagram we showed in Eq. (5.18) that the contributions resulting from different ways to include the orbits in the pseudo-orbit sums cancelled. As can be easily checked the same cancellation also applies to the corresponding contributions from **surrounded** periodic orbits, Fig. 5.2. However, it is not fully general, i.e. it does not work for the two-point correlator of spectral determinants, as was shown in this section and also not for other non-rational correlators of spectral determinants, as can be easily checked.

We finally mention that we concentrated in this part on approaches calculating energy-averaged quantities. Multiply traversed periodic orbits can also occur for zero Ehrenfest-time when studying not averaged semiclassical expressions as for the Kubo conductivity in [24] and for the Wigner time delay in [25].

To summarise, we presented in this chapter in the first section a method to obtain semiclassically the contributions to the spectral form factor $K(\tau)$ in a way consistent with RMT for all τ , i.e. not only for $\tau \leq 1$ as in Chap. 2 first presented in Ref. [1]. Furthermore we explained how the additional correlations appearing in this context are connected with the fact that a correct semiclassical expression for the spectral determinant needs to be real for real energies. In the second section we showed that the semiclassical approach from Ref. [1] applied to the two-point correlator of spectral determinants produces spurious terms coming from pseudo-orbit correlations, spoiling agreement with the universal RMT results. A new additional contribution is thus required, it results from pseudo-orbit correlations represented by encounter diagrams with overlapping encounters. We have shown that these effects

are the semiclassical analogue of the curvature contributions in the field-theoretical approach, thus providing a semiclassical interpretation of the latter. In the discussion of the consistency of our results with previous approaches we explained when RMT results can be obtained in previous semiclassical calculations without considering contributions from multiply traversed periodic orbits.

References

- Heusler, S., Müller, S., Altland, A., Braun, P., Haake, F.: Phys. Rev. Lett. 98, 044103 (2007). arXiv:0610053 (2006)
- 2. Keating, J.P., Müller, S.: Proc. R. Soc. Lond. A 463, 3241 (2007)
- 3. Waltner, D., Heusler, S., Urbina, J.-D., Richter, K.: J. Phys. A 42, 292001(F) (2009)
- 4. Huber, H.: Math. Ann. 138, 1 (1959)
- 5. Voros, A.: Commun. Math. Phys. 110, 439 (1987)
- 6. Steiner, F.: Phys. Lett. B 188, 447 (1987)
- 7. Voros, A.: J. Phys. A 21, 685 (1988)
- 8. Berry, M.V., Keating, J.P.: J. Phys. A 23, 4839 (1990)
- 9. Georgeot, B., Prange, R.: Phys. Rev. Lett. 74, 2851 (1995)
- 10. Sieber, M., Steiner, F.: Phys. Rev. Lett. 67, 1941 (1991)
- 11. Müller, S., Heusler, S., Altland, A., Braun, P., Haake, F.: New J. Phys. 11, 103025 (2009)
- 12. Müller, S., Heusler, S., Braun, P., Haake, F., Altland, A.: Phys. Rev. E 72, 046207 (2005)
- 13. Müller, S.: Periodic-Orbit Approach to Universality in Quantum Chaos. Ph.D. thesis, Universität Duisburg Essen (2005)
- 14. Kettemann, S., Klakow, D., Smilansky, U.: J. Phys. A 30, 3643 (1997)
- 15. Waltner, D., Gutiérrez, M., Urbina, J.-D., Richter, K.: Unpublished (2009)
- 16. Heusler, S.: Private communication (2009)
- 17. Efetov, K.B.: Adv. Phys. 32, 53 (1983)
- 18. Edwards, S.F., Anderson, P.W.: J. Phys. F 5, 965 (1975)
- 19. Veerbaarschot, J.J.M., Zirnbauer, M.: J. Phys. A 18, 1093 (1985)
- 20. Turek, M., Richter, K.: J. Phys. A **36**, L455 (2003)
- 21. Turek, M.: Semiclassics beyond the diagonal approximation. Ph.D. thesis, Universität Regensburg (2004)
- 22. Heusler, S., Müller, S., Braun, P., Haake, F.: Phys. Rev. Lett. 96, 066804 (2006)
- 23. Müller, S., Heusler, S., Braun, P., Haake, F.: New J. Phys. 9, 12 (2007)
- 24. Richter, K.: Europhys. Letters 29, 7 (1995)
- 25. Kuipers, J., Sieber, M.: Phys. Rev. E 77, 046219 (2008)

Chapter 6 Conclusions and Outlook

In this chapter we first summarise our results and afterwards present possible extensions: In general we studied mesoscopic systems with classically chaotic dynamics using semiclassical techniques. On the one hand we confirmed RMT results, on the other hand we considered corrections to the latter results mainly due to Ehrenfest-time effects. After introducing in Chap. 2 the semiclassical approaches for calculating the contributions from correlated orbit pairs to the conductance and spectral correlators, we considered in Chap. 3 two examples of time-dependent processes: the survival probability and the fidelity amplitude. We showed how to obtain semiclassically corrections to the classical results consistent with RMT. This was the first semiclassical treatment of pairs involving *open* orbits starting and ending *inside* the system. Before, only *periodic* orbits or orbits starting and ending on cross sections in the leads had been considered. To calculate the contributions from these open orbit pairs starting and ending inside the system new semiclassical diagrams had to be identified possessing crossings in configuration space at the beginning or at the end of the trajectory. Then we checked that our results and the corresponding RMT results are equal to high order in \hbar in presence and absence of time-reversal symmetry and in the presence of spin-orbit interaction. We furthermore showed that exact relations like the unitarity of the survival probability, the fidelity amplitude and the continuity equation for the survival probability also hold in our semiclassical approach. We could confirm a relation between the fidelity amplitude and the spectral form factor derived before within the RMT framework. In the last part of this chapter we studied effects that were not accessed by RMT, namely the effect of non-diagonal contributions in the Lyapunov regime of the fidelity and in the case of a time-dependent perturbation.

In the next chapter we analysed the effect of a non-zero Ehrenfest-time: After reviewing previous results for the Ehrenfest-time dependence of the leading-order quantum correction in the number of open channels to the conductance of a two lead geometry we calculated the Ehrenfest-time dependence of the survival probability and the fidelity amplitude. The Ehrenfest-time dependence of the survival probability was confirmed by numerical simulations. For the next application we considered

additionally tunnel barriers in the leads. We then described the dependence of the conductance variance contribution linear in the Ehrenfest-time and leading order in the number of open channels on the tunnel probability through the barriers. Due to the large number of diagrams in the analytical calculation and the complicated dependence of the dwell time on the tunnelling rate this calculation was much more involved than the one performed in Ref. [1] for perfectly coupled leads. The calculated tunnel-probability dependence could be confirmed numerically by simulations performed by P. Jacquod. Then we considered the next-to-leading order quantum correction to the dc conductance. In this case we identified previously overlooked diagrams occurring in the case of multiply surrounded periodic orbits and calculated their contributions. We checked that taking these diagrams into account leads to results that fulfil the current conservation relation (2.46). We extended this study by including a finite frequency ω to the ac case and checked in this context that the corresponding contributions we obtained do not affect the Ehrenfest-time independence of the Wigner time delay. Using the gained knowledge about possible orbital configurations we determined the next-to-leading order quantum correction to the spectral form factor in the absence of time-reversal symmetry and found a result consistent with the field-theoretical prediction of Ref. [2] that however differs from the one obtained previously by semiclassical methods [3]. In the next section we calculated the Ehrenfest-time dependence of the correlation function of n pairs of scattering matrices to leading order in the number of open channels for all $n \in \mathbb{N}$. By this, we extended previous approaches that only treated semiclassically cases up to n = 3 [4, 5]. We applied this result to obtain the Ehrenfest-time dependence of the density of states of a chaotic Andreev billiard.

In Chap. 5 we gave semiclassical interpretations of effects occurring in the corresponding field-theoretical calculations. In the first section we studied the connection between the fact that the spectral determinant has to be real for real energies that implies a nontrivial relation for its semiclassical approximation on the one hand and the contributions predicted by RMT for the spectral form factor for $\tau > 1$ on the other. For the two-point correlator of spectral determinants we gave in the second section an interpretation of the integration over a curved manifold in field theory in terms of multiply surrounded periodic orbits in semiclassics. This implies for the relation between the RMT results and the semiclassical approaches to understand it: For some time it was believed that there is a one-to-one correspondence between the contributions from correlated pairs of trajectories in the semiclassical calculation and the contributions from diagrams occurring in the corresponding perturbative supersymmetric treatment studied in Refs. [6, 7]. However our calculation in the second section of the last chapter showed that there exist cases where both calculations contain different effects that also led to different ways for obtaining the RMT results: In the field-theoretical calculation we have an integration over a curved manifold that led to the curvature contributions, however the vertices in field theory that correspond to the semiclassical encounter regions are essentially points, i.e. possess a vanishing extension and thus cannot wind around periodic orbits. This is different in semiclassics where we do not consider a curved manifold but the encounter stretches have a finite length and can thus surround a periodic orbit yielding further contributions.

One possible extension in this case would be to show that the connection between the field-theoretical curvature contributions and the contributions from multiply surrounded periodic orbits we presented here for the second-order contribution in $1/\epsilon$ indeed holds to infinite order in $1/\epsilon$. Probably this would also provide additional information about periodic orbit encounters in general.

One further extension is the search for new classes of correlated trajectories to obtain a semiclassical explanation of further effects predicted by field theory; We have seen in the first section of the last chapter that the fact that the exact spectral determinant is real for real energies implies semiclassically a nontrivial relation between the contributions from orbits of different lengths. This relation, that leads as explained in the last chapter to the behaviour of the spectral form factor for $\tau > 1$ predicted by RMT, should be explained semiclassically in terms of orbit correlations. Up to now this was only achieved for simple chaotic model systems in [8, 9]. Furthermore this would probably not only answer the questions posed after Eq. (5.12), i.e. the role of the upper limit in the time integrations resulting from the application of the Hannay and Ozorio de Almeida sum rule [10] and how the correct semiclassical expression for the inverse spectral determinant looks like, but additionally justify semiclassically the use of finite sums over orbits in semiclassical approximations to the spectral determinant, see the expression in Eq. (5.4). Remember here that claiming that the spectral determinant is real for real energies directly led to the latter expression. The calculation of spectra based on Eq. (5.4) or on a trace formula obtained from the latter equation could be semiclassically justified by such a procedure. Finally we mention that also for other phenomena, for example strong (Anderson) localisation [11], i.e. a localisation of all electronic wavefunctions, not yet identified correlations between orbits could lead to a semiclassical explanation of these effects.

Concerning the approaches for non-zero Ehrenfest-time one can think of two directions for extending our results. First there are several examples where RMT results or semiclassical results for $\tau_E = 0$ are known. Here it would be interesting to extend these results to non-zero Ehrenfest-time and compare them for example with numerical simulations. One concrete application here is transport through a graphene billiard, i.e. through a chaotic cavity fabricated by cutting a cavity out of a two-dimensional graphene flake. The corresponding RMT results characterising this kind of transport are discussed for example in [12].

Second the results obtained in Chap. 4 are a first step towards the semiclassical calculation including the Ehrenfest-time dependence to arbitrary high orders. In Chap. 4 we calculated correlation functions of scattering matrices and spectral densities to some low order in the inverse channel number and the inverse energy difference. A first step towards a generalisation to higher orders would be the identification of a general possible pattern behind the Ehrenfest-time dependencies of the different diagrams. The probability of identifying such a pattern that can be expected to hold to infinite order is quite different for the considered cases: In the case of dc transport we found that the second-order quantum correction is independent of the Ehrenfest-time, whereas the first-order quantum correction turned out to be proportional to $e^{-\tau_E/\tau_D}$ [13]: Comparing the contributions at different orders in the number of open channels, it seems thus not yet possible to identify a general pattern behind the

Ehrenfest-time dependence in this case. For the spectral form factor the final result could however possess a simple structure: The contribution from each discrete diagram (i.e. those considered without the Ehrenfest-time dependence in Chap. 2) to the spectral form factor $K(\tau)$ is given by a function depending on $\tau - n\tau_E/T_H$ where n is the number of encounter stretches of the underlying diagram. In the case of the correlation functions of n pairs of scattering matrices we obtained a huge class of diagrams possessing the same Ehrenfest-time dependence. In this case a general pattern could be that also the higher-order contributions in the inverse channel number possess a simple common Ehrenfest-time dependence. The next step in the last two cases would be to see if these patterns indeed hold semiclassically to arbitrarily high order. This would require a general treatment of arbitrarily sized encounters involving also encounters with periodic orbits and their fringes. Therefore we would need to proceed mainly in two steps: First an efficient method is needed for partitioning the diagrams contributing with the same multiplicity, as we described it when analysing the Ehrenfest-time dependence of the *n*-pair correlator of scattering matrix elements to leading order. Second recursion relations for the corresponding contributions taking, in contrast to the case of zero Ehrenfest-time [14, 15], also diagrams with encounter fringes into account, have to be derived. For example this would mean in the case of the first-order quantum correction to the spectral form factor in the absence of time-reversal symmetry that not only the contributions of two 2-encounters and one 3-encounter have to be captured by the recursion relations, as it was done in Chap. 2, but also the contributions from diagrams containing fringes overlapping at both ends need to be taken into account.

This book is restricted to a semiclassical explanation of quantum features of systems with classically chaotic dynamics. One possible extension is thus to explain semiclassically the corresponding features as the weak-localisation lineshape for systems with regular or mixed classical dynamics. Here these effects are in general system dependent. The current status of this research is the following: Assuming ergodicity of the motion on the tori also for integrable systems sum rules were derived to calculate the contributions to the transmission and reflection from orbit pairs possessing equal actions, i.e. from equal orbits or orbits time-reversed to each other [16]. For a corresponding calculation for the circular billiard, see [17]. These results however do not respect the current conservation relation (2.46), there is a contribution to the reflection but not to the transmission that is affected by a magnetic field. Thus also in this case orbit pairs possessing a small but finite action difference contributing also to the transmission need to be considered. This is however not straightforward: The construction scheme for crossing-anticrossing pairs as depicted in Fig. 2.2 cannot be directly carried over to integrable systems, an essential assumption for the construction was in the chaotic case that the orbits approach and depart from each other exponentially with time, in integrable systems this effect is however linear in time. On the other hand, pairs similar to the ones depicted in Fig. 4.11 were analysed numerically for example in [18] leading to results respecting the current conservation relation, but a corresponding analytical semiclassical approach is still lacking.

We assumed in this book that the considered particles do not interact with each other. Despite this assumption many experimentally observed effects can be explained quite well. Interaction effects due to Coulomb interaction however get important in electron based transport when for example very small dots or dots weakly coupled to the leads by tunnel barriers are considered [19]. A first step to depart from the single particle picture is to describe the state of the system no longer by single particle wavefunctions but by symmetrised or antisymmetrised wavefunctions taking into account that identical particles are considered. Then the effect of interactions, for example due to the Coulomb potential, needs to be taken into account. The standard methods of solid state physics are in general not applicable to mesoscopic systems as they assume translational invariance, that is not given here in good approximation due to the relatively small systems. Furthermore it would be of interest to investigate interacting systems from the quantum chaos perspective, which focuses on identifying the influence of the underlying classical dynamics on the features of the corresponding interacting quantum system. A semiclassical theory taking into account interaction effects is thus highly desireable.

Despite the many achievements made during the last years semiclassical methods thus possess various further interesting applications.

References

- 1. Brouwer, P.W., Rahav, S.: Phys. Rev. B 74, 075322 (2006)
- 2. Tian, C., Larkin, A.I.: Phys Rev. B 70, 035305 (2004)
- 3. Brouwer, P.W., Rahav, S., Tian, C.: Phys. Rev. E 74, 066208 (2006)
- 4. Brouwer, P.W., Rahav, S.: Phys. Rev. B 74, 085313 (2006)
- 5. Whitney, R.S., Jacquod, P.: Phys. Rev. Lett. 96, 206804 (2006)
- 6. Müller, S., Heusler, S., Braun, P., Haake, F., Altland, A.: Phys. Rev. E 72, 046207 (2005)
- 7. Müller, S.: Periodic-Orbit Approach to Universality in Quantum Chaos. Ph.D. thesis, Universität Duisburg Essen (2005)
- 8. Tanner, G.: J. Phys. A 33, 3567 (2000)
- Schanz, H., Smilansky, U.: Proceedings Australian Summer School on Quantum Chaos and Mesoscopics (1999)
- 10. Hannay, J., deAlmeida, A.O.: J. Phys. A 17, 3429 (1984)
- 11. Anderson, P.W.: Phys Rev. 109, 1492 (1958)
- 12. Wurm, J., Rycerz, A., Adagideli, İ., Wimmer, M., Richter, K., Baranger, H.U.: Phys. Rev. Lett. **102**, 056806 (2009)
- 13. Adagideli, İ.: Phys. Rev. B **68**, 233308 (2003)
- 14. Müller, S., Heusler, S., Braun, P., Haake, F., Altland, A.: Phys. Rev. Lett. 93, 014103 (2004)
- 15. Heusler, S., Müller, S., Braun, P., Haake, F.: Phys. Rev. Lett. 96, 066804 (2006)
- 16. Sieber, M.: J. Phys A 32, 7679 (1999)
- 17. Dollinger, T.: Semiclassical Transport and Diffraction Effects in Circular Billiards, diploma thesis, Universität Regensburg, (2009)
- 18. Březinová, I., Stampfer, C., Wirtz, L., Rotter, S., Burgdörfer, J.: Phys. Rev. B 77, 165321 (2008)
- Richter, K.: Semiclassical Theory of Mesoscopic Quantum Systems, Springer Tracts in Modern Physics Vol. 161, Berlin (2000)

Appendix A

Recursion Relations for Transport

To prove the continuity equation for the current (3.126) within our diagrammatic approach we return to the combinatorics of the number of periodic orbit structures described by a vector \mathbf{v} [1, 2], and we start with the unitary case. By considering the number of ways a 2-encounter could merge with a k-encounter [to form a (k+1)-encounter] by shrinking the links connecting the 2-encounters of the structure, they arrived at the relation

$$\frac{2v_2}{L}N(\mathbf{v}) = \sum_{k>2} \frac{(k+1)(v_{k+1}+1)}{L-1} N(\mathbf{v}^{[2,k\to k+1]}), \tag{A.1}$$

where $\mathbf{v}^{[2,k\to k+1]}$ is the vector formed from \mathbf{v} by combining a 2-encounter and a k-encounter to form a (k+1)-encounter, so that v_2 and v_k are reduced by one, while v_{k+1} is increased by one. We want to turn this relation into a version for open systems involving the extra factors we have, in a similar way as was done for parametric correlations in [3]. Including the extra terms and rearranging, we arrive at the following

$$\frac{2v_{2}(N-2\pi i\omega)}{(N-4\pi i\omega)}\hat{N}(\mathbf{v},N)
+ \sum_{k>2} \frac{(k+1)v_{k+1}^{[2,k\to k+1]}(N-2\pi i\omega k)}{(N-2\pi i\omega(k+1))}\hat{N}(\mathbf{v}^{[2,k\to k+1]},N) = 0,$$
(A.2)

where $\hat{N}(\mathbf{v}, N)$ was defined in Eq. (3.110) and $v_{k+1}^{[2,k\to k+1]} = v_{k+1} + 1$. Because this is identically zero, if we sum over all vectors with a common value of L - V = m the result is still zero

$$\sum_{\mathbf{v}}^{L-V=m} \left[\frac{2v_2(N-2\pi i\omega)}{(N-4\pi i\omega)} \hat{N}(\mathbf{v},N) + \sum_{k\geq 2} \frac{(k+1)v_{k+1}^{[2,k\to k+1]}(N-2\pi i\omega k)}{(N-2\pi i\omega(k+1))} \hat{N}(\mathbf{v}^{[2,k\to k+1]},N) \right] = 0. \tag{A.3}$$

As combining a 2-encounter and a k-encounter reduces both L and V by one, the resulting vector $\mathbf{v}^{[2,k\to k+1]}$ has the same value of L-V=m as \mathbf{v} . The important step is then to express the sum over the resulting vectors as

$$\sum_{\mathbf{v}}^{L-V=m} v_{k+1}^{[2,k\to k+1]} \hat{N}(\mathbf{v}^{[2,k\to k+1]}, N) = \sum_{\mathbf{v}'}^{L-V=m} v_{k+1}' \hat{N}(\mathbf{v}', N). \tag{A.4}$$

If we then identify the dummy vector \mathbf{v}' with \mathbf{v} in our original sum, we can rewrite (A.3) as

$$\sum_{\mathbf{v}}^{L-V=m} \left[\frac{2v_2(N-2\pi i\omega)}{(N-4\pi i\omega)} + \sum_{l\geq 3} \frac{lv_l(N-2\pi i\omega(l-1))}{(N-2\pi i\omega l)} \right] \hat{N}(\mathbf{v},N) = 0, \quad (A.5)$$

where l = k + 1. The first term can be included as the l = 2 term in the sum over l, so the result reduces to

$$\sum_{\mathbf{v}}^{L-V=m} \sum_{l>2} \frac{lv_l(N - 2\pi i\omega(l-1))}{(N - 2\pi i\omega l)} \hat{N}(\mathbf{v}, N) = 0.$$
 (A.6)

For the orthogonal case, we can also create a valid periodic orbit structure if we shrink a link that connects a 2-encounter to itself so that the 2-encounter disappears. This means that there is an extra term in the recursion relation. Recasting the relation from [1, 2] into a form we require for our situation, we obtain

$$\frac{2v_{2}(N-2\pi i\omega)}{(N-4\pi i\omega)}\hat{N}(\mathbf{v},N) + \sum_{k\geq 2} \frac{(k+1)v_{k+1}^{[2,k\to k+1]}(N-2\pi i\omega k)}{(N-2\pi i\omega(k+1))}\hat{N}(\mathbf{v}^{[2,k\to k+1]},N) + \frac{L(\mathbf{v}^{[2\to]})}{(N-2\pi i\omega)}\hat{N}(\mathbf{v}^{[2\to]},N) = 0, \tag{A.7}$$

where $\mathbf{v}^{[2\to]}$ is the vector formed from \mathbf{v} by removing a 2-encounter and $L(\mathbf{v}^{[2\to]})$ is the number of links that the new structure has. As well as the resummation in (A.4) we can also express

$$\sum_{\mathbf{v}}^{L-V=m} L(\mathbf{v}^{[2\to]}) \hat{N}(\mathbf{v}^{[2\to]}, N) = \sum_{\mathbf{v}'}^{L-V=m-1} L \hat{N}(\mathbf{v}', N),$$
(A.8)

but now, because removing a 2-encounter reduces L by two and V by only one, the value of L-V of our new summation variable \mathbf{v}' is one less than that of \mathbf{v} . Using these resummations, and the fact that when we sum the relation (A.7) over all vectors \mathbf{v} with the same value of L-V=m the sum is still zero, we obtain a result of

$$\sum_{\mathbf{v}}^{L-V=m} \sum_{l \geq 2} \frac{l v_l (N - 2\pi i \omega(l-1))}{(N - 2\pi i \omega l)} \hat{N}(\mathbf{v}, N) + \sum_{\mathbf{v}}^{L-V=m-1} \frac{L}{(N - 2\pi i \omega)} \hat{N}(\mathbf{v}, N) = 0. \quad (A.9)$$

This result, along with (A.6), allows us to prove (3.126), the continuity equation for the current for both symmetry classes.

Appendix B

Encounter Integrals for Non-zero Ehrenfest-Time

In this Appendix we want to calculate the integrals over the stable and unstable coordinates s and u occurring for encounters with periodic orbits for general prefactors a, b, d in front of $t_{\text{enc},1} + t_{\text{enc},2}$, $t_s + t_u$ and τ_p , respectively. The times $t_{\text{enc},1}$ and $t_{\text{enc},2}$ denote the durations of the encounters with the periodic orbit, t_s and t_u the durations of the fringes, i.e. the correlation times of the two orbits before and after being correlated with the periodic orbit, respectively, and τ_p the duration of it. We therefore consider the expression J defined as

$$J \equiv \left\langle \int_{0}^{\infty} d\tau_{p} \int_{-c}^{c} ds du \int_{0}^{\tau_{p}} dt' \frac{1}{2t_{\text{enc},1}t_{\text{enc},2}} \right.$$

$$\times \exp\left(a\left(t_{\text{enc},1} + t_{\text{enc},2}\right) + b\left(t_{s} + t_{u}\right) - d\tau_{p}\right)$$

$$\times \exp\left(\frac{i}{\hbar} \sum_{i=1}^{2} u_{i} s_{i}\right) \right\rangle_{\Delta k}.$$
(B.1)

The s, u- and the t'-integrals in J are evaluated in [6] yielding

$$J = \int_{0}^{\infty} d\tau_{p} \frac{a^{2}}{T_{H}^{2}} \tau_{p} e^{-\left(d\tau_{p} - 2a\tau_{E}\right)} + \int_{0}^{\infty} d\tau_{p} \frac{b^{2} e^{-d\tau_{p}}}{2T_{H}^{2}(a - b)} \left(e^{2a\tau_{E}} - e^{2b\tau_{E}}\right).$$
(B.2)

Performing the τ_p -integral finally yields

$$J = \frac{a^2}{d^2 T_H^2} e^{2a\tau_E} + \frac{b^2}{2T_H^2 d(a-b)} (e^{2a\tau_E} - e^{2b\tau_E}),$$
 (B.3)

which is frequently used in the main part of this book.

Furthermore we want to consider a 3-encounter and calculate with arbitrary prefactors f and g in front of the encounter duration t_{enc} and the sum of the fringe durations $t_s + t_u$, respectively,

$$K \equiv \left\langle \int_{-c}^{c} ds \, du \, \frac{1}{\Omega^{2} t_{\text{enc}}} \exp(f t_{\text{enc}} + g_{1} t_{s} + g_{2} t_{u}) \right.$$

$$\times \exp\left(\frac{i}{\hbar} \sum_{i=1}^{2} u_{i} s_{i}\right) \right\rangle_{\Delta k}.$$
(B.4)

The first contribution K_1 is obtained by setting g = 0, it yields [4]

$$K_1 = \frac{f}{T_H^2} e^{f\tau_E}. (B.5)$$

The second contribution K_2 , given by $K-K_1$, is obtained for $g_1=g_2\equiv g$ to be [4]

$$K_2 = 3 \frac{g^2}{(2q - f)T_H^2} (e^{2g\tau_E} - e^{f\tau_E}).$$
 (B.6)

For $g_1 \neq g_2$ we have instead [4]

$$K_2 = 3 \frac{g_1 g_2}{(g_1 + g_2 - f) T_H^2} \left(e^{(g_1 + g_2)\tau_E} - e^{f\tau_E} \right).$$
 (B.7)

Appendix C

Conductance Variance with Tunnel Barriers

We give in this Appendix the leading order in N contributions to the variance of the conductance for non-zero Ehrenfest-time in the presence of tunnel barriers. We restrict to terms linear in the Ehrenfest-time τ_E and $N_1 = N_2$ as in the numerics in Fig. 4.12. The results given here are valid in the unitary case; results for the orthogonal case are obtained by multiplying them by a factor 2. After each contribution we give its size in brackets once for $\Gamma = 0.2$ and once for $\Gamma = 0.8$ to illustrate the main contributions responsible for the two peaks in Fig. 4.12. For more details of the calculation, see [5].

If not stated differently the given results are obtained by applying the diagrammatic rules introduced in Chaps. 2–4. The contribution from two 2-encounters in a row (see Fig. 4.9) is given here including also the cases where stretches touch the opening at *one* end by

$$-\frac{\Gamma^2 p_2 \tau_E}{8\tau_D} \tag{C.1}$$

 $(-0.0018\tau_E/\tau_D; -0.0768\tau_E/\tau_D)$. Twice this contribution is also obtained when considering two independent 2-encounters with a periodic orbit, see Fig. 4.14 with the rightmost link cut open.

Furthermore we consider for this diagram also configurations where one encounter stretch in Fig. 4.14 touches *both* openings and the other one touches zero or one time yielding

$$-\frac{\Gamma^2 (1-\Gamma)^2 \tau_E}{4\tau_D} \tag{C.2}$$

 $(-0.0064\tau_E/\tau_D; -0.0064\tau_E/\tau_D)$. This contribution from encounters touching *both* openings is obtained in a similar way as in Sect. 4.5.2. Note that a configuration where *both* encounters touch *both* openings yields a contribution at least quadratic in τ_E .

Two partially overlapping 2-encounters (middle diagram in Fig. 4.13)—the stretches are as before also allowed to touch the opening at *one* end—yield

$$\frac{\Gamma^3 (2-\Gamma)^2 \tau_E}{4\tau_D}.$$
 (C.3)

 $(0.00648\tau_E/\tau_D;~0.18432\tau_E/\tau_D)$. This and also the next contribution can be obtained by taking into account the effect of tunnel barriers in the calculation of K in Appendix B. In the case of the middle diagram in Fig. 4.13 no further contribution due to stretches touching both openings is obtained as can be checked by performing a calculation as in Sect. 4.5.2 for this diagram.

Another contribution results from one 3-encounter with a periodic orbit (leftmost diagram in Fig. 4.13) yielding when again also diagrams with the encounter touching the opening at *one* end are considered

$$\frac{(\Gamma^2 + \Gamma - 1)p_3\tau_E}{8\tau_D} \tag{C.4}$$

 $(-0.04636\tau_E/\tau_D; 0.05456\tau_E/\tau_D)$. Also in this case a diagram similar as in (C.2), i.e. a 3-encounter touching *both* leads, needs to be taken into account

$$\frac{\Gamma^3 (1-\Gamma)^2 \tau_E}{2\tau_D} \tag{C.5}$$

 $(0.00256\tau_E/\tau_D;~0.01024\tau_E/\tau_D)$. The calculation of the last contribution is again similar to the one in Sect. 4.5.2. From (C.5) further configurations can be obtained. In the case of one additional link connecting the encounter to the opening that is back reflected at the lead (similar as in Fig. 4.11) we get compared to Eq. (C.5) a factor Γ less because there is one link more and a factor $1-\Gamma$ more because of the backreflection

$$\frac{\Gamma^2 (1-\Gamma)^3 \tau_E}{\tau_D} \tag{C.6}$$

 $(0.02048\tau_E/\tau_D;~0.00512\tau_E/\tau_D)$ and in the case of two additional links

$$\frac{\Gamma(1-\Gamma)^4 \tau_E}{2\tau_D} \tag{C.7}$$

 $(0.04096\tau_E/\tau_D; 0.00064\tau_E/\tau_D).$

From the rightmost diagram in Fig. 4.13 where the sum of the encounter times is larger than the duration of the periodic orbit and the stretches overlap at both ends we obtain

$$\frac{(p_3 - 2p_2)\tau_E}{8\tau_D} \tag{C.8}$$

 $(-0.029\tau_E/\tau_D; -0.116\tau_E/\tau_D)$. Note that to simplify the expressions below we included some part of this contribution below as k=0-term in (C.18, C.19). Here again also diagrams are taken into account where stretches touch the opening at *one* end, diagrams where the stretches touch the opening at *both* ends yield as for

the configuration considered in (C.3) no contribution.

Up to now we did not treat effects due to correlations of encounter fringes, i.e. correlations between orbit parts before and after they are correlated with the periodic orbit, see Fig. 4.10. Here the contribution is obtained by generalising the calculation of J in Appendix B to this case

$$\frac{\Gamma^3 \tau_E}{8\tau_D} \tag{C.9}$$

 $(0.001\tau_E/\tau_D;~0.064\tau_E/\tau_D)$. In Eq. (C.9) diagrams with fringes inside the system and with fringes touching the lead are considered. Additionally for $\Gamma \neq 1$ we can cut one fringe completely, then the attached encounter stretch touches the opening and only one fringe remains leading to the contribution

$$\frac{(1-\Gamma)(\Gamma^2 - 2\Gamma^4)\tau_E}{4\tau_D} \tag{C.10}$$

 $(0.00736\tau_E/\tau_D; -0.00896\tau_E/\tau_D).$

Up to now we only considered diagrams where the periodic orbit is longer than the encounter stretches. Further contributions in terms of infinite sums derive from the case where the encounter stretches surround the enclosed periodic orbit more than once. In this case we obtain that the k-th term in these sums is the contribution from the k-fold winding of each encounter stretch around the periodic orbit. Configurations where the number of windings of the two stretches differs by more than one do not contribute here, for a justification see Ref. [6]. The contributions considered here are calculated by restricting the integral with respect to the duration of the surrounded periodic orbit appropriately in terms of the encounter durations $t_{\rm enc,1}$ and $t_{\rm enc,2}$. We start with treating a configuration as analysed in Fig. 4.14, now however both orbits encountering the central periodic one surround it k times and first consider the contribution from encounters inside the orbit

$$-\sum_{k=1}^{\infty} \frac{(p_{2k+2} - p_{2k+1})\tau_E}{8k^2(2k+1)\tau_D}$$
 (C.11)

and a corresponding contribution where one stretch touches one opening

$$2\sum_{k=1}^{\infty} \frac{(p_{2k+2} - p_{2k+1})\tau_E}{8k^2(2k+1)\tau_D},$$
 (C.12)

further contributions are not obtained in this case.

Analogous calculations yield for the middle diagram in Fig. 4.13

$$\sum_{k=1}^{\infty} \left[\frac{(p_{2k+3} - p_{2k+2})\tau_E}{4(k+1)(2k+1)\tau_D} - \frac{(p_{2k+2} - p_{2k+1})\tau_E}{4k(2k+1)\tau_D} \right]$$
 (C.13)

and when one stretch touches one opening

$$\sum_{k=1}^{\infty} \left[\frac{(p_{2k+2} - p_{2k+1})\tau_E}{2k(2k+1)\tau_D} - \frac{(p_{2k+3} - p_{2k+2})\tau_E}{2(k+1)(2k+1)\tau_D} - \frac{(2p_{2k+2} - p_{2k+1} - p_{2k+3})\tau_E}{4k(k+1)\tau_D} \right]. \tag{C.14}$$

Turning now to the leftmost diagram in Fig. 4.13 we obtain

$$\sum_{k=1}^{\infty} \frac{(2p_{2k+2} - p_{2k+1} - p_{2k+3})\tau_E}{8(k+1)k\tau_D}$$
 (C.15)

from an encounter inside the orbit and

$$\sum_{k=1}^{\infty} \frac{(2p_{2k+2} - p_{2k+1} - p_{2k+3})\tau_E}{2(k+1)k\tau_D}$$
 (C.16)

from an encounter touching the opening at one end and

$$-\sum_{k=1}^{\infty} \frac{(2p_{2k+2} - p_{2k+1} - p_{2k+3})\tau_E}{4(k+1)k\tau_D},$$
 (C.17)

when one additional link is attached to one stretch that is back reflected at the opening.

The rightmost diagram in Fig. 4.13 contributes

$$-\sum_{k=0}^{\infty} \frac{(p_{2k+3} - p_{2k+2})\tau_E}{8(k+1)^2 (2k+1)\tau_D},$$
(C.18)

when the encounter stretches are inside the system and

$$2\sum_{k=0}^{\infty} \frac{(p_{2k+3} - p_{2k+2})\tau_E}{8(k+1)^2(2k+1)\tau_D},$$
(C.19)

when one stretch touches the lead at one end.

Summing these contributions we obtain from Eqs. (C.15–C.17) and the last summand in Eq. (C.14)

$$\frac{\Gamma^2 \tau_E}{(1 - \Gamma)8\tau_D} \Big[(1 - \Gamma)^2 + p_2 \ln p_2 \Big]$$
 (C.20)

 $(0.0017\tau_E/\tau_D; 0.00032\tau_E/\tau_D)$ and from Eqs. (C.11–C.13, C.18, C.19) and the first two summands in Eq. (C.14)

$$\frac{(p_3 - p_2)\tau_E}{4\tau_D} \tag{C.21}$$

 $(0.032\tau_E/\tau_D; \ 0.008\tau_E/\tau_D)$ and

$$-\frac{\Gamma^2 \text{Li}_2 \left(\left(1 - \Gamma \right)^2 \right) \tau_E}{8 \tau_D} \tag{C.22}$$

 $(-0.00395\tau_E/\tau_D; -0.00323\tau_E/\tau_D)$ with the polylogarithmic function $\text{Li}_2(x)$. The overall contribution to the conductance variance to leading order in N, linear in τ_E and for arbitrary Γ is then obtained to be

$$\frac{\Gamma(\Gamma-1)\left(7\Gamma^{3}-6\Gamma^{2}+4\Gamma-2\right)\tau_{E}}{8\tau_{D}} + \frac{\Gamma^{2}\left(2\Gamma-\Gamma^{2}\right)\tau_{E}}{(1-\Gamma)8\tau_{D}}\ln\left(2\Gamma-\Gamma^{2}\right) - \frac{\Gamma^{2}\operatorname{Li}_{2}\left((1-\Gamma)^{2}\right)\tau_{E}}{8\tau_{D}}, \tag{C.23}$$

which is shown in Fig. 4.12 after multiplication by 2.

References

- 1. Müller, S., Heusler, S., Braun, P., Haake, F., Altland, A.: Phys. Rev. E 72, 046207 (2005)
- Müller, S.: Periodic-Orbit Approach to Universality in Quantum Chaos. Ph.D. thesis, Universität Duisburg Essen (2005)
- 3. Nagao, T., Braun, P., Müller, S., Saito, K., Heusler, S., Haake, F.: J. Phys. A 40, 47 (2007)
- 4. Brouwer, P.W., Rahav, S.: Phys. Rev. B 74, 085313 (2006)
- 5. Waltner, D., Kuipers, J., Jacquod, P., Richter, K.: arXiv:1108.5091, unpublished (2011)
- 6. Brouwer, P.W., Rahav, S.: Phys. Rev. B 74, 075322 (2006)